

*Synthesis and Characterization of Photo-crosslinkable Polymers  
and Hydrogel Thin Films*

**D I S S E R T A T I O N**

**zur Erlangung des akademischen Grades**

**Doctor rerum naturalium**

**(Dr. rer. nat.)**

**vorgelegt**

**der Fakultät Naturwissenschaften**

**der Universität Paderborn**

**von**

**Momen Sayed Ahmed Ali**

**Gutachter: Prof. Dr. Dirk Kuckling**

**Gutachter: Prof. Dr. Klaus Huber**

**Eingereicht am: .....**

**Tag der Verteidigung: .....**

*Synthesis and Characterization of Photo-crosslinkable Polymers  
and Hydrogel Thin Films*

**D I S S E R T A T I O N**

**for the partial fulfillment of the requirements**

**for the academic degree of**

**Doctor rerum naturalium**

**(Dr. rer. nat.)**

**Submitted to**

**Faculty of Science**

**University of Paderborn**

**By**

**Momen Sayed Ahmed Ali**

**Supervised by**

**Prof.Dr. Dirk Kuckling**

**Referees: .....**

.....

.....

**Submitted on:**

# Table of contents

<b>Abbreviations</b>	<b>iii</b>
<b>Abstract</b>	<b>v</b>
<b>Aim</b>	<b>1</b>
<b>1. Introduction</b>	<b>4</b>
<b>2. Experimental</b>	<b>56</b>
2.1. Introduction	56
2.2. Reagents and solvents	56
2.3. Instrumentations	57
2.4. Synthesis of monomers and photo-crosslinkers	61
2.5. Synthesis of monomers	67
2.6. Synthesis of adhesion promoters	76
2.7. Polymer synthesis	78
2.8. Synthesis of PNIPAAm copolymers	84
2.9. Synthesis of photo-crosslinkable polymers	90
2.10. Synthesis of photo-crosslinker functional polymers	95
2.11. Synthesis of grafted polymer	105
2.12. Hydrogel formation	111
<b>3. Results and Discussion</b>	<b>114</b>
3.1. Photo-crosslinkers	114
3.2. Monomers	116
3.3. Adhesion promoters	126
3.4. Polymer characterization	127
3.5. Photo-crosslinker polymers	146
3.6. Formation of photo-crosslinked gel single layer studied by SPR/OWS	176

3.7.	Photo-crosslinked hydrogel bilayer	209
3.8.	Effect of film thickness on the behavior of hydrogel bilayer	225
<b>4.</b>	<b>Summary</b>	<b>233</b>
<b>5.</b>	<b>References</b>	<b>239</b>
<b>6.</b>	<b>Acknowledgments</b>	

## Abbreviations

Abbreviation	Means
<b>APA</b>	4-acetylphenyl acrylate
<b>AFM</b>	Atomic Force Microscopy
<b>AIBN</b>	2,2'-azobis(isobutyronitrile)
<b>ATR</b>	Attenuated Total Reflection
<b>ATRP</b>	Atom Transfer Radical Polymerization
<b>AP</b>	Adhesion promoter
<b>Au</b>	Gold
<b>AVHA</b>	[4-[2-(acryloyloxy)-5-formyl-3-methoxyphenyl] diazenyl}benzoyl) amino] acetic acid
<b>(Boc)<sub>2</sub>O</b>	<i>di-tert</i> -butyldicarbonate
<b>CC</b>	Coexistanse Curve
<b>CP</b>	Cloud Point
<b>DCC</b>	<i>N,N'</i> -dicyclohexylcarbodiimide
<b>d/d<sub>0</sub></b>	Swelling Ratio
<b>DEMAVA</b>	2-[(diethylamino)methyl]-4-formyl-6-methoxyphenyl acrylate
<b>DMF</b>	<i>N,N</i> -dimethylformamide
<b>DHPA</b>	2,3-dihydroxypropyl acrylate
<b>DMIA</b>	1-(2-hydroxyethyl)-3,4-dimethyl-1H-pyrrole-2,5-dione
<b>DMITAc</b>	3-(3,4-dimethyl-2,5-dioxo-2,5-dihydro-pyrrol-yl)-propyl ester
<b>DMIAAm</b>	N-[2'-(3,4-dimethyl-2,5- dioxo-2,5-dihydroxy-pyrrol-1-yl)]-ethyl-acrylamide

---

<b>DSC</b>	Differential Scanning Calorimetry
<b>GPC</b>	Gel Permeation Chromatography
<b>HA</b>	Hippuric Acid
<b>LbL</b>	Layer by Layer
<b>LCST</b>	Lower Critical Solution Temperature
<b>n</b>	Refractive Index
<b>NASI</b>	1-(acryloyloxy)pyrrolidine-2,5-dione
<b>RU</b>	Reflection Unit
<b>RIU</b>	Refractive Index Unit
<b>SPR-OWS</b>	Surface Plasmon Resonance/Optical Waveguide Spectroscopy
<b>T<sub>c</sub></b>	Transition Temperature
<b>TEA</b>	triethylamine
<b>T<sub>g</sub></b>	Glass Temperature
<b>VA</b>	4-formyl-2-methoxyphenylacrylate
<b>ε</b>	Dielectric
<b>θ<sub>SPR</sub></b>	Plasmon Minimum
<b>χ<sub>p</sub></b>	Polymer Fraction
<b>1/χ<sub>p</sub></b>	Volume Degree of Swelling

---

## **Abstract**

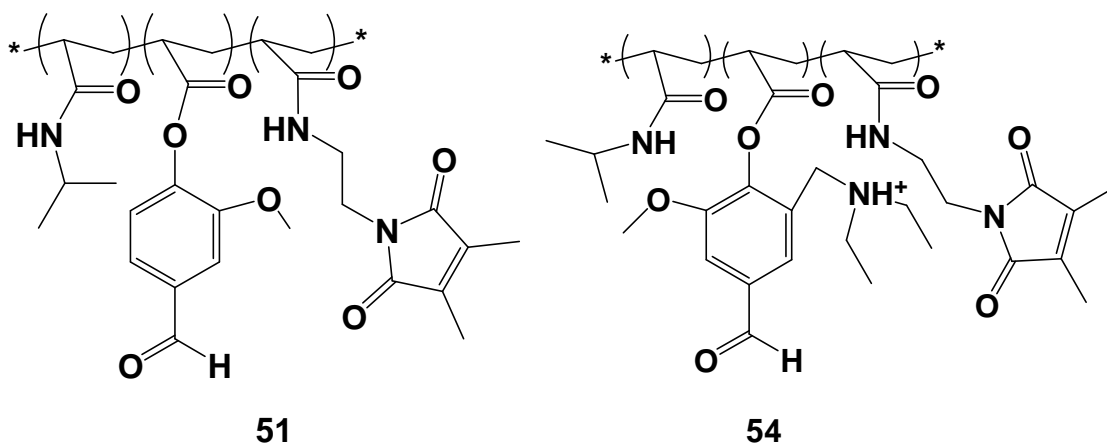
Polymer hydrogels have been our focus of research because of their range of important properties, such as biocompatibility, and responsive behavior. The responsive behavior of special hydrogels is of special concern in this study. The hydrogel is synthesized from stimuli-responsive polymers, sensitive to the surrounding aqueous solution (for example, temperature, and pH). This change in swelling degree refers to changes of many properties of the materials like; refractive index, permeability, elastic modulus, interfacial tension, adhesion, etc. The physical properties of stimuli responsive hydrogels have been explored for the tunable and switchable transport of ions and molecules across the material, controlled uptake and release of chemicals by bulk hydrogels, and various kinds of sensors and actuators. The advantages of hydrogel thin films have been explored for the fabrication of miniaturized devices with fast response times. Hydrogel thin films have also attracted interest as an approach to responsive surfaces and interfaces, where they compete with grafted polymer layers. A 3D polymer network is much more stable at interfaces when compared with polymer brushes, where polymer chains are grafted to the surface via only one functional group while the polymer network is linked to the surface by multiple anchoring points.

Our studies were focused on the following;

- ❖ First of all we focused on the synthesis of new functional monomers; therefore, we used vanillin as start compound in the synthesis of three monomers: 4-formyl-2-methoxyphenylacrylate (VA), 2-[(diethylamino)methyl]-4-formyl-6-methoxyphenyl acrylate (DEMAVA), and [{"4-[2-(acryloyloxy)-5-formyl-3-methoxyphenyl] diazenyl}benzoyl]amino] acetic acid (AHVA). All of these were used in the copolymerization with *N,N*-dimethyl acrylamide (DMAAm) and *N*-isopropylacrylamide (NIPAAm).
- ❖ The homopolymers were synthesized by free radical polymerization of monomers. The polymers investigated by <sup>1</sup>HNMR, and FTIR spectroscopy, GPC and DSC (for T<sub>g</sub> determination). After that it was important to synthesize copolymers based on NIPAAm and study the effect of the incorporated monomers which are hydrophilic (DMAAm, and DEAMVA) or hydrophobic like; 2,2-dimethyl-1,3-dioxolane-4-yl-methylacrylate (SKA) and 1-(acryloyloxy)pyrrolidine-2,5-dione (NASI) on the lower critical solution temperature behavior (T<sub>c</sub>). We observed an increase in T<sub>c</sub> with the

hydrophilic monomers as a function of composition and vice versa for hydrophobic monomers.

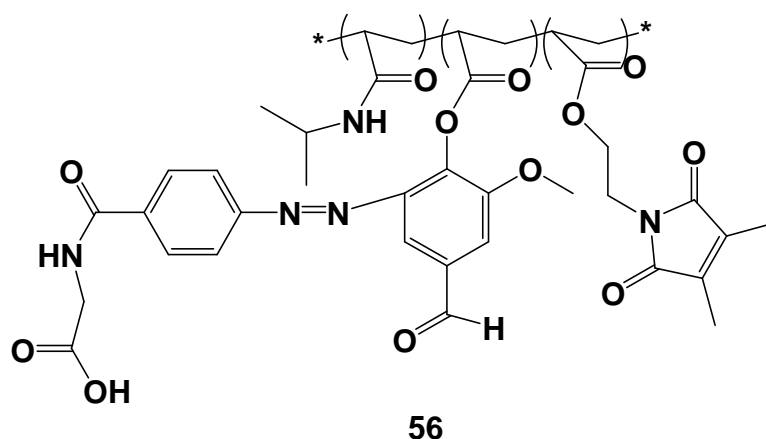
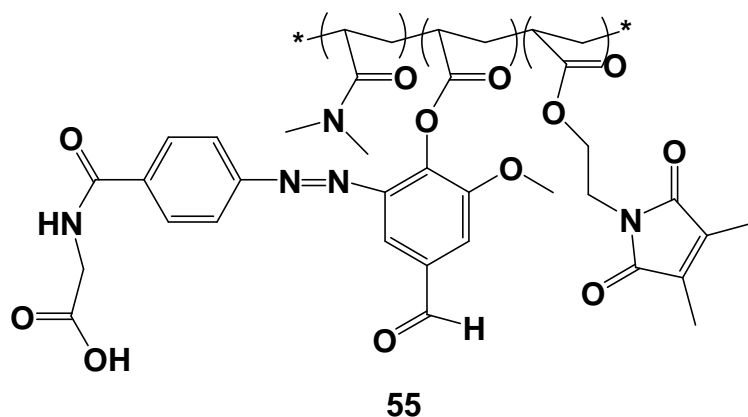
- ❖ Dimethylmaleimide (DMI) moiety was incorporated in the polymers chains and was used to introduce photo-crosslinking by [2+2] cyclodimerization reaction in the presence of UV irradiation. The photo-crosslinkers based on DMI group were DMIAAm, DMIA, and DMIMA. Random free radical polymerization of above monomers with respective photo-crosslinker resulted in formation of photo-crosslinkable polymers of (a) NIPAAm, (b) DMAAm, (c) HEMA, (d) VA, (e) SKA, (f) NIPAAm/VA, (g) DMAAm/DEAMVA, (h) SKA/VA, (i) NIPAAm/DEAMVA, (j) DMAAm/AHVA, and (k) NIPAAm/AHVA. The properties of these polymers were investigated by NMR, UV-vis. Spectroscopy, GPC and SPR. Thin hydrogel layers were prepared by spin coating on gold-coated LaSFN9 glass. The covalent attachment to the surface was achieved through an adhesion promoter.
- ❖ The characterization of responsive thin photo-crosslinked hydrogel layers based on T and pH responsiveness were discussed too.
- ❖ Hydrogel layers were prepared for all kinds of polymers to give different responsive films e.g. temperature responsive for all polymer hydrogel films based on NIPAAm, and pH-responsive behavior for hydrogel films containing (DEAMVA). Furthermore, hydrophilic photo-crosslinked polymer gel based on (DMAAm and HEMA) or hydrophobic photo-crosslinked polymer gel based on SKA and VA were prepared.
- ❖ Formation of dual-responsive polymers and hydrogels were taken in our study e.g. the combination of temperature responsive (NIPAAm) with pH-responsive (DEAMVA) and studying the change in  $T_c$  as a change of pH. We observed an increasing of  $T_c$  as change from acidic to neutral to basic buffer solutions.



- ❖ Swelling behavior of the thin polymer gel layers was investigated by combination of Surface Plasmon Resonance (SPR) and Optical Waveguide Spectroscopy (OWS). SPR

and OWS gave a wide range of information regarding the film thickness ( $d$ ), swelling ratio ( $d/d_0$ ), refractive index ( $n$ ) and volume degree of swelling ( $1/\chi_p$ ) of the thin hydrogel layer.

- ❖ We observed that all  $T_c$  values calculated by SPR/OWS were in agreement with UV.vis. Spectroscopy and DSC with respect of little change demonstrated by the different definitions for each technique.
- ❖ One of the most important observations in our study is demonstrated for azo hydrogels as copolymers with DMAAm or NIPAAm, showing dual responsive behavior. We observed the formation of upper critical solution temperature behavior (UCST) or change of phase separation from LCST to UCST during swelling at pH 11.2. This behavior was interpreted as the effect of hydrogen bonding in the basic media; it rather needs high energy to increase swelling ratio.



- ❖ It was necessary after the formation of single layer to build hydrogel bilayers. For this object we built bilayer hydrogels with temperature responsive photo-crosslinkable NIPAAm as base layer and non-responsive photo-crosslinkable DMAAm as top payer and vice verse. The swelling behavior was discussed as for single layer but here

Fresnel calculations were used as bilayer system yielding two volume degrees of swelling and refractive index for each layer. The lower critical solution temperature was determined as function of  $(1/\chi_p)$  or refractive index for each layer.

- ❖ Formation of bilayer hydrogels based on dual-responsive polymers in the base layer and non-responsive polymers in the upper layer or vice versa was demonstrated. The swelling was studied as a function of both temperature and pH. The lower critical solution temperature was determined as function of  $(1/\chi_p)$  or refractive index for each layer at different pH.
- ❖ The same method was used for T, pH-responsive polymers in the base layer and temperature responsive polymers in the upper layer, with respect to the formation of two ( $T_c$ ) for each layer.
- ❖ The last point studied was the effect of film thickness on the behavior of hydrogel bilayer. For this purpose we used four kinds of bilayer thickness in the temperature responsive and non-responsive system.

## The Problem

Smart hydrogels have been widely used in many applications e.g biomaterials, (micro) actuator and sensors materials, controlled cell attachment/detachment, and controlled drug delivery. Polymer-drug and polymer-protein conjugates typically studied have a tripartite structure: polymer, linker, and therapeutic agent. However, more complex systems now exist that incorporates additional features for targeted delivery or combination therapies. The most common carriers for polymer therapeutics are 2-hydroxyethyl methacrylate (HPMA) (polymer-drug) and poly(ethylene glycol) PEG (polymer- protein), but other systems studied include poly(glutamic acid), dextran, dextrin, chitosans, poly(L-lysine), and poly(aspartamides) as polymeric carriers. Typically such polymers are used as soluble polymers and as particles. However, there is a need to fix such structures to solid substrates. Hence, these applications require the use of hydrogels at surfaces and interfaces. Therefore, the behavior of bulk hydrogel may not be necessarily extended to these types of geometries. Here in our study we were thinking in the synthesis of new responsive functional photo-crosslinkable polymers, which will further be used in the formation of single and bilayer responsive hydrogels and can be used in the immobilization of many biological molecules through on/off system at the surface.

## The Solution

To solve this problem new monomers based on Vanillin have to be synthesized. The presence of aldehyde groups is necessary for the immobilization of many biological molecules through the formation of Schiff base. Three kinds of monomers will provide functional surface; hydrophobic/hydrophilic, pH, functional surface, and T-pH functional surface (**Figure I**). These monomers will be used in the preparation of photo-crosslinkable polymers via free radical polymerization with *N*-isopropylacrylamide (NIPAAm), and *N,N*-dimethylacrylamide (DMAAm) together with a maleimide crosslinker. Hydrogels will be prepared through spin coating of polymer solution followed by irradiation by UV light. The lower critical solution temperature of polymers solutions and hydrogels should be affected by the incorporated monomers as addition of hydrophilic compounds raise  $T_c$ , while the hydrophobic once lower the  $T_c$ . The swelling properties of functional hydrogel films can be used in the delivery/release for many biological molecules or cell attachment/detachment (**see Figure II**). The formation of dual-responsive hydrogels will give the surface more applicability to achieve drug delivery/

release properties in which the control of  $T_c$  with pH expose the surface to different phase separations as shown in **Figure III**.

In order to prepare structures within enhanced properties the formation of bilayer hydrogel is of interest. For this purpose bilayer systems with different responsiveness in the lower and upper layer will be built. Such structures might be used as vessel or gel container for the targeting of biological molecules, as a delivery/release system or for cell attachment/detachment. The bilayer functional hydrogels will have an additional feature, in which the target molecule stay safely inside this gel vessel at different temperature related to  $T_c$  of the functional layer, pH or T with pH (See **Figure IV**).

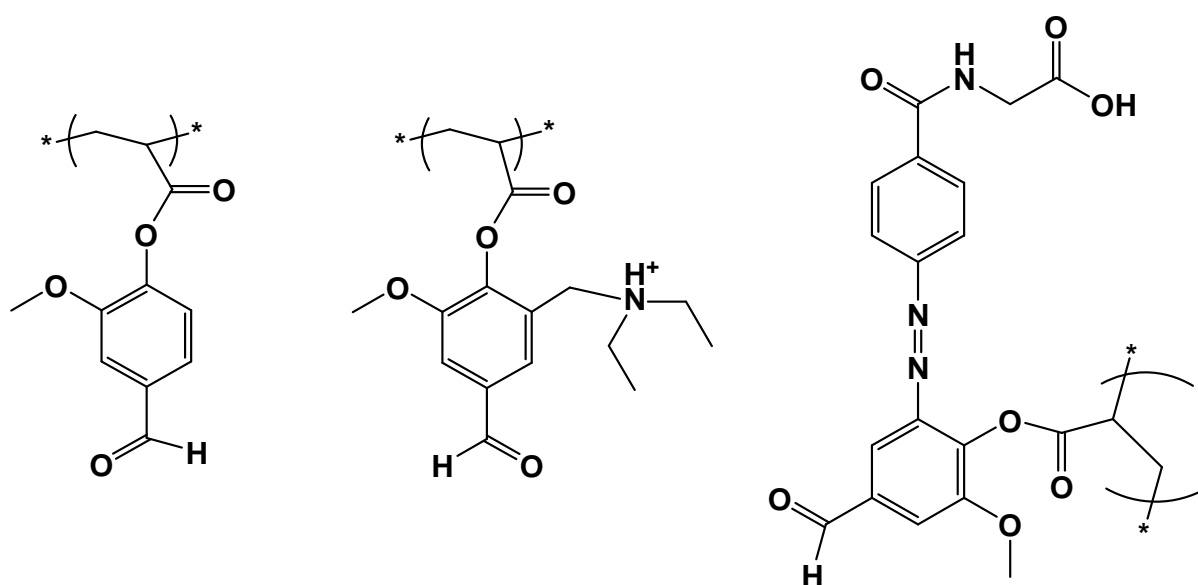


**Figure I:** Vanillin monomers used in our study.

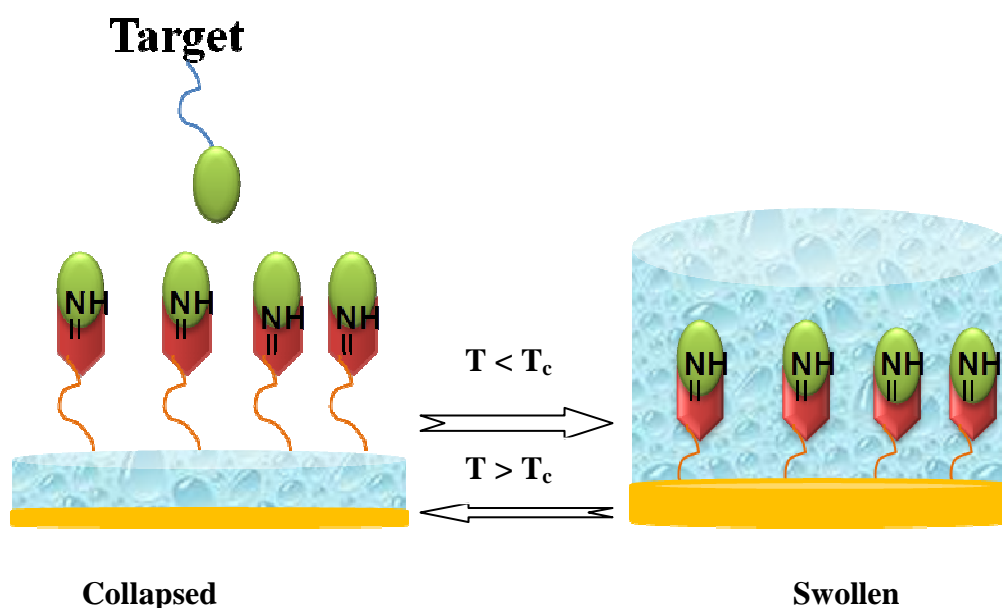


**Figure II:** Swelling and collapsed states of temperature responsive functional hydrogel thin film loaded by bimolecular target through the formation of Schiff base.

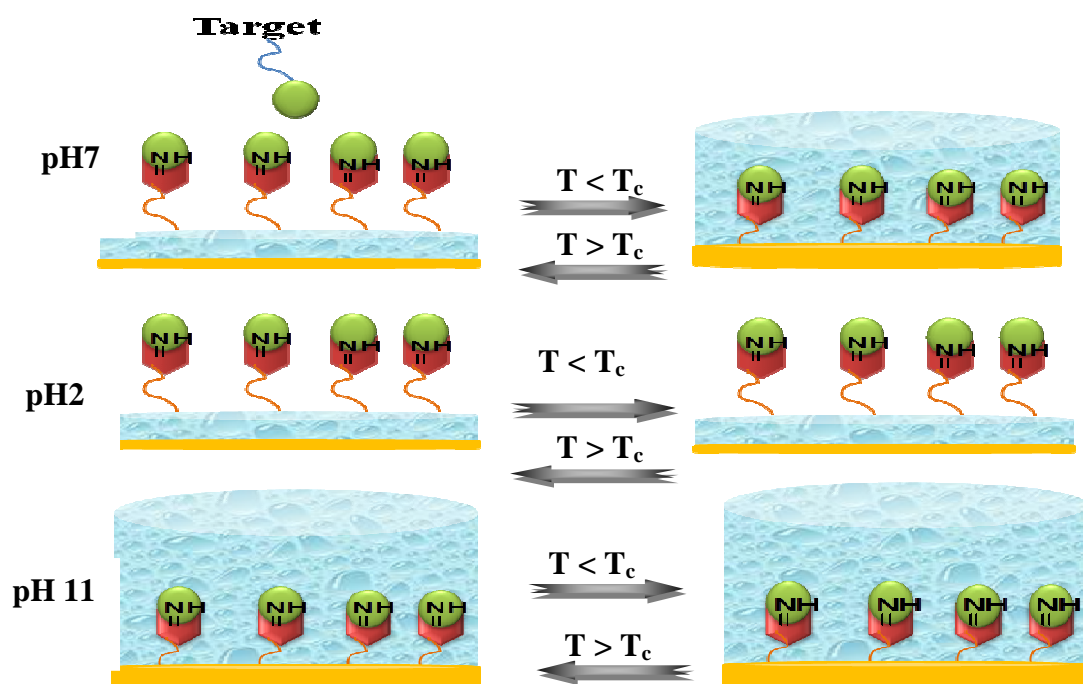


**Figure III:** Swelling and collapsed states of dual-responsive functional hydrogel thin film loaded by bimolecular target through the formation of Schiff base.

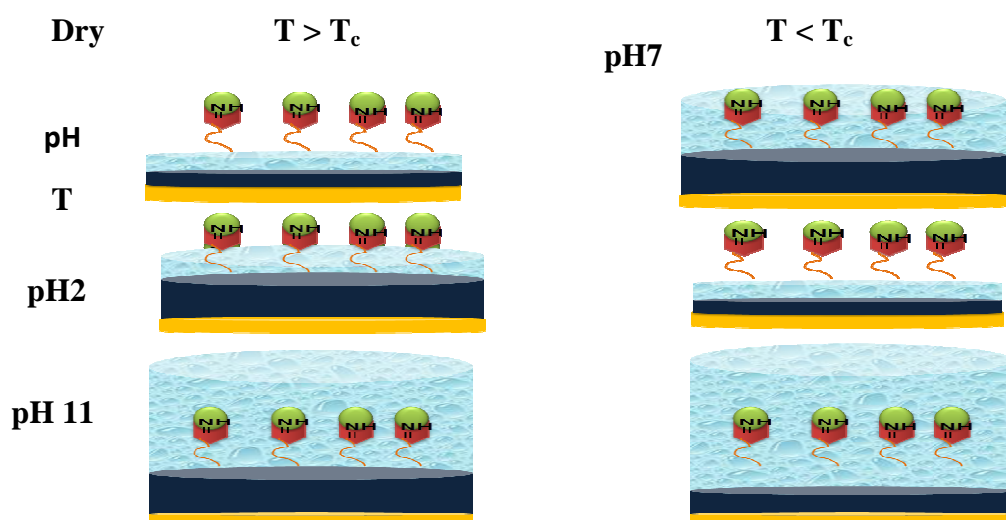


**Figure IV:** Swelling and collapsed states of hydrogel bilayer thin film loaded by bimolecular target through the formation of Schiff base.

# *Chapter(1)*

## *Introduction*

# 1. Hydrogel

## 1.1. Introduction.

Gels, originating from the Latin *gelatus* – frozen, are defined as fine dispersed systems, consisting of solid and liquid or gaseous phases. The solid phase or phases form a three dimensional network, acting as host for the liquid or gaseous phases. In case of a gas as dispersant the system is called aerogel, whereas a host for liquids is referred to as lyogel. In the following lyogels with water as liquid phase, hydrogels are discussed. Silica gels and gelatine are well known examples for physically, non-covalently crosslinked hydrogels or aqueous colloidal dispersions. There, the network is formed and stabilized by van-der-Waals interaction, hydrogen bonding or charge attraction. These gels are stable, but can easily be reliquified, e.g. by shaking. In contrast, chemically, covalently crosslinked hydrogels do not reliquify, they can only loose the accumulated water, turning them back into a solid. This process is reversible. The ability to take up a multiple of their own weight in water is one of the reasons why hydrogels are applied in a broad variety of fields. For instance, polyvinyl alcohol is used as gelatinizing agent in water gel explosives,<sup>(2)</sup> polyhydroxyethyl methacrylate (PHEMA) is found in contact lenses,<sup>(3)</sup> polyacrylates in diapers<sup>(4)</sup> and some, like poly(ethyleneglycol) PEG cover numerous areas from skin cream to solid phase material in gas chromatography<sup>(5, 6)</sup>.



**Figure 1:** Tanakas famous polyelectrolyte hydrogel<sup>(1)</sup>.

## 1.2. Crosslinking methods to design hydrogel.

As the term ‘network’ implies, crosslinks have to be present to avoid dissolution of the hydrophilic polymer chains / segments into the aqueous phase. Hydrogels can also be described in a rheological way. Aqueous solutions of hydrophilic polymers at low or moderate biocompatibilicentration, where no substantial entanglement of chains occurs, normally show Newtonian behavior <sup>(7)</sup>. On the other hand, once crosslinks between the different polymer chains are introduced, the so obtained networks show visco-elastic and sometimes pure elastic behavior. Because of their water-absorbing capacity, hydrogels are not only subject of investigation of researchers interested in fundamental aspects of swollen polymeric networks, but have also found widespread application in different technological areas <sup>(8,9)</sup>.

Many crosslinking methods have been developed and are presently available for the preparation of hydrogel<sup>(7)</sup>. In the present study two kinds of crosslinking methods have been widely used.

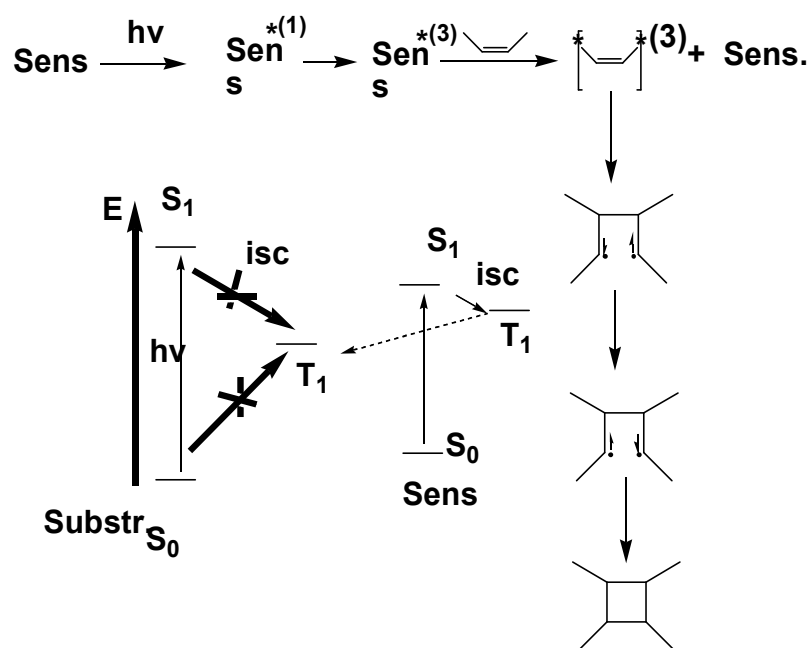
### **1.2.1 Photo-crosslinking hydrogel.**

Suitable groups which undergo photo dimerization and can therefore be used for photo-crosslinking of accordingly functionalized polymers comprise cinnamate (and related) moieties<sup>(10-20)</sup>, coumarins<sup>(21)</sup>, and maleic acid derivatives like dimethylmaleimide (DMMI)<sup>(22-27)</sup>.

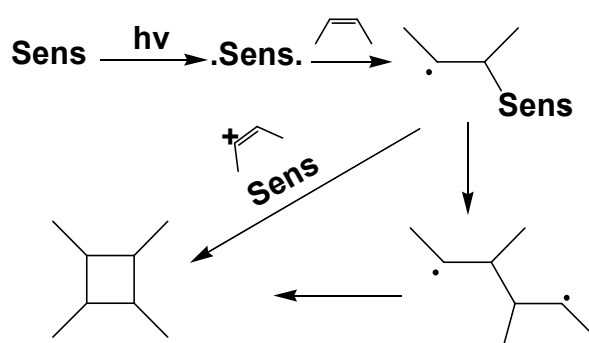
Kuckling *et al.*<sup>(28)</sup>, have used of the photo chemical [2 + 2] dimerization of dimethylmaleimide (DMMI) side groups was made as sketched in **Figure 2**. A sensitizer, thioxanthone disulfonate, was employed to enable the photo reaction by irradiation with long-wave UV light. Although photo chemical crosslinking reactions have been utilized several times to prepare various types of swollen hydrogels<sup>(29,30)</sup>.

Photo chemical [2 + 2]-cycloaddition reactions can principally start from both the excited singlet (S1) and the triplet (T1) states of one of the two molecules eventually forming the dimer. In the first case, the reaction occurs in a concerted action, originating from a syn exciplex that is stabilized by secondary orbital interactions and yields cyclodimers in the stereospecific cis form. The reaction from the T1 state, on the other hand, proceeds in a stepwise manner. Starting from a triplet-exciplex having a long lifetime, the addition occurs via an intermediate 1,4-diradical with wide geometry that finally relaxes to the ground state (S0), where the second bond is formed. Dimeric products thus obtained are a mixture of cis and (favored) trans isomers.

a-



b-



**Figure2:** Mechanism of sensitized [2 + 2]-cycloaddition according to (a) Hammond *et al.*<sup>(31)</sup> and (b) Schenck *et al.*<sup>(32)</sup>.

G. Kaur *et al.*<sup>(33)</sup> have reported bio-inspired core-bound polymeric micelles, based on hydrogen bonding and photo-crosslinking, of thymine have been prepared from poly(vinylbenzylthymine)-b-poly(vinylbenzyltriethylammonium chloride).

L. Zhang *et al.*<sup>(34)</sup> have studied the photografting of acrylic acid (AA) onto poly(ethylene) (PE) films floating on the top surface of a solution and the swelling and pH response properties of the grafted layers. Grafted poly (acrylic acid) (PAAc) layers with ultra-high swelling ratios and pH response rates have been obtained.

### **1.2.2. Crosslinking by hydrogen bond.**

Poly(acrylic acid) and poly(methacrylic acid) form complexes with poly(ethylene glycol). These complexes are held together by hydrogen bonds between the oxygen of the poly(ethylene glycol) and the carboxylic group of poly((meth)acrylic acid), where as for poly((meth)acrylic acid) hydrophobic interactions also play a role <sup>(35)</sup>. Hydrogen bonding does not only occur between poly((meth)acrylic acid) and poly(ethylene glycol), but has also been observed in poly(methacrylic acid-g-ethylene glycol) <sup>(36,37)</sup>.

The hydrogen bonds are only formed when the carboxylic acid groups are protonated. This implies that the swelling of these gels is strongly dependent on the pH. Moreover, the complex of poly(methacrylic acid) and poly(ethylene glycol) prepared at low pH can be dissolved in ethanol. Upon injection, the diffusion of ethanol from the liquid transforms the system into a gel. The gel gradually dissolves in time due to dissociation of the complex <sup>(38)</sup>.

## **1.3. Hydrogel behavior**

### **1.3.1. Thermodynamics.**

Stimuli-responsive polymers are plastic materials with molecule chains cross-linked to a three dimensional network. They are synthesized by a cross-linking reaction between polymer molecules <sup>(39)</sup> or by a cross-linking polymerization, which is simultaneously synthesizing polymer chains and linking them concomitantly <sup>(40)</sup>. Polymer molecules consist of small molecular units, the so-called monomers, which can be arranged in a sequence to form a long polymer chain or to form branched polymer molecules with side chains. Generally, all polymers are solvophilic to certain solvents. Not cross-linked polymers are soluble in presence of these solvents. Due to the interconnections between the polymer chains cross-linked polymers are insoluble but swell by solvent absorption. If they can swell in water they are called hydrogels.

### **1.3.2. Theory of swelling of hydrogel and its behavior in solvents.**

Unlike, normal solvophilic polymers stimuli-responsive hydrogels exhibit a first-order- or a continuous (also called second-order) phase transition behavior. As illustrated in **Figure 3** they exhibit two phases. A separated phase of the gel is dominated by polymer-polymer interactions. In this case the gel reaches its maximal value of hydrophobicity and shrinks. The second phase, a mixed phase, is characterized by solvent-polymer-interactions, which aspire the best mixing of polymer and aqueous solution. Therefore, within the mixed phase the hydrogel gains its maximum of hydrophilicity and swells. Close by the phase interface a small alteration of a thermodynamic variable, namely a solvent concentration, results in a change of

the phase characterised by an abrupt change in physical properties of hydrogel, especially in volume, mass, stiffness and more<sup>(41)</sup>.

The polymer-solvent-interactions of the mixing phase generate osmotic pressures  $\Delta\pi_{mix}$  acting expansively. Due to the polymer-polymer-interactions the polymer network counteracts this expansion by an elastic force respected by  $\Delta\pi_{elast}$ . The hydrogel obtains its swelling equilibrium at the balance of the pressures, which can be described by

$$\Delta\pi = \Delta\pi_{elast} + \Delta\pi_{mix} = 0 \dots\dots\dots(1)$$

The FLORY-REHNER theory<sup>(42, 43)</sup> and the FLORY-HUGGINS theory<sup>(44)</sup> describe these processes in detail.

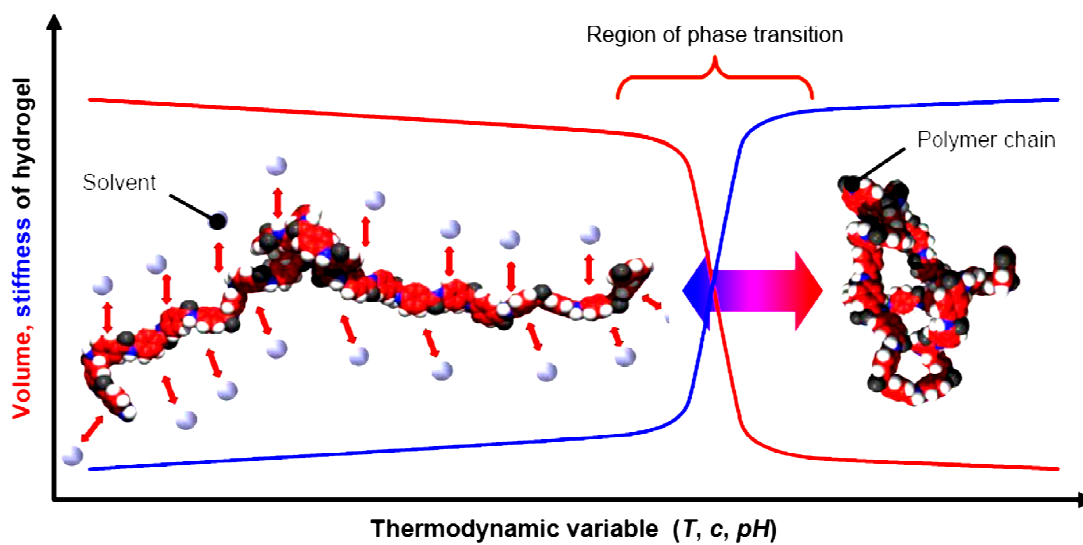


**Figure 3:** Phase transition behaviour of stimuli-responsive hydrogels<sup>(41)</sup>.

The swollen phase of the gel (**left**) is dominated by polymer-solvent interactions obtaining the best mixing of the polymer chains and the aqueous solution. The shrunken phase of the hydrogel (**right**) is determined by polymer-polymer-interactions, which remove solution out of the gel. Near the phase interface, within the range of phase transition, small alterations of a thermodynamic value result in a change of the phase of the hydrogel.

Special solvent-responsive hydrogels can be additionally temperature-sensitive. Such gels have a slightly hydrophobic nature and contain groups, which preferably interact with water molecules by hydrogen bonds which cause the hydrogel swelling. These hydrogen bonds depend on the temperature. Exceeding a critical temperature, called lower critical solution temperature behavior, the hydrogen bonds between polymer and water break apart. Now, the hydrophobic nature of the gel can dominate resulting in a shrinking of the gel<sup>(41)</sup>. The characteristic time of swelling is inversely proportional to the square of the dimensions of the gel and is also proportional to the diffusion coefficient of the gel network.

Swelling can be expressed in weight, volume and length units; data should be given at equilibrium. The weight fraction of the water  $W_f$  in a hydrogel is defined as;

$$W_f = \frac{\text{(Wet weight - Dry weight)}}{\text{(Wet weight)}} \dots\dots\dots(2)$$

The weight % of water is,

$$W_p = W_f \times 100 \dots\dots\dots(3)$$

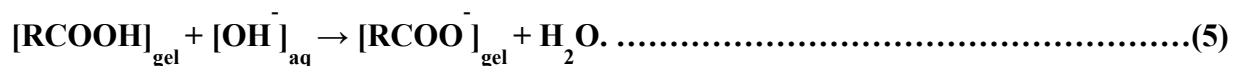
Degree of swelling is expressed as;

$$D_{sw} = \frac{\text{(Wet weight)}}{\text{(Dry weight)}} \quad D_{sw} > 1 \dots\dots\dots(4)$$

In the present study volume degree of swelling for thin hydrogel layers has been calculated from the polymer fraction in the hydrogels <sup>(45)</sup>. The polymer fraction can be obtained from the SPR Fresnel calculations. Degree of swelling in gels depends on synthesis variables, particularly chemical composition and crosslink density <sup>(46, 47)</sup>. Chemical composition can be controlled by taking suitable monomers; however, it is difficult to pin down the crosslinking density. Crosslinking is a random process, and many crosslinks do not function as elastically effective junctions, instead, they are incorporated into loops, dangling ends and densely crosslinked clusters <sup>(48)</sup>.

**1.3.3. Behaviour of polyelectrolyte hydrogels.**

Polyelectrolyte hydrogels comprise weak acidic and weak basic groups, respectively, which can be ionized. For example, gels containing acidic groups are deprotonated in basic surrounding conditions as following:



Therefore, the density of likewise charged groups within the network strongly increases accompanied by an adequate generation of mobile counterions inside the gel, which induces the phase transition due to electrostatic repulsion. In an acidic ambient the acidic gel protonates



resulting in a decrease of both the charge density and the content of mobile counterions within

the hydrogel leading to gel shrinking<sup>(49)</sup>. The phase transition of the gels occurs in a small range close by the apparent acid dissociation constant  $pK_a$  of the hydrogel which is mostly identical with the  $pK_a$  of the ionisable group. Approximately at the apparent  $pK_a$  of the gel the ionisation begins accompanied by a drastic swelling of the hydrogel. If the ionisation of the ionisable component is completed the swelling process stops. Further pH increase only increases the ionic strength. This decreases the osmotic pressure and leads to shrinking of the gel (see **Figure 4**, acidic hydrogel). That figure shows the general behaviors of the three types of polyelectrolyte gels<sup>(41)</sup>.

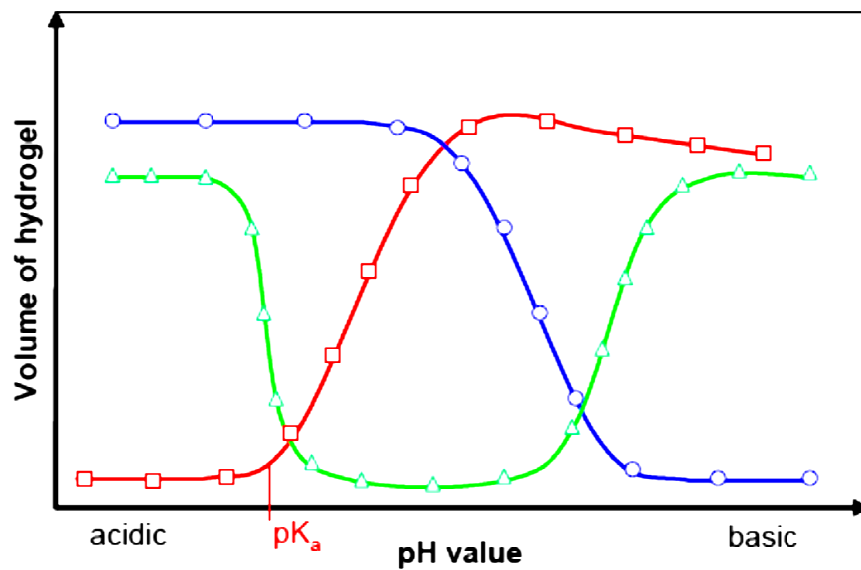


**Figure4:** Relation between pH value and volume of hydrogel, showing the volume degree of swelling of acid and base hydrogel in different pH, demonstrated highly degree in acid media for basic hydrogel as clear for the blue line, and vice versa for acidic hydrogel as clear in the red line. However, the acid-base (ampholytic) polymers show both effects for acid and base as green line<sup>(41)</sup>.

## **1.4. Stimuli-responsive polymers and hydrogels**

### **1.4.1. Introduction**

Stimuli-responsive or “*smart*” polymer or hydrogel systems are polymers or hydrogel that may overcome dramatic property changes responding to small changes in the environment. The most important systems are those sensitive to pH or temperature (T). Human body presents variations on pH along the gastrointestinal tract, and also in some specific areas like certain tissues (and tumoral areas) or sub-cellular compartments. Thermosensitive polymers or hydrogels with critical T close to the physiological value, i.e. poly (*N*-isopropyl acrylamide) (PNIPAAm), offer many possibilities in the biomedical field.

Hoffman *et al.* <sup>(50)</sup> demonstrated, in a very elegant design, that the action of an enzymatic receptor can be modulated when this kind of polymer is conjugated close to its active place. They were able to switch on-off the receptor using the transition between extended and coiled form of the molecule <sup>(51)</sup>. Soluble pH and T-responsive polymers that overcome transition at physiological conditions (37°C and/or physiological pH) have been proposed as minimally invasive injectable systems. The soluble systems may be easily injected, however they precipitate or gel *in situ* forming an implant or scaffold useful for drug delivery systems (DDS) or tissue engineering applications <sup>(52,53)</sup>.

### **1.4.2. Temperature responsive polymers and hydrogel**

#### **1.4.2.1. Introduction**

Polymers sensitive to temperature changes are the most studied class of environmentally sensitive polymers as they have potential applications in the biomedical field <sup>(54)</sup>. This type of systems exhibit a critical solution temperature (typically in water) at which the phase of polymer and solution is changed in accordance with their composition. Those systems exhibiting one phase above certain temperature and phase separation below it, possess an upper critical solution temperature (UCST). On the other hand, polymer solutions that appear as monophasic below a specific temperature and biphasic above it, generally exhibit the so-called lower critical solution temperature (LCST). These represent the type of polymers with most number of applications <sup>(55)</sup>. The typical example is poly (*N*-isopropylacrylamide) (PNIPAAm) that presents a LCST at 32°C in water solution <sup>(56)</sup>. Below that temperature the polymer is soluble as the hydrophilic interactions, due to hydrogen bonding, are predominant, whereas a phase separation occurs above the LCST (cloud point) due to predomination of hydrophobic interactions. Other type of temperature sensitivity is based on the intermolecular association as in the case of Pluronics or Poloxamers (PEO-PPO-PEO) <sup>(57)</sup> where hydrophobic

associations of PPO blocks lead to the formation of micelle structures above critical micelle temperature (CMT).

#### 1.4.2.2. Solubility phase transitions and liquid-liquid coexistence curves.

Different types of “temperature–composition” phase diagrams are schematically presented in **Figure 5**. Typical coexistence curves (CC) with the upper critical solution temperature (UCST, **Figure 5a**) and the lower critical solution temperature (LCST, **Figure 5b**) can be interpreted as parts of the closed-loop CC with two critical temperatures **Figure 5c** when the second critical point lies either beneath the melting point **Figure 5a** or above the boiling point **Figure 5b** of the solution, respectively. It is obvious that **Figure 5d** also shows the closed-loop CC without critical points because the two-phase region expands beyond the liquid phase<sup>(58)</sup>. Interestingly, the two-phase region substantially contracts with an increase in the molecular mass of polyethylene glycol in water<sup>(59)</sup>. Another type of CC with two critical points separated by the total solubility region also exists in **Figure 5e**. In this case, the difference between UCST and LCST is governed by properties of the mixture components. For example, an increase in molecular mass of polystyrene in *tert*-butyl acetate narrows the region of total miscibility,<sup>(60)</sup> so that one can imagine the extreme situation when both two-phase regions coincide to form the CC shown in **Figure 5f**, where the phase separation occurs at any experimentally accessible temperature<sup>(61)</sup>.

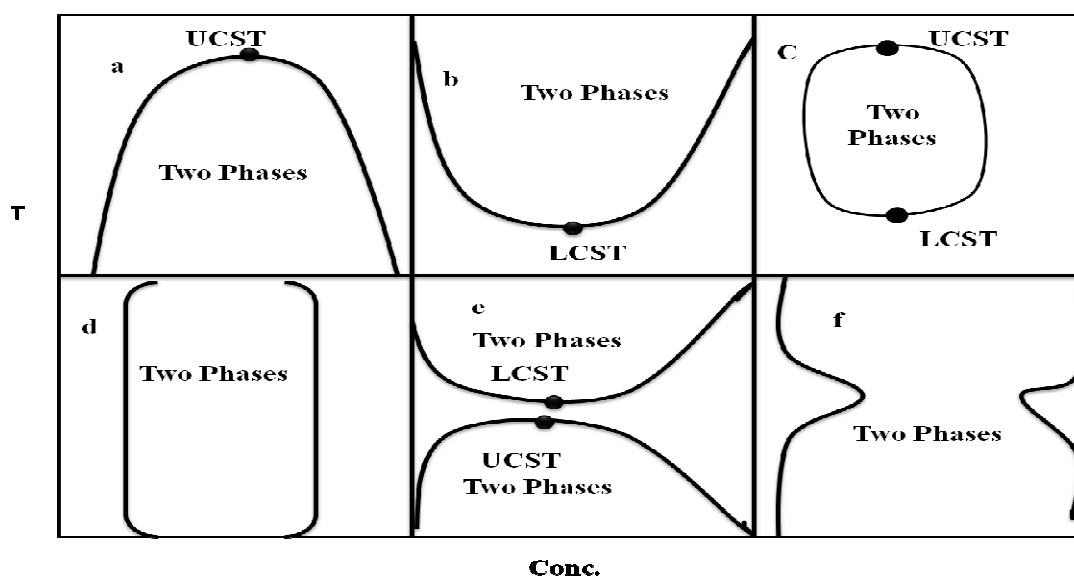


**Figure 5:** Schematic representation of liquid–liquid phase diagrams for mixtures with (a) one UCST; b) one LCST; (c) a closed-loop coexistence curve, UCST > LCST; (d) a closed-loop coexistence curve, where both critical points are beyond the range of measurement; (e) two critical points, UCST < LCST; and (f) two overlapping immiscibility gaps. The frame for

each phase diagram is considered as a window of the experimentally accessible temperatures and concentrations <sup>(61)</sup>.

The occurrence of liquid–liquid phase diagrams with three critical solution points, shown in **Figure 6a**, is striking. However, they are just the broader view of the phase diagrams shown in **Figure 5**, but through a wider window of the experimentally accessible temperatures and concentrations. The closed-loop CCs above an ordinary two-phase region with UCST **Figure 6a**. Interestingly, both two-phase regions tend to expand with a decrease in concentration of 3-butanol, so that LCST and UCST merge, and finally the immiscibility gap with only one UCST, shown in **Figure 5a**, emerges. A liquid–liquid phase equilibrium in a binary 2-butanol/water mixture has been experimentally <sup>(61)</sup> and theoretically <sup>(62)</sup> studied at different pressures. It was found that the effect of pressure was the same as the addition of the third component (2-butanol); the coexistence curve with one UCST **Figure 6b** gradually evolved to the combination of the closed-loop and open two-phase regions with a total of three critical points **Figure 6a**.

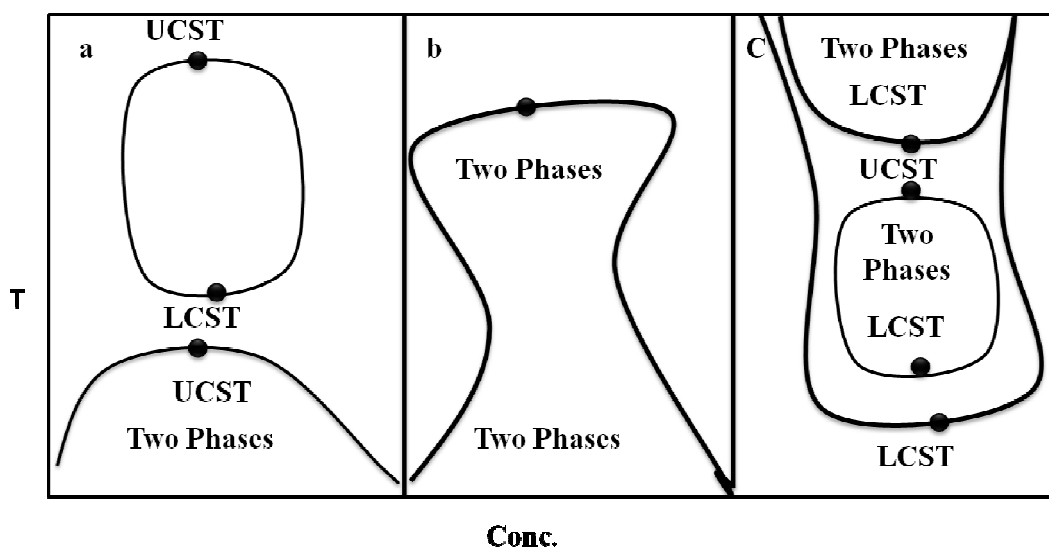


**Figure 6:** Schematic representation of liquid–liquid phase diagrams for mixtures with three critical points: (a) closed-loop immiscibility gap lies above CC with one UCST, (b) overlapping immiscibility gaps, (c) hypothetical CCs with three critical points when closed-loop CC lies beneath CC with one LCST. The frame for each phase diagram is considered as a window of the experimentally accessible temperatures and concentrations <sup>(61)</sup>.

We can conclude phase diagram using some definitions;

**A.** The critical temperature: defined as the temperature at critical condition.

**B.** Lower critical solution temperature (LCST): defined as the lowest point in the coexistence curve, usually water soluble polymers have LCST due to hydrogen bonding, because the hydrogen bonding disrupts at higher temperature <sup>(61)</sup>.

C. Upper critical solution temperature (UCST): defined as the highest point in the coexistence curve. At higher temperatures, the solution is uniform and therefore transparent. At  $T > T_c$  the system has miscibility gap. When cooled to temperature below the coexistence curve, the solution separate into two phases. Each of the two phases is uniform, but they have different composition<sup>(61)</sup>.

### 1.4.3. Transition-point determination (Cloud point).

Several methods have been used for determination of transition temperature, e.g light scattering, turbid-metric analysis by UV-vis. Spectroscopy, differential scanning calorimetry (DSC) and surface Plasmon resonance spectroscopy (SPR). Here we will focus on discussion of three kinds of analysis.

#### 1.4.3.1. UV-vis. Spectrophotometer.

This method have also called turbidity method and used for T-responsive polymers. A specific concentration of polymer (from 0.2 to 3 Wt.%) was dissolved in water, then temperature dependent transmittance were carried out by UV.vis Spectrometer<sup>(63-68)</sup>. **Figure 7** and **Figure 8** show the relation between transmittance as a temperature change the first change at the intersect refers to  $T_c$  which is LCST or UCST, which is the beginning of turbidity or formation of two phases, after that, sharp change has been occurred and the solution is milky, this is a completely phase separation and the cloud point has been formed.

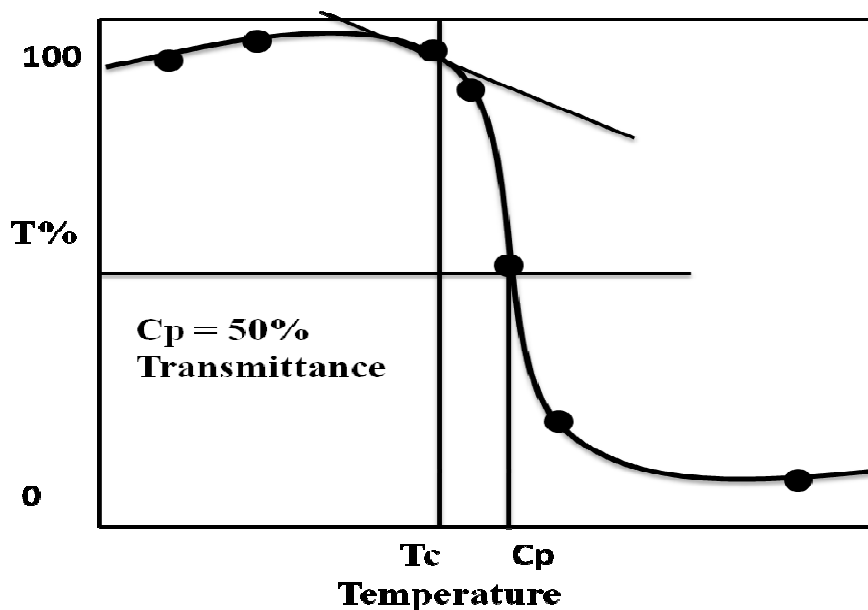


**Figure7:** Schematic diagram of temperature dependent transmittance for determination of transition temperature and cloud point.

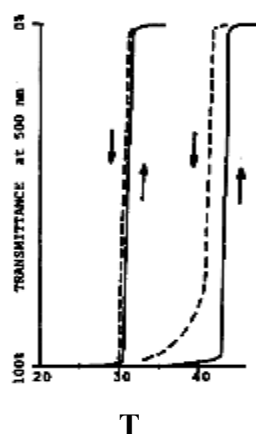


**Figure 8:** Phase diagram of 1 wt % aqueous solution of poly (N-isopropylacrylamide) <sup>(64)</sup>.

### **1.4.3.2. Differential scanning calorimetry.**

DSC is a vital tool to measure the LCST of a polymer system. Depending on the type of reaction, a peak is obtained in the DSC thermogram, which gives information about transition temperature and heat of transition. An endothermic peak is observed at the LCST upon heating aqueous solution of PNIPAAm <sup>(69-72)</sup>. The measured transition heats varies with concentration, this is attributed to the energy required to break hydrogen bonds between polymer and water molecules. Large differences have been found to exist in the shape and height of the endotherms between polymers of different molecular weight distribution, although all the endotherms have a similar enthalpy which is typical for hydrogen bond interactions. The characteristics (height, width, peak position) of the endotherm are independent of concentration for at least the range 0.4-4.0 mg/ml. In this study DSC has been used for LCST determination of thermosensitive linear polymer and results are compared with other techniques like SPR.

### **1.4.3.3. Surface Plasmon Resonance spectroscopy (SPR).**

SPR-OW will discuss in detail in **chapter 3**, but, here we will discuss an application of SPR is the determination of LCST of hydrogel. The swelling of hydrogel film has been used to study the change in thickness with temperature also; refractive indexes with temperature were used in the determination of LCST <sup>(45, 73-76)</sup>.

### **1.4.4. Polymers with LCST.**

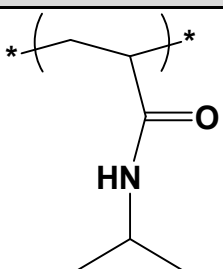
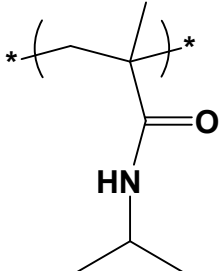
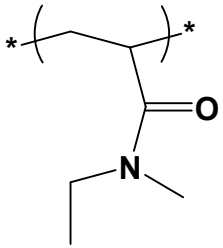
The LCST can be defined as the critical temperature at which polymer solution undergo phase separation from one phase (isotropic state) to two phases (anisotropic state) rich and poor in polymer <sup>(54)</sup>. Below the LCST the enthalpy term, related to the hydrogen bonding between the polymer and the water molecules, is responsible for the polymer dissolution. When raising the

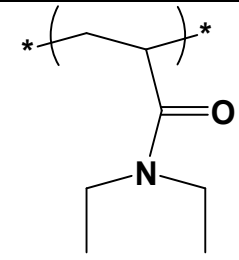
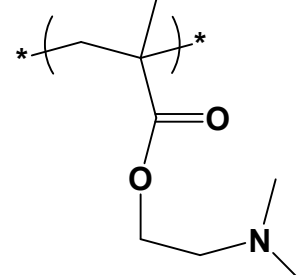
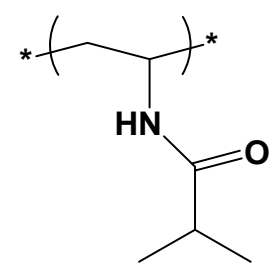
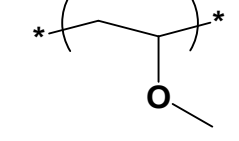
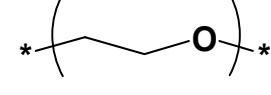
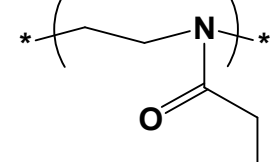
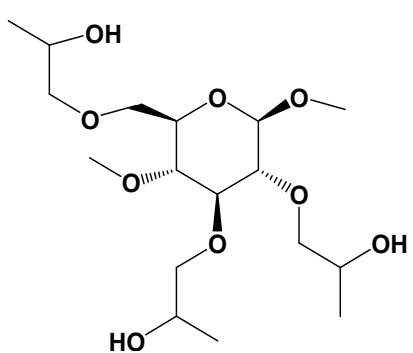
temperature above the LCST, the entropy term (hydrophobic interactions) dominates leading to polymer precipitation. The LCST of polymers in water solutions can be modulated by incorporating hydrophilic or hydrophobic moieties. For example, when NIPAAm is copolymerized with hydrophilic monomers such as AAm, the LCST increases up to about 45°C when 18% of AAm is incorporated to the polymer, whereas LCST decreases to about 10°C when 40% of hydrophobic *N*-tert-butylacrylamide (N-tBAAm) is added to the polymer (77).

When hydrogels are prepared by crosslinking T-responsive polymers the temperature sensitivity in water results in changes in the polymer hydration degree. Below the transition temperature the polymer swells up to equilibrium hydration degree being in an expanded state. By increasing the temperature above the transition hydrogel deswells to a collapsed state. This process is generally reversible and can be applied in a pulsatile manner making the polymer to behave as an on-off system when the stimulus is applied or removed.

The most representative group of polymers showing LCST is the poly(*N*-substituted acrylamide) family. A selection of frequently studied polymers with a LCST in water is listed in **Table (1)**.

**Table 1:** List of polymers with LCST in water.

Polymer name	Polymer structure	LCST	Ref.
Poly( <i>N</i> -isopropylacrylamide)		33°C	(78)
Poly( <i>N</i> -isopropylmethacrylamide)		40°C	(79)
Poly( <i>N</i> -ethyl- <i>N</i> -methylacrylamide)		56°C	(80)

<p><b>Poly(<i>N,N</i>-diethylacrylamide)</b></p>		<p>32°C (81)</p>
<p><b>Poly(<i>N,N</i>-dimethylaminoethylmethacrylate)</b></p>		<p>50°C (82)</p>
<p><b>Poly(vinylisobutyroamide)</b></p>		<p>35°C (83)</p>
<p><b>Poly(methylvinylether)</b></p>		<p>36°C (84)</p>
<p><b>Poly(ethylene glycol)</b></p>		<p>96°C (85)</p>
<p><b>Poly(2-ethylloxazoline)</b></p>		<p>65°C (86)</p>
<p><b>Hydroxypropylcellulose</b></p>		<p>44°C (87)</p>

### 1.4.5. Applications of LCST polymers and hydrogels.

#### 1.4.5.1. Clinical applications.

T-responsive hydrogel based NIPAAm have limitations since they are not biodegradable but have been evaluated as drug release carriers consisting in semi-IPN of PNIPAAm and poly(tetramethylene glycol) crosslinked with MBAAm, analysing the release of indomethacin as a model drug, showing also an on-off pulsatile release behaviour <sup>(88)</sup>. Other combinations with biodegradable systems have been prepared by dispersing PNIPAAm hydrogel microparticles into a crosslinked gelatine matrix <sup>(89)</sup> or by encapsulating the drug core with ethylcellulose containing nano-sized PNIPAAm hydrogel particles <sup>(90)</sup>. Novel hydrogels showing both T-sensitivity and biodegradability have been prepared using PNIPAAm crosslinked with degradable poly (amino acid) <sup>(91)</sup>. Kumashiro *et al.* <sup>(92)</sup> have designed a new semi-interpenetrating network (SIPN) based on dextran grafted with T-sensitive polymer chains, that is degraded by specific enzymes at a definite temperature range.

#### 1.4.5.2. Tissue engineering.

Many approaches have been achieved in field of tissue engineering, as temperature sensitive scaffolds or surface modifications for the manipulation of cell sheets. Poly (NIPAAm-co-acrylic acid) (poly (NIPAAm-co-AA)) gels have been applied as extracellular matrix for pancreatic islets in biohybrid pancreas <sup>(93)</sup>. Composite membranes have also been prepared maintaining and exploiting the LCST. For example, NIPAAm has been crosslinked on the surface of glass disks forming hydrogels inside the glass pores. For making stable thermally controlled on-off devices.

PNIPAAm hydrogel had been grafted onto the entire surface of a rigid porous polymer membrane <sup>(94)</sup>. Disks were placed between donor and receptor cells by a permeation chamber and the transport of salicylic acid and bovine serum albumin were tested as a function of temperature. The delivery rate of both drugs across the composite membrane was found to be temperature dependent as the rate was increased when the temperature raised from 20 to 40 °C, going from an expanded state to a collapsed state where pores are opened <sup>(95)</sup>.

#### 1.4.5.3. Surface modifications.

The surface can be modified by T-responsive polymer to exploit the fact that most proteins show significantly greater adsorption on hydrophobic surfaces than in hydrophilic ones. Above the LCST the T-sensitive polymer will adsorb peptides and proteins from a solution and these biomolecules can be desorbed by decreasing the temperature as has been done in chromatographic supports incorporating PNIPAAm and using water as eluent <sup>(96)</sup>. Another

approach has shown that the surface of tissue culture polystyrene grafted with PNIPAAm allows cells to adhere and proliferate above the LCST of the polymer whereas a cell detachment was detected at temperatures below LCST<sup>(96)</sup>. Moreover, this type of application has been tested on biodegradable polymers such as poly (L-lactic acid)<sup>(97)</sup>.

This type of grafting has also been performed on reversible 3D-matrix for the culture of articular chondrocytes, cells that proliferate adequately on the matrix that are then removed by temperature lowering<sup>(98)</sup>.

### **1.4.6. pH-responsive polymers and hydrogel.**

pH-responsive polymers are polyelectrolytes that bear in their structure weak acidic or basic groups that either accept or release protons in response to changes in environmental pH. The pendant acidic or basic groups on polyelectrolytes undergo ionization just like acidic or basic groups of monoacids or monobases<sup>(99)</sup>. However, complete ionization on polyelectrolytes is more difficult due to electrostatic effects exerted by other adjacent ionized groups. This makes the apparent dissociation constant ( $K_a$ ) different from that of the corresponding monoacid or monobase<sup>(99)</sup>.

By generating the charge along the polymer backbone, the electrostatic repulsion results in an increase in the hydrodynamic volume of the polymer<sup>(100)</sup>. This transition between tightly coiled and swollen state is influenced by any condition that modify electrostatic repulsion, such as pH, ionic strength, and type of counterions. The transition from collapsed state to expanded state has been explained by changes in the osmotic pressure exerted by mobile counterions neutralizing the network charges<sup>(54)</sup>.

The pH range that a reversible phase transition occurs can be generally modulated by two strategies:

1. Selecting the ionizable moiety with a  $pK_a$  matching the desired pH range. Therefore, the proper selection between polyacid or polybase should be considered for the desired application<sup>(99)</sup>.
2. Incorporating hydrophobic moieties into the polymer backbone and controlling their nature, amount and distribution. When ionizable groups become neutral non-ionized- and electrostatic repulsion forces disappear within the polymer network, hydrophobic interactions dominate. The introduction of a more hydrophobic moiety can offer a more compact conformation in the uncharged state and a more accused phase transition. The hydrophobicity of these polymers can be controlled by the copolymerization of hydrophilic ionisable monomers with more hydrophobic monomers with or without pH-sensitive moieties, such as 2-hydroxyethyl methacrylate, methyl methacrylate and maleic anhydride<sup>(99)</sup>. Polyacidic

polymers will be unswollen at low pH, since the acidic groups will be protonated and unionized. When increasing the pH, a negatively charged polymer will swell. The opposite behaviour is found in polybasic polymers, since the ionization of the basic groups will increase when decreasing the pH. Typical examples of pH-responsive polymers with anionic groups are poly (carboxylic acids) as poly (acrylic acid) (PAA) or poly(methacrylic acid) **Figure 9**. Another kind of polyacidic polymer is the polysulfonamides (derivatives of *p*-aminobenzenesulfonamide). These weak polyacids present a pKa that narrowly varies from 3 to 11, depending on the electrowithdrawing nature of the substituent on the nitrogen <sup>(101)</sup>. A few examples of pH-responsive polyacids and, polybases;

**Polyacids**

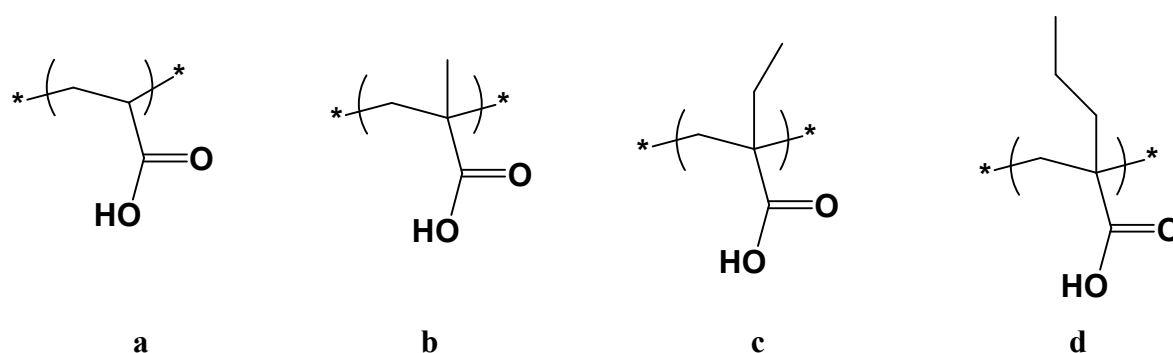


**Figure 9:** Chemical structure of pH-sensitive polyacids (a) poly(acrylic acid); (b) poly(methacrylic acid); (c) poly(2-ethylacrylic acid); (d) poly(2-propylacrylic acid) <sup>(99)</sup>.

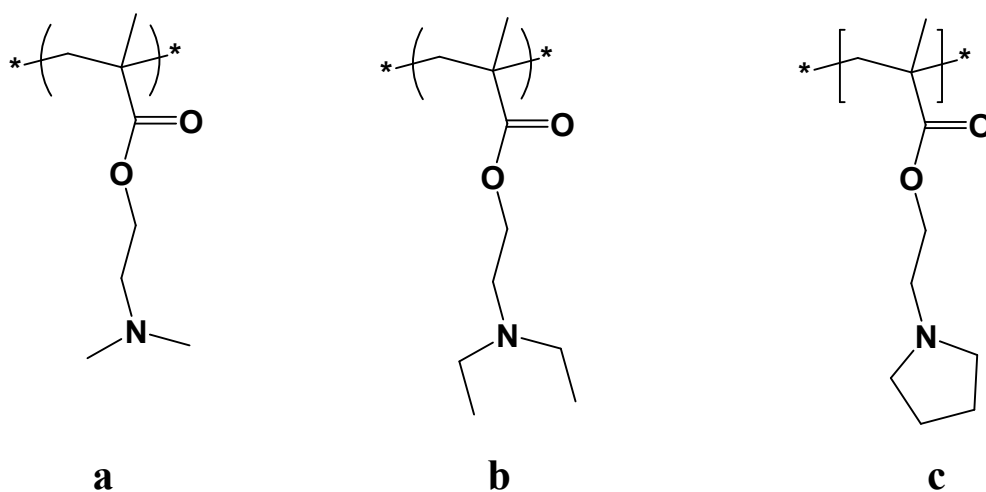


**Figure 10:** Chemical structure of pH-sensitive polybases. (a) PDMAEMA; (b) PDEAEMA; (c) PEPyM<sup>(99)</sup>.

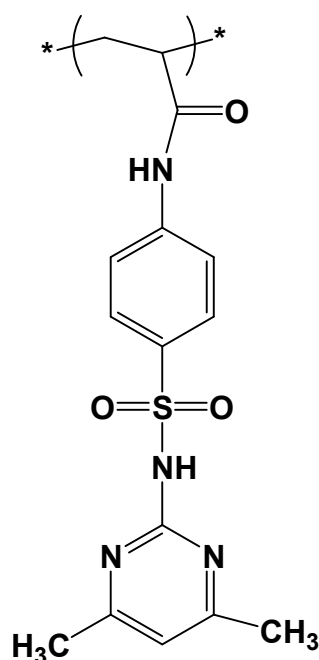


**Figure11.** Chemical structure of 4-amino-*N*-[4,6-dimethyl-2-pyrimidinyl]-benzenesulfonamide (sulfomethazine) containing polymer<sup>(102,103)</sup>.

Researchers have designed more sophisticated pH-responsive polymers in order to take advantage of the pH changes that occur in nature. These materials are inspired by living organisms trying to mimic their response mechanisms. Sauer *et al.*<sup>(104)</sup> have reported the synthesis of pH-responsive hollow nanocontainers inspired in virion particles. The poly (acrylic acid) vehicles were synthesized by vesicular polymerization and emulsion polymerization (using core-shell latex particles). These nanocapsules combined the protective ability of the nanocontainers in combination with controlled permeability and therefore can be used to trigger the release of encapsulated materials from the inner core.

When pH-sensitive polymeric chains are crosslinked forming hydrogels, their behaviour is not only influenced by the nature of the ionizable groups, the polymer composition, and the hydrophobicity of the polymer backbone, but also by the crosslinking density. This affects the solute permeability in terms of bioactive compounds release in several applications; the higher the crosslinking density, the lower the permeability, especially significant in the case of high molecular weight solutes.

Most of the materials described in the literature that respond to external stimuli are acrylic hydrogels. In a swollen state, each polymer chain is isolated by solvent molecules and is therefore, exposed as a single molecular unit to tension and shear forces produced during a gel deformation process. Most polyelectrolyte gels exhibit a decrease in modulus with increasing swelling degree. However, poly(silamine), **Figure12** hardened on swelling by formation of the rigid molecular locks through ionic interactions<sup>(104)</sup>. The system described by Lou *et al.*

consists on a silicon-based polymer, comprising alternating units of *N,N*-diethylethylenediamine and 3,3-dimethyl-3-silapentamethylene. They developed hydrogel microspheres based on this chemistry which formed a very stable skin layer when swollen in acidic media <sup>(105)</sup>. The externally stable skin layer was explained in terms of the high activation energy for the rod/globule transition along with a lowered mass transport through the skin layer.

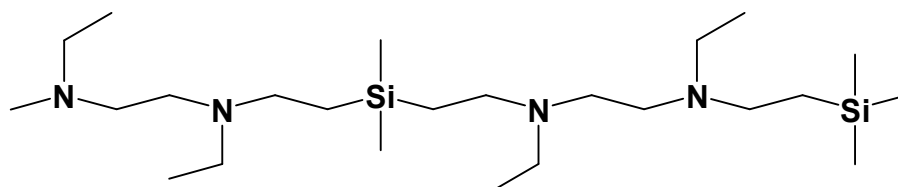


**Figure 12.** Non-protonated polysilamine <sup>(105)</sup>.

### 1.4.7. Applications.

Several applications for pH-responsive polymers and hydrogel especially in the field of biomedicine, here we report the most attractive examples have been reported in the last years.

#### 1.4.7.1. Drug delivery systems.

It is important to know that pH changes along the gastrointestinal tract (GIT) between 2 (stomach) and 10 (colon), for this condition pH-responsive polymers are ideal for colon specific drug delivery.

The most common approach utilizes enteric polymers that resist degradation in acidic environment and release drug in alkaline media due to the formation of salt.

Several groups have developed polymeric prodrugs (polymers in which the drug is covalently attached to the macromolecular chain) susceptible to hydrolytic cleavage dependent upon the pH and hence suitable for colon drug delivery. This is the case of poly(*N*-methacryloylaminoethyl 5-aminosalicylamide) or poly(methacryloylethoxyethyl-5-aminosalicylic acid) <sup>(106)</sup> or the copolymeric system was developed based on 2-acrylamido-2-methylpropane sulfonic acid (AMPS) and a methacrylic derivative of an antiaggregant drug called Triflusal <sup>(107)</sup> **Figure 13.**

Some scientists tried to design some natural pH-responsive polymer these materials are inspired by living organisms trying to mimic their response mechanisms.

Sauer *et al.* <sup>(108)</sup> have reported the synthesis of pH-sensitive hollow nanocontainers inspired in virion particles. The poly (acrylic acid) vehicles were synthesized by vesicular polymerization and emulsion polymerization (using core-shell latex particles). These nanocapsules combined

the protective ability of the nanocontainers in combination with controlled permeability and therefore can be used to trigger the release of encapsulated materials from the inner core.

A new kind of synthetic vesicles with a high degree of architectural control made of amphiphilic block copolypeptides has been prepared by Bellomo and co-workers<sup>(109)</sup>.

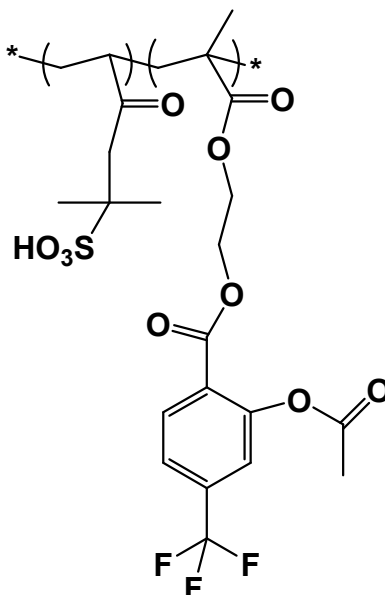


**Figure 13:** Schematic structure of the copolymeric system based on AMPS and the methacrylic derivative of Triflusal<sup>(107)</sup>.

The hydrophilic block was made of lysine, decorated with a few water soluble ethylene glycol units and the hydrophobic block was constituted by leucine peptide. The synthetic polymer forms a supramolecular structure highly sensitive to environmental signals and able to respond precisely to pH changes and actuate as drug delivery carriers.

Most of smart drug release systems are driven by the phase-volume transition. However, Liu and co-workers<sup>(110)</sup> reported the preparation of novel  $\beta$ - cyclodextrin microgels for drug delivery applications driven by inclusion effects.

### 1.4.7.2. Gene carriers.

One of the most promising applications of pH-sensitive polymers is as non-viral gene carriers. Naked DNA is very difficult to incorporate into the cells because it is negatively charged and it has a very large size at physiological conditions. Liposomes and polycations are the two major classes of chemical (non-viral) gene delivery methods to condense DNA in charge balanced nanoparticles that can be carried into cell compartments.

Godbey and Mikos reviewed some of the advances in non-viral gene delivery research<sup>(111)</sup> describing the use of poly (ethylenimine) (PEI) and poly (L-lysine) (PLL) as two of the most successful candidates for this application. PEI is a highly polycationic synthetic polymer that condense DNA in solution, forming complexes that are readily endocytosed by many cell

types. Chitosan, a biocompatible and resorbable cationic aminopolysaccharide, has also extensively been used as DNA carrier <sup>(112-116)</sup>.

Lim *et al.* [38] prepared a self-destroying, biodegradable, polycationic polyester, poly (*trans*-4-hydroxy-L-proline ester) (PHP ester), with hydroxyproline, a major constituent of collagen, gelatine, and other proteins, as a repeating unit. PHP ester formed soluble polymer/DNA complexes with average diameters of less than 200 nm. These complexes could transfect the mammalian cells, being comparable to the transfection obtained with PLL, the most common polymer for gene delivery.

Lim *et al.* also presented <sup>(117)</sup> a degradable non-toxic PLL analogue employing poly[ $\alpha$ -(4-aminobutyl)-L-glycolic acid] (PAGA) for its application as gene carrier. This polymer condensed DNA into a spherical shaped polymer and showed accelerated degradation when free, and decreased degradation during the formation of complexes with DNA. The transfection efficiency of PAGA/DNA complexes was about twice that of PLL/DNA complexes. The most important characteristics of this polymer against cationic liposomes and polyamidoamine (PANAM) dendrimers are its high solubility, non-toxicity and degradability when used as systemic gene carrier.

Kataoka <sup>(118)</sup> recently communicated the development of polymeric micelles as nanocarriers for gene and drug delivery based on doxorubicin-conjugated block copolymer poly(ethylene glycol)-poly(aspartame hydrazinedoxorubicin) [(PEG-p(Asp-Hid-dox))]. The polymer retained drugs and genes at physiological pH and released the drugs as pH decrease below 6.0.

Hoffman's group has dedicated great efforts to obtain new delivery systems to introduce efficiently biomolecules to intracellular targets <sup>(119-121)</sup>. They mimicked the molecular machinery of some viruses and pathogens that are able to sense the lowered pH gradient of the endosomal compartment and become activated to destabilize the endosomal membrane. This mechanism enhances protein or DNA transport to the cytoplasm from intracellular compartments such as endosome. They demonstrated the utility of poly (2-propylacrylic acid) (PPAA) to enhance protein and DNA intracellular delivery. They also constructed more versatile carrier systems, designing a new functionalized monomer (pyridyl disulfide acrylate, PDSA), that allows efficient conjugation through disulfide linkages that can be reduced in the cytoplasm after endosomal translocation of the therapeutics. PDSA was copolymerized with alkylacrylic acid monomers and alkylacrylate monomers. The membrane destabilizing activity of the polymers depended on the lengths of the alkyl segment and their ratio in the final polymer chains <sup>(122)</sup>.

### 1.4.7.3. Glucose sensors.

pH-sensitive polymers is the fabrication of insulin delivery systems for the treatment of diabetic patients. Delivering insulin is different from delivering other drugs, since insulin has to be delivered in an exact amount at the exact time of need. Many devices have been developed for this purpose and all of them have a glucose sensor built into the system. In a glucose-rich environment, such as the bloodstream after a meal, the oxidation of glucose to gluconic acid catalysed by glucose oxidase (GluOx) can lower the pH to approximately 5.8. This enzyme is probably the most widely used in glucose sensing, and makes possible to apply different types of pH-sensitive hydrogels for modulated insulin delivery<sup>(123)</sup>.

### 1.4.8. Polymers and hydrogels with dual stimuli-responsiveness.

These polymers and hydrogels are multiresponsive, but, the majority of studies have focused on pH and temperature variation<sup>(124-126)</sup>. It has been achieved by a combination of ionisable and hydrophobic functional group<sup>(127-129, 71)</sup>.

Several authors have recently presented their advances in this field, as Leung *et al.*<sup>(130)</sup> that have prepared smart core-shell microgels based on PNIPAAm, MBAAm and chitosan or poly(ethyleneimine) in the absence of surfactants. The materials were obtained by graft copolymerization and presented a well defined core-shell structure consisting of temperature-sensitive cores (based on PNIPAAm) with pH-sensitive shells (based on cationic water-soluble polymers).

Rodríguez-Cabello's group<sup>(131)</sup> has extensively worked in the development of elastin-like polymers (ELPs) by genetic engineering showing their extraordinary potential. Well defined and tailored polymers were obtained covering a wide range of properties. They developed different materials by fermentation, which showed clear environmental advantages. The ELPs presented a modulated pH- and T-sensitivity covering the most interesting range of biomedical applications. ELPs have also been modified with photo responsive molecules as azobenzenes<sup>(131)</sup> and spiropyranes<sup>(132)</sup> getting photo sensitive macromolecules. Kurata and Dobashi<sup>(133)</sup> published the preparation of potential intelligent drug carriers based on *N*-acryloyl-*N'*-alkylamide derivatives of both L-glutamic acid and L-aspartic acid.

New copolymeric systems derived from *N,N*-dimethylaminoethyl methacrylate (DMAEM) and acrylic acid (AAc) or itaconic acid (IAc) were obtained by UV-irradiation. They responded to both pH and temperature as a polyampholyte according to the monomeric compositions and combination of temperature and pH conditions.

Kuckling *et al.* presented a systematic study of how LCST varies depending on hydrophilic/hydrophobic balance. With this purpose they prepared copolymers of NIPAAm

with acrylamide derivatives bearing carboxylic groups attached to spacers with different chain length <sup>(71)</sup> and deeply studied the influence of both temperature and pH on their properties.

Other authors combined NIPAAm with butylmethacrylate and acrylic acid in order to obtain pH-/temperature-sensitive vehicles for peptide delivery. They confirmed that loading efficiency increased with increasing ionic strength, which is predominantly governed by hydrophobic interactions and/or specific interactions between the polymer molecules <sup>(134)</sup>.

Alginate has been modified using PNIPAAm forming dual stimuli responsive SIPNs that could be useful in biomedical fields for stimuli-responsive drug delivery systems <sup>(135)</sup>.

Moreover, Benrebouh *et al.* <sup>(136)</sup> synthesised and characterised copolymers based on NIPAAm and methacrylate monomers derived from cholic acid (**Figure 14**) in order to improve the biocompatibility of the polymer.

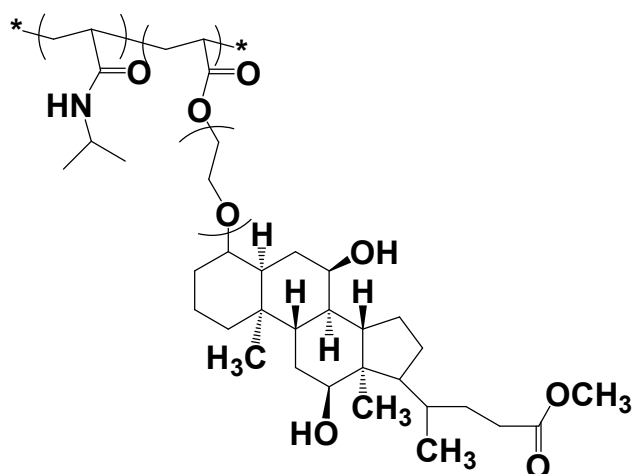


**Figure14:** Chemical structure of the copolymer of NIPAAm and methacrylate monomers derived from cholic acid <sup>(136)</sup>.

Ning *et al.* presented in 2001 <sup>(137)</sup> the synthesis by  $\gamma$ -irradiation and characterization of poly(*N,N*-dimethylaminoethyl methacrylate) (PDMAEMA), a temperature-sensitive material in a temperature range of 38-40°C and pH-sensitive at pH = 2.5. Electricity-responsive behaviour at a field voltage of approximately 3.0 V was shown to take place. As the synthesised materials were transparent, elastic, and had a good swelling capacity their utilization as drug delivery systems was proposed. Poly (*N,N*-diethylaminoethyl methacrylate) PDEAEMA has also been copolymerized with PEO in order to obtain pH- and T-sensitive copolymers for injectable delivery applications <sup>(138)</sup>.

Gan *et al.* <sup>(139)</sup> prepared and studied a new water soluble pH- and T-sensitive polymer based on poly(acryloyl-*N*-propylpiperazine) (PAcrNPP) (**Figure 15**) that exhibited a lower critical solution temperature (LCST) in water at 37°C.

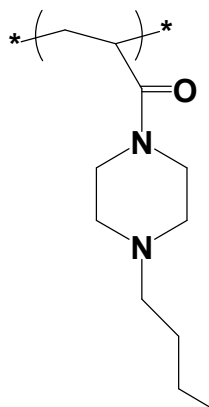


**Figure15:** poly(*N*-acryloyl-*N*-propylpiperazine) structure <sup>(139)</sup>.

Dumitriu *et.al* <sup>(140)</sup> synthesized hydrogels consisting of sodium alginate and *N*-isopropylacrylamide covalently crosslinked with *N,N*-methylenebisacrylamide. The thermo- and pH-responsive properties of these hydrogels were evidenced by their swelling behavior, which depended also on the amount of crosslinking agent and hydrogel composition.

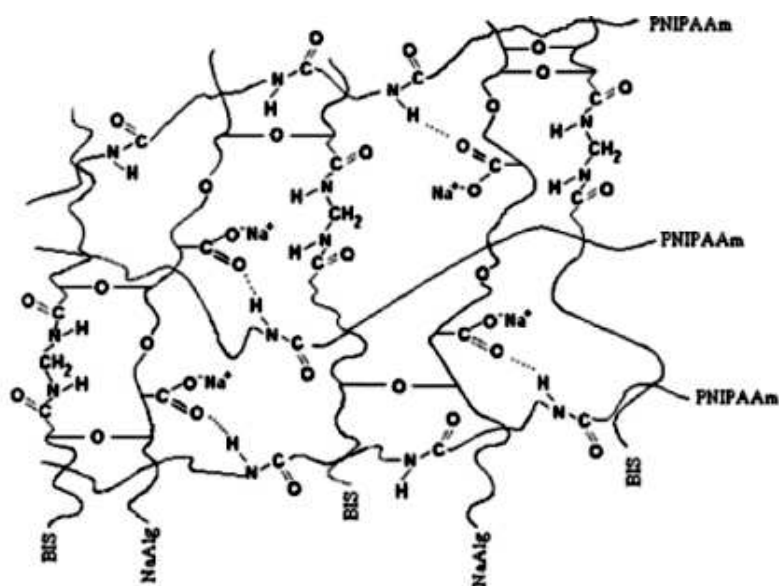


**Figure16:** Schematic of the formation of PNIPAAm/Alg three-dimensional mixed-IPN <sup>(140)</sup>.

Dong Chen *et.al* <sup>(141)</sup> prepared multiresponsive reversible gels with a carboxylic azo polymer (PM6AzCOOH) in dimethyl sulfoxide (DMSO) based on formation of H-aggregation and hydrogen bonds. Due to the specifically designed molecular structure of the polymer PM6AzCOOH, the obtained gel showed multiresponsive behaviors to several stimuli, such as temperature, solvent polarity, and light. Their reversibly multiresponsive behaviors were systematically studied. It was found that the resulting gels could be destroyed by heating, adding a solvent with lower polarity, or irradiating with UV light. The gel could then be reformed by reverse processes with full reproducibility.

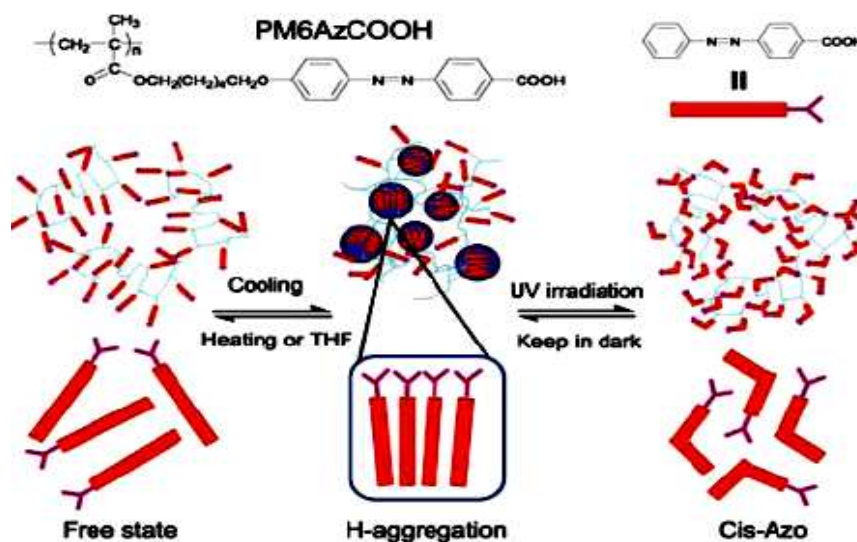


**Figure 17:** A schematic illustration of multi-responsive reversible gels formed with PM6AzCOOH in DMSO <sup>(141)</sup>.

On the other hand, supramolecular gels of rather complex nanostructure are derived by the combination of inorganic components with organic counterparts capable of associative interactions leading to hybrid gel formation. Despite their structural complexity these gels are unique in a sense that their properties and functions are dominated by the synergistic effect of the two functionalities. An intriguing approach to the formation of hybrid supramolecular gels employs reversible metal–ligand interactions to build the self-assembled construction, which is afforded extra optical or magnetic properties by the metal complex <sup>(142)</sup>. To this end, Beck and Rowan <sup>(143)</sup> synthesized a novel class of hybrid supramolecular gels that exhibit intriguing responsive behavior to heat, metal binding, and light irradiation **Figure 17**. The polymers were prepared from a bifunctional oligoethylene glycol derivative end capped with a bis (2,6-bis(10-methylbenzimidazolyl)-4-hydroxypyridine) tridentate ligand capable to bind transition metals. The organic ligand formed linear polymers with gel like texture in the presence of selective metal ions at an appropriate organic/ inorganic content. The metal type (i.e. Zn, La, Co, Eu) affected the physicochemical properties of the gel resulting in temperature dependent sol–gel transition, thixotropic polymers with mechanoresponsive (shear-thinning) behavior and gels with unique photo responsive properties. The versatility of this method allows for the development of polymers with tailor made properties by the rational choice of the building blocks and therefore provides access to an important range of multi-responsive materials.

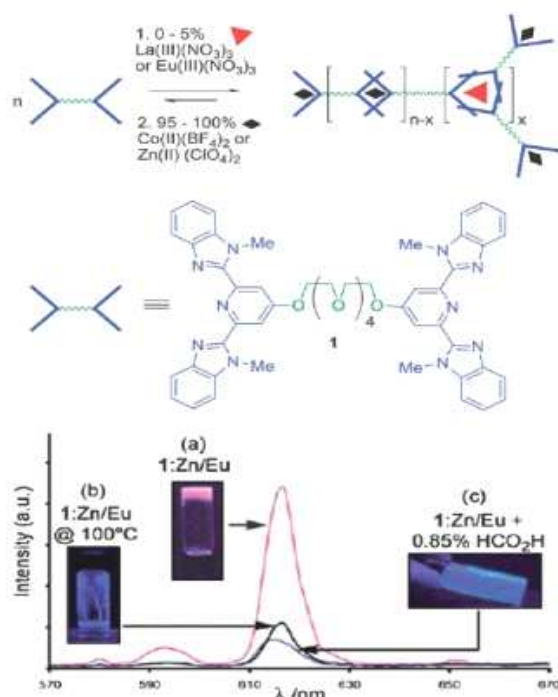


**Figure18:** Supramolecular hydrogels responsive to temperature, metals and light formed by coordination of lanthanoid and transition metal ions by a bifunctional oligoethylene glycol tridentate ligand. <sup>(143)</sup>

Jiang *et.al.* <sup>(144)</sup> extended the wettability variations of a surface in response to three different stimuli, pH, and temperature and glucose concentration by grafting a PNIPAAm–poly (acrylamido phenylboronic acid) copolymer onto a rough silicon substrate **Figure19**. The surface exhibited a complex cooperative wetting behavior in response to all three stimuli. A switch from superhydrophobicity to superhydrophilicity was induced by either cooling the surface at neutral pH or increasing the pH at low temperature in the presence of glucose or alternatively by exposing the surface to glucose at neutral pH and low temperature. An increase of the LCST of the copolymer with the glucose concentration at neutral and high pH was found which supported the observed changes in wettability. The response of this system to a combination of biochemical stimuli in a synergistic manner renders it very promising for use in diagnostics, drug delivery or cell culture applications.

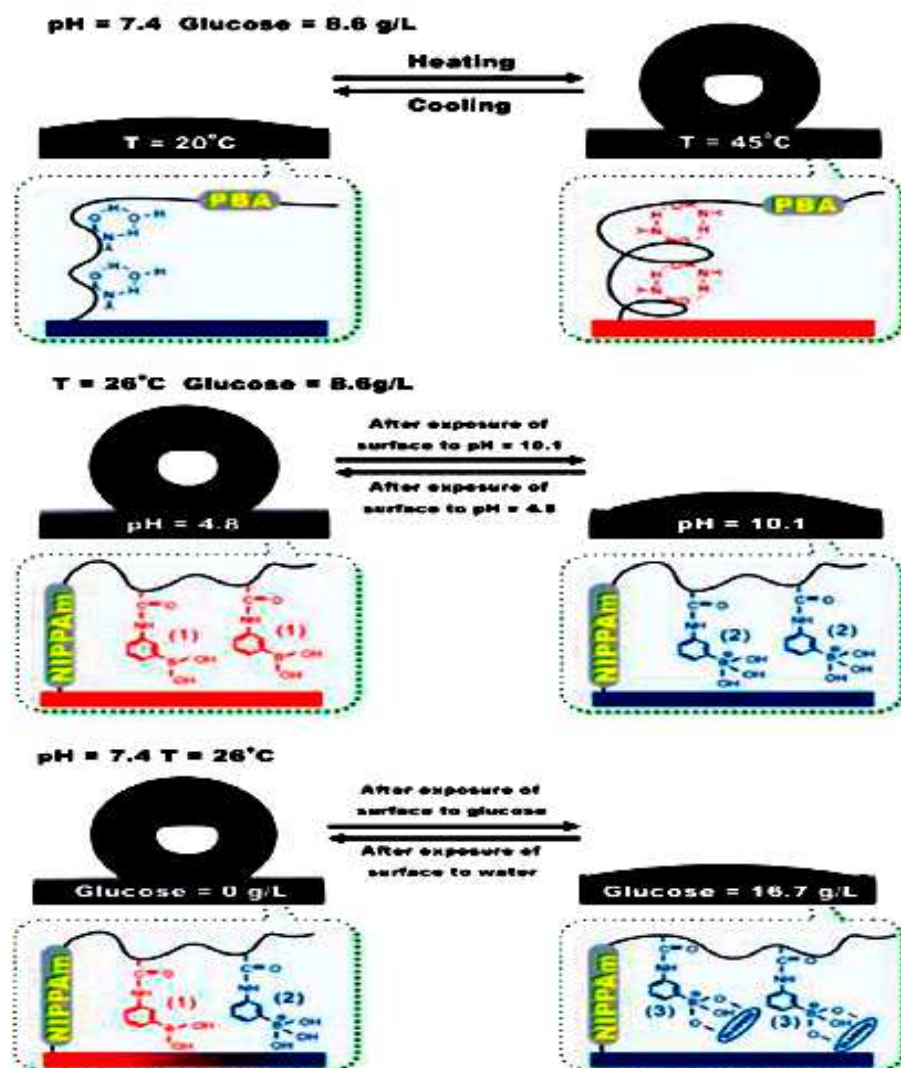


**Figure19:** PNIPA-co-PBA surfaces change between superhydrophilicity and super hydrophobicity by pH, temperature and glucose concentration variations <sup>(144)</sup>.

An alternative approach for the development of multiresponsive surfaces that alter their wetting and structural characteristics in a complex manner in response to three different stimuli were proposed by Rodriguez-Hernandez and coworkers. They employed homopolymer/block copolymer blends, deposited on a surface by spin coating, to obtain films with thicknesses above 100 nm and thus eliminate possible effects of the support on the surface characteristics <sup>(145)</sup>.

## 1.5. Functional Hydrogels.

Functional hydrogels consist of at least one polymer segment that enables polymer analogous reactions. The possible routes utilize active ester chemistry, click chemistry, polymeric anhydrides, epoxides, aldehydes and ketones. Including Michael-type and Friedel-Crafts reactions as well as methylations, polymer analogous reactions involve almost all high yield organic reactions<sup>(146–148)</sup>. Furthermore, for most of these transformations, both reaction partners are polymerizable or can be provided by functionalization of a precursor polymer. For example PHEMA can be transformed into a carboxylate with cyclic anhydrides and carbamates.

These reactive sites allow for the modification with a variety of biomolecules for biosensor applications and chromatography based on affinity binding<sup>(149–153)</sup>, additionally, attaching molecular recognition sites diversified cell culturing, and polymer assisted drug delivery advanced medication<sup>(100)</sup>. As mentioned above, responsive behavior can be implemented to create a functional responsive hydrogel or to diversify the responsiveness, i.e. to a magnetic field by incorporating magnetite nanoparticles<sup>(154, 155)</sup>.

The combination of functionality and responsive behavior allows for the development of advanced biosensors<sup>(156)</sup>. The concept is described in **Figure 20**.

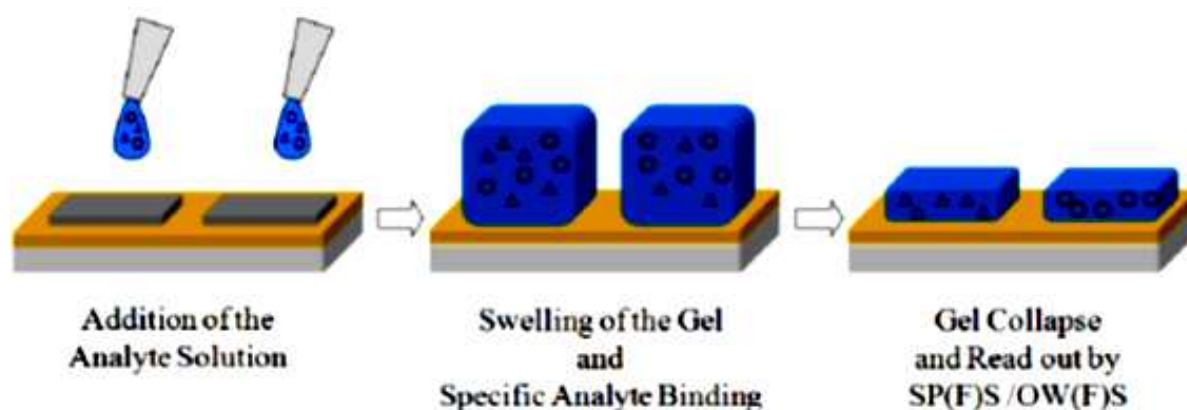
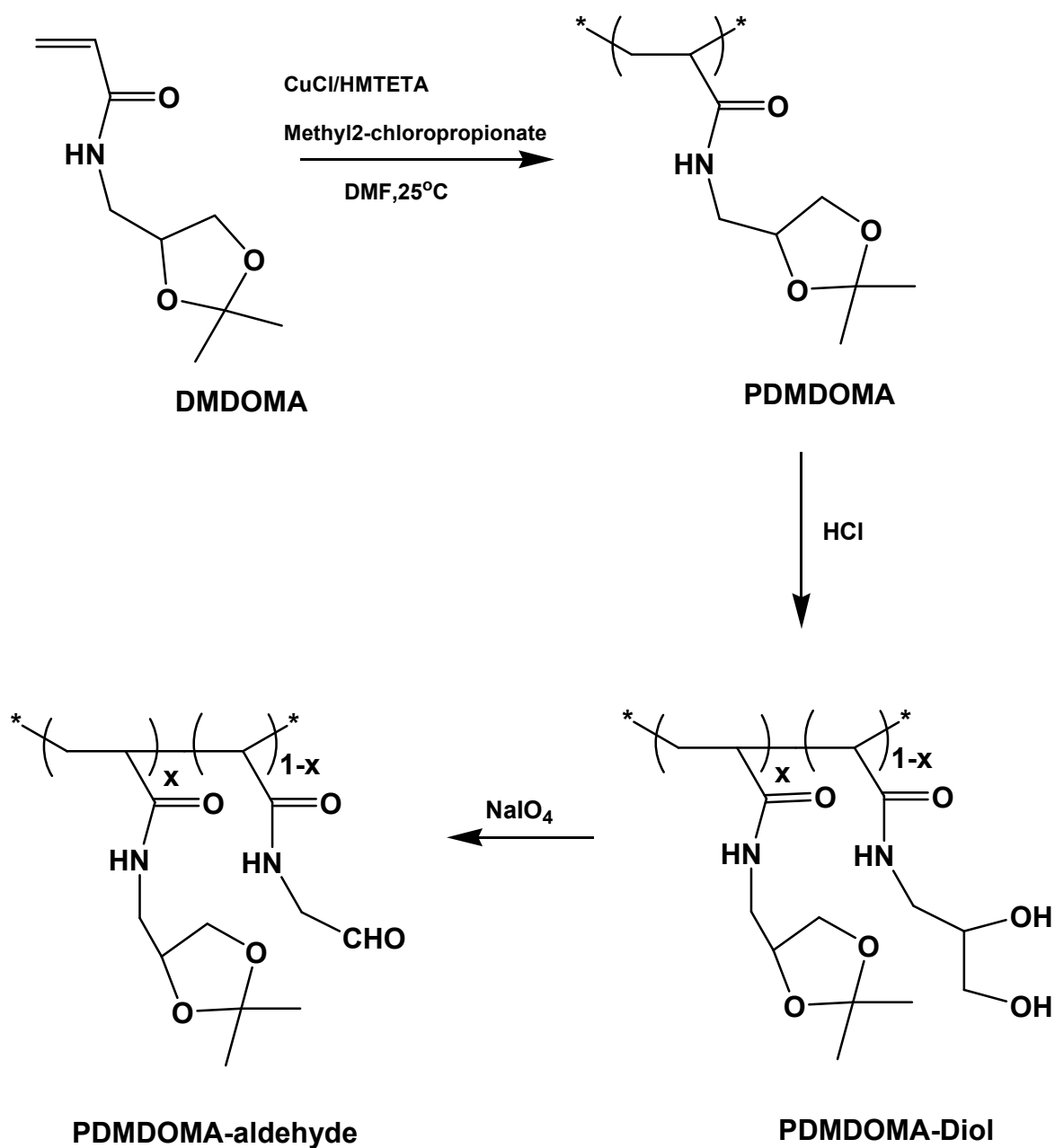


**Figure20:** Sensor concept with a functional responsive hydrogel<sup>(156)</sup>.

Zou *et al.*<sup>(157)</sup> have synthesized thermo-responsive aldehyde polymers by cleaving the pendant dioxolane groups and subsequently oxidizing the 1,2-diols. The reactivity of Poly(*N*-[(2,2-dimethyl-1,3-dioxolane)methyl]acrylamide)aldehyde PDMDOMA-aldehyde was verified by the reductive amination reactions with aniline and propylamine. The LCST of PDMDOMA derivatives depends on the hydrophilic or hydrophobic content in the polymer. An increase in the hydrophilicity (e.g., 1,2-diol or 1,1-diol) led to an increase in the phase

transition temperature, while the addition of propylamine or aniline (hydrophobic components) caused a decrease in the phase transition temperature.



**Scheme 1.** Synthesis of PDMDOMA, PDMDOMA-Diol, and PDMDOMA-Aldehyde <sup>(157)</sup>.

## **1.6. Stimuli-responsive hydrogel thin films.**

Recent advances in nanotechnology have led to increased interest in hydrogel thin films. The advantages of hydrogel thin films have been explored for the fabrication of miniaturized devices with fast response times. Hydrogel thin films have also attracted interest as an approach to responsive surfaces and interfaces, where they compete with grafted polymer layers. A 3D polymer network is much more stable at interfaces when compared with polymer brushes, where polymer chains are grafted to the surface via only one functional group while the polymer network is linked to the surface by multiple anchoring points. Unlike polymer brushes, the thin gel film can be transferred from the surface of one material to the surface of another material or used as a free-standing film. The storage function of the hydrogel thin films (their ability to accommodate various nanoparticles, chemicals, dyes, enzymes, etc.) can be explored for the substantial increase in the range of functional properties they will demonstrate and external signals they will respond to <sup>(158)</sup>.

### **1.6.1 Preparation of hydrogel thin film.**

Chemically crosslinked stimuli responsive hydrogel thin film can be prepared according to these methods;

#### **1.6.1.1. Crosslinking copolymerization (adding multifunctional co-monomers).**

In this method solvent-based free-radical polymerization techniques are broadly used. A reaction mixture containing monomers, a crosslinking agent, and a free-radical initiator is either spin-coated onto a planar substrate or confined between two planar substrates (one of them is non-sticky) using micrometer thick spacers and polymerized in situ <sup>(159)</sup>. Among the free-radical polymerization techniques, a UV-initiated polymerization technique has gained popularity because it allows micro-patterning of films via a projection mask <sup>(160,161)</sup>. Peppas and coworkers used a mask aligner to precisely position hydrogel patterns on a substrate surface <sup>(161)</sup>. The photo initiator is either added to a reaction mixture or chemically immobilized on a substrate. In the latter case, the growth of a film is initiated from a surface, and the thickness can be controlled by varying the exposure time <sup>(159)</sup>. This method is also suitable for coating substrates with complex geometry <sup>(162)</sup>. Another free-radical polymerization technique is electrochemically-induced polymerization. For example, the polymerization of PNIPAM hydrogel thin films was initiated by electron transfer from a conducting substrate to a redox-active initiator (potassium persulfate) <sup>(163)</sup>. In another example, the hydrogel thin films of an m-acrylamidophenylboronic acid-acrylamide

copolymer were grown by Zn (II)-catalyzed electropolymerization<sup>(164)</sup>. In both cases, the film thickness was controlled by the electrolysis time. Recently, a simple method for the generation of hydrogel films with a thickness gradient has been reported<sup>(165)</sup>. In this method, Zn(II)- catalyzed electropolymerization of poly(acrylic acid) (PAA) was carried out in the presence of an in-plane electrochemical potential gradient applied to a resistive working electrode.

Plasma polymerization is an attractive one-step, solvent-free, vapor-phase deposition technique used for producing highly crosslinked hydrogel thin films (typically ranging from tens to hundreds of nanometres thick) without the use of crosslink agents (crosslinking occurs due to ion/electron bombardment of the material during the deposition)<sup>(166-169)</sup>. Film thickness is conveniently controlled by polymerization time and plasma power. The substrates are often surface modified with an adhesion promoter (e.g., self-assembled monolayer or polymer brush) to improve the stability of the films. Some monomers (e.g., *N*-isopropylacrylamide) have to be heated to achieve an appropriate vapor pressure during plasma polymerization. Initiated chemical vapor deposition (ICVD) is another solvent-free, onestep technique suitable for the generation of uniform thin films of crosslinked polymers<sup>(170)</sup>.

### **1.6.1.2 Crosslinking after thin film deposition in the dry state.**

The crosslinking of copolymers containing photo reactive pendent groups or monomers (e.g., benzophenone or 4-cinnamoylphenyl methacrylate) with UV irradiation is a popular approach<sup>(124,73,171-174)</sup>. It is compatible with photo lithography and is suitable for the preparation of films with a wide range of thicknesses in the dry state (from tens of nanometers to tens of micrometres)<sup>(175,176)</sup>. Photo-crosslinkable films can also be obtained by mixing a polymer with a photo initiator<sup>(177)</sup>. Alternatively, polymer thin films are immobilized to the substrate's surface and internally crosslinked by plasma treatment<sup>(178,179)</sup>.

### **1.6.1.3 Multiple Layer-by-Layers (LbL) assembled thin film.**

The polymer films fabricated in this way are multilayered<sup>(180)</sup>. The main advantages of the LbL technique are in the fine control of a film's structure and chemical composition, and in the fact that LbL films can be assembled on substrates of any shape and in confined environments. For example, LbL deposition was used to modify the walls of microchannels<sup>(181)</sup>.

LbL films exhibit pH responsive swelling behavior. For example, poly(allylamine hydrochloride)/poly(styrene sulfonate) (PAH/PSS) films were rendered pH-sensitive by selecting appropriate assembly conditions (pH).<sup>36</sup> A strong excess of COO<sup>-</sup> -groups can be

built into multilayers by using partially esterified PAA. As the assembly of a multilayer is completed, the ester groups are hydrolyzed to yield carboxyl groups <sup>(182)</sup>.

LbL films of water-soluble non-ionic polymers and PEs can also be obtained via hydrogen-bonded self-assembly <sup>(183)</sup>. For example, the hydrogen-bonded LbL assembly was utilized to produce temperature-responsive films <sup>(184,185)</sup>.

In highly acidic and basic solutions, LbL films become unstable due to internal ionization, large swelling forces, and partial dissociation of ionic bonds, resulting in film detachment, decomposition, or phase separation <sup>(186-189)</sup>. In order to secure their stability, the films are chemically attached to substrates and internally crosslinked. For example, PE (polyelectrolyte) chains were functionalized with photo reactive groups (e.g., benzophenone) to enable crosslinking with UV light <sup>(190,191)</sup>. Condensation reactions (e.g. carbodiimide chemistry) were used for crosslinking polymers containing carboxylic acids and amines <sup>(192)</sup>.

### **1.6.1.4. Ultrathin LbL hydrogels via click chemistry.**

In click chemistry, covalent reactions with high yields can be performed under mild conditions. Using azide- or alkyne- modified PAA polymers, stepwise growth of LbL films was demonstrated in the presence of copper(I) and sodium ascorbate in aqueous solution <sup>(193)</sup>. Deposition was promoted by the formation of 1,2,3-triazole crosslinks **Figure 21**.

Single-component PAA capsules prepared via this approach were stable over a pH range from 2 to 10, and showed reversible changes in size, up to 70%, when cycled between high and low pH environments <sup>(194)</sup>. However, the requirement for the use of copper in the azide-alkyne click chemistry reaction prevents the use of this approach for biological applications. Recently, another click chemistry route based on thiol-ene reaction was used for the fabrication of LbL hydrogels **Figure 21B** <sup>(195)</sup>. In this case, instead of allowing polymers to react during each deposition cycle, the precursor platforms for hydrogel poly (methacrylic acid) (PMAA) layered films were first pre-assembled using thiol-PMAA, ene-PMAA and polyvinylpyrrolidone (PVPON). The cross-linking of PMAA layers was then carried out via thiol-ene reaction initiated by exposure to UV-light. The exposure of cross-linked films to aqueous solution at pH 7 resulted in release of PVPON from the PMAA film and formation of layered PMAA hydrogel films or capsules.

A synthesis of single-component polyallylamine hydrochloride (PAH) films and capsules was also accomplished through direct covalent LbL assembly mediated by Glutaraldehyde (GA) <sup>(196)</sup>. The stepwise deposition of ~2.2 nm of PAH per layer could be achieved by alternating immersion of flat or particulate templates into PAH and GA solutions. Film growth occurred as Schiff bases formed between the cross-linker and amine groups of the polymer.



## **1.6.2. Applications of stimuli-responsive hydrogel films.**

### **1.6.2.1. Storage and regulation of mass-transport.**

#### **1.6.2.1.1. Tunable ion-selective permeability (ion “gating”).**

The tunable permeability was attributed to the pH-dependent swelling of the multilayers. The chemical crosslinking of the PAA/PAH multilayers allowed stabilization of the films, which otherwise showed delaminating at basic pH because of strong swelling <sup>(182)</sup>. Reversible temperature-induced modulation of ion transport across LbL multilayers assembled from ionically modified PNIPAM random copolymers (PAH-co-PNIPAM and PSS-co-PNIPAM) has been demonstrated by Jaber and Schlenoff <sup>(199)</sup>. Because of the high density of ionic crosslinks, the multilayers showed very limited swelling with no delaminating problem. Highly stable ion perm selective membranes based on chemically crosslinked LbL multilayers and hydrogel thin films have been reported by several groups. Akashi and coworkers have demonstrated the switching on/off of ionic permeability of crosslinked LbL multilayers (PAA-co-PNIPAM/PVAm, where PVAm is poly (vinylamine hydrochloride)) below and above the LCST of PNIPAM <sup>(192)</sup>. Advincula and coworkers have reported on pH-sensitive bipolar ion-permeable hydrogel films prepared by LbL assembly and photo-crosslinking of benzophenone modified PAA and PAH <sup>(190)</sup>. The ionization degree of the groups in the multilayers was controlled by pH, thereby allowing the switching on/off of ion transport for either cationic or anionic species. Ion permselectivity occurs because the charges present in the multilayer reject ions of the same sign and favor transport of ions of the opposite sign. This approach was later extended to films having the dual response <sup>(200)</sup>. The films had a binary architecture, where a temperature-sensitive brush (PNIPAM) was grafted atop a pH-sensitive LbL multilayer (PAH/PAA), thus enabling a dual control mechanism for ionic permeability across the films. pH-switchable perm selective membranes from photo-crosslinked LbL multilayers containing carboxylic acid and imine groups have also been reported by Sun and coworkers <sup>(191)</sup>. Aoyagi and coworkers prepared photo-crosslinked hydrogel films of PNIPAM-co-poly (2-carboxyisopropyl acrylamide) and demonstrated that the ion transport across the films was strongly affected by temperature and pH <sup>(125)</sup>.

#### **1.6.2.1.2. Regulation of flow and permeability (“chemical valves”).**

A responsive hydrogel material immobilized inside a microfluidic channel can operate as a valve which opens and closes the channel for a water flow. “Smart” hydrogel valves eliminate the need for external power and external control and thus allow the creation of autonomous “lab-on-a-chip” systems for analytics <sup>(158)</sup>.

Chu *et al.* have reported chemical valves with the temperature response opposite to that found in PNIPAM-based systems <sup>(201)</sup>. To achieve this behavior, they modified a porous nylon 6 membrane with a layer of an interpenetrated polymer network (IPN) composed of PAM and PAA **Figure 22**. The resulting gel exhibited UCST behavior due to the temperature induced dissociation of the zipper-type H-bond complex between the polymers.

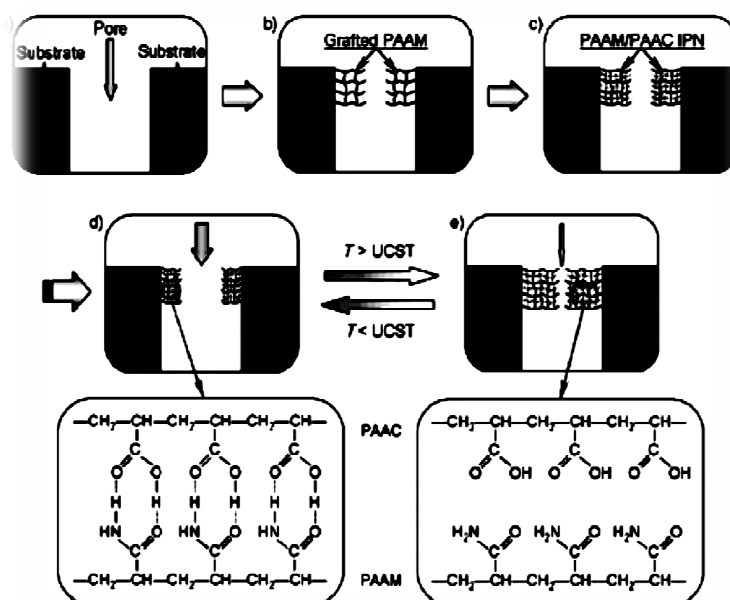


**Figure22:** Schematic illustration of the temperature-responsive gating membrane and the fabrication procedure: (a) porous membrane support; (b) membrane support after plasma-graft polymerization of PAM; (c) the subsequent synthesis of PAA results in the formation of PAM/PAA hydrogel gate inside the membrane's pores; (d) below the UCST the membrane's pores open as a result of the formation of an insoluble hydrogen-bonded complex between PAM and PAAC; (e) above the UCST the membrane's pores close because of the complex dissociation and swelling of the hydrogel <sup>(201)</sup>.

Rubner, Cohen, and coworkers have fabricated pH-controlled valves from commercial track-etch membranes whose pores were modified with PAH/PSS LbL multilayers <sup>(181)</sup>. The valve showed discontinuous changes in the trans-membrane water flux and permeability of high molecular weight poly (ethylene oxide) (PEO) caused by pH-induced swelling and shrinking of the multilayer. The swelling of the multilayer was found to be hysteretic; meaning an open or closed state of the valve could be attained at a single pH value.

An alternative approach to chemical valves based on macroporous hydrogel thin film membranes has been recently suggested <sup>(202)</sup>. The 100 to 200 nm thick membranes (chemically crosslinked P2VP) were prepared on a planar substrate and then transferred onto 200 nm pore size polycarbonate track-etch support membranes to form a pH-responsive skin

layer **Figure 23**. The pore size was altered (from wide open pores to completely closed pores) by the expansion/shrinkage of the entire hydrogel body of the membranes. This property was explored for controlling the water transport through the membranes.

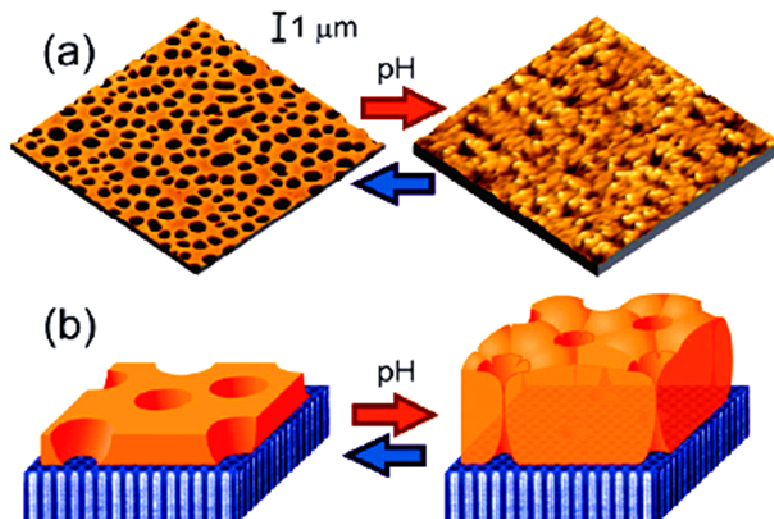


**Figure 23.** (a) SPM images ( $7.5 \times 7.5 \mu\text{m}^2$ ) of a P2VP gel membrane under water of pH 5.5 (left) and 2 (right). (b) Schematic representation of the gel membrane with the open (left) and closed (right) pores; the gel membrane is deposited on the surface of a porous substrate <sup>(202)</sup>.

### 1.6.3. Chemical sensors based on hydrogel films.

The stimuli-triggered volumetric transition in hydrogel layers was explored for various sensors. Hydrogel thin films were used to sense temperature, pH, and various kinds of analytes. Sensors are classified by a scheme used to transduce analyte-induced chemical or physical changes in a hydrogel into an electrical or optical signal <sup>(158)</sup>.

#### 1.6.3.1. Microgravimetric transducers.

Several groups used mass-sensitive quartz crystal microbalance (QCM) resonators coupled with stimuli-responsive hydrogel coatings to monitor changes in hydrogel swelling. Absorption and release of water by the hydrogel are followed by changes in the surface load, which results in a shift of the resonance frequency of a QCM resonator. The response is typically nonlinear because both stiffness and density of the hydrogel coating decrease upon swelling. Such changes in the mechanical properties also cause damping of the signal amplitude, which can be monitored in parallel with the frequency. Richter et al. discussed physical aspects of the operation of hydrogel-based QCM sensors and their limitations <sup>(203)</sup>. Their pH sensor, based on PVA/PAA hydrogel, showed high pH-sensitivity but suffered from swelling hysteresis. The pH-sensitive thin films of crosslinked P4VP prepared on QCM crystals have been also reported by Ramstrom, Yan, and coworkers <sup>(204)</sup>.

Shinkai and coworkers prepared a nucleotide-sensitive molecularly imprinted multilayer by carrying out the LbL deposition of boronic acid containing polyanion and polycation in the presence of the anionic nucleotide (adenosine monophosphate, AMP) on a QCM resonator surface <sup>(205)</sup>. The subsequent removal of AMP from the multilayer yielded the swollen hydrogel from the cation-excess polyion complex. Rebinding of AMP neutralized the complex, and thus the hydrogel shrank. The swelling-shrinking of the hydrogel was sensed using a QCM resonator.

An ultrasensitive pH sensor based on micromachined cantilevers has been reported by Peppas' group <sup>(161,206)</sup>. Patterned layers of PMAA/poly (ethylene glycol) dimethacrylate were formed on silicon wafers containing cantilevers by free-radical UV polymerization.

### **1.6.4. Actuators.**

#### **1.6.4.1. Cell-culture supports with the triggered release.**

A promising application of responsive hydrogel thin films is related to tissue engineering. The idea of controlling adhesion of mammalian cells using substrates from thermoresponsive polymers dates back to 1990 when it was first reported by Okano's group <sup>(207)</sup>. Since then, several groups have studied different aspects of this process, which has resulted in a large number of publications. Recent reviews on the subject can be found in the papers of Kikuchi and Okano <sup>(208)</sup> and da Silva et al. <sup>(209)</sup>. In many studies, thermoresponsive surfaces have been formed by 10 to 100 nm thick crosslinked PNIPAM-based copolymer films <sup>(209)</sup>. At temperatures above the LCST, the cells adhere, spread, and proliferate on the relatively hydrophobic PNIPAM surfaces the same way they do on the traditional polystyrene tissue culture dishes. However, when the temperature is lowered well below the LCST, all cultured cells spontaneously detach due to the PNIPAM transition into the hydrophilic state. Such temperature-responsive culture supports have been demonstrated as useful in regenerative medicine and tissue engineering applications. Specifically, sheets of cultured cells along with their extracellular matrix are harvested from the dishes and transplanted to tissue beds with minimal cell loss <sup>(210)</sup>. They can be micro-patterned to include cells of different types and **Figure 24** layered to create complex 3D tissue-like structures <sup>(211)</sup>.

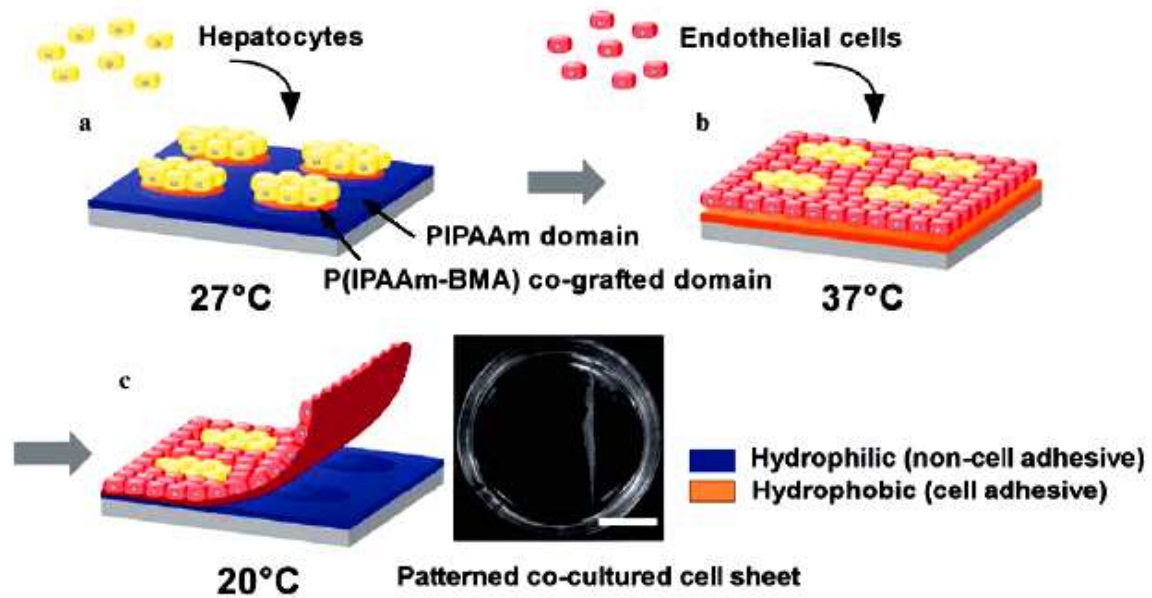


**Figure 24.** Schematic representation of the methods for patterning cell co-culture and harvesting of co-cultured cell sheets using a dual patterned surface. (a) The first cell type, hepatocytes, is seeded and cultured at 27°C, resulting in localization of hepatocytes onto PNIPAM-poly (n-butyl methacrylate) co-grafted islands showing a hydrophobic nature. (b) The second cell type, endothelial cells, is seeded and cultured at 37°C, resulting in the generation of patterned co-cultures. (c) Decreasing the temperature to 20°C induces the detachment of the co-cultured cell sheet. Harvested patterned co-cultured cell sheet (right). Bar: 1 cm <sup>(211)</sup>.

## 1.7. Surface plasmon resonance and optical waveguide (SPR-OW) or SPW spectroscopy.

### 1.7.1. Waveguide introduction.

Waveguides are a physical medium through which light can be guided, similar to the way that a conductor can guide an electric current. Many different physical configurations of optical waveguides are possible. A simplistic example would be a bent glass rod a few millimeters in diameter used to guide light to an inaccessible location. A common device based on this principle would be a bore light which directs light at right angles from the source. Of greater interest to a researcher investigating sensing mechanisms are fiber optics and planar waveguides, both of which are frequently used as the basis for optical sensors. The waveguiding nature of optical waveguides is illustrated in Figure 4, where the propagation of light through the waveguide occurs via total internal reflection. Within the dimensions of the waveguide with very little leakage into the surroundings. As **Figure 25** indicates, the

**Introduction**

refractive index of medium-1 ( $n_1$ ) is higher than that of medium-2 ( $n_2$ ). For any waveguide, the guiding medium must have a higher index of when this phenomenon occurs; the propagating light ray is confined refraction than the surroundings in order for light to propagate by total internal reflection <sup>(212)</sup>.

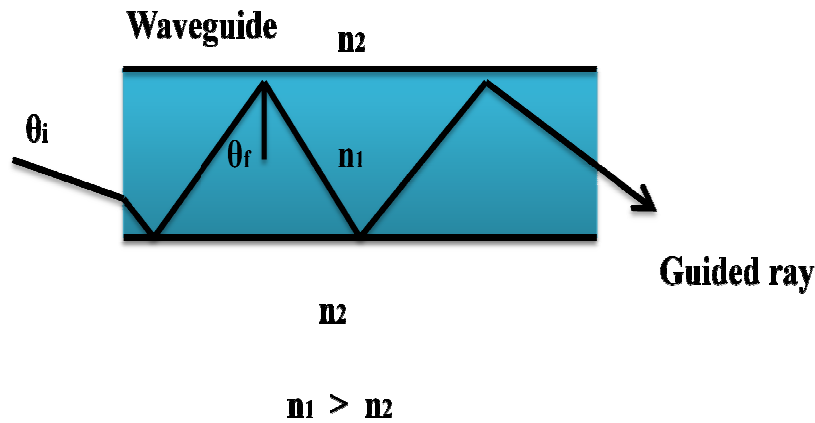


**Figure25:** Waveguiding of Light;  $n$  is refractive index,  $\theta$  denotes angle of incidence and reflection respectively.

Total internal reflection can occur at a boundary interface between any two media of different refractive indices, provided that the critical angle of reflection is met, as defined by Snell’s law. The relevant portion of Snell’s law is shown in Equation 9.

**Sin  $\theta_c = n_1/n_2$  ..... (8)**

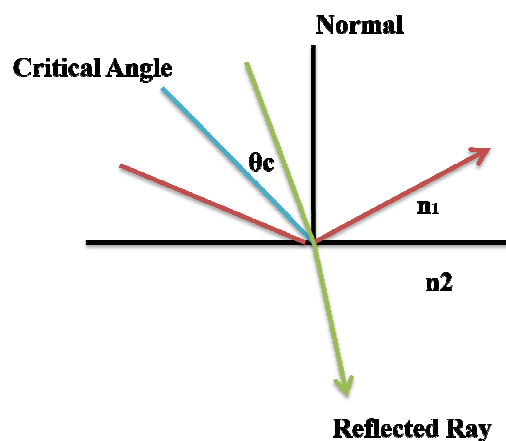


**Figure26:** shows a two dimensional representation of an incident light ray impinging on the interface between two media.

Snell’s law relates a critical angle of reflection  $\theta_c$  to the refractive indices of a waveguide and its surroundings  $n_1$  and  $n_2$ . The critical angle defines a minimum angle of incidence for a

particular interface. A light ray's angle of incidence at the waveguide interface must be equal to, or greater than,  $\theta_c$  for total internal reflection to occur.

A light ray that does not satisfy the critical angle criteria is refracted into medium 2. Light that does satisfy the critical angle is internally reflected into medium 1. Simply, Snell's law shows that the critical angle for a particular waveguiding system depends upon the ratio of the refractive indices of the involved media. This elementary model will serve to describe light propagation and simple reflection at a single boundary with macro scale dimensions such as the Kretschmann prism arrangement. However, SPR is not confined to large scale optical waveguides. Fiber and planar waveguides have advantages for certain sensing situations <sup>(212)</sup>.

### **1.7.2. Surface plasmon resonance spectroscopy.**

#### **1.7.2.1. Historical background.**

Plasmonics is concerned with conduction electrons at metal surfaces and their interaction with electromagnetic radiation <sup>(213)</sup>. The quantization of the collective oscillations of electrons in the conduction band of a metal produces the plasmon. There are three types of plasmons: volume plasmons, surface plasmon polaritons, and localized surface plasmons. Surface plasmons are basically the quanta of plasma oscillations at a metal surface. When a surface plasmon couples with a photon, a quasiparticle called the surface plasmon polariton (SPP) is formed. Volume plasmons are the excitation of the conduction electron sea that occurs in bulk metals and localized surface plasmons are the excitations (non-propagating) of conduction electrons in metallic nanostructures coupled to the electromagnetic field. Classical mechanics and the Drude model can be used to describe plasmons and predict behavior <sup>(214,215)</sup>. The focus herein will be placed on surface plasmon resonance and the practical applications of this technology.

Although a mathematical prediction of SPR was developed in the late 1890's, the SPR phenomenon was first physically witnessed in the early 20<sup>th</sup> century by R. W. Wood at Johns Hopkins University <sup>(216)</sup>. He was observed the spectra resulting from the illumination of the gratings on a dividing engine. Wood noticed through experimentation that the intensity of reflected light was a function of angle. There were points in the spectra where there was almost no reflected light, and these minima occurred within 600 nm of the point of maximum reflection <sup>(217)</sup>. This prompted his hypothesis that the theories governing these diffraction gratings were insufficient. This was an extreme notion, considering the diffraction grating theories were first introduced by James Gregory soon after Newton's famous prism experiments in the 17th century.

Maxwell's equations **9** are classical descriptors of electromagnetic behavior and there are many solutions in existence. In 1907, Ze-neck developed a set of solutions to Maxwell's equations that explained Wood's earlier observation <sup>(218)</sup>. However, it wasn't until the 1960's that the configurations most familiar to SPR were born. After the development of the prism configuration, SPR grew into an established analytical technique that complimented the results of other techniques. Since then, the growth of the field has progressed into broader applications.

### **1.7.2.2. Theory.**

SPR is a collective density oscillation of free electrons confined to and propagating along a metal (typically silver or gold) surface. This density oscillation is coupled with an electromagnetic (evanescent) wave whose electric field is decaying exponentially from the surface. The SPR can be excited on the surface of a thin metal film deposited on the base of a prism (the Kretschmann configuration) by monochromatic light incident at the prism-film interface. The SPR is detected through a narrow minimum in the reflection coefficient at a particular angle of incident light. The angle at which the minimum occurs depends strongly on the refractive index and the thickness of the dielectric layer deposited on the metal surface. Because of the evanescent nature of SPR, the probing depth of this technique is limited to layers of two to three hundred nanometers in thickness. Here we will discuss SPR theory with some detail as followed <sup>(213)</sup>.

### **1.7.2.3. Prism-based configurations.**

A conventional description of an SPR instrument is best understood in terms of a prism-based configuration. A traditional light source is unable to excite the surface plasmons independently. Therefore, this configuration allows the light to exploit reflecting properties of a glass prism. In 1968, both Otto <sup>(219)</sup> and Kretschmann <sup>(220)</sup> developed prism coupling configurations for SPR excitation based on concepts involving attenuated total reflectance (ATR). In the Otto configuration **Figure 27**, the prism and metal surface are separated by a dielectric (commonly air). The Kretschmann configuration (sometimes called Kretschmann-Raether configuration; **Figure 28** places the metal film between the dielectric and the prism. The latter configuration is less susceptible to Fresnel loss and easier to implement as the metal film can be deposited directly on the prism face. Consequently, the Kretschmann configuration is widely accepted as the superior configuration.

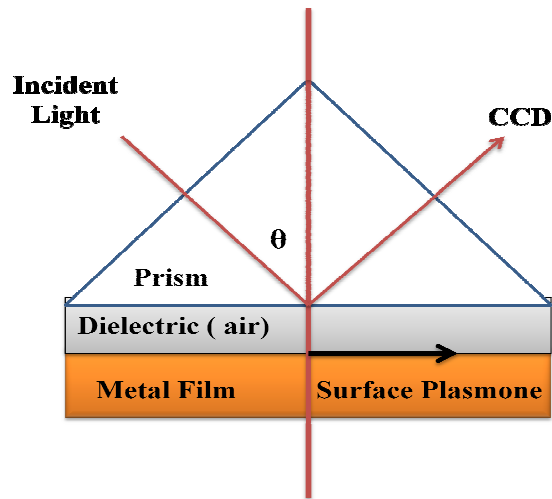


Figure27: Otto configuration.

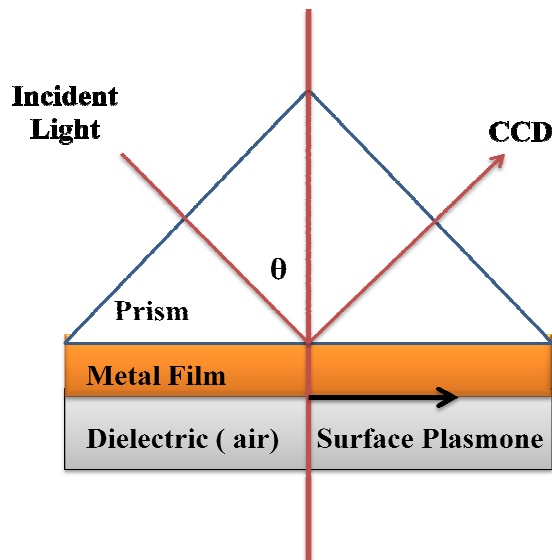


Figure28: Kretschmann configuration.

#### 1.7.2.4. Attenuated total reflectance.

ATR uses the evanescent wave concept of total internal reflection (TIR) to measure the variations that occur when a total internally reflected light beam interacts with a sample. TIR begins with the light beam. Light is a transverse wave composed of an electric field and a magnetic field set perpendicular to each other (hence electromagnetic). When incident light is passed through a higher refractive index ( $n$ ) material to a lower refractive index material, the electrical field part of the light wave penetrates the material with the lower refractive index. The evanescent wave, propagates and decays exponentially along the interface of the two

media, when the angle of incident light is greater than the critical angle, total internal reflection occurs. The critical angle may be calculated as;

$$\theta_{\text{crit.}} = \text{Sin}^{-1} n_2/n_1 \dots\dots\dots(9)$$

Where  $n_1$  is the refractive index of the denser medium and  $n_2$  is the refractive index of the less dense medium<sup>(221)</sup>.

**1.7.2.5. Surface plasmon excitation.**

SPR relies on the ability of a “source” to excite the surface plasmons that reside in the conduction band of a noble-type metal thin film. Standard excitation sources are electromagnetic radiation and electron beams. If a light source is used, it must be p-polarized (parallel to the plane of incidence). Wood’s early work demonstrated that using s-polarized light would not produce the same excitation (in electronic surface plasmons) outcome as p-polarized light<sup>(222)</sup>. Common light sources can be in the far-infrared (10-1000  $\mu\text{m}$ ), mid-infrared (2.5-10  $\mu\text{m}$ ), near-infrared (750 nm-2.5 $\mu\text{m}$ ), or visible light ranges (400-700 nm). Lasers that operate at the desired wavelength are often used since they are monochromatic and coherent.

The light from the source passes through an optically dense medium (usually a prism) at a defined angle and reflects off of the other side of the medium that borders the dielectric or metal film. The reflected light then travels to the detector (typically a charged coupled device (CCD) or a 2D array of photo diodes<sup>(223)</sup>. An evanescent wave propagates (and decays exponentially) from the point of irradiation and stimulates the excitation of surface plasmons. The angle at which the resonant excitation of a surface plasmon occurs is precise and depends on the vector representation of the waves of the surface plasmon ( $K_{\text{sp}}$ ) and the evanescent field ( $K_{\text{ev}}$ ) (calculated using equations 11 and 12).

$$K_{\text{sp}} = \omega_0/C \sqrt{\epsilon_m n_s^2 / \epsilon_m + n_s^2} \dots\dots\dots(10)$$

$$K_{\text{ev}} = \omega_0/C n_g \text{Sin}\theta \dots\dots\dots(11)$$

Where  $\omega_0$  is the frequency of the incident light source,  $C$  is the speed of light,  $n_g$  is the refractive index of the dense medium,  $\epsilon_m$  is the dielectric constant of the metal film, and  $n_s$  are the refractive index of the dielectric).

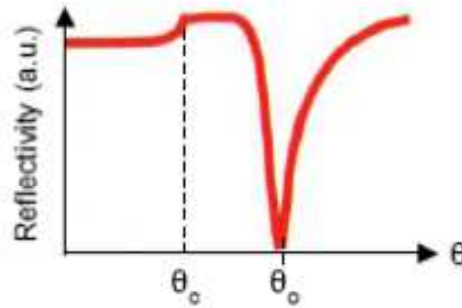


**Figure29.** Typical SPR spectrum.

A wave vector is simply the vector representation of a wave. The magnitude of a wave vector indicates the wavenumber and the direction indicates the direction of wave propagation.

When these two wave vectors are equal, the evanescent wave and the plasmon are coupled and surface plasmon resonance occurs. This resonance can be physically observed by the sudden drop in angle dependent reflectance accompanied by energy loss. This is called the minimum of reflectance and is the typical data point recorded in experimentation. The angle associated with this resonance is referred to as the resonance angle and depends on the refractive index associated with the sample (illustrated in **Figure 29**).

The excitation of a surface plasmon is one of the energy loss interactions that take place within the energy levels. The energy of the surface plasmon may be estimated using the free electron model (Equation 12, where  $n$  is the conduction electron density,  $e$  is the elementary charge,  $m$  is the mass of an electron, and  $\epsilon_0$  is the permittivity of free space) which brought together the Drude model and the Fermi-Dirac statistics from quantum mechanics.

$$\mathbf{k}_{sp} = \mathbf{k} \sqrt{\epsilon_0 n^2 / m \epsilon_0} \dots \dots \dots (12)$$

**1.7.2.6. Metal films.**

The metal films used in SPR fall under the chemical designation of noble metals. By this definition, any noble metal may be used to propagate SPs. A physical definition of noble metals indicates that the metal must have a d-subshell that is completely full. This explanation would limit the noble metals to silver, gold, and copper. Consequently, the most commonly used metals are gold and silver (occasionally copper). Silver films produce the sharpest peaks in SPR spectra when used as the metal interface <sup>(224)</sup>, but they are susceptible to oxidation. Gold is the more stable of the two and has a reasonably sharp SPR peak. The surface chemistry of gold is also quite desirable, allowing for facile attachment of molecules in sensor systems <sup>(225)</sup>.

### 1.7.3. Applications.

#### 1.7.3.1. Thickness of hydrogel thin film and multilayers.

The surface plasmon resonance (SPR) technique has been widely used to monitor changes in the thickness of polymer thin films and multilayers. The SPR is detected through a narrow minimum in the reflection coefficient at a particular angle of incident light. The angle at which the minimum occurs depends strongly on the refractive index and the thickness of the dielectric layer deposited on the metal surface. Because of the evanescent nature of SPR, the probing depth of this technique is limited to layers of two to three hundred nanometres in thickness.

D. Kuckling *et al.* <sup>(226)</sup> have been prepared two hydrogel layers based on photo-crosslinkable poly(dimethyl acrylamide) (PDMAAm) as base layer and poly (*N*-isopropyl acrylamide) (PNIPAAm) as top layer forms a bilayer assembly where, the base layer is highly swollen and the top layer shows temperature responsive swelling. Swelling characterization has been done using a combination of surface plasmon resonance spectroscopy and optical waveguide spectroscopy. The PDMAAm and PNIPAAm within the bilayer assembly retain their swelling behavior, which they showed as a separate layer. Due to the presence of the photo-cross-linker such bilayer films can be patterned to develop surfaces with different properties at different regions.

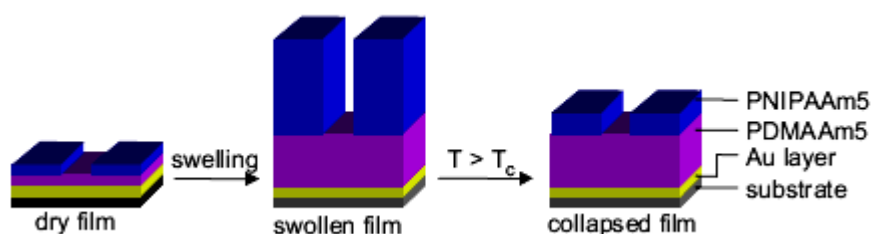


**Figure30:** Schematic representation of a patterned photo-crosslinked bilayer assembly with bottom layer as a hydrophilic layer and top layer as a stimuli- sensitive layer <sup>(226)</sup>.

Frank and coworkers used the SPR technique to study the effects of temperature and hydrostatic pressure on the swelling degree of 4  $\mu\text{m}$  thick (dry state) PNIPAM hydrogel films. They detected broadening of the volume phase transition region and a shift in the transition temperature to higher values with an increase in pressure. It has been demonstrated that the film confinement has a significant effect on the transition temperature and the swelling degree <sup>(159)</sup>.

Willner and coworkers measured the kinetics of swelling and shrinking of the glucose-sensitive hydrogel film (acrylamide copolymer containing boronic acid groups) using the SPR

technique<sup>(164)</sup>. They found that the film swelling upon addition of glucose was rapid, whereas the shrinking as a result of the glucose depletion was a slow process (tens of minutes), which indicated strong interactions between the sugar molecules and the boronic acid groups.

In several studies, hydrogel thin films were used as platforms for immobilization of various bioreceptors for SPR monitoring of biomolecular binding events, including DNA hybridization, DNA-protein, protein-protein, and other receptor-ligand pair associations<sup>(227–229)</sup>. The hydrogel films (usually carboxylated dextran and ethylenediamine) enable better surface coverage and adhesion of the receptor groups than is usually achieved when they are directly immobilized on a metal surface. Being highly hydrophilic, the hydrogel layers demonstrate low non-specific adsorption of proteins on the detector surface. Furthermore, protein bioreceptors are less prone to denaturation on hydrogel substrates<sup>(228)</sup>.

A metallic thin film with a lithographically manufactured periodic array of cylindrical nanoscopic wells (so-called plasmonic crystal, **Figure 30a**) is another promising sensing platform that does not require a prism to excite the SPR by incident light. The plasmonic crystal exhibits a complex, multi-peak transmission spectrum in the visible and near-infrared regions. Mack *et al.* immobilized a ~500 nm thick pH-responsive hydrogel film (copolymer containing acrylic acid groups) on the surface of the plasmonic crystal **Figure 31b**<sup>(230)</sup>. They found that the pH-induced swelling transitions occurring in the hydrogel film strongly altered the positions and intensities of plasmon resonance peaks in the spectra. Summing the absolute magnitudes of the difference spectra (as referenced to a spectrum acquired at a specific pH value) over all wavelengths yielded an integrated plasmonic response that directly correlated with pH-dependent changes in the properties of the hydrogel film **Figure 30c,d**.

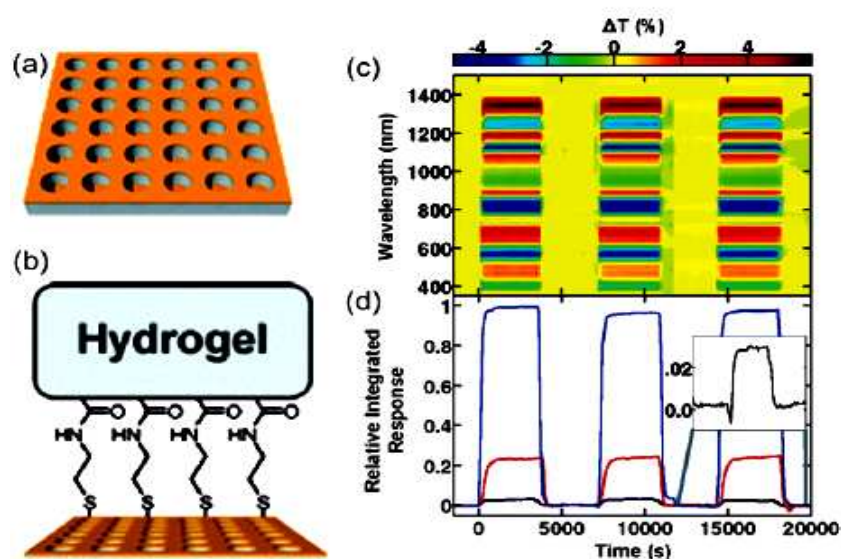


**Figure31:** Schematic representation of a plasmonic crystal before (a) and after modification with a pH-responsive hydrogel layer (b). (c) Spectral sensitivity map consisting of difference spectra from the hydrogel modified crystal referenced to  $t = 0$  s, after which the analyte solution was cycled between pH 7.86 and 1.44. (d) The integrated plasmonic response corresponding to reversible changes in analyte solution from pH 7.86 to 1.44 (blue), 6.42 to 5.13 (red), and 5.76 to 5.66 (black). The smallest pH change (0.10) is well differentiated from the stable background signal (inset) <sup>(230)</sup>.

The SPR can also be excited in noble metal nanoparticles by exposing them to light of a specific wavelength. This phenomenon, known as localized surface plasmon resonance (LSPR), is observed for surface immobilized nanoparticles (islands) and colloidal dispersions. The LSPR leads to a pronounced extinction peak (or peaks) in a transmission UV-vis spectrum (also referred to as a T-LSPR spectrum) that is noticeable even for nanoparticle monolayers and sub-millimolar concentrations of nanoparticle dispersions. The intensity and position of the peak depend on the size and shape of nanoparticles, their size distribution and spatial organization, shell thickness (for the core-shell particles), and the dielectric constant of the surrounding medium <sup>(231,232)</sup>. If the metal nanoparticles are coupled with a polymer, the stimuli-induced changes in the polymeric material can be transformed into an optical signal. Although T-LSPR spectroscopy was widely used for the registration of molecular recognition events, it was only recently employed for sensing stimuli-induced changes in polymeric materials.

Lee and Perez-Luna reported on the reversible aggregation of gold colloidal nanoparticles linked to the surface-grafted carboxylated dextran chains in solvents of different polarity and the associated changes in the optical properties <sup>(233)</sup>. The observed shifts in the position of the plasmon resonance peak were assigned to changes in the refractive index of the hydrogel and in the strength of electromagnetic inter-particle coupling.

Lowe and coworkers have developed a range of hydrogel based holographic sensors for detecting bacterial spores <sup>(160)</sup> measuring pH, <sup>(234)</sup> ionic strength, <sup>(235)</sup> and the content of ethanol in aqueous solutions, <sup>(236)</sup> as well as the concentration of metal ions, <sup>(237,238)</sup> glucose, <sup>(239)</sup> and metabolites of enzymatic reactions <sup>(240)</sup> Holographic diffraction gratings comprised of fringes of silver particles were generated in ~10 mm hydrogel films (mainly poly (2-hydroxyethyl methacrylate) (PHEMA) copolymers containing analyte-sensitive groups and, in one study, immobilized enzymes) and acted as a tunable wavelength filter. The operation principle was based on recording a reflection spectrum that was sensitive to the swelling degree of the hydrogel.

Integrated optical sensor chips suitable for high-resolution pH measurements have been fabricated by Kunz and coworkers<sup>(241)</sup>. Compact dual-channel chipped grating coupler sensor chips were coated with the 90 to 300 nm thick photo patterned films of pH-responsive hydrogels (photo-crosslinkable PHEMA copolymer containing amino groups). The sensor detected changes in a refractive index occurring upon swelling and shrinking of the hydrogel. A resolution  $\Delta\text{pH} < \pm 1.1 \times 10^{-4}$  (at pH 7.5) has been reported.

### **1.7.3.2. Biosensor applications.**

Biosensors have been impacting the sciences for many years. L. D. Clark and his oxygen electrode began the biosensor movement in 1953<sup>(242)</sup>. The first SPR biosensor was reported in 1983 by Liedberg *et al.*<sup>(243)</sup> Their biosensor was originally designed to detect the irreversible binding of antihuman  $\gamma$ -globulin (a-IgG) to human  $\gamma$ -globulin (IgG). The experiments were successful in establishing SPR as a highly sensitive candidate for detection in biosensors. Within a year Biacore was conceived with the help of the group from Linköping (Liedberg *et al.*), becoming the first company to develop the SPR technology for commercial biosensing purposes. Today, Biacore is a subsidiary of GE Healthcare and offers an array of sensor chips and instruments based on the aforementioned technology.

### **1.7.3.2. Binding events.**

One of the main uses of SPR in biosensors is the monitoring of a binding event. In biosensor applications there are two most commonly two major parts involved in monitoring a binding event: the biological recognition component (BRC) and the recognized component (RC). In the Liedberg experiment IgG was the BRC and a-IgG was the RC.<sup>20</sup> The BRC is immobilized on the metal film. The minimum of reflectance is then measured by SPR with the BRC adsorbed. Next, the RC is allowed to come in contact with the film surface and interact. The minimum of reflectance is measured after this step. The difference between the two minima allows for facile conclusion that the binding event has taken place<sup>(221)</sup>.

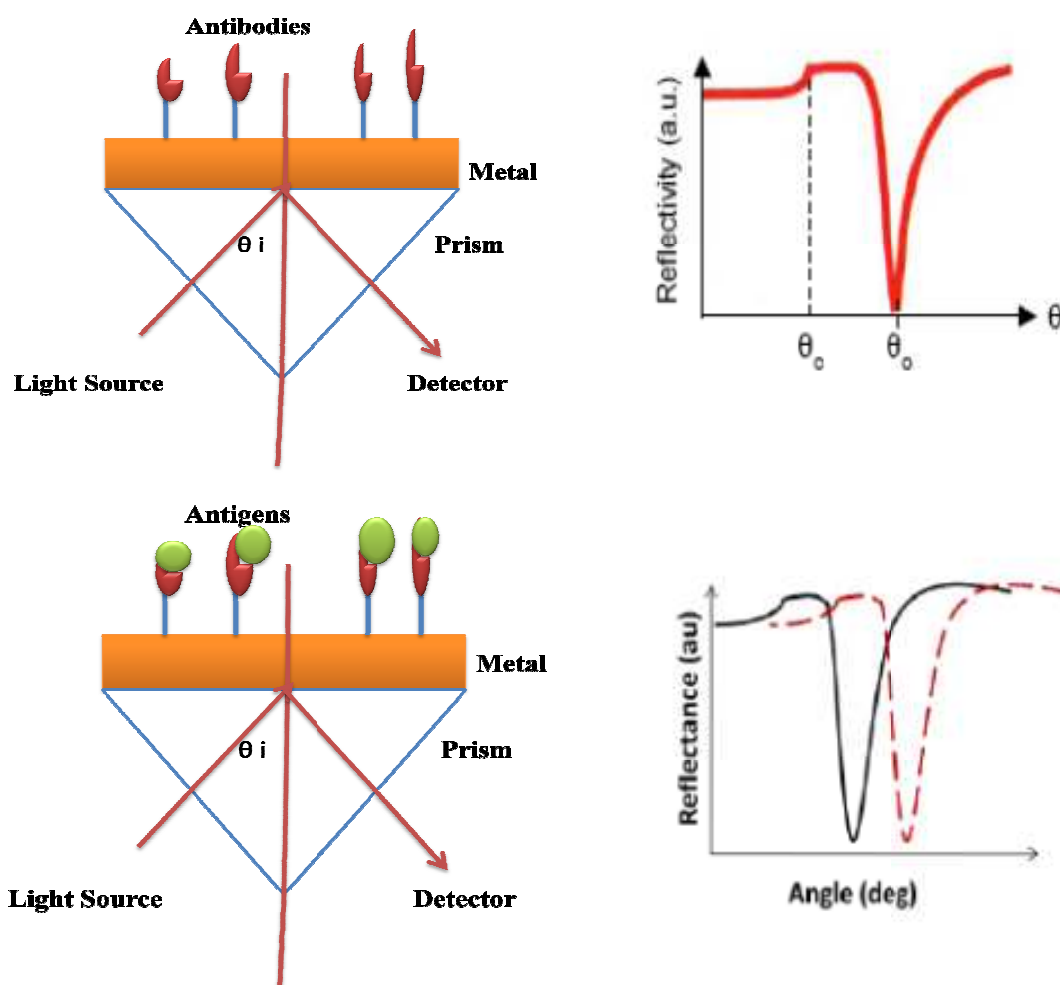


Fig.32. SPR monitoring of bending event.

### 1.7.3.3. Quantitative applications of SPR.

The adsorbate film thickness can be calculated as an average value. A simple method for converting local reflectivity changes measured in surface plasmon resonance (SPR) microscopy to effective layer thicknesses and absolute surface coverages of adsorbed species is presented. For a range of high-contrast angles near the SPR resonance where the local metal surface's reflectivity changes linearly with angle, the change in reflectivity at fixed angle is proportional to the change in effective refractive index ( $\epsilon_{\text{eff}}$ ) near the surface. This change in ( $\epsilon_{\text{eff}}$ ) can be converted to absolute adsorbate coverage using methods developed for quantitative SPR spectroscopy. A measurement of the change in reflectivity due to changes in refractive index of bulk solutions, i.e., percent reflectivity change per refractive index unit (RIU), is the only calibration required<sup>(244,245)</sup>. Stenberg *et al.* have determined protein surface concentration using SPR. The SPR response measured defined as the change in surface plasmon resonance angle, was correlated to the absolute amount of protein surface

concentration <sup>(246,247)</sup>. The general procedure can be shortly described in **Figure 33**, and equation 13 <sup>(248)</sup>.

$$\Delta\theta_0 = C1 \Delta n + C2\Delta d \quad \dots\dots\dots (13)$$

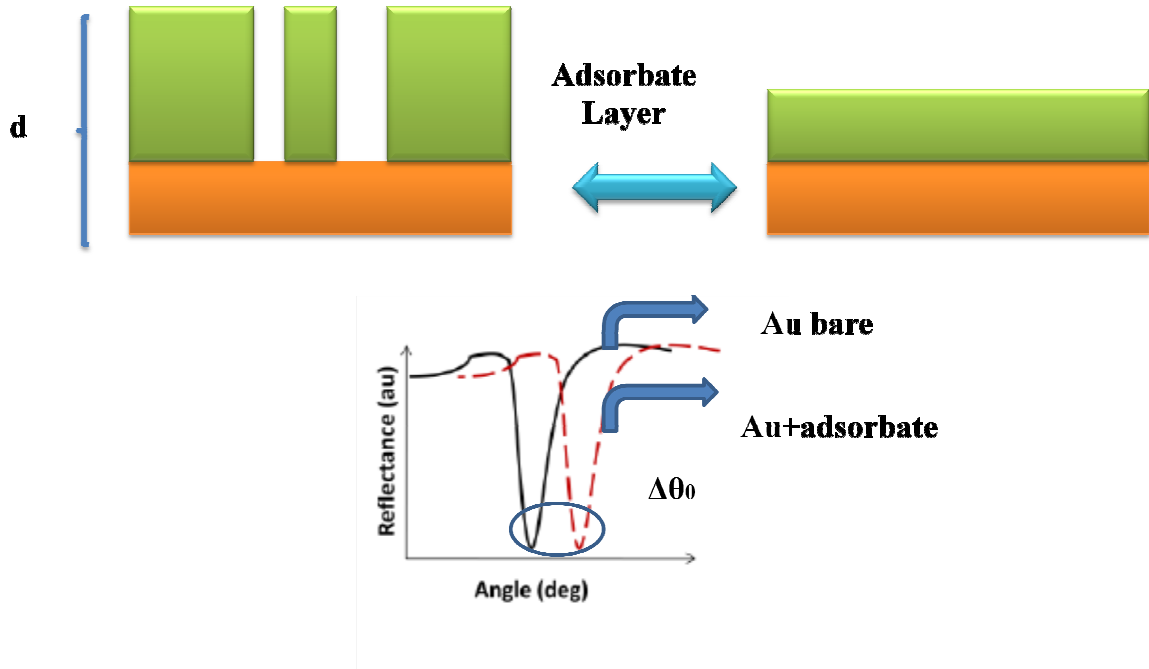


**Figure33:** Adsorbante layer and SPR for Au-bare and Au-adsorbate.

**1.7.3.4. Kinetics.**

Biosensors are not merely limited to sensing binding events. The kinetics of systems are frequently studied using SPR biosensors with flow-through ability. In 1997 at the National Insitutes of Health (NIH), Schuck utilized SPR to investigate the binding affinities and kinetic constants involved with binding events between biomolecules<sup>(249)</sup>. His extensive studies approached the problems associated with kinetic studies and proposed ways of minimizing their effects.

The rate of change of the SPR angle as a binding event occurs provides the kinetic parameters. Pseudo first-order kinetics is assumed, and the change in SPR angle is recorded as a function of time <sup>(223)</sup>. The reaction is performed at differing concentrations. There will be a rate constant for both the formation of the bound and the dissociated complex. The ratio of the two ( $KD=k_{association}/k_{dissoci}$ ) rate constants provides the dissociation constant (KD).

## **1.8. Adhesion**

### **1.8.1. Introduction**

Ideally, the adhesion linking layer provides a stable link between substrate material and immobilization matrix and also shields the substrate from the sample buffer with a dense and homogeneous film. With respect to the exponentially decaying strength of the evanescent field, thicknesses above 10 nm would be caused by swelling effects. On the other hand, thicknesses below 1 nm usually result in unstable and inhomogeneous coatings, so preferably the thickness of adhesion linking layer is between 2 and 5 nm. Finally, the refractive index of the adhesion linking layer should be lower than that of the substrate material. Depending on the surface-exposed material of the biochip substrate typically gold or glass different routes are chosen to address the above requirements <sup>(250)</sup>.

### **1.8.2. Adhesion linking layers for metal surfaces**

The cationic surfaces of many transition metals are soft electron pair acceptors and exhibit a strong affinity towards soft electron pair donors such as thiols, disulfides and thioethers. Due to the negative imaginary part of their electromagnetic wavefunction in combination with their chemical inertness, gold, silver or platinum are suited for use in SPR and as electrochemical sensors. Alkyl derivatives of above-mentioned functional groups with a chain length of >10 carbon atoms assemble spontaneously on such substrates and form self-assembled monolayers (SAMs) with high packing densities <sup>(251)</sup>. Shorter thiols also assemble, but the SAMs are not well defined and relatively unstable <sup>(252)</sup>. Monofunctional mercaptoalkyls yield hydrophobic surfaces having contact angles higher than 100°. Bifunctional derivatives form monolayers with defined chemistry which are useful intermediates for covalent coupling of ligands or for further derivatization <sup>(253)</sup>. Typical examples for such compounds are 16-hydroxyhexadecane-1-thiol and the corresponding carboxylated compound 15-carboxypentadecane-1-thiol. The adsorption of these long-chain thiols usually takes place in 1–5 mM ethanolic solutions in 8–24 h. Although the formation of a monolayer is almost complete after a few minutes, the initially formed monolayer is not well ordered and contains many gauche defects within the chains. Over time, the layer becomes more ordered and well packed. In addition to thiols, dithiols and thioethers are also suitable, as all of these groups exhibit sufficiently high adsorption energy on surfaces of Group 7–12 metals, which is typically in the range 40–50 kJ mol<sup>-1</sup> – 50% of the strength of a C–C bond. The stabilizing characteristics of the resulting surface, i.e. its inertness against adsorption of proteins and other sample components, depend critically on the functionality of

the surface exposed to the sample. However, the long term stability of SAMs is limited as they show desorption after a few weeks of exposure to buffer or serum <sup>(254)</sup>.

A less common approach for the derivatization of noble metal surfaces is the adsorption of positively charged or mercapto-derivatized polymers to the negatively charged metal surface. Due to electrostatic attraction and the cooperative effect of several adsorption sites, stable monolayers can be formed.

### **1.8.3. Adhesion linking layers for plastics**

Although at present gold and glass dominate as chip surface materials used for direct optical biosensors, it is foreseeable that future low-cost devices will increasingly rely on injection molded consumables made from, e.g., poly(methyl methacrylate) (PMMA), polystyrene, polycarbonate or cycloolefin copolymers (COC). The surface of these materials is a complex, heterogeneous mix of amorphous and crystalline regions consisting of mostly hydrophobic polymer chains which often slowly migrate and rearrange over time. Modification of this kind of substrate usually begins with an oxidative pretreatment either via a wet-etch step <sup>(255)</sup> or more reproducibly – oxygen plasma treatment <sup>(246)</sup>. The immobilization matrix can then be coupled either directly or via subsequently adsorbed stabilizing polymer layers <sup>(256)</sup>. Adhesion linking layers can be further applied via plasma deposition, allowing fast and simultaneous processing of regardless of the substrate material, large batch volumes, and can yield homogeneous coatings with different chemical functionalities at relatively low cost per unit. Typical thick film preparation methods such as dip or spin coating are less suited as the necessary coating thickness of a few nanometers is difficult to control reproducibly with these techniques.

# *Chapter(2)*

## *Experimentals*

## 2. Experimentals

### 2.1. Introduction

This chapter describes the experimental procedures for synthesizing and characterizing various photo-crosslinkers, adhesion promoters and polymers. The chapter is divided in twelve sections. **Section 2.2** provides information about the reagents and solvents used in this study. The instrumental part is described in the **Section 2.3** with special emphasis on SPR (Surface Plasmon Resonance) spectroscopy and Optical Waveguide Spectroscopy (OWS). The **Section 2.4** presents synthesis and characterization of photo-cross-linkers. **Section 2.5** monomers synthesis and **section 2.6** for adhesion promoter. **Sections 2.7-2.11.;** are for polymers synthesis. The last section briefly describes the process of film formation, and determination of refractive index from SPR data.

### 2.2. Reagents and solvents

N-isopropylacrylamide (NIPAAm; Acrōs) was recrystallized from distilled hexane.

- ❖ N,N-dimethylacrylamide (DMAAm; Aldrich), 2-hydroxyethylmethacrylate (HEMA; Acrōs) and ethoxy ethyl glycidyl ether were distilled under vacuum and stored at low temperature (- 20°C).
- ❖ Di-tert-butylidicarbonate ((boc)<sub>2</sub>O, Acros), acryloyl chloride (AcrCl, Merck), sodium carbonate (Na<sub>2</sub>CO<sub>3</sub>) and trifluoroacetic acid (TFA) were of reagent quality grade and used as received.

Diaminoethane (Fluka), dimethyl maleic anhydride (98%, Aldrich), 1M ZnEt<sub>2</sub> in hexane (Aldrich), sodium dodecyl sulfate (SDS), acrylic acid (99.5%, Acrōs), N,N'-dicyclohexylcarbodiimide (DCC, Merck), (Acrōs), thioxanthone (Acrōs), 2-hydroxyethylamine (Acrōs), (DMAP, Fluka), triethylamine (Merck), thiolacetic acid (Merck) and allyl amine (Merck) were used as received, Vanillin (99% Acrōs), 4-aminohippuric acid (99% Acrōs), N-hydroxysuccinimide (99% Merck), 4-hydroxyacetophenone (98% Acrōs), diethylamine (Merck), N,N-dimethylethane-1,2-diamine(Merck).

- ❖ 2,2'-azobis(isobutyronitrile) (AIBN) was recrystallized from methanol prior to use.
- ❖ Silica gel 60 (0.040-0.063mm, Merck) was used as received.
- ❖ Sodium chloride (J. T. Baker), sodium sulfate (Merck) sodium carbonate (Grüssing) magnesium sulfate (Merck), hydrogen peroxide (J. T. Baker) and sulphuric acid (Merck) were used as received.

- ❖ Solvents: 1,4-dioxane, toluene, dichloromethane, petroleum ether, diethylether, n- hexane, ethylacetate, chloroform, N,N-dimethylformamide (DMF), tetrahydrofuran (THF), glacial acetic acid (Appli Chem), N-methyl-2-pyrrolidone (NMP), dimethylsulphoxide (DMSO), ethanol, pyridine, 2 ethoxy ethylacetate and butanone.
- ❖ All these solvents were dried and purified using standard procedures or used as received.

### **2.3 Instrumentation:**

#### **NMR spectroscopy**

The  $^1\text{H}$  NMR and  $^{13}\text{C}$  NMR spectra were recorded on a Bruker AVANCE 500 spectrometer (500 MHz for  $^1\text{H}$  NMR and 125 MHz for  $^{13}\text{C}$ ).

#### **DSC**

Measurements were carried out with a micro DSC III from setaramto to determine the  $T_c$  of the polymer solutions. The DSC thermograms of the polymer solutions were recorded at a heating rate of  $5\text{ }^\circ\text{C}/\text{min}$ . The polymer concentration was 50 mg/ml in deionised water and the onset value of the transition was taken as  $T_c$ .

PERKIN ELMER Differential Scanning Calorimeter Pyris 1 was used for the determination of  $T_g$  of solid polymers. The thermogram was recorded at heating and cooling rate of  $5\text{ }^\circ\text{C}/\text{min}$ .

#### **Gel-Permeation Chromatography (GPC)**

Molecular weight ( $M_n$ ) and molecular weight distribution ( $M_w/M_n$ ) of all polymers, copolymers and terpolymers were determined by Gel-Permeation Chromatography with Knauer DMAc, Polymer samples (6 g/L) were prepared with 2,6-di-tert-butyl-4-methylphenol (BHT) as an internal standard. The measurements were performed at  $30\text{ }^\circ\text{C}$  and calibrated with PMMA.

#### **UV-vis.Spectroscopy**

UV-vis. Spectra were recorded on UV-vis. Perkin Elmer Lambda 45 Spectrometer. For the estimation of photo-crosslinker content, 1 mol% of polymer solution in methanol for NIPAAm, DMAAm and their copolymers and terpolymers, and THF was used for HEMA samples.

UV.Spectroscopy was also used for the determination of LCST of NIPAAm polymers, using metal covet stand and water cycle injected from water bath (Julabo F12), with thermostat, and cooling system. Over manual thermostat (TEMPERATUR-MESSGERÄT MD 3040, BECKMANN+EGLE) was also used to adjust the actual temperature inside the solution. The polymer solution was 1 wt% in water.

### **IR Spectroscopy**

IR spectras were recorded on VERTEX 70 Fourier transform infrared instrument. The samples were milled with KBr pellet. Some samples were measured as solution in water and pH11, also the solution was added to KBr.

### **Spin coating**

Spin coater model G3P-8 SpinCoat (Speciality Coating System, INT.) was used to prepare thin film (~ 200 nm dry thickness) on the glass substrate with 250 rpm for 30 sec and 2000 rpm for 140 sec. thicker films were obtained by increasing the polymer concentration to 10% and using 1000 rpm.

### **UV Lamp**

UV lamp (OSRAM, 100W, Hg lamp, wavelength > 250 nm) equipped with an optical lens, a mirror and a double wall glass reactor connected to water circulating thermostat was used for photo-crosslinking process.

UV lamp (Dr. Hönle, metal halide high pressure lamp, wavelength >310 nm) equipped with H-1 filter.

### **Surface Plasmon Resonance Spectroscopy (SPR) and Optical Waveguide Spectroscopy (OWS).**

SPR along with OWS were used to determine the film thickness and swelling ratios of photo-crosslinked thin films. This technique provides an in dept information about the polymer in thin films and at interfaces. It is a non-destructive and surface sensitive technique due to the evanescent field of the surface plasmon (SPs). Method does not require labeling and is well suited for solid-air or solid-liquid interfaces and allows a real time analysis of changes in the probed zone. Excitation of the surface plasmon results in simultaneous determination of film thickness and refractive index of hydrogel film.

Surface plasmon is an electromagnetic wave traveling along the interface between the metal and a dielectric. For SPs to exist at such an interface, the real part of the dielectric constant of the two media must be of opposite sign. This condition is met in the infrared (IR)-visible region for air / metal and water / metal interfaces (where the  $\epsilon$  of metal is negative and that of air or water is positive). SPs cannot be excited directly at planar air / metal or water / metal interfaces because momentum matching condition cannot be satisfied. Therefore, it becomes necessary to use a prism-coupling arrangement.

He-Ne laser beam with a wavelength of 632.8 nm was used for excitation of SPs in Kretschmann configuration. The substrate was LaSFN9 glass slides with 45 nm gold film.

## Experimentals

The Au film was deposited PVD-Anlage (physical vapor deposition), company (tectra GmbH). After adsorption of DMITAc adhesion promoter on Au, photo-cross-linkable polymer solution was spin coated and irradiated with UV light as described in **Section 12**. For measuring temperature dependent swelling a set up was constructed. 3-4mL of distilled water was injected manually to the SPR cell (SPR cell consists of an sample holder, LaSFN9 with gold coating, a prism, water bath to maintain temperature). The temperature inside the cell was measured with a thermocouple of 0.1 °C accuracy.

Film thickness and swelling were determined in distilled water, and phosphate-citrate buffer solution for preparation of different pH from pH2 to pH8, and phosphate buffer solution for pH9 to pH11.

- ❖ Preparation of pH2-pH8 using phosphate-citrate buffer solution. A solution **A** of 35.6g of dibasic phosphate ( $\text{Na}_2\text{HPO}_4 \cdot 2\text{H}_2\text{O}$ ) was dissolved in 1L distilled water. A solution **B** of 21,014g of citric acid ( $\text{C}_6\text{H}_8\text{O}_7 \cdot \text{H}_2\text{O}$ ) was dissolved in 1L of distilled water, both solutions were used in the adjustment of pH-solutions are cleared in the table below.

**Table 2:** The amounts used for preparation of pH buffer solutions.

pH	Solution A (ml)	Solution B (ml)
pH2.2	2	98
pH3	20.5	79.5
pH5	51.5	48.5
pH8	97.2	2.8

After addition all pH-buffer solutions were measured using pH-meter model VWR pH100.

- ❖ Preparation of pH9-pH11 using phosphate buffer solution. A solution of 0.1M disodium hydrogen phosphate 14.2g in 1L distilled water, 0.1M HCl, and 0,1M NaOH, both solutions were used in the adjustment of pH-solutions are clear in the table below,

❖ **Table 3:** The amounts used for preparation of pH buffer solutions.

pH	Phosphate solution (ml)	0.1 M HCl (ml)	0.1 M NaOH (ml)
pH9	95.50	4.5	-
pH10	96.64	-	3.36
pH11	96.53	-	4.7

After additions all pH-buffer solutions were measured using pH-meter model VWR pH100.

The laser beam after reflecting from the gold-coated sample with a prism (mounted on a goniometer) was monitored by means of a photodiode detector. Time dependent SPR changes in gel were observed by SPR kinetic scans where the reflected intensity versus time scans were recorded at a fixed angle. Reflected intensity versus angle scans were monitored by varying the angle of incidence from 18° to 90° for dry polymer film and 40° to 90° for swollen hydrogel film. When the momentum and energy of the laser beam and the surface plasmon excitation is matched, minima  $\theta_{SPR}$  is observed. Thickness and the refractive index of the polymer layer determine the angle of excitation. Small size (in terms of thickness) of hydrogel layer results in faster response, in the order of seconds, however it takes some time (min) to change temperature in SPR cell. After each angular scans, an equilibrium time of 15-20 minutes was given to obtain a desired temperature in SPR cell.

Optical Waveguide Spectroscopy utilizes the same principle and was used when the film were sufficiently thick (>500 nm dry thickness). Additional minima were observed, corresponding to the laser beam coupling into waveguide mode. Resulting scans from SPR and OWS were fit to Fresnel calculations for determination of refractive index and thickness. Refractive index was converted to polymer fraction  $\chi_p$ , which finally gave volume degree of swelling ( $1/\chi_p$ ) according to the linear equation;

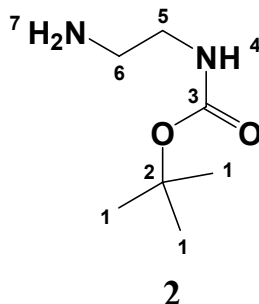
$$n = 0.00190 \chi_p + 1.33123 \dots \dots \dots (14)$$

The plot of refractive index versus temperature was fit to a sigmoidal curve and the inflection point of the curve was defined as the transition temperature for all thermoresponsive thin hydrogel films. Laser beam covers an area of around 1 mm<sup>2</sup> and SPR data obtained was an average over this size. A slight difference in the film thickness and refractive index resulted in broader minima than those of the Fresnel calculations.

## 2.4 Synthesis of monomers and photo-crosslinkers

### 2.4.1. Synthesis of acrylate photo-crossliker ( DMIAAm )

#### Step1: Synthesis of tert-butyl-N-(2-aminoethyl)-carbamate



The first step involve the protection of amino group of diaminoethane using *di-tert-butylidicarbonate*

#### Procedure:

21.825g (0.1mol) of di-tert-butylidicarbonate in 250 mL dest. 1,4-dioxane was added slowly to a stirred solution 46.465g (0.7731mol) diaminoethane in 100 mL dest. 1,4-dioxane over period 3h at room temperature. The reaction mixture was allowed for stirring 2d. The precipitate was filtered, and the excess of 1,4-dioxane and diaminoethane was evaporated under vacuum. 300 mL dest. water was added, and again the precipitate was filtered. The aqua's solution was saturated with sodium chloride and extracted 5 times with 150ml dichloromethane. The organic phase was dried with sodium sulfate and then the excess of solvent was removed under vacuum. The compound was characterized by  $^1\text{H}$  NMR,  $^{13}\text{C}$  and IR spectroscopy.

**Yield:** 87% (lit.: 80%)<sup>(257)</sup>.

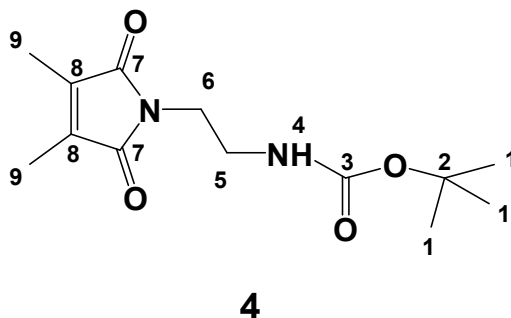
**Physical state:** colorless viscous liquid.

$^1\text{H}$  NMR, (500 MHz,  $\text{CDCl}_3$ ):  $\delta$  (ppm) = 1.12 (s, 9H, 1- $\text{CH}_3$ ), 1.33 (s, 2H, 7- $\text{NH}_2$ ), 2.73 (m, 2H, 6- $\text{CH}_2$ ), 3.11 (t, 2H, J= 5.5 Hz, 5- $\text{CH}_2$ ), 5.1 (s, 1H, 4-NH).

$^{13}\text{C}$ -NMR (125 MHz,  $\text{CDCl}_3$ ):  $\delta$  (ppm) = 28.36 (3C, 1- $\text{CH}_3$ ), 41.79 (1C, 6- $\text{CH}_2$ ), 43,1 (1C, 5- $\text{CH}_2$ ), 78.3 (1C, 2-C ), 156,23 ( 1C, 3-C=O).

IR (KBr):  $\nu$  ( $\text{cm}^{-1}$ ): 3342 (m) (N-H), 2963 (s) ( $\text{CH}_2$ ,  $\text{CH}_3$ ), 1706 (C=O), 1525(s) (N-H).

**Step2: Synthesis of N-[2'-(3,4-Dimethyl-2,5-dioxo-2,5-dihydro-pyrrol-1-yl)-aminoethyl]-tert-butylcarbonat.**



**Procedure:**

13,05g (81.5mmol) of tert-butyl-N-(2-aminoethyl)-carbamate (**1**) in 150 mL dry toluene was added slowly to stirred solution of 10.27 (81.5mmol) dimethyl maleic anhydride in 200mL dry toluene. The reaction mixture was refluxed at 130-135°C in oil bath for 3h, and using water trap to remove water as a side products. The resultant solution was filtered and then evaporated under reduced pressure. The solution was precipitated using 500 mL cold n-pentane, then filtered and washed two times with n-pentane. The product was dried under vacuum overnight.

**Yield %:** 96% (lit.: 98%)<sup>(257)</sup>

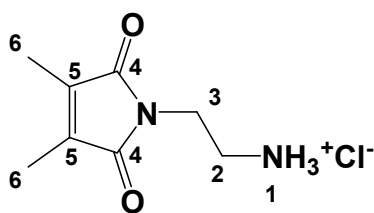
**Physical state:** brownish white solid.

**<sup>1</sup>H NMR (500 MHz, CDCl<sub>3</sub>):** δ (ppm) = 1.41(s, 9H, 1-CH<sub>3</sub>), 1.96 (s, 6H, 9-CH<sub>3</sub>), 3.31 (dd, 2H, <sup>3</sup>J = 4.6 Hz, 5-CH<sub>2</sub>), 3.37 (t, 2H, <sup>3</sup>J = 5.8 Hz, 5-CH<sub>2</sub>), 4.77 (s, 1H, NH).

**<sup>13</sup>C-NMR (125 MHz, CDCl<sub>3</sub>):** δ (ppm) = 8.66 (2C, 9-CH<sub>3</sub>), 28.29 (3C, 1-CH<sub>3</sub>), 37.99 (1C, 6-CH<sub>2</sub>), 39.80 (1C, 5-CH<sub>2</sub>), 79.34 (1C, 2-C), 137.29 (2C, 8-C=C), 155.98 (1C, 3-C=O), 172.20 (1C, 7-C=O).

**IR (KBr):** ν (cm<sup>-1</sup>): 3395 (s) (N-H), 2983 (s) (CH<sub>2</sub>, CH<sub>3</sub>), 1716 (C=O), 1683(s) (C=C).

**Step3: Synthesis of N-[2-(3,4-dimethyl-2,5-dioxo-2,5-dihydro-pyrrol-1-yl)]-ethylamino hydrochloride**



5

**Procedure:**

In two neck flask fitted with drying tubes and dropping funnel. 15g (0.056mol) of (4) was suspended in 110 mL ethylacetate, the solution changed to brown. 9.26 mL (90.91 mmol) HCl conc. was dropped during 45min., and then the reaction mixture was stirred overnight at RT. The precipitate was filtered and washed with ethylacetate. The solid product was dried overnight under vacuum.

**Yield %:** 96% (lit.: 95%)<sup>(257)</sup>.

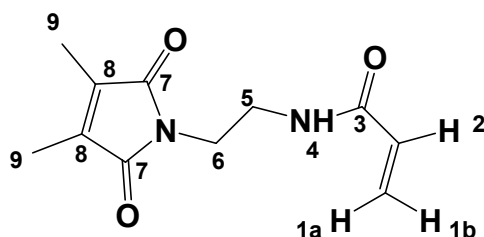
**Physical state:** brownish white solid.

**<sup>1</sup>H NMR (500 MHz, DMSO-*d*<sub>6</sub>):**  $\delta$ (ppm) = 1.91 (s, 6H, 6-CH<sub>3</sub>), 2.96 (br.; 2H, 2-CH<sub>2</sub>), 3.65 (t, 2H, <sup>3</sup>J = 6.1Hz, 3-CH<sub>2</sub>), 8.14 (s, 3H, 4NH<sub>3</sub><sup>+</sup>).

**<sup>13</sup>C-NMR (125 MHz, CDCl<sub>3</sub>):**  $\delta$  (ppm) = 8.92 (2C, 6-CH<sub>3</sub>), 35.55 (1C, 2-CH<sub>2</sub>), 39.87 (1C, 3-CH<sub>2</sub>), 137.44 (2C, 5-C=C), 172.09 (2C, 4-C=O).

**IR (KBr):**  $\nu$  (cm<sup>-1</sup>): 2995 (s) (CH<sub>2</sub>, CH<sub>3</sub>), 2005 (m) (NH<sub>3</sub><sup>+</sup>), 1705 (C=O), 1616(s) (C=C).

**Step4: Synthesis of N-[2-(3,4-dimethyl-2,5-dioxo-2,5-dihydroxy-pyrrol-1-yl)]-ethylacrylamide**



6

**Procedure:**

In three neck flask fitted with reflux condenser for cooling, and under argon. 7g (0.034 mol) of (**5**) was suspended in 300ml dry THF, then allowed to strong stirring. 13.83g (0,13mol) of TEA was added slowly, then the mixture was allowed to cool to 0-5°C and 7.74g(0.085mol) acryloylchloride was added slowly during 1h.; the reaction mixture was stirred at RT.; 6h. The precipitate was filtered and washed two times with 50 mL THF. The solvent was removed under reduced pressure then, the product was extracted by CH<sub>2</sub>Cl<sub>2</sub> and three times with 30 mL dest. water, two times with 30 mL sodium bicarbonate solution and two times with 0.1M HCl. The organic phase was dried with MgSO<sub>4</sub> overnight, then filtered and the product was purified by column chromatography, using ethylacetate as eluent R<sub>f</sub>= 0.32.

**Yield %:**60% (lit.: 59%)<sup>(257)</sup>.

**Physical state:** yellowish white solid.

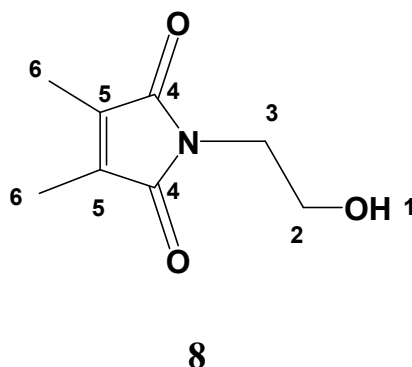
**<sup>1</sup>H NMR ( 500 MHz , CDCl<sub>3</sub>):** δ(ppm) =1.96 (s, 6H, 9-CH<sub>3</sub>), 3.51 (q, 2H, J=3.7 Hz, 5-CH<sub>2</sub>), 3.69 (t, 2H, J = 3.6 Hz, 6-CH<sub>2</sub>), 5.62 (dd, 1H, <sup>2</sup>J = 1.4 HZ, <sup>3</sup>J = 8.9 Hz, 1a-CH), 6,07 (dd, 1H, <sup>3</sup>J=10.7 Hz, <sup>3</sup>J = 17 2-CH), 6.20 (s, 1H, 4-NH), 6.24 (dd, 1H, <sup>2</sup>J = 1.4 HZ, <sup>3</sup>J = 9.3 Hz, 1b-CH).

**<sup>13</sup>C-NMR (125 MHz, CDCl<sub>3</sub>):** δ (ppm) =8.71 (2C, 9-CH<sub>3</sub>), 37.39 (1C, 5-CH<sub>2</sub>), 39.70 (1C, 6-CH<sub>2</sub>), 126.27 (1C, 1-CH<sub>2</sub>), 130.83 (1C, 2-CH), 137.50 (2C, 8-C=C), 165.78 (1C, 3-C=O), 172.45 (2C, 7-C=O).

**IR (KBr):** ν (cm<sup>-1</sup>): 3300 (s) (NH), 3080-2945 (s) (CH<sub>2</sub>, CH<sub>3</sub>), 1706 (C=O), 1646(s) (C=C).

## 2.4.2. Synthesis of dimethylmaleimidoacrylate (DMIA).

*Step1: Synthesis of dimethylmaleimido ethanol or 1-(2-hydroxyethyl)-3,4-dimethyl-1H-pyrrole-2,5-dione.*



### Procedure:

In round bottom flask with water trap to collect water; 12.623g (0.206 mol) of 2-aminoethanol was added to stirred solution of 12.611g (0.1 mol) dimethylmaleic anhydride in 300 mL toluene. The mixture was refluxed at the boiling point of solvent about 135°C in oil bath for 4h. The solution was cooled to RT. The solvent was evaporated under reduced pressure. The product was purified by TLC using 1:1 n-hexane: ethylacetate as eluent and silica ( $R_f = 0.32$ ).

**Yield %:** 72% (lit.: 74%)<sup>(48)</sup>.

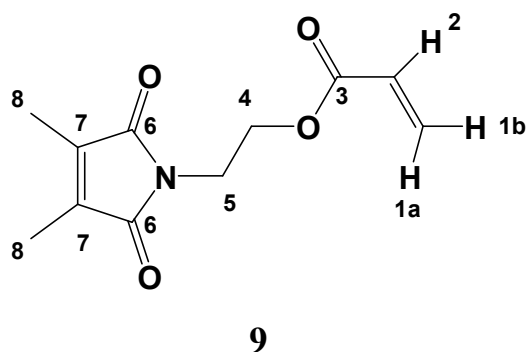
**Physical state:** Colorless crystals

**<sup>1</sup>H NMR (500 MHz, CDCl<sub>3</sub>):**  $\delta$  (ppm) = 1.97 (s, 6H, 6-CH<sub>3</sub>), 2.19 (br.; 1H, 1-OH), 3.70 (t, 2H, <sup>3</sup>J = 5.9 Hz, 3-CH<sub>2</sub>), 3.77 (m, 2H, <sup>3</sup>J = 4.9 Hz, 2-CH<sub>2</sub>).

**<sup>13</sup>C-NMR (125 MHz, CDCl<sub>3</sub>):**  $\delta$  (ppm) = 8.70 (2C, 6-CH<sub>3</sub>), 40.91 (1C, 3-CH<sub>2</sub>), 61.38 (1C, 2-CH<sub>2</sub>), 137.42 (2C, 5-C=C), 172.82 (2C, 4-C=O).

**IR (KBr):**  $\nu$  (cm<sup>-1</sup>): 3500 (m) (OH), 3080-2945 (s) (CH<sub>2</sub>, CH<sub>3</sub>), 1765 (C=O), 1705 (s) (C=C), 1005 (s) (OH).

**Step2: Synthesis dimethylmaleimidoacrylate (DMIA).**



**Procedure:**

In two neck flask fitted with argon balloon. 5,57g (0,032mol) of **(8)** in 100 mL dry CH<sub>2</sub>Cl<sub>2</sub> was stirred and, 6.70g (0.066 mol) of TEA was added. The mixture was allowed to cool to 5-0°C in an ice bath. 3.33g (0.0368 mol) of acryloyl chloride was added drop wise. The yellowish suspension was stirred at 5°C for 1h, and then allowed to stir at RT overnight. The suspension was filtered and, the filtrate was evaporated under reduced pressure to remove the solvent. The product was purified by column chromatography with 1:2 n-hexane to ethylacetate R<sub>f</sub> = 0,45.

**Yield %:** 97%. (lit.: 98%)<sup>(48)</sup>.

**Physical state:** colorless viscous liquid.

**<sup>1</sup>H NMR (500 MHz, CDCl<sub>3</sub>):** δ(ppm) = 1.94 (s, 6H, 8-CH<sub>3</sub>), 3.78 (t, 2H, <sup>3</sup>J = 5.5 Hz, 5-CH<sub>2</sub>), 4.3 (t, 2H, <sup>3</sup>J = 5.3 Hz, 4-CH<sub>2</sub>), 5.79 (dd, <sup>2</sup>J = 1.4 Hz, <sup>3</sup>J = 10.3 Hz, 1a-CH), 6.07 (dd, <sup>3</sup>J = 10.4 Hz, <sup>3</sup>J = 17.3 Hz, 1 H, 2-CH), 6.37 (dd, <sup>2</sup>J = 1.4 Hz, <sup>3</sup>J = 17.3 Hz, 1b-CH).

**<sup>13</sup>C-NMR (125 MHz, CDCl<sub>3</sub>):** δ (ppm) = 8.66 (2C, 8-CH<sub>3</sub>), 36.81 (1C, 5-CH<sub>2</sub>), 61.79 (1C, 4-CH<sub>2</sub>), 128.01 (1C, 1-CH<sub>2</sub>), 131.28 (1C, 2-CH), 137.36 (2C, 7-C=C), 165.76 (1C, 3-C=O), 172.45 (2C, 6-C=O).

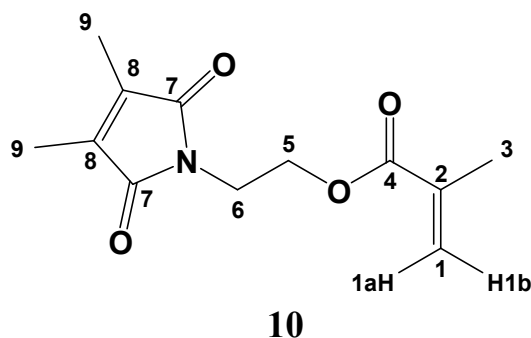
**IR (KBr):** ν (cm<sup>-1</sup>): 3080-2945 (s) (CH<sub>2</sub>, CH<sub>3</sub>), 1670-1730 (s) (C=O), 1640 (s) (C=C).

### 2.4.3. Synthesis of dimethylmaleimidomethacrylate (DMIMA).

#### Step1: Synthesis of dimethylmaleimido ethanol or 1-(2-hydroxyethyl)-3,4-dimethyl-1H-pyrrole-2,5-dione.

As discussed earlier in the synthesis of DMIA (8).

#### Step2: Synthesis of dimethylmaleimidomethacrylate (DMIMA).



#### Procedure:

In two neck flask fitted with argon balloon. 0.4g (0.0033mol) of (4-dimethylaminopyridine) DMAP was added to a solution of dimethylmaleimidoethanol 6.76g (0.04 mol) and methacrylic acid 3.4 mL (0,04mol) in 150 mL of dry CH<sub>2</sub>Cl<sub>2</sub>. The reaction mixture was cooled in ice bath to 0-5°C and DCC (dicyclohexylcarbodiimide) 8 g (0.04mol) was added. The reaction mixture was stirred at 5°C for 15 min., and then allowed to stir at RT for 3h. The mixture was filtered and the white precipitate was washed three times by 50 mL diethylether. The collected solvent was evaporated under reduced pressure. The product was purified by column chromatography with a 4:1 of n-hexane to ethyacetate as eluent and with silca gel as stationary phase R<sub>f</sub> = 0.5.

**Yield %:** 70% (lit.: 70%)<sup>(171)</sup>.

**Physical state:** white, slurrish solid.

**<sup>1</sup>H NMR (500 MHz, CDCl<sub>3</sub>):** δ(ppm) = 1.87 (s, 3H, 3-CH<sub>3</sub>), 1.93(s, 6H, 9-2CH<sub>3</sub>), 3.76 (t, <sup>3</sup>J = 4.6 Hz, 2H, 6-CH<sub>2</sub>), 4.24 (t, <sup>3</sup>J = 4.5 Hz, 2H, 5-CH<sub>2</sub>), 5.51(s, 1H, 1a-CH), 6.07 (s, 1H, 1b-1-CH).

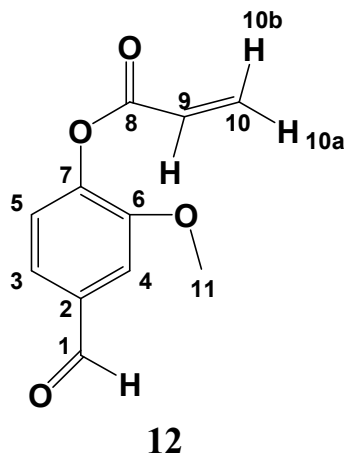
**<sup>13</sup>C-NMR (125 MHz, CDCl<sub>3</sub>):** δ(ppm) = 8.66 (2C, 9-CH<sub>3</sub>), 18.19, (CH<sub>3</sub>), 36.81 (1C, 6-CH<sub>2</sub>), 61.89 (1C, 5-CH<sub>2</sub>), 126.21 (1C, 1-CH<sub>2</sub>), 131.28 (1C, 2-CH), 137.36 (2C, 8-C=C), 165.76 (1C, 4-C=O), 172.45 (2C, 7-C=O).

**IR (KBr):** ν (cm<sup>-1</sup>): 3080-2945 (s) (CH<sub>2</sub>, CH<sub>3</sub>), 1670-1730 (C=O), 1630 (s) (C=C).

## 2.5. Synthesis of monomers.

### 2.5.1 Synthesis of vanilline monomers.

Synthesis of vanillin acrylate or 4-formyl-2-methoxyphenylacrylate (VA).



#### Procedure:

In two neck flask fitted with argon balloon. 8g (0.052 mol) was dissolved in 100mL dry  $\text{CH}_2\text{Cl}_2$  and allowed to stir strongly and 10.52g (0.1 mol) of TEA was added. The reaction mixture allowed cooling in ice bath to  $0-5^\circ\text{C}$ . 5.4g (0.059 mol) acryloyl chloride was added drop wise. The yellowish suspension was stirred at  $5^\circ\text{C}$  for 1h then, allowed to stir at RT overnight. The precipitate was filtered and solvent was evaporated under reduced pressure. The product was extracted by  $\text{CH}_2\text{Cl}_2$  and washed three times with distilled water, one with sodium carbonate and one with 0.1M HCl. The organic phase was dried with  $\text{MgSO}_4$  overnight, then filtered and the product was distilled using oil pump and at  $100^\circ\text{C}$ .

**Yield %:** 85%

**Physical state:** Colorless oil changed to white, slurrish solid after cooling overnight in refrigerator.

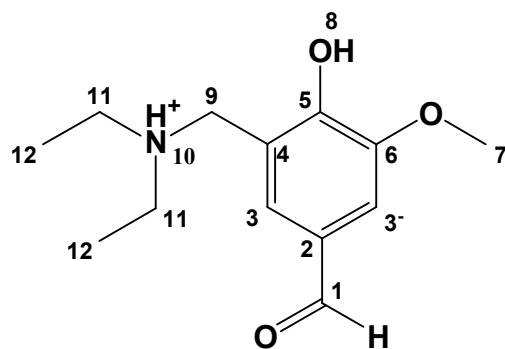
**$^1\text{H NMR}$  (500 MHz,  $\text{CDCl}_3$ ):**  $\delta(\text{ppm}) = 3.73(\text{s}, 3\text{H}, 11\text{-CH}_3)$ , 5.93 (dd,  $^2\text{J} = 0.7 \text{ Hz}$ ,  $^3\text{J} = 10.5 \text{ Hz}$ , 1H, 10a-CH), 6.23 (dd,  $^3\text{J} = 10.4 \text{ Hz}$ ,  $^3\text{J} = 17.3 \text{ Hz}$ , 1 H, 9-CH), 6.47 (dd,  $^2\text{J} = 0.7 \text{ Hz}$ ,  $^3\text{J} = 17.3 \text{ Hz}$ , 10b-CH), 7.12(d,  $^2\text{J} = 7.9 \text{ Hz}$  1H, 5-Ar-CH), 7.36 (dd,  $^3\text{J} = 13.8 \text{ Hz}$ ,  $^4\text{J} = 1.6$ , 1H, 3-Ar-CH, d,  $^4\text{J} = 1.2 \text{ Hz}$ , 4-Ar-CH), 9.96(s, 1H, 1-CHO).

**$^{13}\text{C-NMR}$  (125 MHz,  $\text{CDCl}_3$ ):**  $\delta(\text{ppm}) = 55.91$  (1C, 11- $\text{CH}_3$ ), 111.09 (1C, 4-Ar-CH), 123.36 (1C, 3-Ar-CH), 124.24 (1C, 5-Ar-CH), 127.08 (1C, 9-CH), 133.16 (1C, 10-CH), 135.26 (1C, 2-Ar-C), 144.62 (1C, 7-Ar-CH), 151.09 (1C, 6- Ar-C), 163.22 (1C, 8-C=O), 190.99 (1C, 1-C=O).

**IR (KBr):**  $\nu$  ( $\text{cm}^{-1}$ ): 2950-2970 (s) ( $\text{CH}_2$ ,  $\text{CH}_3$ ), 2840 (m) ( $\text{OCH}_3$ ), 1745 (s) ( $\text{C}=\text{O}$ , carbonyl), 1695 (s) ( $\text{C}=\text{O}$ , aldehyde), 1600(s) ( $\text{C}=\text{C}$ ), 784- 885 (m) ( $\text{Ar-CH}$ ).

### 2.5.2. Synthesis of 2-[(diethylamino)methyl]-4-formyl-6-methoxyphenyl acrylate (DEMAVA).

**Step1: Synthesis of 3-[(diethylamino) methyl]-4-hydroxy-5-methoxybenzaldehyde**



13

#### Procedure:

In 250 mL round bottomed flask fitted with reflux condenser, 10g (0.065 mol) of vanillin, (4-hydroxy-3-methoxy benzaldehyde), 10g (0.33 mol) of formaldehyde and 10g of diethylamine (0.136 mol) in 150 mL ethanol. The mixture was refluxed in oil bath at 90-100°C for 3h. Then allowed the mixture to cool to room temperature. The solvent was removed under reduced pressure to collect the product.

**Yield %:** 97%

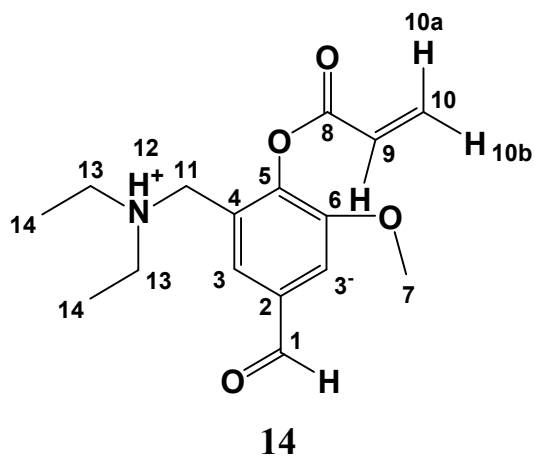
**Physical state:** Yellowish white solid

**$^1\text{H NMR}$  (500 MHz,  $\text{CDCl}_3$ ):**  $\delta$ (ppm) = 1.18(t, 6H, 12- $\text{CH}_3$ ), 1.26 (br., s, 1H, 8-OH), 2.73 (q, 4H, 11- $\text{CH}_2$ ), 3.92 (s, 2H, 9- $\text{CH}_2$ ), 3.94 (s, 3H, 7- $\text{CH}_3$ ), 7.25, 7.34 (dd, 2H,  $^4J = 1.6$ , 3,3'-Ar-CH, 10- $\text{NH}^+$ ), 9.77 (s, 1H, 1-CHO).

**$^{13}\text{C-NMR}$  (125 MHz,  $\text{CDCl}_3$ ):**  $\delta$ (ppm) = 10.82 (2C, 12- $\text{CH}_3$ ), 46.35 (2C, 11- $\text{CH}_2$ ), 55.85 (1C, 10- $\text{CH}_2$ ), 56.01 (1C, 8- $\text{CH}_3$ ), 109.68 (1C, 4'-Ar-CH), 120.84 (1C, 4-Ar-CH), 125.75 (1C, 5-Ar-C), 127.99 (1C, 3-Ar-CH), 148.65 (1C, 6-Ar-CH), 154.87 (1C, 7-Ar-C), 191.65 (1C, 2-C=O).

**IR (KBr):**  $\nu$  ( $\text{cm}^{-1}$ ): 2987 (s) ( $\text{CH}_2$ ,  $\text{CH}_3$ ), 2325 (br.) ( $\text{NH}^+$ ), 1650 (s) (2-C=O), 1706 (s) (7-C=O), 1584(s) ( $\text{NH}^+$ ), 820- 868 (m) ( $\text{Ar-CH}$ ).

**Step2: Synthesis of 2-[(diethylamino) methyl]-4-formyl-6-methoxyphenyl acrylate**



**Procedure:**

In two neck flask fitted with argon balloon. 13.9g (0.058 mol) of (**13**) was dissolved in 200 mL dry CH<sub>2</sub>Cl<sub>2</sub> and allowed to stir strongly and 12.3g (0.12 mol) of TEA was added. The reaction mixture allowed cooling in ice bath to 0-5°C. 5.4g (0.059 mol) acryloyl chloride was added drop wise. The yellowish suspension was stirred at 5°C for 1h, and then allowed to stir at RT for 6 h. The precipitate was filtered and solvent was evaporated under reduced pressure. The product was extracted by CH<sub>2</sub>Cl<sub>2</sub> and wash three times with 100ml dest. water then one time with 0.1M Na<sub>2</sub>CO<sub>3</sub>, and again with 100 mL dest. Water, then product dried with MgSO<sub>4</sub> overnight.

**Yield %:** 80%

**Physical state:** Orange solid

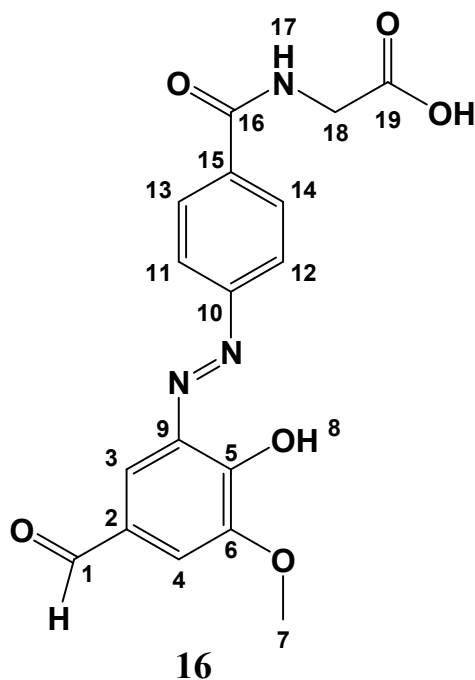
<sup>1</sup>H NMR (500 MHz, CDCl<sub>3</sub>): δ(ppm) = 1.1(t, 6H, 14-CH<sub>3</sub>), 2.49 (q, 4H, 13-CH<sub>2</sub>), 3.52 (s, 2H, 11-CH<sub>2</sub>), 3.87 (s, 3H, 7-CH<sub>3</sub>), 6.05 (dd, <sup>2</sup>J = 1.3 Hz, <sup>3</sup>J = 10.4 Hz, 1H, 10a-CH), 6.36 (dd, <sup>3</sup>J = 10.4 Hz, <sup>3</sup>J = 17.3 Hz, 1 H, 9-CH), 6.64 (dd, <sup>2</sup>J = 1.3 Hz, <sup>3</sup>J = 17.3 Hz, 10b-CH), 7.25, 7.34 (dd, 3H, <sup>4</sup>J = 1.6, <sup>4</sup>J = 1.9, 3,3'- Ar-CH, 12-NH<sup>+</sup>), 9.77 (s, 1H, 1-CHO).

<sup>13</sup>C-NMR (125 MHz, CDCl<sub>3</sub>): δ(ppm) = 10.82 (2C, 12-CH<sub>3</sub>), 46.35 (2C, 11-CH<sub>2</sub>), 55.85 (1C, 10-CH<sub>2</sub>), 56.01 (1C, 8-CH<sub>3</sub>), 109.68 (1C, 4'-Ar-CH), 120.84 (1C, 4-Ar-CH), 125.75 (1C, 5-Ar-C), 127.99 (1C, 3-Ar-CH), 148.65 (1C, 6-Ar-CH), 154.87 (1C, 7-Ar-C), 191.65 (1C, 2-C=O).

IR (KBr): ν (cm<sup>-1</sup>): 2987 (s) (CH<sub>2</sub>, CH<sub>3</sub>), 2325 (br.) (NH<sup>+</sup>), 1650 (s) (2-C=O), 1706 (s) (8-C=O), 1584(s) (NH<sup>+</sup>), 820- 868 (m) (Ar-CH).

### 2.5.3. Synthesis of [4-[2-(acryloyloxy)-5-formyl-3-methoxyphenyl] diazenyl] benzoyl] amino] acetic acid.

*Step1: Synthesis of (4-[5-formyl-2-hydroxy-3-methoxyphenyl] diazenyl] benzoyl] amino)acetic acid.*



#### Procedure:

10.49g (0.054mol) of 4-aminohippuric acid was dissolved in 25 mL concentrated hydrochloric acid and 25 mL distilled water. Diazotize by addition of solution of 4g (0.058mol) of sodium nitrite in 20 mL water. A solution of 8.22g (0.054mol) of vanillin in 60 ml of 10% sodium hydroxide in 250 ml beaker was prepared; the solution mixture was cooled to 5°C using ice bath and 30g of ice was added to the solution. The mixture of vanillin was allowed to stir vigorously followed by addition of cold solution of diazonium salt slowly; a deep red color was developed and deep red crystals of compound (**18**) was separated. The mixture was stirred for 30 min.. The solution was filtered and washed by 100 ml. distilled water. The product was purified by re-crystallization from ethanol.

**Yield %:** 60%

**Physical state:** deep red solid.

**Melting point:**

$^1\text{H NMR}$  (500 MHz,  $\text{CDCl}_3$ ):  $\delta(\text{ppm}) = 3.93$  (s, 3H, 7-OCH<sub>3</sub>), 3.97 (d, 2H,  $^3\text{J} = 5.8\text{Hz}$ , 18-CH<sub>2</sub>), 6.98 (d, 1H,  $^3\text{J} = 7.9\text{ Hz}$ , 4-Ar-CH), 7.40 (dd, 1H,  $^3\text{J} = 13.2\text{ Hz}$ ,  $^4\text{J} = 1.8\text{ Hz}$ , 11-Ar-CH), 7.46 (dd, 1H,  $^3\text{J} = 10.3\text{ Hz}$ ,  $^4\text{J} = 1.8\text{ Hz}$ , 12-Ar-CH), 7.61 (d, 1H,  $^4\text{J} = 2.3\text{ Hz}$ , 3-Ar-CH), 7.89

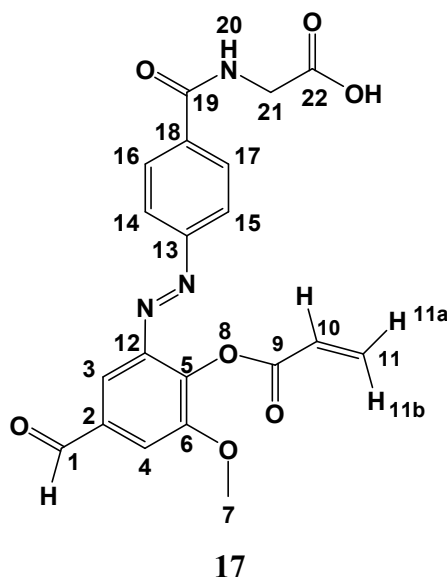
## Experimentals

(d, 1H,  $^4J$  13,1-Ar-CH), 8.99 (t, 1H,  $^3J$  = 5,8, 17-NH), 9.78 (s, 1H, 1-CHO), 9.85(s, 1H, 19-COOH).

$^{13}\text{C-NMR}$  (125 MHz,  $\text{CDCl}_3$ ):  $\delta(\text{ppm})$  = 41.85 (1C, 18- $\text{CH}_2$ ), 56.08 (1C, 7- $\text{CH}_3$ ), 115.89 (1C, 3-Ar-CH), 116.58 (1C, 4-Ar-CH), 123.14 (2C, 11,12-Ar-CH), 126.5 (1C, 9-Ar-CH), 128.92 (2C, 13,14-Ar-CH), 129.17 (1C, 1-Ar-C), 136.01 (1C, 15-Ar-C), 139.71 (1C,5-Ar-C), 148.65 (1C, 6-Ar-C), 153.55(1C, 10-Ar-C), 166.25(1C, 16-C=O), 171.63(1C, 19-C=O), 191.45(1C, 1-C=O).

*IR* (KBr):  $\nu$  ( $\text{cm}^{-1}$ ): 3310 (s) (NH), 2948 (m) (CH) Aliphatic, 1742 (s) (C=O) carbonyl, 1655(s) (CONH<sub>2</sub>), 1580 (m) (N=N), 1135(s) (OCH<sub>3</sub>), 788- 850 (m) (Ar-CH).

**Step2: Synthesis of [4-[2-(acryloyloxy)-5-formyl-3-methoxyphenyl] diazenyl]-benzoyl amino] acetic acid(AHVA).**



### Procedure:

In two neck flask fitted with argon balloon. 6g (0.0167 mol) of **(18)** was dissolved in 100mL dry  $\text{CH}_2\text{Cl}_2$  and allowed to stir strongly and 3.39g (0.335 mol) of TEA was added. The reaction mixture allowed cooling in ice bath to 0-5°C. 1.5g (0.0167 mol) acryloyl chloride was added drop wise. The reddish suspension was stirred at 5°C for 1h, and then allowed to stirred at RT for 6 h. The precipitate was filtered and solvent was evaporated under reduced pressure. The product was extracted by  $\text{CH}_2\text{Cl}_2$  and wash three times with 100ml dest. water then product dried with  $\text{MgSO}_4$  overnight and dissolved again in 100ml diethylether then filtered and solvent was removed under reduced pressure.

**Yield %:** 40%

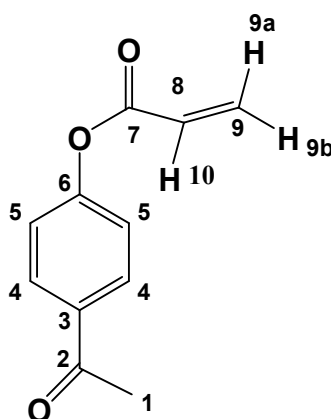
**Physical state:** deep red solid.

$^1\text{H NMR}$  (500 MHz,  $\text{CDCl}_3$ ):  $\delta(\text{ppm})$  = 3.95 (s, 3H, 7-OCH<sub>3</sub>), 3.98 (d, 2H,  $^3\text{J}$  = 5.8 Hz, 21-CH<sub>2</sub>), 6.04 (dd,  $^2\text{J}$  = 1.2 Hz,  $^3\text{J}$  = 10.4 Hz, 1H, 11a-CH), 6.36 (dd,  $^3\text{J}$  = 10.4 Hz,  $^3\text{J}$  = 17.3 Hz, 1 H, 10-CH), 6.62 (dd,  $^2\text{J}$  = 1.2 Hz,  $^3\text{J}$  = 17.3 Hz, 11b-CH), 7.04 (d, 1H,  $^3\text{J}$  = 8.5 Hz, 4-Ar-CH), 7.26 (t, 1H,  $^3\text{J}$  = 7.9, 20-NH), 7.50 (m, 5H, 3, 14-17-Ar-CH), 9.81 (s, 1H, 1-CHO), 9.95 (s, 1H, 22-COOH).

$^{13}\text{C-NMR}$  (125 MHz,  $\text{CDCl}_3$ ):  $\delta(\text{ppm})$  = 41.76 (1C, 21-CH<sub>2</sub>), 56.12 (1C, 7-CH<sub>3</sub>), 110.97 (1C, 3-Ar-CH), 114.41 (1C, 4-Ar-CH), 123.44 (2C, 14,15-Ar-CH), 127.49 (2C, 16,17-Ar-CH), 129.90 (1C, 10-Ar-CH), 133.28 (1C, 12-Ar-C), 135.28 (1C, 11-C=C), 144.84 (1C, 2-Ar-C), 147.19 (1C, 5-Ar-C), 151.74 (1C, 13-Ar-C), 152.07 (1C, 6-Ar-C), 163.40 (1C, 9-C=O), 163.60 (1C, 19-C=O), 190.91 (1C, 1-C=O), 191.06 (1C, 22-C=O).

$\text{IR (KBr)}$ :  $\nu(\text{cm}^{-1})$ : 3370 (s) (NH), 2937 (s) (CH) Aliphatic, 1748 (s) (C=O) carbonyl, 1694 (s) (CONH, C=C), 1577 (m) (N=N), 1136 (s) (OCH<sub>3</sub>), 788, 857 (m) (Ar-CH).

#### 2.5.4. Synthesis of 4-acetylphenyl acrylate



19

#### Procedure:

In two neck flask fitted with argon balloon. 8g (0.058 mol) of 4-hydroxyacetophenone was dissolved in 150mL dry  $\text{CH}_2\text{Cl}_2$  and allowed to stir strongly and 11.7g (0.11 mol) of TEA was added. The reaction mixture allowed cooling in ice bath to 0-5°C. 5.24g (0.058 mol) acryloyl chloride was added drop wise. The yellowish suspension was stirred at 5°C for 1h then, allowed to stir at RT overnight. The precipitate was filtered and solvent was evaporated under reduced pressure. The product was extracted by  $\text{CH}_2\text{Cl}_2$  and washed three times with distilled water, two with sodium carbonate and two with 0.1M HCl. The organic phase was dried with  $\text{MgSO}_4$  overnight, then filtered and the solvent was removed under reduced pressure.

**Yield %:** 75%

**Physical state:** brownish solid.

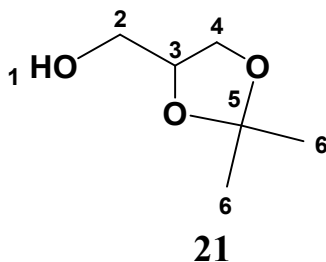
**<sup>1</sup>H NMR (500 MHz, CDCl<sub>3</sub>):**  $\delta$ (ppm) = 2.63(s, 3H,1-CH<sub>3</sub>), 6.09 (dd, <sup>2</sup>J = 0.7 Hz, <sup>3</sup>J = 10.3 Hz,1H, 9a-CH), 6.36(dd, <sup>3</sup>J =10.2 Hz, 1 H, 9b-CH), 6.76 (dd, <sup>2</sup>J =10.2 Hz, <sup>3</sup>J =17 Hz, 10-CH), 7.28 (dd, <sup>3</sup>J = 12.5 Hz, <sup>4</sup>J = 2.6 Hz, 2H, 4,4-Ar-CH), 8.04(dd, <sup>3</sup>J = 10.5 Hz, <sup>4</sup>J = 2.1 Hz, 2H, 5,5-Ar-CH).

**<sup>13</sup>C-NMR (125 MHz, CDCl<sub>3</sub>):**  $\delta$ (ppm) =26.56 (1C, 11-CH<sub>3</sub>), 121.71 (2C, 5,5-Ar-CH), 127.57 (1C, 8-CH), 129.94 (2C, 4,4-Ar-CH), 133.21 (1C, 9-CH), 154.31 (1C, 16-Ar-C), 163.89 (1C, 7-C=O), 196.77 (1C, 1-C=O).

**IR (KBr):**  $\nu$  (cm<sup>-1</sup>): 2950-2970 (s) (CH<sub>2</sub>, CH<sub>3</sub>), 1727 (s) (2-C=O,), 1706 (s) (7-C=O,), 1600(s) (C=C), 784- 885 (m) (Ar-CH).

### 2.5.5. Synthesis of 2,2-dimethyl-1,3-dioxolane-4-yl-methylacrylate (Solketalacrylate)(SKA).

**Step1: Synthesis of isopropylidene glyceol.**



#### **Procedure:**

In 250 mL round bottomed flask fitted with reflux condenser and, water trap to collect water. 36g (0.62 mol) acetone, 30g (0.44 mol) glycerol in 100 mL CHCl<sub>3</sub>. The mixture was stirred and 1.2g (6.2 mol) of p-Toluenesulfonic acid. The reaction mixture was refluxed and, stirred in oil bath at 80°C. After, the time ended about 1.8 mL water was collected. The reaction mixture allowed cooling and, 1.3g of sodium carbonate was added and refluxed again for 1/2h. The precipitate was filtered and, solvent was evaporated under reduced pressure.

**Yield %:** 86% (lit.: 82%)<sup>(257)</sup>.

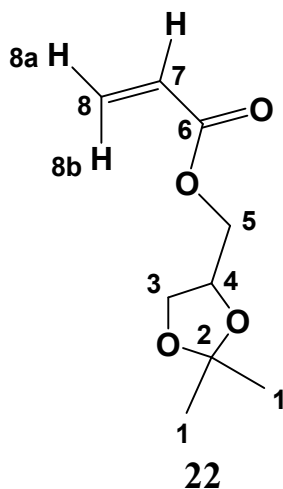
**Physical state:** colorless viscous liquid.

**<sup>1</sup>H NMR (500 MHz, CDCl<sub>3</sub>):**  $\delta$ (ppm) = 1.29 (s, 1H, 6-CH<sub>3</sub>), 1.34 (s, 1H, 6-CH<sub>3</sub>), 2.77 (br., 1H, OH), 3.52 (m, 1H, 2-CH<sub>2</sub>), 3.58 (m, 1H, 2CH<sub>2</sub>), 3.68 (m, 1H, 2CH<sub>2</sub>), 3.93 (m, 1H, 4-CH<sub>2</sub>), 4.13 (m,1H, 3-CH).

**<sup>13</sup>C-NMR (125 MHz, CDCl<sub>3</sub>):**  $\delta$ (ppm) = 25.19 (1C, 1-CH<sub>3</sub>), 26.60 (1C, 1-CH<sub>3</sub>), 62.97 (1C, 5-CH<sub>2</sub>), 65.83 (1C, 3-CH<sub>2</sub>), 76.2 (1C, 4-CH), 109.27 (1C, 2-C).

*IR (KBr):*  $\nu$  ( $\text{cm}^{-1}$ ): 3400 (s) (OH), 2970(s) (CH-Aliphatic), 1050 (s) (C-O-C ether).

**Step2: Synthesis of of 2,2-dimethyl-1,3-dioxolan-4-yl-methylacrylate.**



**Procedure:**

In 500 mL two neck flask fitted with argon balloon. 37g (0.28 mol) of **(21)** in 300 mL dry  $\text{CH}_2\text{Cl}_2$  and allowed to stir strongly and 30,4g (0.3 mol) of TEA was added. The reaction mixture allowed cooling in ice bath to  $0-5^\circ\text{C}$ . 22g (0.24 mol) acryloyl chloride was added drop wise. The yellowish reaction mixture was stirred at  $0-5^\circ\text{C}$  for 1h, and then allowed to stirred at RT for 2d. The precipitate was filtered and solvent was evaporated under reduced pressure. The product was extracted by 60 mL  $\text{CH}_2\text{Cl}_2$  and washed three times with 300 mL distilled water. The organic phase was dried with  $\text{MgSO}_4$  overnight, then filtered and solvent was evaporated under reduced pressure. The crude product was purified by vacuum distillation using oil pump at  $85-90^\circ\text{C}$  ( $10^{-2}$  bar).

**Yield %:** 83% (lit.: 85%)<sup>(257)</sup>.

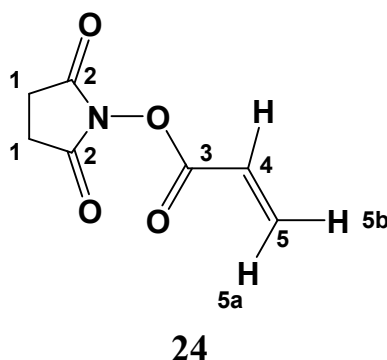
**Physical state:** colorless viscous liquid.

**$^1\text{H NMR}$  (500 MHz,  $\text{CDCl}_3$ ):**  $\delta$ (ppm) = 1.32 (s, 3H, 1- $\text{CH}_3$ ), 1.38 (s, 3H, 1- $\text{CH}_3$ ), 3.72 (m, 1H, 5- $\text{CH}_2$ ), 4.04 (m, 1H, 4-CH), 4.13 (m, 1H, 3- $\text{CH}_2$ ), 4.19 (m, 1H, 3- $\text{CH}_2$ ), 4.29 (m, 1H, 4-CH), 5.81 (dd,  $^2\text{J}=1,3$  Hz,  $^3\text{J} = 10.4$  Hz, 8a-CH), 6.11 (dd,  $^3\text{J}=10.7$  Hz,  $^3\text{J} = 17.3$  Hz, 1H, 7-CH), 6.34 (dd,  $^2\text{J}=1.3$ ,  $^3\text{J} = 17.3$  Hz, 1H, 8b- $\text{CH}_2$ ).

**$^{13}\text{C-NMR}$  (125 MHz,  $\text{CDCl}_3$ ):**  $\delta$ (ppm) =25.33 (1C, 1- $\text{CH}_3$ ), 26.62 (1C, 1- $\text{CH}_3$ ), 64.71 (2C, 5-  $\text{CH}_2$ ), 66.30 (2C, 3- $\text{CH}_2$ ), 73.57 (1C, 4-CH), 109.79 (1C, 2-C), 127.96 (1C, 7-CH), 131.25 (2C, 8- $\text{CH}_2$ ), 165.80 (1C, 6-C=O).

***IR (KBr):***  $\nu$  ( $\text{cm}^{-1}$ ): 2960(s) (CH-Aliphatic), 1721(s) (C=O), 1630 (s) (C=C), 1180 (s) (C-O-C ether).

## 2.5.6. Synthesis of 1-(acryloyloxy) pyrrolidine-2,5-dione ( NASI )



### Procedure:

In two neck flask fitted with argon balloon. 5g (0.043 mol) of N-hydroxysuccinimide was dissolved in 100mL dry CH<sub>2</sub>Cl<sub>2</sub> and allowed to stir strongly; 5.54g (0.054 mol) of TEA was added. The reaction mixture allowed cooling in ice bath to 0-5°C. 4.5g (0.049 mol) acryloyl chloride was added drop wise. The yellowish suspension was stirred at 0-5°C for 1h then, allowed to stir at RT overnight. The precipitate was filtered and solvent was evaporated under reduced pressure. The product was extracted by CH<sub>2</sub>Cl<sub>2</sub> and washed two times with 50 mL distilled water, one with 1M sodium carbonate. The organic phase was dried with MgSO<sub>4</sub> overnight, then filtered and The product was purified by column chromatography with a 1:1 of n-hexane to ethylacetate as eluent and with silica gel as stationary phase R<sub>f</sub> = 0.32.

**Yield %:** 75%

**Physical state:** colorless viscous liquid.

<sup>1</sup>H NMR (500 MHz, CDCl<sub>3</sub>): δ(ppm) = 2.85 (s, 4H, 1-2CH<sub>2</sub>), 6.36 (dd, 1H, <sup>2</sup>J = 0.8 Hz, <sup>3</sup>J = 10.5 Hz, 5b-CH), 6.53 (dd, 1H, <sup>3</sup>J = 10.6 Hz, <sup>3</sup>J = 17.3 Hz, 6-CH), 6.66 (dd, 1H, <sup>2</sup>J = 0.9 Hz, <sup>3</sup>J = 17.3 Hz, 7a-CH).

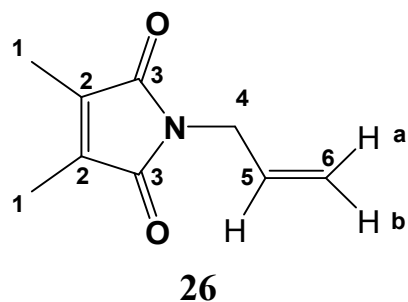
<sup>13</sup>C-NMR (125 MHz, CDCl<sub>3</sub>): δ(ppm) = 25.95 (2C, 1-CH<sub>2</sub>), 123.43 (1C, 4-CH), 138.01 (1C, 5-CH), 161.84 (2C, 2-C=O), 170.64 (1C, 1-C=O).

IR(KBr): ν (cm<sup>-1</sup>): 2990 (s) (CH-Aliphatic), 1740 (s) (C=O), 1630 (s) (C=O).

## 2.6. Synthesis of adhesion promoters.

### 5.1. Synthesis of thioacetic acid 3-(3,4-dimethyl-2,5-dioxo-2,5-dihydro-pyrrol-yl)-propyl ester ( DMITAc ).

*Step1: Synthesis of 1-allyl-3,4-dimethyl-pyrrol-2,5-dione.*



#### Procedure:

In 250mL round bottomed flask fitted with water trap to collect water. 5.71g (0,1mol) of allyl amine was added to a stirred solution of 6.305g (0.05 mol) of dimethylmaleic anhydride in 200mL toluene. The reaction mixture was refluxed with stirring in oil bath at 130°C for 4h. After, the time ended 1.5mL of water was collected. The mixture allowed cooling at room temperature and, was filtered; solvent removed under reduced pressure. The crude product was purified by column chromatography using 4:1 n-hexane to ethylacetate as eluent and silica gel as stationary phase  $R_f = 0.5$ .

**Yield %:** 70 % (lit.: 75%)<sup>(48)</sup>.

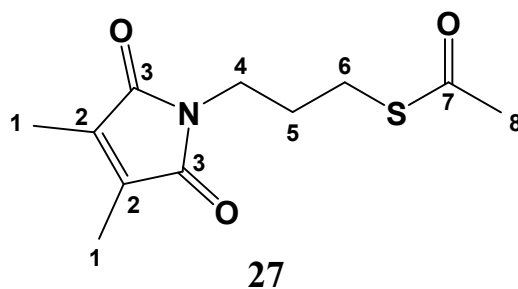
**Physical state:** white, slurrish solid

<sup>1</sup>**H NMR (500 MHz, CDCl<sub>3</sub>):**  $\delta$ (ppm) = 1.96 (s, 6H, 1-2CH<sub>3</sub>), 4.08 (tt, 2H, <sup>2</sup>J = 1.5 Hz, <sup>3</sup>J = 5.6 Hz, 4-CH<sub>2</sub>), 5.14 (ddd, 1H, <sup>2</sup>J = 1.2 Hz, <sup>3</sup>J = 27.1 Hz, <sup>3</sup>J = 10.2 Hz, <sup>3</sup>J = 17.1 Hz, <sup>4</sup>J = 1.1 Hz, 6 a,b-CH), 5.80 (ddd, 1H, <sup>3</sup>J = 27.3, <sup>3</sup>J = 17.2 Hz, <sup>3</sup>J = 6.97 Hz, <sup>3</sup>J = 5.7 Hz, 5-CH).

<sup>13</sup>**C-NMR (125 MHz, CDCl<sub>3</sub>):**  $\delta$ (ppm) = 8.64 (2C, 1-CH<sub>3</sub>), 39.97 (1C, 4-CH<sub>2</sub>), 117.25 (1C, 6-CH<sub>2</sub>), 132.04 (1C, 5-CH), 137.32 (2C, 2-C=C), 171.73 (1C, C=O).

**IR(KBr):**  $\nu$  (cm<sup>-1</sup>): 2960 (s) (CH-Aliphatic), 1720-1740 (s) (C=C),(C=O).

**Step2: Synthesis of thioacetic acid 3-(3,4-dimethyl-2,5-dioxo-2,5-dihydro-pyrrol-yl)-propyl ester ( DMITAc ).**



**Procedure:**

In 50mL round bottom flask with reflux condenser. 3.454g (0.045 mol) of thioacetic acid was added to stir solution of 5g (0.03 mol) in 30 mL  $\text{CHCl}_3$ ; and 0.294g (1.79mmol) was also added. The reaction mixture was refluxed at  $80^\circ\text{C}$  for 5h in oil bath. The mixture allowed to cool at room temperature, after this, 50 mL of 1M sodium bicarbonate was added. The aqueous solution was extracted two times 60mL diethylether each time, then, the ether phase washed with saturated solution of NaCl, dried with  $\text{MgSO}_4$  overnight. The product was purified by column chromatography using 4:1 n-hexane to ethylacetate as eluent and silica gel as stationary phase  $R_f = 0.32$ , followed by vacuum distillation for extra purification.

**Yield %:** 88 % ( lit.: 84%)<sup>(48)</sup>.

**Physical state:** Colorless viscous liquid

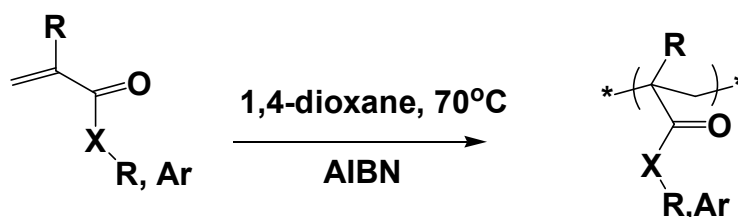
**$^1\text{H NMR}$  (500 MHz,  $\text{CDCl}_3$ ):**  $\delta(\text{ppm}) = 1.83$  (p, 2H,  $^3J = 6.9$ , 1-5 $\text{CH}_2$ ), 1.93 (s, 6H, 1- $\text{CH}_3$ ), 2.28 (s, 3H, 8-CH), 2.81 (t, 2H,  $^3J = 7.3$ , 6-CH), 3.51(t, 2H,  $^3J = 6.9$ , 4-CH).

**$^{13}\text{C-NMR}$  (125 MHz,  $\text{CDCl}_3$ ):**  $\delta(\text{ppm}) = 8.6$  (2C, 1- $\text{CH}_3$ ), 26.28 (1C, 6- $\text{CH}_2$ ), 28.70 (1C, 4- $\text{CH}_2$ ), 30.51, (1C, 8- $\text{CH}_3$ ), 36.72 (1C, 5- $\text{CH}_2$ ), 137.17 (2C, 2- $\text{C}=\text{C}$ ), 172.07 (1C, 3- $\text{C}=\text{O}$ ), 195.33 (1C, 7- $\text{C}=\text{O}$ ).

**IR (KBr):**  $\nu(\text{cm}^{-1})$ : 2960 (s) (CH-Aliphatic), 1740-1720 (s) (3- $\text{C}=\text{O}$ ),(2- $\text{C}=\text{C}$ ), 1705 (7- $\text{C}=\text{O}$ ).

## 2.7. Polymers synthesis.

### 2.7.1. Synthesis of homopolymers.



X= O, NH; R = H, CH<sub>3</sub>

**Scheme 18:** General synthesis of homopolymers.

#### General procedure.

All polymers were polymerized using free radical polymerization in solution and AIBN as initiator.

In 250mL round bottom flask, (0.0424mol) of monomer was added to 80 mL of solvent. (0.0426 mmol) of Azobisisobutyronitrile (AIBN) was added. The reaction mixture was purged in argon for 20 min., and then heated in oil bath at 70°C for 8h. After this the mixture cooled first at room temperature, then in refrigerator. The polymer was precipitated in 500 mL diethylether at -40°C. The precipitate was re-dissolved in THF and re-precipitated in diethylether to remove the un-reacted monomers and impurities.

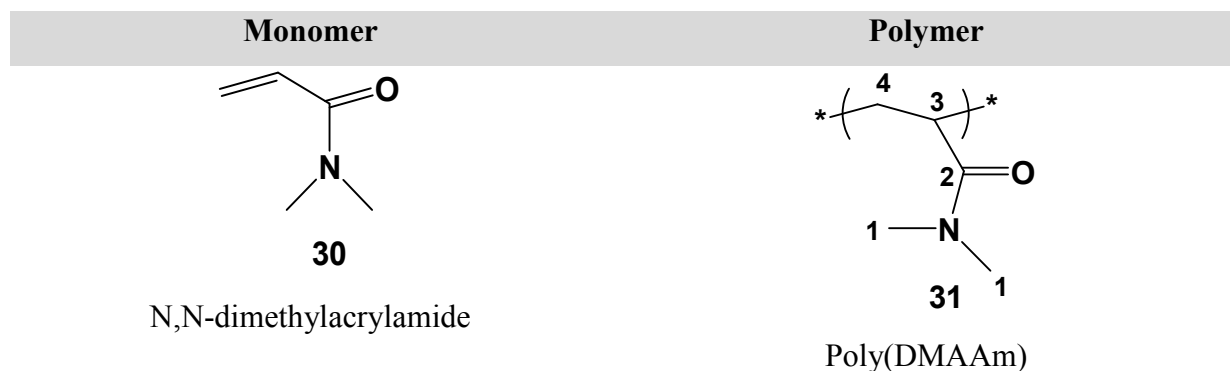
**Table 4:** Shows monomers, polymers and solvent, yield and physical state, also the chemical analysis (1H NMR, IR) of each polymer.

Monomer	Polymer	
<p style="text-align: center;"><b>28</b></p> <p style="text-align: center;">N-isopropylacrylamide</p>	<p style="text-align: center;"><b>29</b></p> <p style="text-align: center;">Poly(NIPAAm)</p>	
Solvent	Yield%	Physical state
1,4- dioxane	95	Solid
<sup>1</sup> H NMR	IR (KBr)	
<sup>1</sup> H NMR (500 MHz, CDCl <sub>3</sub> ): δ(ppm) = 1-1,88 (m, 6H, 1-2CH <sub>3</sub> ), 1.47-2.36 (m, 3H, 5-	IR (KBr): ν (cm <sup>-1</sup> ): 3442 (N-H), 2967 (C-H), 1646 (CONH), 1548 (NHCH).	

## Experimentals

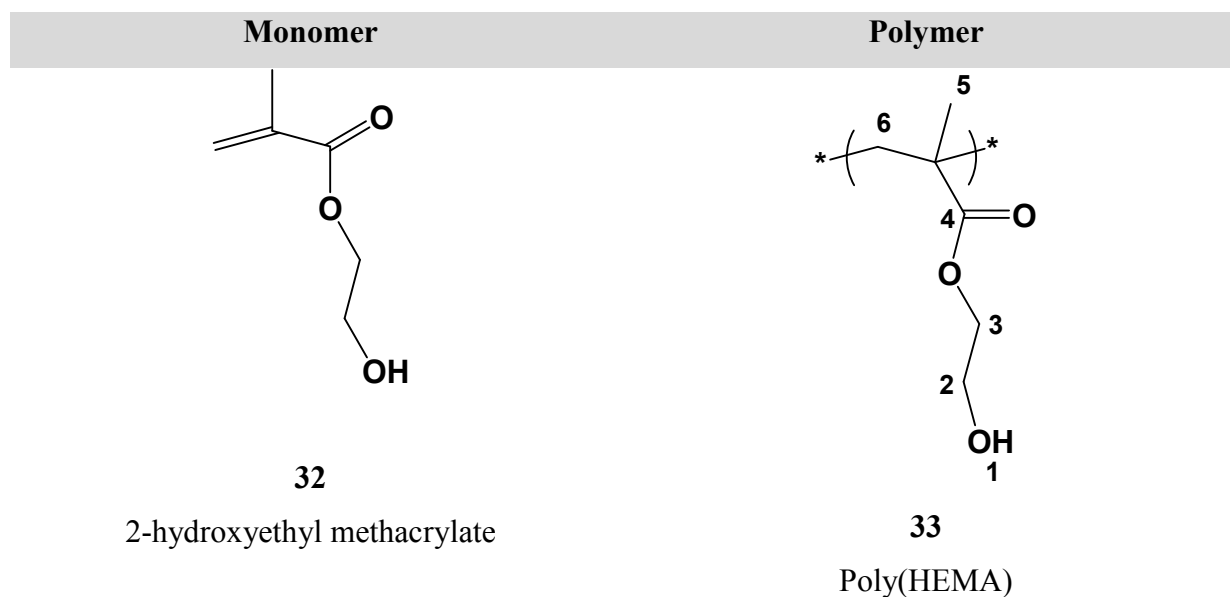
CH, 6-CH<sub>2</sub>), 3.99-4.2 (m, 1H, 2-CH), 6.28

(br. s, 1H, 3-NH).



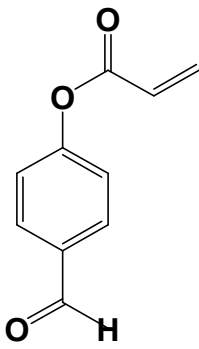
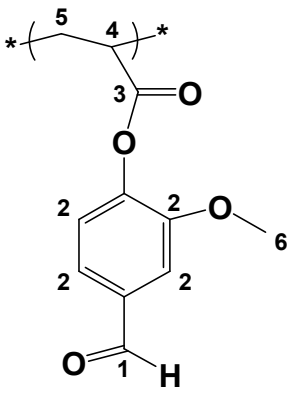
Solvent	Yield%	Physical state
1,4- dioxane	93	Solid

<sup>1</sup> H NMR	IR (KBr)
<sup>1</sup> H NMR (500 MHz, CDCl <sub>3</sub> ): δ(ppm) = 1.32-1.89 (m, 2 H, 4-CH <sub>2</sub> ), 2.15-3.18 (m, 7 H, 3-CH, 1-2CH <sub>3</sub> ).	IR (KBr): ν (cm <sup>-1</sup> ): 2930 and 2868 (CH-Aliphatic), 1708 and 1625 (2-C=O).



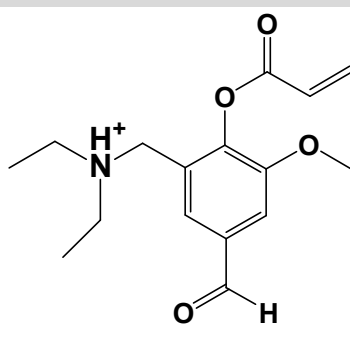
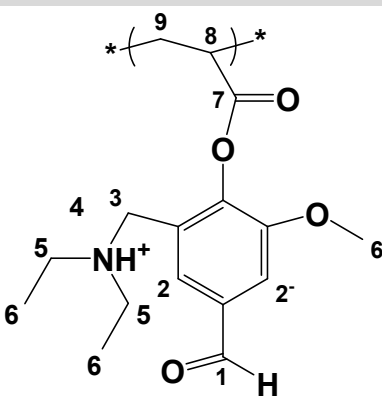
Solvent	Yield%	Physical state
Ethanol	95	Solid

<sup>1</sup> H NMR	IR (KBr)
<sup>1</sup> H NMR (500 MHz, DMSO): δ(ppm) = 1H, 1-OH), 3,77-3,84(m, 2H, 2-CH <sub>2</sub> ), 4,03-4,13 (m, 2H, 3-CH <sub>2</sub> ).	IR (KBr): ν (cm <sup>-1</sup> ): 3447 (O-H), 2950 (C-H-Aliphatic), 1726 (C=O).

Monomer	Polymer
 <p style="text-align: center;"><b>12</b></p> <p style="text-align: center;">4-formyl-2-methoxyphenyl acrylate (VA)</p>	 <p style="text-align: center;"><b>34</b></p> <p style="text-align: center;">Poly (VA)</p>

Solvent	Yield%	Physical state
1,4- dioxane	88	Solid

<sup>1</sup> H NMR	IR (KBr)
<sup>1</sup> H NMR (500 MHz, CDCl <sub>3</sub> ): δ(ppm) = 1,66-2,47(m, 2H, 5-CH <sub>2</sub> ), 2,65-3,23 (m, 1H, 4-CH), 3,46-3,99 (m, 3H, 6-CH <sub>3</sub> ), 6,87-7,66 (m, 3H, 2-CH-Ar.), 9,68-10,03 (m, 1H, 1-CHO).	IR (KBr): ν (cm <sup>-1</sup> ): 2951(s) (4,5-CH-Aliphatic), 1714-1543 (s) (3-C=O), 1633 (s) (1-C=O), 1135 (s) (6-OCH <sub>3</sub> ).

Monomer	Polymer
 <p style="text-align: center;"><b>14</b></p> <p style="text-align: center;">2-[(diethylamino)methyl]-4-formyl-6-methoxyphenyl acrylate ( DEMA VA ).</p>	 <p style="text-align: center;"><b>35</b></p> <p style="text-align: center;">Poly(DEMA VA)</p>

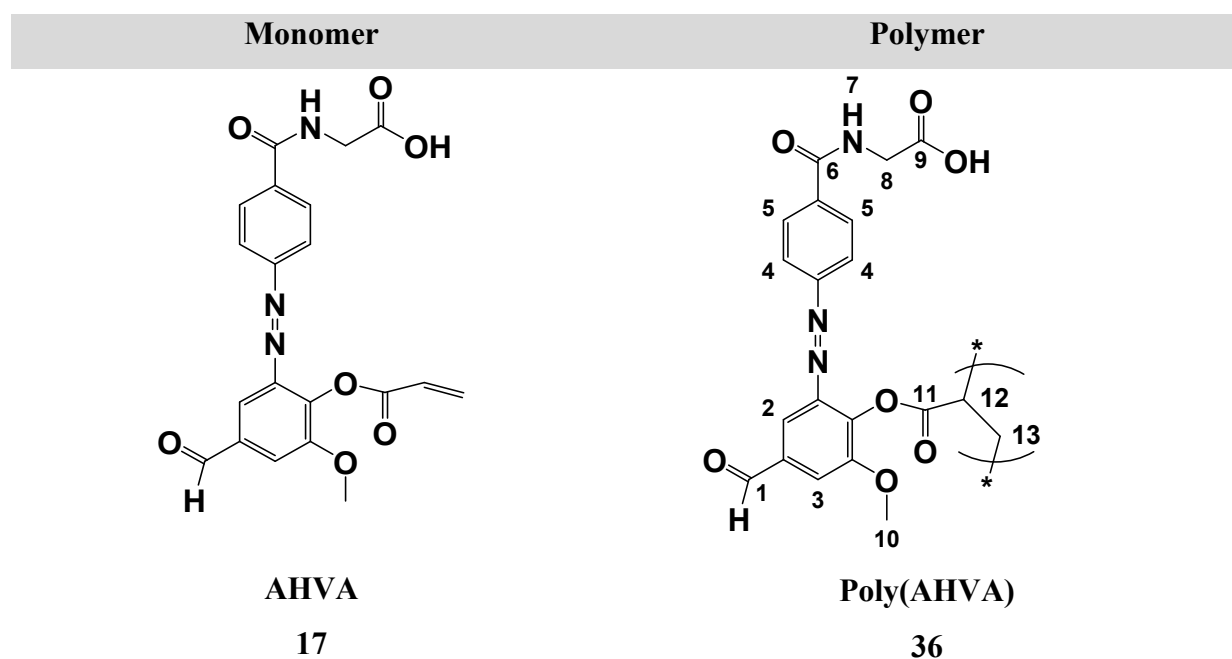
Solvent	Yield%	Physical state
1,4- dioxane	20	Solid

<sup>1</sup> H NMR	IR (KBr)
--------------------	----------

## Experimentals

$^1\text{H NMR}$  (500 MHz,  $\text{CDCl}_3$ ):  $\delta(\text{ppm})$  1,04-1,23(m, 6H, 6- $2\text{CH}_3$ ), 1,29-1,58 (m, 2H, 9- $\text{CH}_2$ ), 1,68-1,99 (m, 1H, 8- $\text{CH}_3$ ), 2,52-2,80 (m, 4H, 5- $2\text{CH}_2$ ), 3,81-4,01(m, 5H, 3- $\text{CH}_2$ , 6- $\text{CH}_3$ ), 6,28-6,78 (m, 1H, 2'- $\text{CH-Ar.}$ ), 6,86-7,18 (m, 2H, 2- $\text{CH-Ar.}$ , 4- $\text{NH}^+$ ) 9,67-10,02 (m, 1H, 1- $\text{CHO}$ ).

$\text{IR (KBr): } \nu (\text{cm}^{-1})$ : 2951(s) (4,5- $\text{CH-Aliphatic}$ ), 2353(br.)  $\text{NH}^+$  1710 (s) (7- $\text{C=O}$ ), 1690 (s) (1- $\text{C=O}$ ), 1150 (s) (6- $\text{OCH}_3$ ).

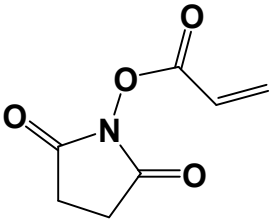
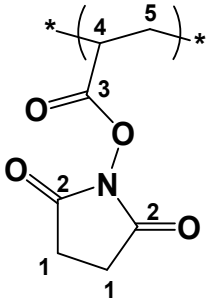


Solvent	Yield%	Physical state
1,4- dioxane	32	Solid

$^1\text{H NMR}$	$\text{IR (KBr)}$
------------------	-------------------

$^1\text{H NMR}$  (500 MHz,  $\text{CDCl}_3$ ):  $\delta(\text{ppm})$  1,094-1,49(m, 2H, 12- $\text{CH}_2$ ), 1,57-2,77 (br., 1H, 13- $\text{CH}$ ), 3,52-4,24 (m, 5H, 8- $\text{CH}_2$ , 10- $\text{CH}_3$ ), 5,85-6,86 (m, 1H, 3- $\text{CH-Ar.}$ ), 6,98-7,21 (m, 1H, 7- $\text{NH}$ ), 7,32-7,54 (m, 2H, 4,4- $\text{CH-Ar.}$ ), 7,55-8,16 (m, 3H, 2,5,5- $\text{CH-Ar.}$ ).

$\text{IR (KBr): } \nu (\text{cm}^{-1})$ : 3370 (s) (NH), 2937 (s) (CH) Aliphatic, 1748 (s) (C=O) carbonyl, 1694(s) (CONH, C=C), 1584 (m) (N=N), 1127(s) ( $\text{OCH}_3$ ), 780, 867 (m) (Ar-CH).

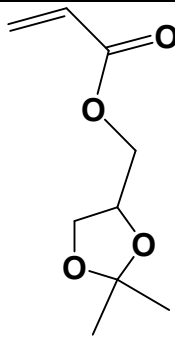
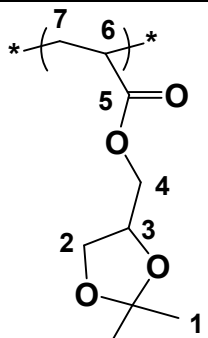
Monomer	Polymer	
 <p style="text-align: center;">24</p>	 <p style="text-align: center;">37</p>	
Solvent	Yield%	Physical state
1,4-dioxane	90	Solid
<sup>1</sup> H NMR	IR (KBr)	
<sup>1</sup> H NMR (500 MHz, DMSO): $\delta$ (ppm) = 1,87-2,29 (m, 2H, 5-CH <sub>2</sub> ), 2,66-2,95 (m, 4H, 1-2CH <sub>2</sub> ), 3,02-3,23 (m, 1H, 4-CH).	IR (KBr): $\nu$ (cm <sup>-1</sup> ): 3065 (s) (CH) Aliphatic, 1730 (s) (C=O carbonyl), 1665, (s), (C=O amide).	

### 2.7.2. Synthesis of Poly (SKA).

#### Procedure

A mixture of 3g of (2,2-dimethyl-1,3-dioxolan-4-yl)methyl acrylate (SKA) (0.016mol), was dissolved in 60mL 1,4-dioxane, and (2.64) mg of AIBN was added in 100mL round flask. The mixture was sealed and purged with argon for 20min., then allowed to stir at 70°C in oil bath for 8h. The polymer solution was cooled at room temperature and then frozen in refrigerator. The solution was poured in 200mL diethylether, polymer was separated as oily spot in the bottom of the flask. Solvent was decanted and re-dissolved in THF then separated again by 50 mL diethylether. Solvent was removed under reduced pressure and then dried overnight under vacuum.

**Table 5:** Shows monomers, polymers and solvent, yield and physical state, also the chemical analysis ( $^1\text{H}$  NMR, IR) of poly (SKA).

Monomer	Polymer	
 <p style="text-align: center;"><b>22</b></p> <p style="text-align: center;">(2,2-dimethyl-1,3-dioxolan-4-yl)methyl acrylate</p>	 <p style="text-align: center;"><b>38</b></p> <p style="text-align: center;">Poly(SKA)</p>	
Solvent	Yield%	Physical state
1,4- dioxane	57	Viscous liquid
$^1\text{H}$ NMR	IR (KBr)	
$^1\text{H}$ NMR (500 MHz, $\text{CDCl}_3$ ) : $\delta(\text{ppm}) =$ IR (KBr): $\nu(\text{cm}^{-1})$ : 3065 (s) (CH) Aliphatic, 1,22-1,41(m, 6H, 1-2 $\text{CH}_3$ ), 1,97-2,06(m, 3H, 6-CH, 7- $\text{CH}_2$ ), 2,19-2,43 (m, 2H, 7- $\text{CH}_2$ ), 3,30-3,43 (m, 2H, 2- $\text{CH}_2$ ), 3,61-3,72 (m, 2H, 4- $\text{CH}_2$ ), 3,82-4,23 (m, 1H, 3-CH).		

### 2.7.3. Synthesis of Poly(2,3-dihydroxypropyl acrylate) (DHPA).

In 50 mL round flask, fitted with reflux condenser. A mixture of 2g of (**38**) dissolved in 10 mL THF, and 15 mL glacial acetic acid was refluxed at 90°C for 6h. After time finished solution was cooled at room temperature, and solvent was removed under reduced pressure. Polymer was dried under freeze-drying overnight.

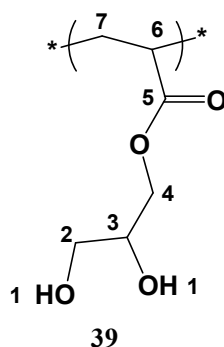


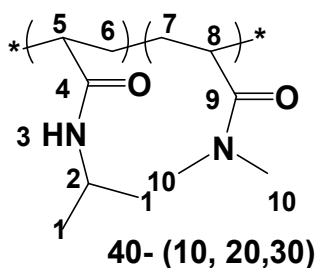
**Table 6:** Shows monomers, polymers and solvent, yield and physical state, also the chemical analysis ( $^1\text{H NMR}$ , IR) of poly (SKA).

Solvent	Yield%	Physical state
THF	23	Viscous liquid
$^1\text{H NMR}$	IR (KBr)	
$^1\text{H NMR}$ (500 MHz, $\text{CDCl}_3$ ) : $\delta(\text{ppm}) =$ IR (KBr): $\nu$ ( $\text{cm}^{-1}$ ): 3065 (s) (CH) Aliphatic, 1,22-1,41(m, 2H, 1-2 $\text{CH}_3$ ), 1,97-2,06(m, 2H, ,1,1-OH), 2,25-2,49 (m, 1H, 6-CH), 3,26-3,47 (m, 2H, 2- $\text{CH}_2$ ), 3,53-3,74 (m, 1H, 3-CH), 3,84-4,13 (m, 2H, 4- $\text{CH}_2$ ).		

## 2.8. Synthesis of *N*-isopropylacrylamide (NIPAAm) copolymers.

Here we focused in the synthesis of copolymers based on NIPAAm, as the main part with different mole ratios of hydrophilic and hydrophobic monomers in order to, increase or decrease lower critical solution temperature (LCST), as will discuss in chapter (3).

### 2.8.1. Synthesis of Poly (NIPAAm-*Co*-DMAAm) with 10, 20, and 30 mol% of DMAAm.



#### Procedure

In round bottom flask 10, 20 and 30 mol% of *N,N*-dimethylacrylamide was added to 4g (0.0353mol) NIPAAm in 80 mL 1,4-dioxane and AIBN was also added. The reaction mixture was purged in argon for 20 min., and then heated in oil bath at 70°C for 8h. After cooling at room temperature and also in refrigerator, the polymer was precipitated in diethylether, at -40°C, then dissolved in THF, and reprecipitated in diethylether to remove the unreacted monomers and impurities.

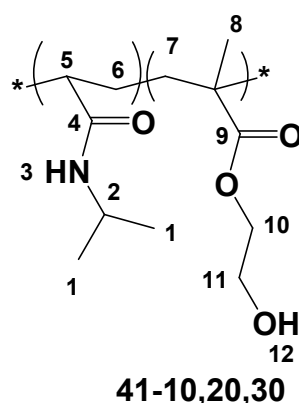
**Table 7:** Shows the mole ratios of DMAAm and amount of AIBN, yield and physical state, also the chemical analysis ( $^1\text{H NMR}$ , IR) of poly(NIPAAm-*Co*-DMAAm).

Polymer	DMAAm	AIBN	Yield%	Physical state
40-10	0.349g (3.53 mmol)	8.23 mg	92	Solid
40-20	0.699g (7,06 mmol)	8.987mg	95	Solid
40-30	1.049g (10.6 mmol)	9.738mg	96	Solid

$^1\text{H NMR}$	IR (KBr)
$^1\text{H NMR (500 MHz, CDCl}_3\text{): } \delta \text{ (ppm) = 1-1.88 (m, 6H, 1-2CH}_3\text{), 1.47-2.36 (m, 3H, 5-CH, 6-CH}_2\text{), 2.77-3.14(m, 7H, 8-CH, 10-CH}_3\text{), 3.99-4.2 (m, 1H, 2-CH), 6.28 (br. s, 1H, 3-NH).$	$\text{IR (KBr): } \nu \text{ (cm}^{-1}\text{): 3442 (N-H), 2967 (C-H), 1646 (CONH), 1548 (NHCH).$

### 2.8.2. Synthesis of Poly (NIPAAm-*Co*-HEMA) with 10, 20, and 30 mol% of HEMA.



#### Procedure

As discussed later in **section 2.8.1.**

**Table 8:** shows the mole ratios of DMAAm and amount of AIBN, yield and physical state, also the chemical analysis ( $^1\text{H NMR}$ , IR) of poly (NIPAAm-*Co*-HEMA).

Polymer	HEMA	AIBN	Yield%	Physical state
41-10	0.460g (3,53 mmol)	9.447 mg	92	Solid
41-20	0.920g (7,06 mmol)	10.310mg	92	Solid
41-30	1.380g (10,6 mmol)	11.167mg	96	Solid

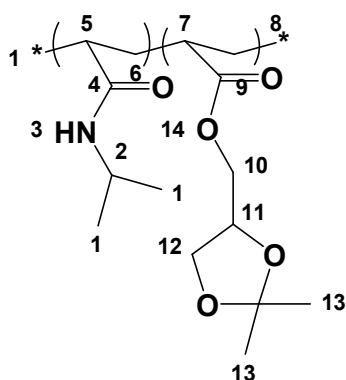
  

$^1\text{H NMR}$	IR (KBr)
$^1\text{H NMR (500 MHz, DMSO): } \delta \text{ (ppm) = 0.71-1.16 (m, 6H, 1-2CH}_3\text{), 1.17-1.64 (m, 3H, 5-CH, 6-CH}_2\text{), 3.07-3.30 (m, 7H, 8-CH, 10-CH}_3\text{), 3.99-4.2 (m, 1H, 2-CH), 6.28 (br. s, 1H, 3-NH).$	$\text{IR(KBr): } \nu \text{ (cm}^{-1}\text{): 3450 (br.) (OH), 3072, 2982 (br.) (CH) Aliphatic,$

1.77-2.11(m, 2H, 7-CH<sub>2</sub>), 3.48-3.69 (m, 3H, 8-CH<sub>3</sub>), 1730(s) (C=O, carbonyl), 1650(C=O, 3.70-4.15 (m., 5H, 2-CH, 10-CH<sub>2</sub>, 11-CH<sub>2</sub>), 4.81- amide).

5.15(br., 1H, 12-OH), 6.86-7.71 (br., 1H, 3-NH).

### 2.8.3. Synthesis of Poly (NIPAAm-*Co*-SKA) with 10, 20, and 30 mol% of SKA.



42-10,20,30

#### Procedure

As previously discussed in **section 2.8.1**

**Table 9:** Shows the mole ratios of SKA and amount of AIBN, yield and physical state, also the chemical analysis (<sup>1</sup>H NMR, IR) of poly (NIPAAm-*Co*-SKA).

Polymer	SKA	AIBN	Yield%	Physical state
42-10	0.658g (3.534 mmol)	11.625 mg	90	Solid
42-20	1.314g (7.06 mmol)	12.680mg	78	Solid
42-30	1.973g (10.6 mmol)	13.740mg	60	Solid

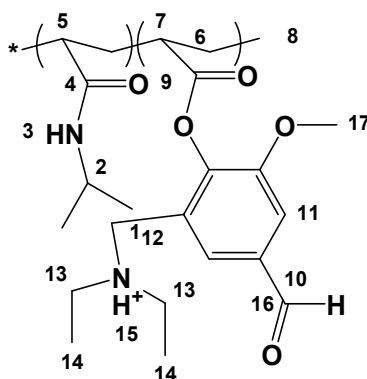
#### <sup>1</sup>H NMR

<sup>1</sup>H NMR (500 MHz CDCl<sub>3</sub>): δ(ppm) = 1.09-1.22 (m, 6H, 1-2CH<sub>3</sub>), 1.23-1.49 (m, 6H, 13-2CH<sub>3</sub>), 1.48-1.71(m, 1H, 6-CH), 1.72-1.94 (m, 2H, 5-CH<sub>2</sub>), 1.95-2.46 (m, 3H, 7-CH, 8-CH<sub>2</sub>), 2.79-3.01(m, 1H, 12-CH<sub>2</sub>), 3.84-4.16 (m, 1H, 2-CH), 4.19-4.43(m, 1H, 11-CH), 5.76-6.82 (br., 1H, 3-NH).

#### IR (KBr)

IR(KBr): ν (cm<sup>-1</sup>): 3090, 2982 (br.) (CH) Aliphatic, 1748(s) (C=O, carbonyl), 1676(C=O, amide).

### 2.8.4. Synthesis of Poly (NIPAAm-Co-DEMAVA) with 10, 20, and 30 mol% of DEMAVA.



**43-10,20,30**

**Table 10:** Shows the mole ratios of DEMAVA and amount of AIBN, yield and physical state, also the chemical analysis (<sup>1</sup>H NMR, IR) of poly (NIPAAm-Co-DEMAVA).

Polymer	DEMAVA	AIBN	Yield%	Physical state
<b>43-10</b>	1.319g (3.534 mmol)	15.747 mg	70	Solid
<b>43-20</b>	2.638g (7.06 mmol)	17.176mg	65	Solid
<b>43-30</b>	3.957g (10.6 mmol)	18.612mg	65	Solid

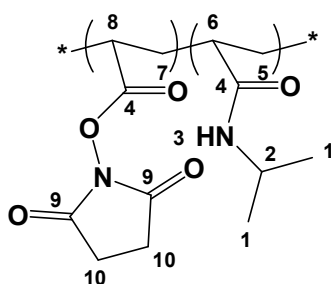
**<sup>1</sup>H NMR**

**IR (KBr)**

<sup>1</sup>H NMR (500 MHz, CDCl<sub>3</sub>): δ(ppm) = 0.66-1.33 (m, 6H, 1-2CH<sub>3</sub>), 1.37-1.72 (m, 2H, 6-CH<sub>2</sub>), 1.72-1.94 (m, 6H, 14,14-CH<sub>3</sub>), 1.94-2.26 (m, 2H, 5,7-CH), 2.27-2.82 (m, 2H, 8-CH<sub>2</sub>), 3.31-3.37 (m, 4H, 13,13-CH<sub>2</sub>), 3.78-4.16 (m, 6H, 2-CH, 12-CH<sub>2</sub>, 17-CH<sub>3</sub>), 5.61-7.008 (br., 1H, 3-NH), 7.07-7.52 (m, 2H, 11-CH-Aromatic, 15-NH<sup>+</sup>), 7.55-7.90 (br., (s) 1H, 10-CH-Aromatic), 9.79-10.1 (br. (s),1H, 16-CHO).

IR (KBr): ν (cm<sup>-1</sup>): 3342(s) (NH), 3090, 2987 (s) (CH) Aliphatic, 2300 (br.) (NH<sup>+</sup>), 1773(s) (C=O, carbonyl), 1655 (C=O, amide).

### 2.8.5. Synthesis of poly (NASI-Co-NIPAAm) with 10, and 15 mol% of NASI.



**44-10,15**

#### Procedure:

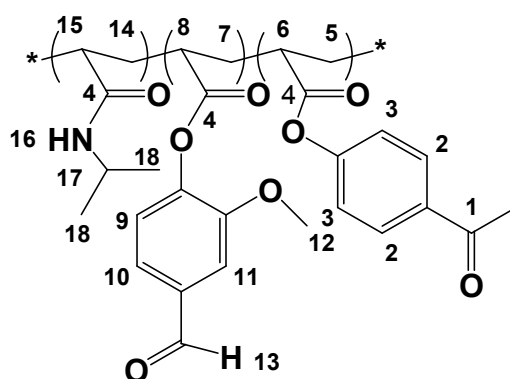
The same method used in copolymerization of (NIPAAm), also used in synthesis of 10, 15 mol% poly (NASI-Co-NIPAAm) using 2.00g (0.0176mol) of NIPAAm, and 50mL 1,4-dioxane.

Actual amounts for both monomers and initiator are cleared in the table below.

**Table 11:** Shows the mole ratios of VA, VPA and amount of AIBN, yield and physical state, also the chemical analysis (<sup>1</sup>H NMR, IR) of poly(NIPAAm-Co-VA-Co-VPA).

Polymer	NASI	AIBN	Yield%	Physical state	NASI	
					Feeding mol%	<sup>1</sup> H NMR mol%
44-10	0.295g(1.75 mmol)	6 mg	93	Solid	10	9,98
44-15	0.45g(2.67mmol)	10 mg	93	Solid	15	12,8
<sup>1</sup> H NMR				IR (KBr)		
<sup>1</sup> H NMR (500 MHz, CDCl <sub>3</sub> ): δ(ppm) = 0.89-1.36(m, 6H, 1-2CH <sub>3</sub> ), 1.45-2.68 (m, 6H, 5,7-CH <sub>2</sub> , 6,8-CH), 2.75-3.01 (m, 4H, 10-2CH <sub>2</sub> ), 3.87-4.15 (m, 1H, 2-CH), 6.01-6.81(m, 1H, 3-NH)				IR (KBr): ν (cm <sup>-1</sup> ): 3069 and 2978 (CH-Aliphatic), 1755 (s) (C=O, carbonyl), 1690 (s) (C=O, amide).		

### 2.8.6. Synthesis of terpolymer of poly (NIPAAm-Co-VA-Co-APA).



45-10-10

#### Procedure:

In 100 mL round bottom flask, 10 mol% of (12) was added to 10 mol% (14) respectively and to 2.00g (0.0176mol) NIPAAm in 50mL 1,4-dioxane and AIBN was also added. The reaction mixture was purged in argon for 20 min., and then heated in oil bath at 70°C for 8h. After cooling at room temperature and also in refrigerator, the polymer was precipitated in diethylether, at -60°C, then dissolved in THF, and reprecipitated in diethylether to remove the unreacted monomers and impurities.

Actual amounts for both monomers and initiator are cleared in the table below.

**Table 12:** Shows the mole ratios of VA, VPA and amount of AIBN, yield and physical state, also the chemical analysis (<sup>1</sup>H NMR, IR) of poly (NIPAAm-Co-VA-Co-VPA).

Polymer	VA	APA	AIBN	Yield%	Physical state
45-10-10	0.362g (1,76mmol)	0.334g (1,76 mmol)	10mg	90	Solid
	<sup>1</sup> H NMR	IR (KBr)			
	<sup>1</sup> H NMR (500 MHz, CDCl <sub>3</sub> ): δ(ppm) = 0.79-1.35(m, 6H, 18-2CH <sub>3</sub> ), 1.43-2.46 (m, 9H, 5,7,14-CH <sub>2</sub> , 6,8,15-CH), 2.47-2.66 (m, 3H, 1-CH <sub>3</sub> ), 3.78-4.19 (m, 1H, 17-CH), 5.88-6.72(m, 1H, 16-NH), 7.07-7.23 (m, 3H, 3,9-3CH-Ar.), 7.38-7.59 (m, 2H, 10,11-2CH), 7.84-8.05 (m, 2H, 2-2CH), 9.86-10.04(m, 1H, 13-CHO).	IR (KBr): ν (cm <sup>-1</sup> ): 3363 (N-H), 3069 and 2978 (CH-Aliphatic), 1762 (s) (C=O, carbonyl), 1690 (s) (C=O, aldehyde), 1570,(s)(C=O amide), 1104 (m) (OCH <sub>3</sub> ), 860 (m) (CH-Ar.).			

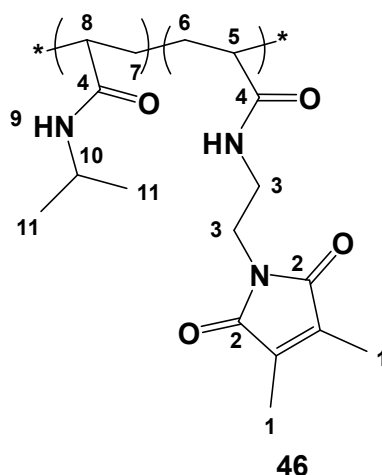
**Table 13:** Clear mole ratio of feeding of DMIAAm, and calculated using <sup>1</sup>HNMR and UV-spectroscopy.

Polymer	Feeding mol%		<sup>1</sup> HNMR (mol%)	
	VA	APA	VA	APA
45-10-10	10	10	6,5	9,8

## 2.9. Synthesis of photo-crosslinker polymers.

### 2.9.1. Synthesis of poly (NIPAAm-*Co*-DMIAAm) with 2, 5 and 10 mol% of acrylamide crosslinker.

Photo-crosslinkable polymers of NIPAAm were synthesized by free radical polymerization of NIPAAm with varying mol-% of acrylamide photo-crosslinker.



#### General procedure

In round bottom flask, 2, 5 and 10 mol% of acrylamide cross-linker was added to 3.00g (0,0265mol) NIPAAm in 60 mL 1,4-dioxane and AIBN was also added. The reaction mixture was purged in argon for 20 min., and then heated in oil bath at 70°C for 8h. After cooling at room temperature and also in refrigerator, the polymer was precipitated in diethylether, at -50 °C, then dissolved in THF, and reprecipitated in diethylether to remove the unreacted monomers and impurities.

**Table 14:** Clears the mole ratios of DMIAAm and amount of AIBN, yield and physical state, also the chemical analysis (<sup>1</sup>H NMR, IR) of poly(NIPAAm-*Co*-DMIAAm).

Polymer	DMIAAm	AIBN	Yield%	Physical state
46-02	0.1178g (0.53 mmol)	9.06mg	89	Solid
46-05	0.294g (1.325 mmol)	9.33mg	85	Solid

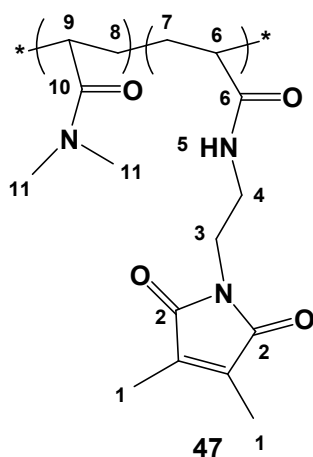
## Experimentals

46-10	0.588g (2.65 mmol)	9.77mg	83	Solid
<sup>1</sup> H NMR		IR (KBr)		
<sup>1</sup> H NMR (500 MHz, CDCl <sub>3</sub> ): δ(ppm) = 0.97-1.25 (m, 6H, 11-2CH <sub>3</sub> ), 1.26-1.46 (m, 5H, 5-CH, 6,7-CH <sub>2</sub> ), 1.88-1.99 (m, 6H, 1-CH <sub>3</sub> ), 2.01-2.34 (m, 1H, 8-CH), 3.86-4.12 (m, 1H, 10-CH), 6.28 (br. s, 1H, 3-NH).		IR (KBr): ν (cm <sup>-1</sup> ): 3326 (N-H), 3090 and 2945 (CH-Aliphatic), 1660 (4-C=O, NIPAAm), 1550 (4-C=O, DMIAAm).		

**Table 15:** Clear mole ratio of feeding of DMIAAm and calculated using <sup>1</sup>HNMR and UV-spectroscopy.

polymer	Feeding mol%	<sup>1</sup> HNMR (mol %)	UV (mol %)
46-02	2	1.96	1.98
46-05	5	4.15	4.33
46-10	10	6.25	7.32

### 2.9.2. Synthesis of photo-crosslinker poly(DMAAm-Co-DMIAAm) with 2, 5 and 10 mol% of maleimido crosslinker.



#### General procedure:

The same method used in synthesis of poly(NIPAAm-Co-DMIAAm), also used in synthesis of poly(DMAAm-Co-DMIAAm) using 3.00g (0.03026mol), in 60 mL 1,4-dioxane.

Actual amounts for both monomers, and initiator were used, also the volume of solvent are cleared in the table below.

**Table 16:** Clears the mole ratios of DMIAAm, and amount of AIBN, yield and physical state, also the chemical analysis ( $^1\text{H NMR}$ , IR) of poly (DMAAm-*Co*-DMIAAm).

Polymer	DMIAAm	AIBN	Yield%	Physical state
47-02	0.1344g (0.6 mmol)	9.89mg	93	Solid
47-05	0.335g (1.51 mmol)	10.19mg	94	Solid
47-10	0.671g (3.02 mmol)	10.67mg	89	Solid

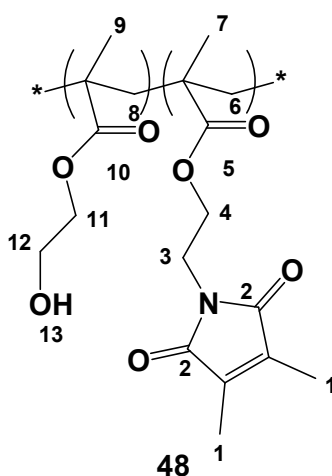
  

$^1\text{H NMR}$	IR (KBr)
$^1\text{H NMR}$ (500 MHz, $\text{CDCl}_3$ ): $\delta(\text{ppm}) =$ 1.41-1.85 (m, 2H, 8- $\text{CH}_2$ ), 1.88-1.99 (m, 6H, 1-2 $\text{CH}_3$ ), 2.33-2.75(m, 3H, 6-CH, 7- $\text{CH}_2$ ), 2.74-3.22 (m, 7H, 9-CH, 11- $\text{CH}_3$ ), 3.48-3.68 (m, 4H, 3,4- $\text{CH}_2$ ).	IR (KBr): $\nu$ ( $\text{cm}^{-1}$ ): 2945 (CH-Aliphatic), 1710 (10-C=O, DMAAm), 1647 (2-C=O, DMIAAm).

**Table 17:** Clear mole ratio of feeding of DMIAAm, and calculated using  $^1\text{HNMR}$  and UV-spectroscopy.

polymer	Feeding mol%	$^1\text{HNMR}$ (mol%)	UV (mol%)
47-02	2	1.87	1.89
47-05	5	3.65	4.21
47-10	10	9.33	9.56

### 2.9.3. Synthesis of photo-crosslinker poly(HEMA-*Co*-DMIMA) with 2, 5 and 10 mol% of acrylamide crosslinker.



**General procedure:**

The same method used above, also used in synthesis of poly (HEMA-*Co*-DMIMA). 2.00g (0,015mol) of HEMA and AIBN was added to 2, 5, 10 mol% of DMIMA, dissolved in 40mL absolute ethanol.

Actual amounts for both monomers and initiator were used, also the volume of solvent are cleared in the table below.

**Table 18:** Clears the mole ratios of DMIAAm and amount of AIBN, yield and physical state, also the chemical analysis (<sup>1</sup>H NMR, IR) of poly (HEMA-*Co*-DMIAAm).

Polymer	DMIMA	AIBN	Yield%	Physical state
<b>48-02</b>	0.07g(0.295 mmol)	5.61 mg	84	Solid
<b>48-05</b>	0.182g(0.767 mmol)	5.79 mg	91	Solid
<b>48-10</b>	0.365g(1.538 mmol)	6.07 mg	86	Solid

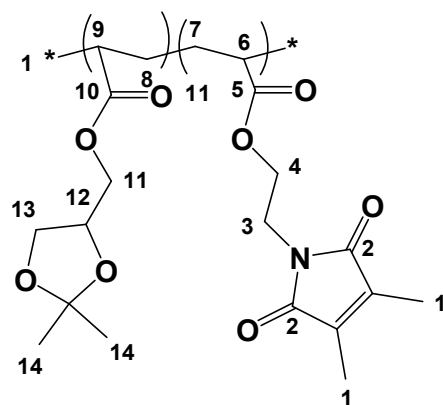
  

<sup>1</sup> H NMR	IR (KBr)
<sup>1</sup> H NMR (500 MHz, DMSO): $\delta(\text{ppm}) = 0.70\text{-}1.02$ (m, , 6 H, 7.9-CH <sub>3</sub> ), 1.36-1.60(m, 2H. 6-CH <sub>2</sub> )1.72-1.98 (m, 8H, 1-CH <sub>3</sub> , , 8-CH <sub>2</sub> ), 3.52-3.65 (m, 2 H, 12-CH <sub>2</sub> ), 3.74-4.22 (m, , 2 H, 11-CH <sub>2</sub> ), 4.68-4.98 (m, , 1 H, 11-OH).	IR (KBr): $\nu (\text{cm}^{-1})$ : 3460 (s) br. (OH), 2952(s) (CH-Aliphatic), 1724(s).

**Table 19:** Clear mole ratio of feeding of DMIMA, and calculated using <sup>1</sup>HNMR, and UV-spectroscopy.

polymer	Feeding mol%	<sup>1</sup> HNMR (mol%)	UV (mol%)
<b>48-02</b>	2	1.93	1.95
<b>48-05</b>	5	4.77	4.88
<b>48-10</b>	10	6.33	7.45

### 2.9.4. Synthesis of photo-crosslinker poly (SKA-Co-DMIA) with 2, 5 and 10 mol% of acrylamide crosslinker.



49

#### General procedure:

In round bottom flask 2, 5 and 10 mol% of acrylamide cross-linker was added to 2.00g (0,01mol) SKA in 1,4-dioxane and AIBN was also added. The reaction mixture was purged in argon for 20 min., and then heated in oil bath at 60°C for 8h. After cooling at room temperature and also in refrigerator, the polymer was extracted in diethylether, at -50°C, and then the solvent was removed under reduced pressure to collect the viscous oil polymer. After this the crude polymer was purified by dissolving in THF and re-extracted in diethylether as too viscous oil which, solidify under reduced pressure.

Actual amounts for both photo-crosslinker and initiator were used also, are cleared in the table below.

**Table 20:** The mole ratios of DMIAAm, and amount of AIBN, yield and physical state, also the chemical analysis (<sup>1</sup>H NMR, IR) of poly (SKA-Co-DMIAAm).

Polymer	DMIMA	AIBN	Yield%	Physical state
49-02	0.048g(0.257 mmol)	4.19 mg	45	Solid under pressure
49-05	0.25g(0.767 mmol)	4.40 mg	50	Solid under pressure
49-10	0.365g(1.538 mmol)	4.72 mg	47	Solid under pressure
<sup>1</sup> H NMR			IR (KBr)	
<sup>1</sup> H NMR (500 MHz, CDCl <sub>3</sub> ): δ(ppm) = 1.29-			IR (KBr): ν (cm <sup>-1</sup> ): 2987-2940(s)	
1.46(m, 6H, 14-2CH <sub>3</sub> ), 1.47-1.78(m, 3H, 6-CH, 7-			(CH-Aliphatic), 1747(s) (C=O),	
CH <sub>2</sub> ), 1.90-2.01 (m, 6H, 1-2CH <sub>3</sub> ), 2.19-2.49 (m,			1680(s) (C=C).	
3H, 8-CH <sub>2</sub> , 9-CH), 3.63-3.86 (m, 2H, 13-CH <sub>2</sub> ),				

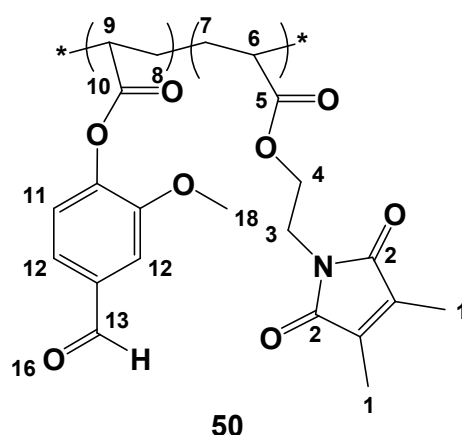
## Experimentals

3.94-4.21 (m, 6H, 11-CH<sub>2</sub>, 3,4-CH<sub>2</sub>), 4.22-4.39(m, 1H, 12CH).

**Table 21:** The mole ratios of feeding of DMIMA, and calculated using <sup>1</sup>HNMR and UV-spectroscopy.

Polymer	Feeding mol%	<sup>1</sup> HNMR (mol%)	UV (mol%)
49-02	2	3.19	3.56
49-05	5	10.5	11.23
49-10	10	14.08	14.22

### 2.9.6. Synthesis of functionalized photo-crosslinker poly(VA-Co-DMIA) with 2, 5 and 10 mol% of acrylamide crosslinker.



#### General procedure:

In 100mL round bottom flask. 5 and 10 mol% of acrylamide cross-linker (DMIA) was added to 2.00g (0.0112mol) 4-formyl-2-methoxyphenyl acrylate in 40mL 1,4-dioxane and AIBN was also added. The reaction mixture was purged in argon for 20 min., and then heated in oil bath at 70°C for 8h. After cooling at room temperature and also in refrigerator, the polymer was precipitated in diethylether, at -20°C, then dissolved in THF, and reprecipitated in diethylether to remove the unreacted monomers and impurities.

Actual amounts for both photo-crosslinker and initiator are cleared in the table below.

## Experimentals

**Table 22:** The mole ratios of DMIAAm and amount of AIBN, yield and physical state, also the chemical analysis (<sup>1</sup>H NMR, IR) of poly(VA-Co-DMIA).

Polymer	DMIMA	AIBN	Yield%	Physical state
50-02	0.05g(0.22 mmol)	4.90 mg	74	Solid
50-05	0.151g(0.6 mmol)	5.06 mg	78	Solid
50-10	0.302g(1.2 mmol)	5.32 mg	73	Solid

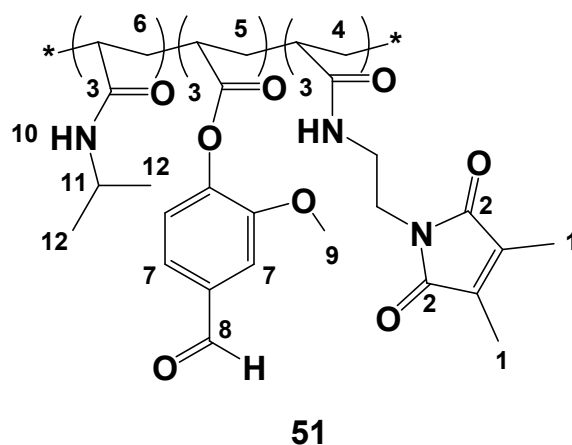
<sup>1</sup> H NMR	IR (KBr)
<sup>1</sup> H NMR (500 MHz, DMSO): $\delta$ (ppm) = 1.50-2.23(m, 8H, 1-2CH <sub>3</sub> , 7-CH <sub>2</sub> ), 2.61-3.20(m, 1H, 6-CH), 3.45-3.95 (m, 6H, 18-CH <sub>3</sub> ,8-CH <sub>2</sub> , 9-CH ), 6.92-7.67 (m, 3H, 11,12-CH-Ar.), 9.86-10.08 (m, 1H, 13-CHO).	IR (KBr): $\nu$ (cm <sup>-1</sup> ): 2995-2850(s) (CH-Aliphatic), 1760(s) (C=O, carbonyl), 1706(s) (C=O, Aldehyde), 1600(s) (C=C), 1096 (s) (O-CH <sub>3</sub> ), 725-852 (m) (CH-Aromatic).

**Table 23:** The mole ratios of feeding of DMIA, and calculated using <sup>1</sup>HNMR and UV-spectroscopy.

Polymer	Feeding mol%	<sup>1</sup> HNMR (mol%)	UV (mol%)
50-02	2	1.83	1.83
50-05	5	3.99	4.11
50-10	10	9.09	9.21

## 2.10. Synthesis of photo-crosslinker functional polymers.

2.10.1 Synthesis of functionalized photo-crosslinker poly(NIPAAm-*Co*-VA-*Co*-DMIAAm) with 2, 5 and 10 mol% of acrylamide cross-linkable and 5, 10 and 15 mol% of VA respectively.



### General procedure:

In 100mL round bottom flask. 2, 5 and 10 mol% of maleimido crosslinker (DMIAAm) was added to 5, 10 and 15 mol% 4-formyl-2-methoxyphenyl acrylate respectively and to 2.00g (0,0176mol) NIPAAm in 50mL 1,4-dioxane and AIBN was also added. The reaction mixture was purged in argon for 20 min., and then heated in oil bath at 70°C for 8h. After cooling at room temperature and also in refrigerator, the polymer was precipitated in diethylether, at -50°C, then dissolved in THF, and reprecipitated in diethylether to remove the unreacted monomers and impurities.

Actual amounts for (VA), photo-crosslinker and initiator are cleared in the table below.

**Table 24:** The mole ratios of VA, DMIA and amount of AIBN, yield and physical state, also the chemical analysis (<sup>1</sup>H NMR, IR) of poly (NIPAAm-*Co*-VA-*Co*-DMIA).

Polymer	VA	DMIA	AIBN	Yield%	Physical state
51-02-05	0.182g(0.88mmol)	0.05g(0.22 mmol)	10.12 mg	85	Solid
51-05-10	0.363g(1.76mmol)	0.151g(0.6 mmol)	10.81 mg	83	Solid
51-10-15	0.545g(2.64mmol)	0.302g(1.2 mmol)	11.61 mg	75	Solid

<sup>1</sup>H NMR

IR (KBr)

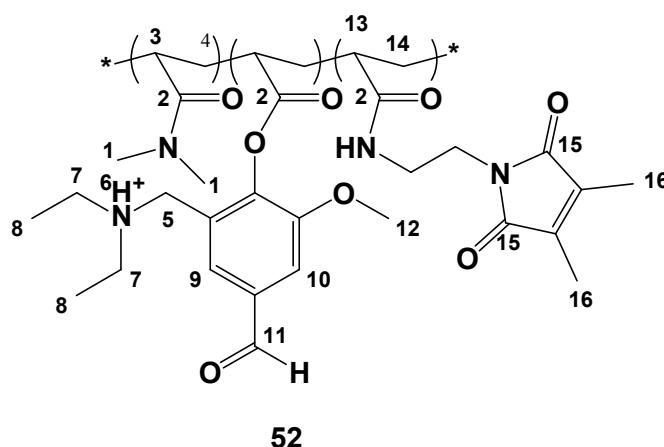
<sup>1</sup>H NMR (500 MHz, CDCl<sub>3</sub>): δ(ppm) = 1.10- IR(KBr): ν (cm<sup>-1</sup>): 3097-2987(s) (CH-

1.41(m, 6H, 12-2CH<sub>3</sub>), 1.44-1.81(m, 6H, 4- Aliphatic), 1760(s) (C=O, carbonyl), 3CH<sub>2</sub>), 1.82-1.99 (m, 6H, 1-2CH<sub>3</sub>), 2.02-2.64 1706(s) (C=O, Aldehyde), 1600(s) (m, 3H, 5-3CH), 3.64-3.73 (m, 3H, 9-CH<sub>3</sub>), (C=C), 1104 (s) (O-CH<sub>3</sub>), 800-852 (m) 3.87-4.22(m, 1H, 11-CH), 5.86-6.82 (br., 1H, (CH-Aromatic). 10-NH), 7.11-7.30 (m, 1H, 6-CH-Ar.), 7.37-7.60 (m, 2H, 7-2CH-Ar.), 9.86-10.04 (m, 1H, 8-CHO).

**Table 25:** The mole ratios of feeding of DMIA, VA, and calculated using <sup>1</sup>HNMR and UV-spectroscopy.

Polymer	Feeding mol%		<sup>1</sup> HNMR (mol%)		UV (mol%)
	DMIAAm	VA	DMIAAm	VA	DMIAAm
51-02-05	2	5	1.9	4.2	1.96
51-05-10	5	10	5.88	11.11	5.97
51-10-15	10	15	7.69	14.28	7.85

**2.10.2. Synthesis of functionalized photo-crosslinker poly(DMAAm-Co-DEAMVA-Co-DMIAAm) with 2, 5 and 10 mol% of acrylamide crosslinker and 5, 10 and 15 mol% of DEAMVA respectively.**



**General procedure:**

The same method used above, also used in synthesis of poly (DMAAm-Co-DEAMVA-Co-DMIAAm), using 2.00g (0.02mol) of DMAAm, and 40mL 1,4-dioxane.

Actual amounts for both monomers and initiator were used, are cleared in the table below.

## Experimentals

**Table 26:** The mole ratios of DEAMVA, DMIAAm and amount of AIBN, yield and physical state, also the chemical analysis (<sup>1</sup>H NMR, IR) of poly (DMAAm-Co-DEAMVA-Co-DMIAAm).

Polymer	DEAMVA	DMIA	AIBN	Yield%	Physical state
52-02-05	0.291g(0.99mmol)	0.088g(0.39 mmol)	10.12 mg	90	Solid
52-05-10	0.582g(1.99mmol)	0.224g(1 mmol)	10.81 mg	65	Solid
52-10-15	0.874g(2.99mmol)	0.518g(2mmol)	11.61 mg	45	Solid

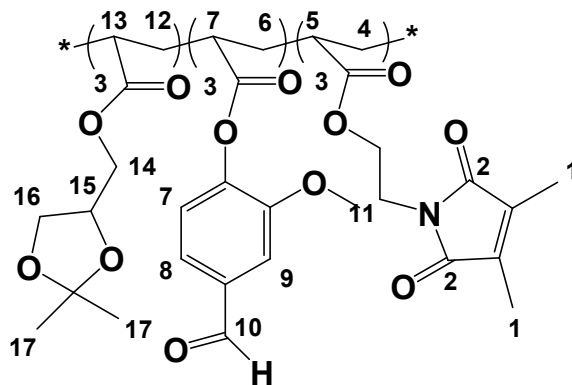
  

<sup>1</sup> H NMR	IR (KBr)
<sup>1</sup> H NMR (500 MHz, CDCl <sub>3</sub> ): δ(ppm) = 0,83-1,08(m, 6H, 8-2CH <sub>3</sub> ), 1,09-1,41(m, 1H, 3-CH), 1,42-1,87 (m, 2H, 4-CH <sub>2</sub> ), 1,88-2.04 (m, 6H, 16-2CH <sub>3</sub> ), , 2.23-2.73 (m, 7H, 7-2CH <sub>2</sub> , 13-CH, 14-CH <sub>2</sub> ),2.74-3.26(m, 6H, 1-CH <sub>3</sub> ), 3.38-3.71 (m, 3H, 4-CH, 5-CH <sub>2</sub> ), 3.76-3.98 (m, 5H, 7-CH <sub>2</sub> , 12-CH <sub>3</sub> ), 7.29-7.43 (m, 2H, 10-CH-Ar.,6-NH <sup>+</sup> ), 7.63-7.80(m, 1H, 9-CH-Ar.), 9.87-10.01 (m, 1H, 11-CHO).	IR (KBr): ν (cm <sup>-1</sup> ): 2943(s) (CH-Aliphatic), 2349(w) br. (NH <sup>+</sup> ), 1760(s) (C=O, carbonyl), 1715(s) (C=O, Aldehyde), 1635(s) (C=C), 1151 (s) (O-CH <sub>3</sub> ), 840-852 (m) (CH-Ar.).

**Table 27:** The mole ratios of feeding of DMIA, DEAMVA, and calculated using <sup>1</sup>HNMR and UV-spectroscopy.

Polymer	Feeding mol%		<sup>1</sup> HNMR (mol%)		UV (mol%)
	DMIAAm	DEAMVA	DMIAAm	DEAMVA	DMIAAm
52-02-05	2	5	4.38	1.46	4.93
52-05-10	5	10	7.45	4.85	8.54
52-10-15	10	15	7.75	4.05	8.33

### 2.10.3. Synthesis of photo-crosslinker poly(SKA-Co-VA-Co-DMIA) with 5 and 10 mol% of acrylamide crosslinker and 10, and 15 mol% of VA.



53

#### General procedure:

In round bottom flask. 5mol% of acrylamide cross-linker was added to 2.00g (0,01mol) SKA and 10 and 15 mol% of VA in 40mL 1,4-dioxane and AIBN was also added. The reaction mixture was purged in argon for 20 min., and then heated in oil bath at 70°C for 12h. After cooling at room temperature and also in refrigerator, the polymer was extracted in diethylether, at -50°C, and then the solvent was removed under reduced pressure to collect the viscous oil polymer. After this the crude polymer was purified by dissolving in THF and reextracted in diethylether as too viscous oil which, solidify under reduced pressure.

Actual amounts for VA, photo-cross-linker, and initiator are cleared in the table below.

**Table 28:** The mole ratios of VA, DMIA and amount of AIBN, yield and physical state, also the chemical analysis (<sup>1</sup>H NMR, IR) of poly (SKA-Co-VA-Co-DMIA).

Polymer	VA	DMIA	AIBN	Yield%	Physical state
53-05-10	0.2g(1mmol)	0.119g(0.5 mmol)	7 mg	50	Solid
53-7,5-15	0.3g(1.5mmol)	0.167g(0.75 mmol)	7.7 mg	46	Solid

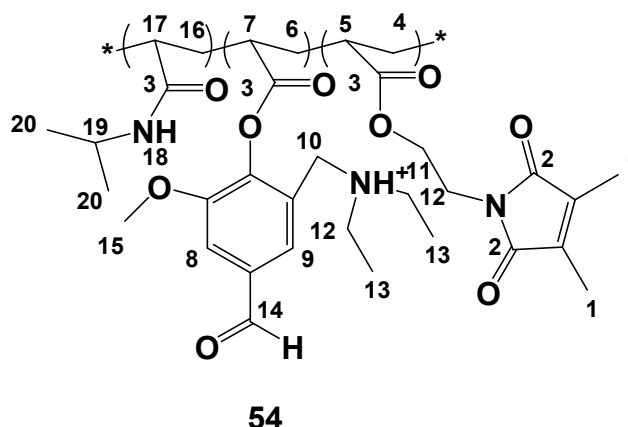
<sup>1</sup> H NMR	IR (KBr)
<sup>1</sup> H NMR (CDCl <sub>3</sub> ): δ(ppm) = 1.22-1.47(m, 6H, 17-2CH <sub>3</sub> ), 1.54-1.87(m, 3H, 12-CH, 13-CH <sub>2</sub> ), 1.88-2.06 (m, 6H, 1-2CH <sub>3</sub> ), 3.61-3.81 (m, 2H, 16-CH), 3.82-3.94 (m, 3H, 11-CH <sub>3</sub> ), 3.95-4.06	IR (KBr): ν (cm <sup>-1</sup> ): 2958-2940(s) (CH-Aliphatic), 1720(s) (C=O), 1600(s) (C=C), 820(s) (CH-Ar.).

(m, 2H, 14-2CH<sub>2</sub>), 4.07-4.26 (m, 1H, 15-CH),  
7.17-7.34(m, 1H, 8-CH-Ar. ), 7.38-7.53(m, 2H,  
7,9-2CH-Ar.), 9.85-9.99 (m, 1H, 10-CHO).

**Table 29:** The mole ratios of feeding of DMIA, VA, and calculated using <sup>1</sup>HNMR and UV-spectroscopy.

Polymer	Feeding mol%		<sup>1</sup> HNMR (mol%)		UV (mol%)
	DMIA	VA	DMIA	VA	DMIA
53-05-10	5	10	4.5	9	4.73
53-7.5-15	7.5	15	7.3	12.3	8.12

#### 2.10.4. Synthesis of photo-crosslinker Poly(NIPAAm-*Co*-DMEAVA-*Co*-DMIAAm) with 5, 7.5 and 10 mol% of acrylamide crosslinker and 10, 15 and 20 mol% of DEMAVA.



#### General procedure:

In 100mL round bottom flask. 5, 7.5 and 10 mol% of maleimido crosslinker (DMIAAm) was added to 10 and 15, 20 mol% of 2-[(diethylamino)methyl]-4-formyl-6-methoxyphenyl acrylate ( DEMAVA ) respectively and to 2.00g (0,0176mol) NIPAAm in 40 mL 1,4-dioxane and AIBN was also added. The reaction mixture was purged in argon for 20 min., and then heated in oil bath at 70°C for 8h. After cooling at room temperature and also in refrigerator, the polymer was precipitated in diethylether, at -30°C, then dissolved in THF, and reprecipitated in diethylether to remove the unreacted monomers and impurities.

Actual amounts for both monomers and initiator are cleared in the table below.

## Experimentals

**Table 30:** The mole ratios of DEMA VA, DMIAAm and amount of AIBN, yield and physical state, also the chemical analysis ( $^1\text{H}$  NMR, IR) of poly (NIPAAm-Co-DEMAVA-Co-DMIAAm).

Polymer	DEMAVA	DMIAAm	AIBN	Yield%	Physical state
54-05-10	0.51g(1.76mmol)	0.195g(0.88 mmol)	12.5mg	60	Solid
54-7,5-15	0.769g(2.64mmol)	0.29g(1.32mmol)	13.51g	57	Solid
54-10-20	1.02g(3.52mmol)	0.39g(1.76 mmol)	14.3mg	58	Solid

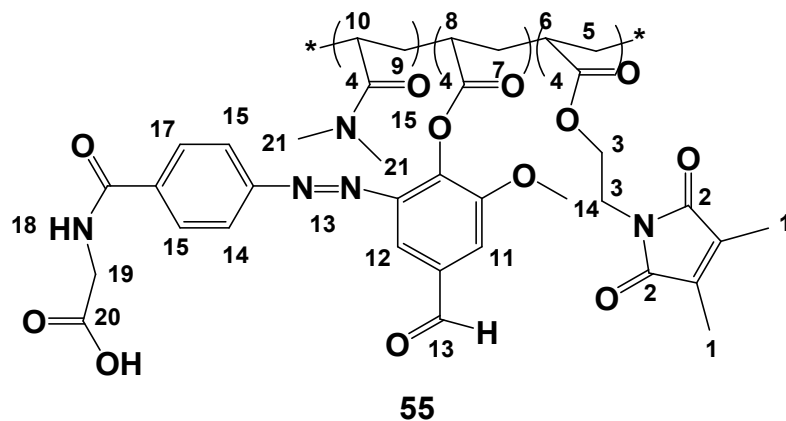
  

$^1\text{H}$ NMR	IR (KBr)
$^1\text{H}$ NMR (500 MHz, $\text{CDCl}_3$ ): $\delta(\text{ppm}) = 0.76-1.30$ (m, 6H, 20-2 $\text{CH}_3$ ), 1.45-1.70 (m, 1H, 16- $\text{CH}_2$ ), 1.70-1.87 (m, 6H, 13,13-2 $\text{CH}_3$ ), 1.89-2.02 (m, 6H, 1-2 $\text{CH}_3$ ), 2.03-2.22 (m, 6H, 4,6-2 $\text{CH}_2$ , 5,7-2CH), 3.39-3.53 (m, 4H, 12,12-2 $\text{CH}_2$ ), 3.56-3.77 (m, 5H, 10- $\text{CH}_2$ , 15- $\text{CH}_3$ ), 3.80-4.18 ( m, 1H, 19-CH), 5.91-6.90 (br., 1H, 18- $\text{NH}^+$ ), 7.30-7.47 (m, 2H, 8-CH-Ar., 11- $\text{NH}^+$ ), 7.59-7.79 (m, 1H, 9-CH-Ar.), 9.79-10.10 (m,1H, 14-CHO).	IR(KBr): $\nu$ ( $\text{cm}^{-1}$ ): 3100, 2948(s) (CH-Aliphatic), 2350(w) br. ( $\text{NH}^+$ ), 1761(s) (C=O, carbonyl), 1710(s) (C=O, Aldehyde), 1630(s) (C=C), 1154 (s) (O- $\text{CH}_3$ ),830-840 (m) (CH-Ar.).

**Table 31:** The mole ratios of feeding of DMIAAm, DEAMVA, and calculated using  $^1\text{HNMR}$  and UV-spectroscopy.

Polymer	Feeding mol%		$^1\text{HNMR}$ (mol%)		UV (mol%)
	DMIAAm	DEMAVA	DMIAAm	DEMAVA	DMIAAm
54-05-10	5	10	4.3	3	5.13
54-7.5-15	7.5	15	5.5	3.77	5.93
54-10-20	10	20	7.40	6.54	8.20

### 2.10.5. Synthesis of photo-crosslinker Poly(DMAAm-Co-AHVA-Co-DMIA) with 5 and 10 mol% of acrylamide crosslinker and 5 and 10 mol% of AHVA.



#### General procedure:

In 100mL round bottom flask. 5 and 10 mol% of acrylamide cross-linker (DMIA) was added to 5 and 10 mol% of [4-[2-(acryloyloxy)-5-formyl-3-methoxyphenyl] diazenyl}benzoyl amino] acetic acid (AHVA) respectively and to 2.00g (0,02mol) DMAAm in 40 mL 1,4-dioxane and AIBN was also added. The reaction mixture was purged in argon for 20 min., and then heated in oil bath at 70°C for 8h. After cooling at room temperature and also in refrigerator, the polymer was precipitated in diethylether, at -20°C, then dissolved in THF, and reprecipitated in diethylether to remove the unreacted monomers and impurities.

Actual amounts for both monomers and initiator are cleared in the table below.

**Table 32:** The mole ratios of AHVA, DMIA and amount of AIBN, yield and physical state, also the chemical analysis (1H NMR, IR) of poly (DMAAm-Co-AHVA-Co-DMIA).

Polymer	AHVA	DMIA	AIBN	Yield%	Physical state
55-05-05	0.41g(1mmol)	0.22g(1 mmol)	16.15mg	65	Solid
55-10-10	0.82g(2mmol)	0.44g(2mmol)	17.60mg	53	Solid

<sup>1</sup> H NMR	IR (KBr)
<sup>1</sup> H NMR (500 MHz, CDCl <sub>3</sub> ): δ(ppm) = 0.72-0.92 (m, 1H, 6-CH), 1.05-1.42 (m, 2H, 7-CH <sub>2</sub> ), 1.47-1.98 (m, 8H, 1-2CH <sub>3</sub> , 9-CH <sub>2</sub> ), 2.70-3.25 (m, 8H, 8-CH, 10-CH, 21-2CH <sub>3</sub> ), 3.60-3.69 (m, 3H,	IR (KBr): ν (cm <sup>-1</sup> ): 2937(s) (CH-Aliphatic), 1748(s) (C=O, carbonyl), 1712(s) (C=O, Aldehyde), 1650(s) (C=C, CONH), 1505 (m) (-N=N-),



**Table 34:** The mole ratios of AHVA, DMIA and amount of AIBN, yield and physical state, also the chemical analysis (<sup>1</sup>H NMR, IR) of poly (DMAAm-*Co*-AHVA-*Co*-DMIA).

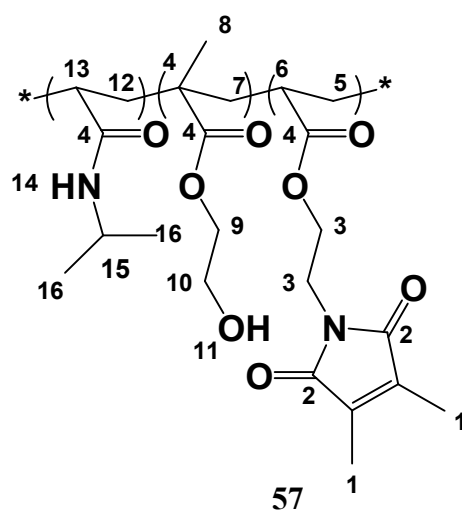
Polymer	AHVA	DMIA	AIBN	Yield%	Physical state
56-10-20	0.41g(1mmol)	0.22g(1 mmol)	16.15mg	40	Solid
<sup>1</sup> H NMR			IR (KBr)		
<sup>1</sup> H NMR (500 MHz, DMSO): δ(ppm) = 0.77-1.13 (m, 6H, 20-2CH <sub>3</sub> ), 1.34-1.64 (m, 4H, 6,17-2CH <sub>2</sub> ), 1.78-1.99 (m, 6H, 1-2CH <sub>3</sub> ), 2.01-2.34(m, 2H, 7,18-CH) 3.50-4.48 (m, 6H, 13-CH <sub>2</sub> , 16-CH <sub>3</sub> , 19-CH), 5.99-6.75 (m, 1H, 8-CH-Ar.), 6.99-8.50 (m, 6H, 8 <sup>-</sup> , 10,11-CH-Ar., 12-NH), 9.25-10.19 (m, 2H, 14-COOH, 15-CHO).			IR (KBr): ν (cm <sup>-1</sup> ): 2962(s) (CH-Aliphatic), 1750(s) (C=O, carbonyl), 1715(s) (C=O, Aldehyde), 1643(s) (C=C, CONH), 1550 (m) (-N=N-), 1108 (s) (O-CH <sub>3</sub> ), 760,835 (m) (CH-Ar.).		

**Table 35:** The mole ratios of feeding of DMIA, AHVA, and calculated using <sup>1</sup>HNMR and UV-spectroscopy.

Polymer	Feeding mol%		<sup>1</sup> HNMR (mol%)		UV (mol%)
	DMIA	AHVA	DMIA	AHVA	DMIA
56-10-20	10	20	4.1	51.9	4.75

## 2.11. Synthesis of grafted polymers.

### 2.11.2. Synthesis of poly(NIPAAm-*Co*-HEMA-*Co*-DMIA)



**Procedure**

The same method used above, also used in synthesis of poly(NIPAAm-*Co*-NASI-*Co*-DMIAAm), using a mixture of 3.00g (26.5mmol) of NIPAAm, 5 mol% and 10 mol% of DMIAAm and HEMA respectively in 60mL 1,4-dioxane.

Actual amounts for both monomers and initiator are cleared in the table below.

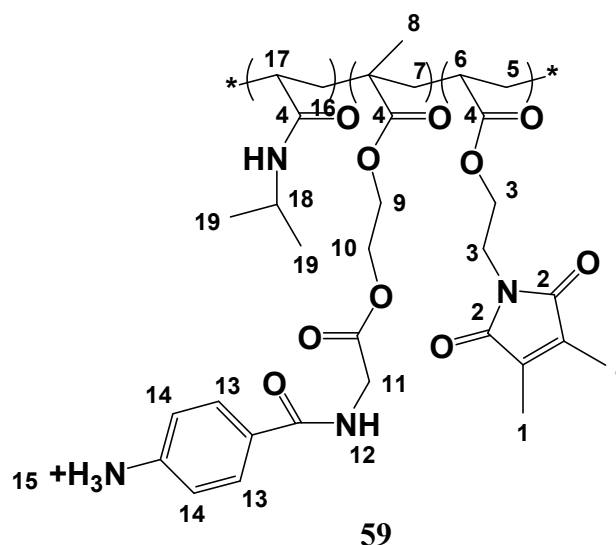
**Table 36:** The mole ratios of NASI, DMIAAm and amount of AIBN, yield and physical state, also the chemical analysis (<sup>1</sup>H NMR, IR) of poly (NIPAAm-*Co*-HEMA-*Co*-DMIA).

Polymer	HEMA	DMIA	AIBN	Yield%	Physical state
57-05-10	0.344g(2.65mmol)	0.294g(1.32 mmol)	14mg	90	Solid
<sup>1</sup> H NMR			IR (KBr)		
<sup>1</sup> H NMR (500 MHz, CDCl <sub>3</sub> ): δ(ppm) = 0.76-0.91 (m, 1H, 6-CH), 0.95-1.38 (m, 6H, 15-2CH <sub>3</sub> ), 1.43-1.70 (m, 6H, 7,12-CH <sub>2</sub> , 13-CH), 1.70-1.91 (m, 3H, 8-CH <sub>3</sub> ), 1.92-2.01(m, 6H, 1-2CH <sub>3</sub> ), 2.02-2.36 (m, 2H, 6-CH <sub>2</sub> ), 3.68-3.71 (m, 1H, 11-OH), 3.72-3.77 (m, 2H, 10-CH <sub>2</sub> ), 3.80-4.2(m, 1H,15-CH), 4.2-4.30 (m, 2H, 9-CH <sub>2</sub> ), 5.94-6.65(m, 1H, 14-NH).			IR (KBr): ν (cm <sup>-1</sup> ): 3060, 2979(s) (CH-Aliphatic), 1711 (s) (C=O, carbonyl), 1663(s) (C=C).		

**Table 37:** The mole ratios of feeding of DMIA, HEMA, and calculated using <sup>1</sup>HNMR and UV-spectroscopy.

Polymer	Feeding mol%		<sup>1</sup> HNMR (mol%)		UV (mol%)
	DMIA	HEMA	DMIA	HEMA	DMIA
57-05-10	5	10	4.9	7.9	4.9

### 2.11.4. Synthesis of poly(NIPAAm-Co-HEMA-Co-DMIAAm) grafted 4-aminohippuric acid.



#### Procedure:

0.38g (0.002mol) 4-aminohippuric acid, was dissolved in 20mL dry DMF, then 0,468g (0.00226mol) DCC was added. After that a solution of 1.00g of polymer (**59**) in 15mL dry DMF, and 0.28g (0.00229mol) DMAP was added. The mixture was purged in argon for 20min., and then stirred at room temperature for 2d. After that polymer was precipitated in diethylether and dissolved again in THF and re-precipitated in diethylether, then dried overnight under vacuum.

**Table 38:** The chemical analysis (<sup>1</sup>H NMR, IR) of poly (NIPAAm-Co-HEMA-g-HA -Co-DMIA).

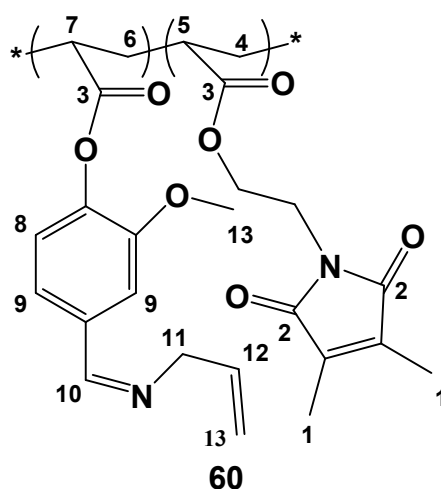
<sup>1</sup> H NMR	IR (KBr)
<sup>1</sup> H NMR (DMSO): $\delta(\text{ppm}) = 0.79\text{-}1.16(\text{m}, 6\text{H}, 19\text{-}2\text{CH}_3)$ , $1.17\text{-}1.67(\text{m}, 6\text{H}, 7,16\text{-CH}_2, 17\text{-CH})$ , $1.69\text{-}2.16(\text{m}, 10\text{H}, 1,8\text{-}3\text{CH}_3)$ , $3.11\text{-}3.50(\text{m}, 6\text{H}, 9,10,11\text{-}3\text{CH}_2)$ , $3.56\text{-}3.69(\text{m}, 2\text{H}, 3\text{-CH}_2)$ , $3.70\text{-}4.17(\text{m}, 3\text{H}, 5\text{-CH}_2, 18\text{-CH})$ , $6.35\text{-}7.639(\text{m}, 4\text{H}, 13,14\text{-CH-Ar.})$ , $7.88\text{-}8.02(\text{m}, 1\text{H}, 12\text{-NH})$ , $8.04\text{-}8.20(\text{m}, 3\text{H}, 15\text{NH}_3^+)$ .	IR (KBr): $\nu(\text{cm}^{-1})$ : 3300 (s) ( $\text{NH}_3^+$ ), 3074, 2940(s) (CH-Aliphatic), 2100 (br.) ( $\text{NH}_3^+$ ), 1718 (s) (C=O, carbonyl), 1665(s) (C=C).

**Table 39:** The mole ratios of feeding of DMIA, HEMA, HEMA-g-HA, and calculated using  $^1\text{H NMR}$ .

Polymer	Feeding mol%		$^1\text{H NMR}$ (mol%)	
	DMIA	HEMA	DMIA	HEMA-g-HA
59	4.9	7.9	4.76	32.5

### 2.11.5. Synthesis poly( VA-Co-DMIA)-g(AA)-g-(NIPAAm).

#### Step1: Synthesis of poly (VA-Co-DMIA)-g-(AA).



**Scheme 41:** Synthesis poly (VA-Co-DMIA)-g-(AA).

#### Procedure:

In 50 mL round bottom flask, 2.00g of poly (VA-Co-DMIA), was dissolved in 30mL ethanol, and 1.1g (0.0193mol) allyl amine (AA) was added. The reaction mixture allowed refluxing with stirring at 100°C for 3h. The mixture was cooled at room temperature, then solvent removed under reduced pressure to collect reddish solid product, and 65% yield.

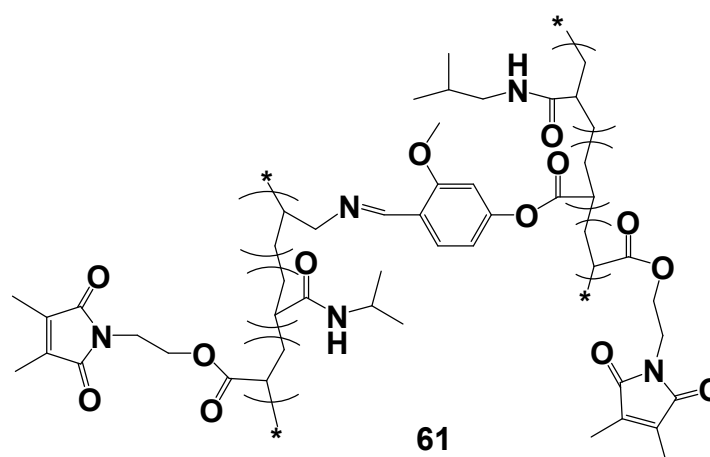
**Table 40:** The chemical analysis ( $^1\text{H NMR}$ , IR) poly (VA-Co-DMIA)-g-AA.

$^1\text{H NMR}$	IR (KBr)
$^1\text{H NMR}$ (500 MHz, $\text{CDCl}_3$ ): $\delta(\text{ppm}) =$ 0.70-0.92(m,1H,5-CH) 1.70-2.02(m, 6H,1-2CH <sub>3</sub> ), 2.75-3.33 (m, 2H, 6-CH <sub>2</sub> ), 3.34-3.44(m, 1H, 5-CH), 3.59-3.89(m, 3H, 13-CH <sub>3</sub> ), 4.02-4.36(m, 3H, 7-CH, 11-CH <sub>2</sub> ), 4.95-5.34 (m, 2H, 13-CH <sub>2</sub> ), 5.79-6.18 (m, 1H, 12-CH), 6.80-7.17 (m, 1H, 8-CH-Ar.), 7.30-7.53 (m, 2H, 9-2CH), 8.05-8.25 (m, 1H, 10-CH).	IR (KBr): $\nu$ ( $\text{cm}^{-1}$ ): 3066, 2940(s) (CH-Aliphatic), 1645(s) (-CH=N-), 870 (s) (CH-Ar.).

**Table 41:** The mole ratios of feeding of DMIA, and calculated using  $^1\text{H NMR}$ .

Polymer	Feeding mol%	$^1\text{H NMR}$ (mol%)
	DMIA	DMIA
60	10	9,09

**Step2: Synthesis poly( VA-Co-DMIA)-g-(NIPAAm).**



**Procedure:**

2g (0.0176mol) of NIPAAm, 0.7g of poly(VA-Co-DMIA)-g-(AA), and 16mg of AIBN were dissolved in 40 mL 1,4-dioxane in 100mL round bottom flask. The solution mixture was purged in argon for 20min., and stirred in oil bath at 70°C for 10h. The solution mixtures were cold to room temperature, then freeze in refrigerator for 3h, and then defreeze. Polymer was precipitated in 200mL diethylether at RT., filter, and dissolved again in THF, and reprecipitated in diethylether. The solution was filtered and dried overnight under reduced pressure, giving orange-reddish solid product, yield 63%.

**Table 42:** The chemical analysis ( $^1\text{H NMR}$ , IR) poly (VA-Co-DMIA)-g- NIPAAm.

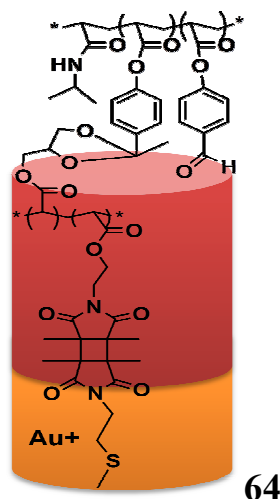
$^1\text{H NMR}$	IR (KBr)
$^1\text{H NMR}$ (500 MHz, $\text{CDCl}_3$ ): $\delta(\text{ppm}) =$ 0.70-0.92(m,1H,4-CH), 0.95-1.25(m, 6H, 17-2CH <sub>3</sub> ), 1.39-1.71(m, 3H,6-CH,8-CH <sub>2</sub> ), 1.72-1.93 (m, 6H, 1-CH <sub>3</sub> ), 1.95-2.41(m, 2H, 14-CH <sub>2</sub> ), 3.53-3.88 (m, 3H, 10-CH <sub>3</sub> ), 3.89-4.10(m, 1H, 16-CH), 4.11-4.32 (m, 4H, 3-CH <sub>2</sub> ,12-CH <sub>2</sub> ), 4.96-5.26 (m, 2H, 13-CH <sub>2</sub> ), 5.73-6.13 (m, 1H, 13-CH), 6.85-7.21 (m, 2H, 9-CH-	IR (KBr): $\nu$ ( $\text{cm}^{-1}$ ): 3066, 2940(s) (CH-Aliphatic), 1770 (s) (C=O), 1640(s) (-CH=N-), 870 (s) (CH-Ar.).

Ar.), 7.30-7.53 (m, 1H, 10-CH-Ar.), 8.03-8.23(m,1H, 11-CH).

**Table 43:** The mole ratios of feeding of DMIA, and calculated using  $^1\text{HNMR}$ .

Polymer	Feeding mol%	$^1\text{HNMR}$ (mol%)
	DMIA	DMIA
61	9	3.7

### 2.11.6. Synthesis of self-assembled layer-by-layer using hydrogel thin film of poly(DHPA-*Co*-DMIA)-*g*-Poly(NIPAAm-*Co*-APA-*Co*-VA).



It was achieved in two steps.

#### ***Step1: Ring opening of SKA to form DHPA.***

##### **Procedure:**

100 ml round flask fitted by reflux condenser. A glass slid with surface of (gold + adhesion) promoter and was spin coated by P( SKA-*Co*-DMIA) 10wt%, 2000rpm and UV irradiated for 1h, then was immersed in a mixture of 15ml THF and 15mL glacial acetic acid. The mixture was refluxed for 5h at 90°C. The slid was removed and washed by THF, and distilled water, then dried under vacuum overnight. IR was used to see the change in surface, SPR-OW was used to measure thickness, and refractive index in the dry case, and also the swelling properties was discussed.

**IR  $\nu$  ( $\text{cm}^{-1}$ ):** 3500-3900(s, br. Multipeaks) (OH, CH-Aliphatic), 1672-1738 (br. Multipeaks)(C=O),1570-1588(s, multipeak)(C=C).

**Step2: self-assembled layer by layer (LbL) using hydrogel thin film of poly (DHPA-Co-DMIA)-g-Poly(NIPAAm-Co-APA-Co-VA).**

**Procedure:**

In 50 mL round bottomed flask fitted with reflux condenser. A slide coated by poly (DHPA-Co-DMIA) was immersed in solution of Poly (NIPAAm-Co-APA-Co-VA) in 25 mL CHCl<sub>3</sub>. The mixture was stirred and 0.1g (0.58 mmol) of p-Toluenesulfonic acid was also added. The solution with glass slide was refluxed and, stirred in oil bath at 80°C. After that, the reaction mixture allowed cooling and, 0.2g of sodium carbonate was added and refluxed again for 30min. The slide was removed and washed by THF, and water, then dried under vacuum for 4h.

IR was used to see the change in surface, SPR-OW was used to measure thickness, and refractive index in the dry case, and also the swelling properties was discussed.

**IR  $\nu$  ( $cm^{-1}$ ):** 3500-3700(m,br. Multipeaks) (NH, CH-Aliphatic), 2350(s)(O-C-O), 1668-1730 (br. Multipeaks)(C=O),1570-1588(s, multipeak) (C=C), 720(m) (CH-Ar.).

## **2.12. Hydrogel formation.**

### **2.12.1. Modification of Gold surface.**

45 nm of gold was coated on LaSFN9 substrate by chemical vapor deposition. Gold surface then was modified by absorption of DMITAc adhesion promoter. SPR substrates with 45 nm gold were submerged in 5 mM solution of adhesion promoter in absolute ethanol for 24 h, rinsed with ethanol and dried under Ar atmosphere. The presence of adhesion promoter was confirmed by SPR (angle).

### **2.12.2. Film formation.**

Polymer solutions (5-15 wt-%) of photo-crosslinker polymer based on NIPAAm, DMAAm, and HEMA and their copolymers and terpolymers in various solvents were spin coated at 2000 rpm for 180 sec. Spin coated polymer films were then dried under vacuum for 1 h, irradiated with suitable UV lamp for 1 h. **Table44** shows the combination of substrate and solvent used to obtain thin film.

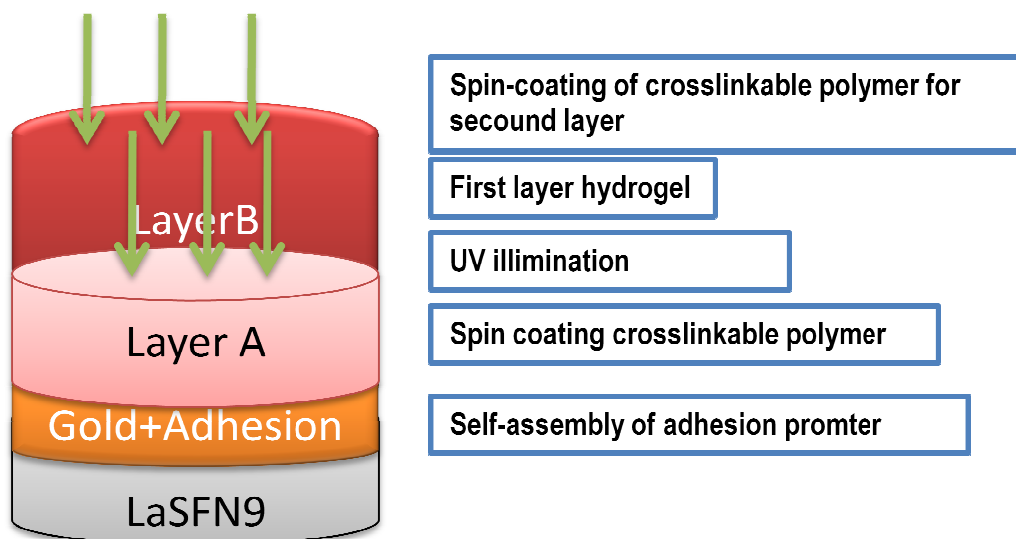


**Figure34:** Schematic diagram for formation of hydrogel layers.

**Table 44:** List of solvent used for dissolving polymers used in the formation of hydrogel thin film.

Photo-crosslinkable polymer solution	Solvent	Photo-crosslinkable polymer solution	Solvent
NIPAAm	Cyclohexanone	DMEAAm	DMSO
DMAAm	Cyclohexanone	VA	Cyclohexanone
HEMA	DMSO	DEMAVA	Cyclohexanone
SKA	Cyclohexanone	AVHA	Cyclohexanone
DMEAMA	Cyclohexanone	-	-

Similar procedures involving spin coating and irradiation were used to obtain multilayer assembly of polymer on top of a photo-crosslinked film.

### 2.12.3. Determination of refractive index from SPR

The refractive index of hydrogel layers on LaSFN9 substrate was determined by Fresnel calculations as described below. The parameters shown in (Table45) were modified to obtain a good fit for the SPR curve.

**Table 45:** Parameters for calculating film thickness and refractive index of Au.

	Film thickness (nm)	Eps (real)	Eps (image)
LaSFN9	-	3.4036	-
Au	45	-12.3	1.29
Air	-	1	-

## *Experimentals*

---

For polymer layers, the thickness of dry polymer film was also inserted in the Fresnel calculations. The refractive index of air and refractive index of PBS buffer as outermost layer were inserted to determine the properties of film in dry and swollen state respectively (**Table46**). Notable features obtained from the Fresnel calculations are film thickness and refractive index. Latter was obtained by calculating the square root of Eps (real). The interpretation of results from Fresnel calculations is mentioned in (**Sections 3.6, 7 and 8**).

**Table 46:** Parameters for calculating film thickness and refractive index of polymer layer.

	<b>Film thickness (nm)</b>	<b>Eps (real)</b>	<b>Eps (image)</b>
	-	3.4036	-
<b>LaSFN9</b>			
<b>Au</b>	45	-12.3	1.29
<b>Polymer</b>	200	2.1	-
<b>Water</b>	0	1.77	-

In the case of formation of bilayer hydrogels, polymer thickness should be multiple,

**Table 47:** Parameters for calculating film thickness and refractive index of polymer bilayer.

	<b>Film thickness (nm)</b>	<b>Eps (real)</b>	<b>Eps (image)</b>
	-	3.4036	-
<b>LaSFN9</b>			
<b>Au</b>	45	-12.3	1.29
<b>Polymer(LayerA)</b>	200	2.1	-
<b>Polymer(LayerB)</b>	200	2.1	-
<b>Water</b>	-	1.77	-

For simulation of pH-responsive polymer hydrogel layer or bilayer Esp(real), was calculated for water (1.77).

# *Chapter(3)*

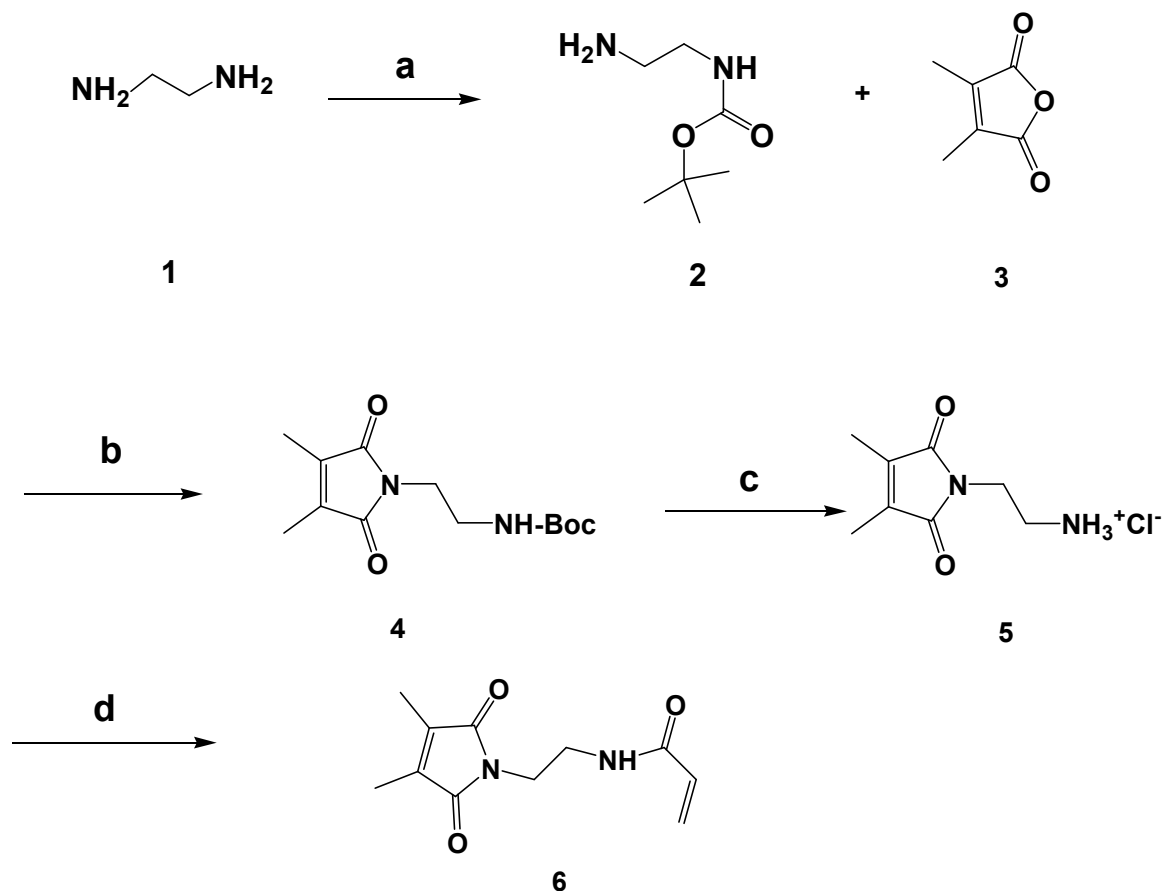
*Results and discussions*

### 3. Results and discussions.

#### 3.1. Photo-crosslinkers.

##### 3.1.1. Acrylate photo-crosslinker (DMIAAm).

Acrylamide photo-crosslinker (DMIAAm) (**6**) was synthesized in a four-step process as outlined in the **Scheme2**. It was used as a crosslinker for NIPAAm, DMAAm and their copolymers with VA and DEAMVA in a free radical polymerization. The first step in the synthesis of DMIAAm involved the protection of amine group of diaminoethane by tert-butyloxycarbonyl (Boc) group. The resulting product was then reacted with dimethyl maleic anhydride. Removal of the Boc group by reaction with hydrochloride acid to produce (**5**) and subsequent reaction with acryloyl chloride produced the final product (**6**). This process has been already reported in the literature <sup>(257)</sup>. The conversion of (**4**) to (**5**) is a condensation reaction and this process involved the formation of a dimethylmaleimide moiety and removal of water as a side product. In the reported synthesis of DMIAAm, no further work up was used to purify the intermediate compound (**5**). A high quantitative yield of 60 % for product (**6**) in this study has been attributed to the use of purified intermediates in all reactions steps.

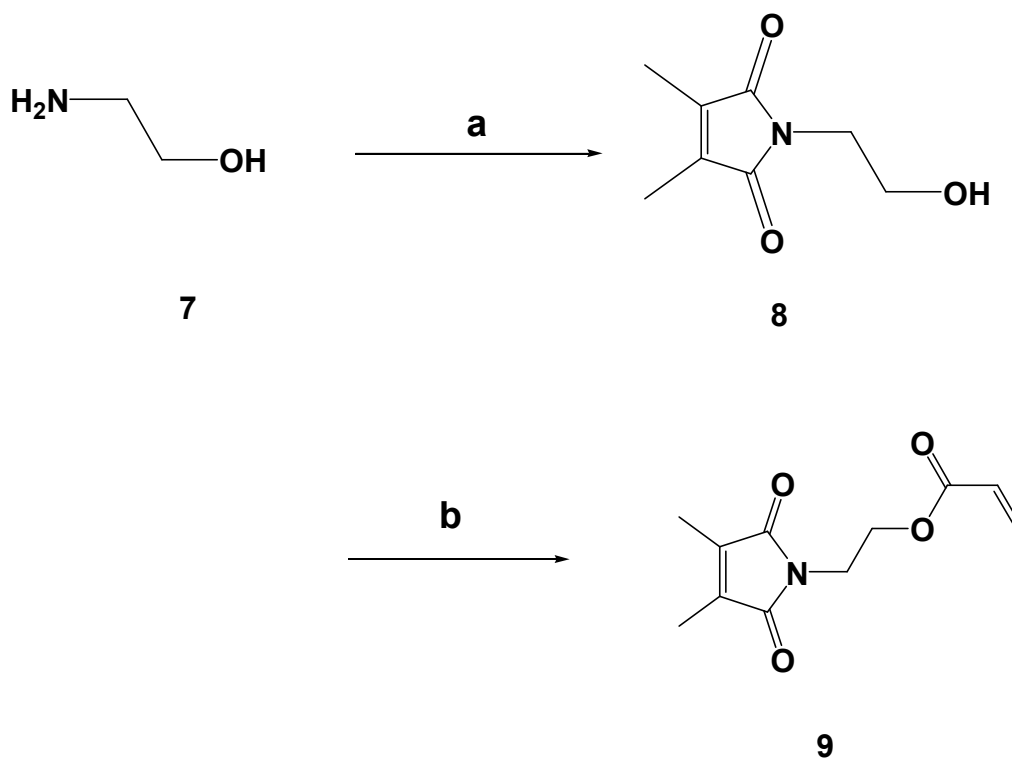


**Scheme2:** Synthesis of photo-crosslinker N-[2'-(3,4-dimethyl-2,5- dioxo-2,5- dihydroxy-pyrrol-1-yl)]-ethyl-acrylamide (DMIAAm).

- (a)  $(\text{Boc})_2\text{O}$  / 1, 4- Dioxane, RT, 48 h.
- (b) Dimethylmaleic anhydride / toluene, 130-135°C, 3 h.
- (c) HCl / Ethylacetate, RT, 24 h.
- (d) acryloyl chloride, TEA /  $\text{CH}_2\text{Cl}_2$ , 1h at 0-5°C, 6 h at RT.

### 3.1.2. Acrylate photo-crosslinker (DMIA).

Acrylate photo-crosslinker (DMIA) (**9**) was synthesized in a two-step process as outlined in the **Scheme3**. It was used as a crosslinker for HEMA, VA and AVHA in a free radical polymerization. The first step in the synthesis of DMIA involved a condensation reaction between dimethyl maleic anhydride and aminoethanol with the subsequent removal of water as a by-product. The resulting colorless crystalline solid (**8**) was reacted with acryloyl chloride in presence of triethylamine as base catalysis and dichloromethane and finally lead to the formation of (**9**) the product in high yield (97 %).

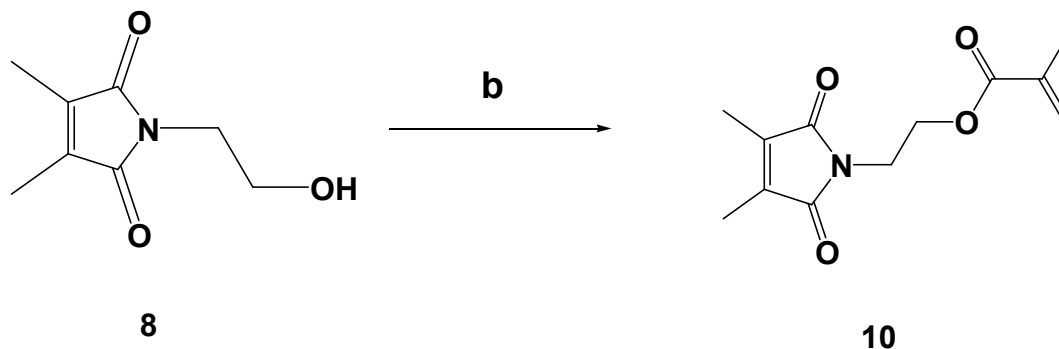


**Scheme 3:** Synthesis of dimethylmaleimido ethanol or 1-(2-hydroxyethyl)-3,4-dimethyl-1H-pyrrole-2,5-dione (DMI) (**8**) and dimethylmaleimidoacrylate (DMIA) (**9**).

- (a) Toluene, 130-160°C, 5 h.
- (b) Acryloyl chloride,  $\text{Et}_3\text{N}$  /  $\text{CH}_2\text{Cl}_2$ , 0-5°C (1 h), RT (24 h).

### 3.1.3. Acrylate photo-crosslinker (DMIMA).

Methacrylate photo-crosslinker (DMIMA) (**10**) was synthesized in a two-step process as outlined in **scheme 4**. The first step was discussed previously for compound (**8**). The second step in a similar to last compound **9** but we used methacryloyl chloride.



**Scheme 4:** Synthesis of dimethylmaleimidomethacrylate.

(b) Methacryloyl chloride/ DCC, DMAP/ $\text{CHCl}_2$  0-5°C (1 h), RT (24 h).

## 3.2. Monomers.

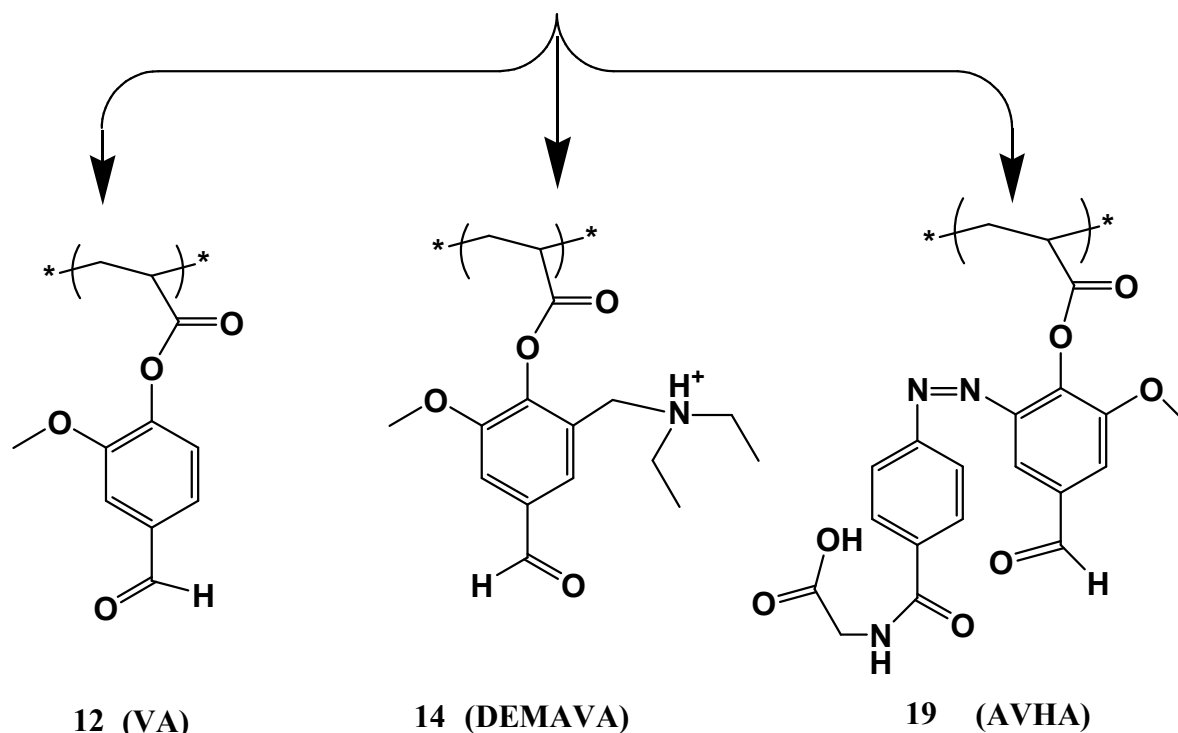
### 3.2.1. Vanillin monomers.

Vanillin (4-hydroxy-3-methoxybenzaldehyde) and related flavor compounds are of great economical importance because of the demand and their price. Inexpensive biotechnological processes therefore are of great interest. The demand for vanillin, for example exceeds its natural production. Only 0.2% of the flavor's world market is presently covered by natural resources; the major part is resources; the major part is synthetic material<sup>(258)</sup>. The tendency to use the products from natural sources increases because it is found that they frequently are healthier so that vanillin, for example, can be applied in higher concentration. The drawback however, is the high price. Biotechnologically produced vanillin is considered as "natural." The first large scale production of synthetic vanillin was started from sulphated lignin waste waters in 1936 by the Salvo Corporation in the USA<sup>(259)</sup>.

*T. Gumí et al.* report on the preparation of various polysulfone capsules containing different vanillin concentrations. Vanillin release from the capsules has been monitored along with time. High performance liquid chromatography (HPLC) has been used as analytical technique to determine vanillin concentration<sup>(260)</sup>.

Vanillin's monomers have a great advantage in the formation of aldehyde functional polymers and hydrogels, which have been widely used to couple with protein and peptides<sup>(261, 262,263)</sup>.

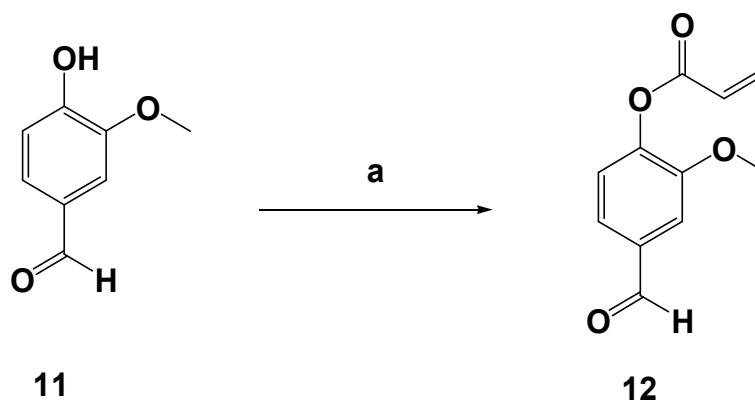
Here in the present study we used vanillin compound for the synthesis of three new kinds of acrylate monomers.



**Scheme 5:** Vanillin's monomers.

### 3.2.2. 4-Formyl-2-methoxyphenylacrylate (VA) monomer.

Vanillin acrylate (VA) was synthesized in one step process. Compound (11) was reacted with acryloyl chloride in the presence of triethylamine as base catalysis for the elimination of hydrochloride as triethylamine hydrochloride, and yielded product (12).



**Scheme 6:** Synthesis of 4-formyl-2-methoxyphenylacrylate (VA).

a.  $\text{CH}_2\text{Cl}_2$ /Acryloyl chloride/ Triethylamine.

The  $^1\text{H}$  NMR spectra for (12) was in a good agreement with the number of protons. and the integrations were acceptable for all protons as shown in **Figure35**.  $^{13}\text{C}$  NMR, and IR were also used for the deduction of compound (12) and all were in a good agreement with the chemical structure.

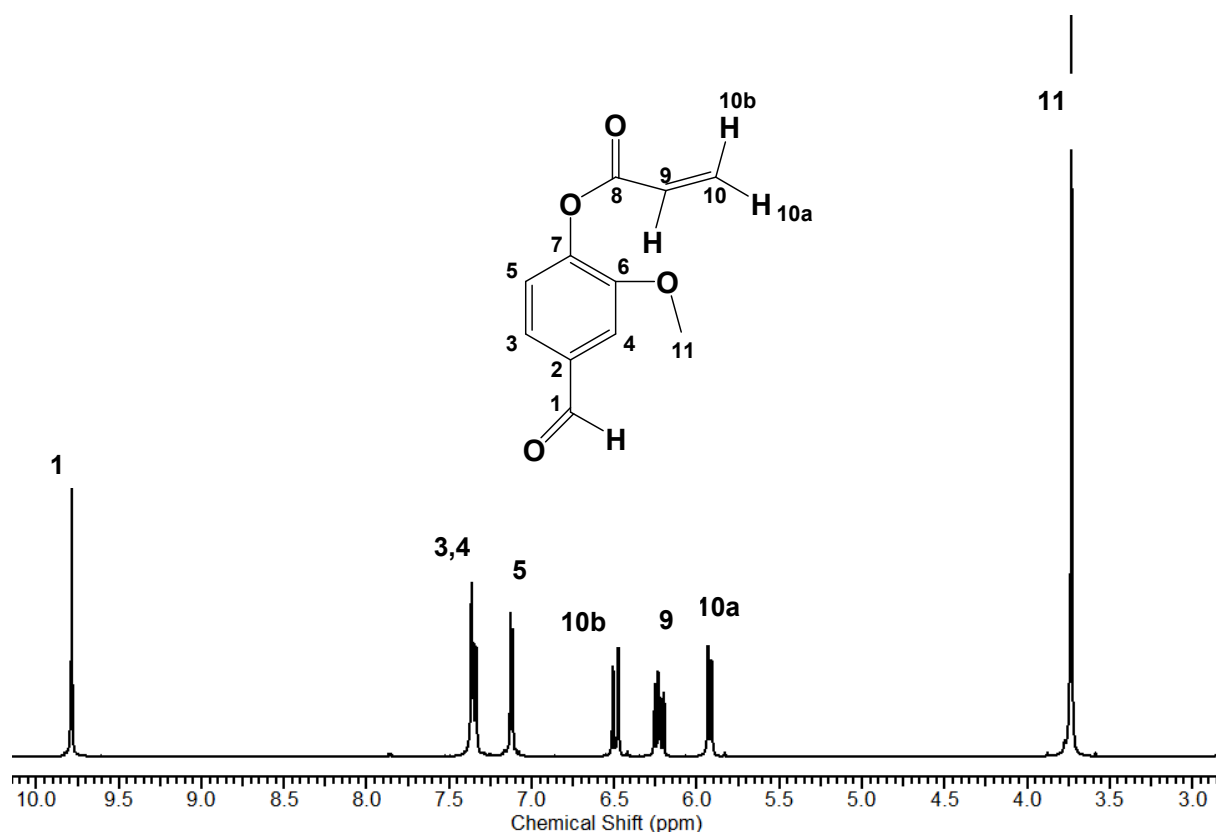
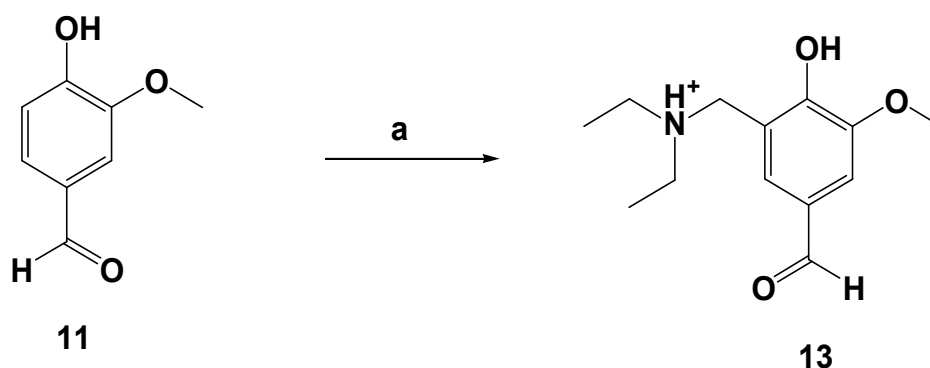


Figure 35: <sup>1</sup>H NMR spectra (CDCl<sub>3</sub>) of (VA).

### 3.2.3.2- [(diethylamino)methyl]-4-formyl-6-methoxyphenyl acrylate (DEMAVA).

DEMAVA was synthesized in two steps as discussed in detail below.

**Step 1:** Is the formation of (3-[(diethylamino)methyl]-4-hydroxy-5-methoxy-benzaldehyde).



**Scheme 7:** Synthesis of 3-[(diethylamino)methyl]-4-hydroxy-5-methoxy-benzaldehyde.

**a.** Formaldehyde, diethylamine/ ethanol, reflux, 100°C, 3h.

This has been done by the reaction of vanillin with diethylamine and formaldehyde according to Mannich reaction mechanism. In this reaction we did not use any catalysis especially acid catalysis which famous to use in Mannich reaction therefore protonated tertiary amine has been yielded.

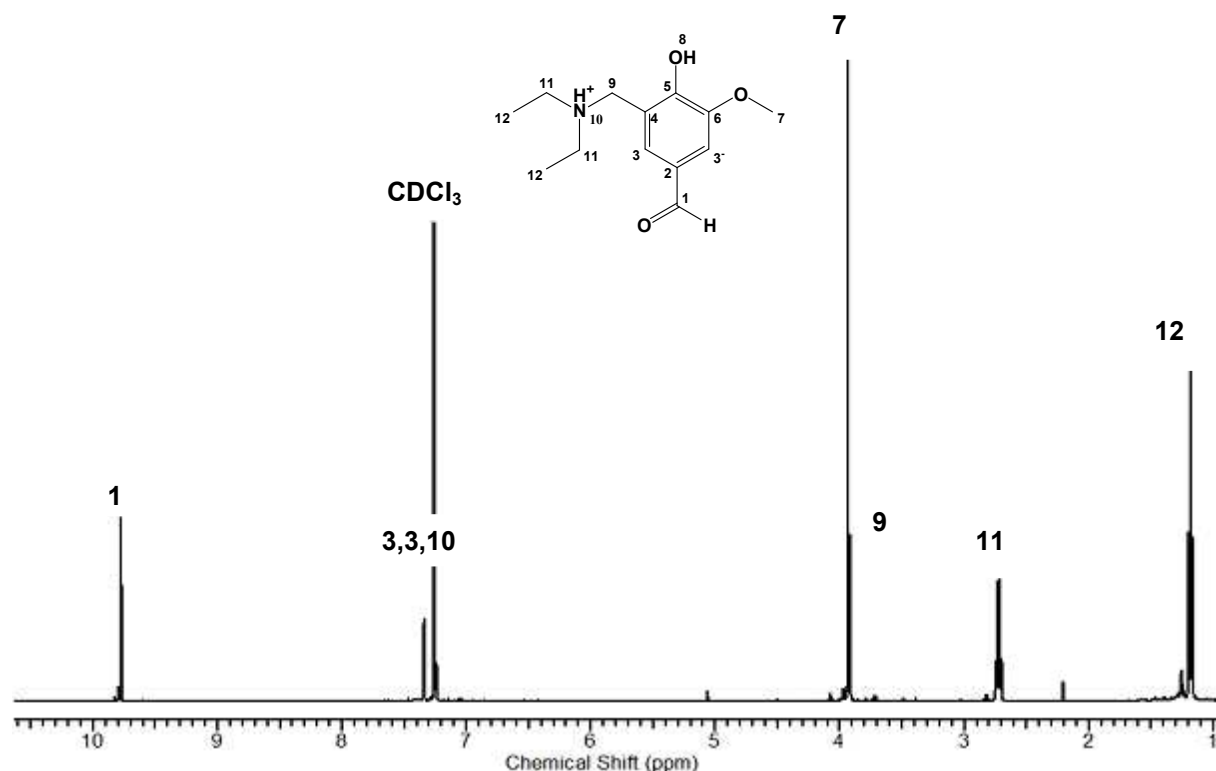
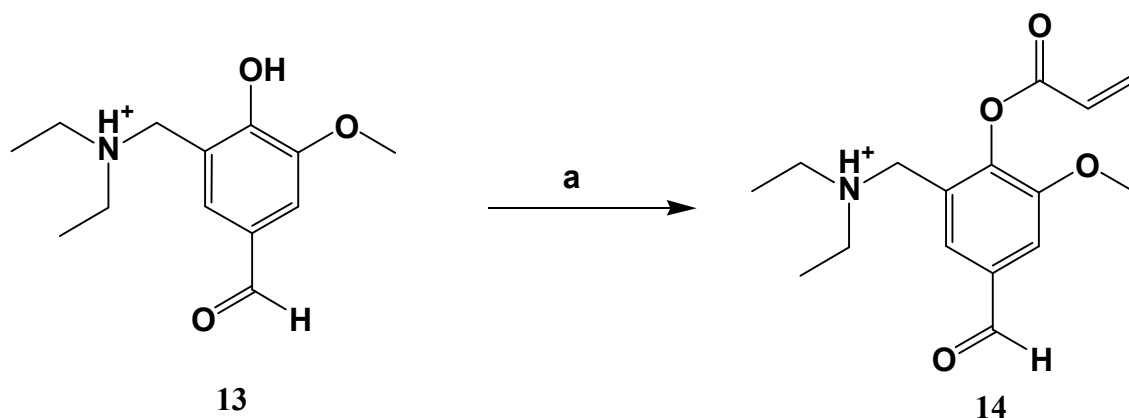


**Figure 36:** <sup>1</sup>H NMR (CDCl<sub>3</sub>) of 2-[(diethylamino)methyl]-4-formyl-6-methoxyphenyl acrylate.

**Step2:** Is the formation of 2-[(diethylamino)methyl]-4-formyl-6-methoxyphenyl acrylate (DEMAVA).

This was achieved by reaction of compound **13** with acryloyl chloride in the presence TEA to form **14**.



**Scheme 8:** 2-[(diethylamino)methyl]-4-formyl-6-methoxyphenyl acrylate (DEMAVA).

a. CH<sub>2</sub>Cl<sub>2</sub>/Acryloyl chloride/ TEA.

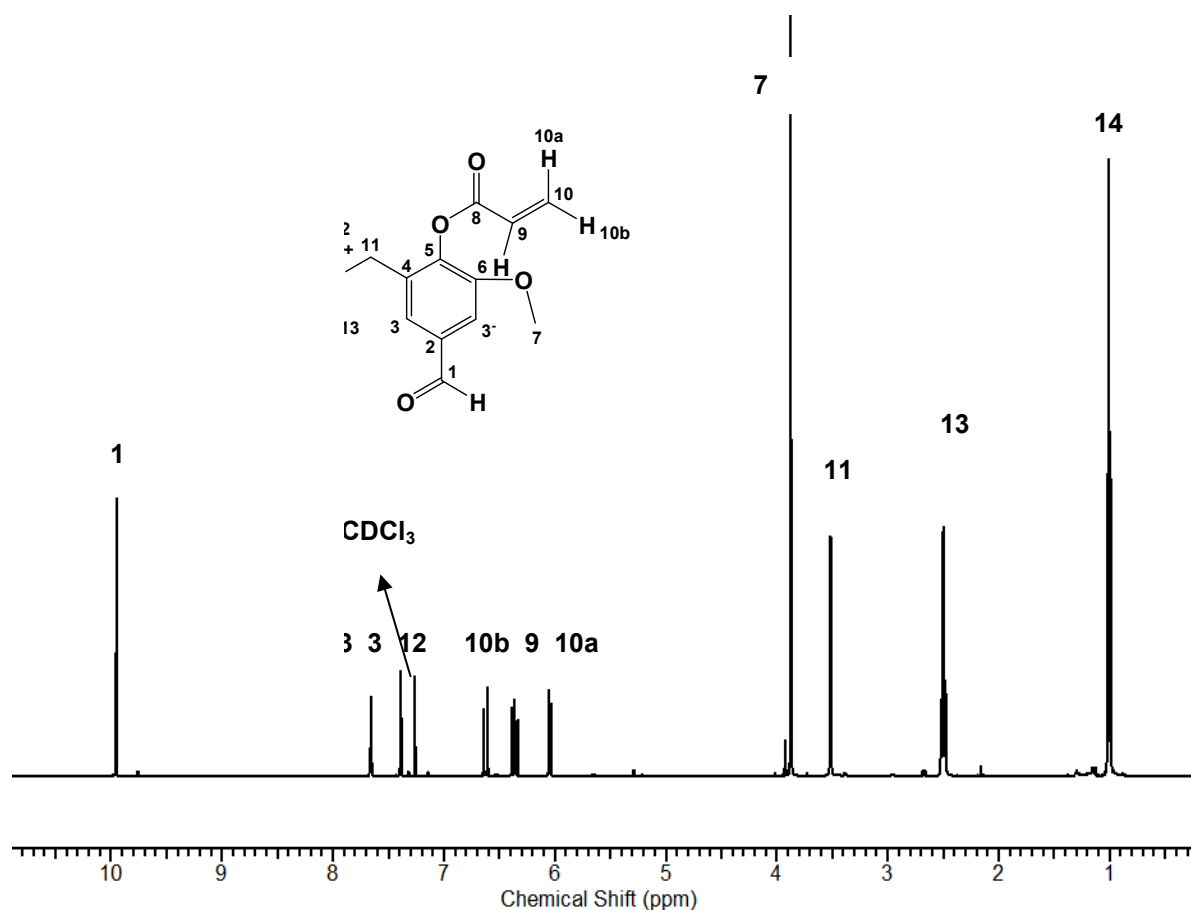


**Figure 37:**  $^1\text{H}$  NMR ( $\text{CDCl}_3$ ) of DEMAVA.

IR-spectra illustrated the presence of ( $\text{NH}^+$ ) in step1 and 2 as a broad peak at  $\nu$  ( $\text{cm}^{-1}$ ) = 2325, as shown in the **Figure38**.

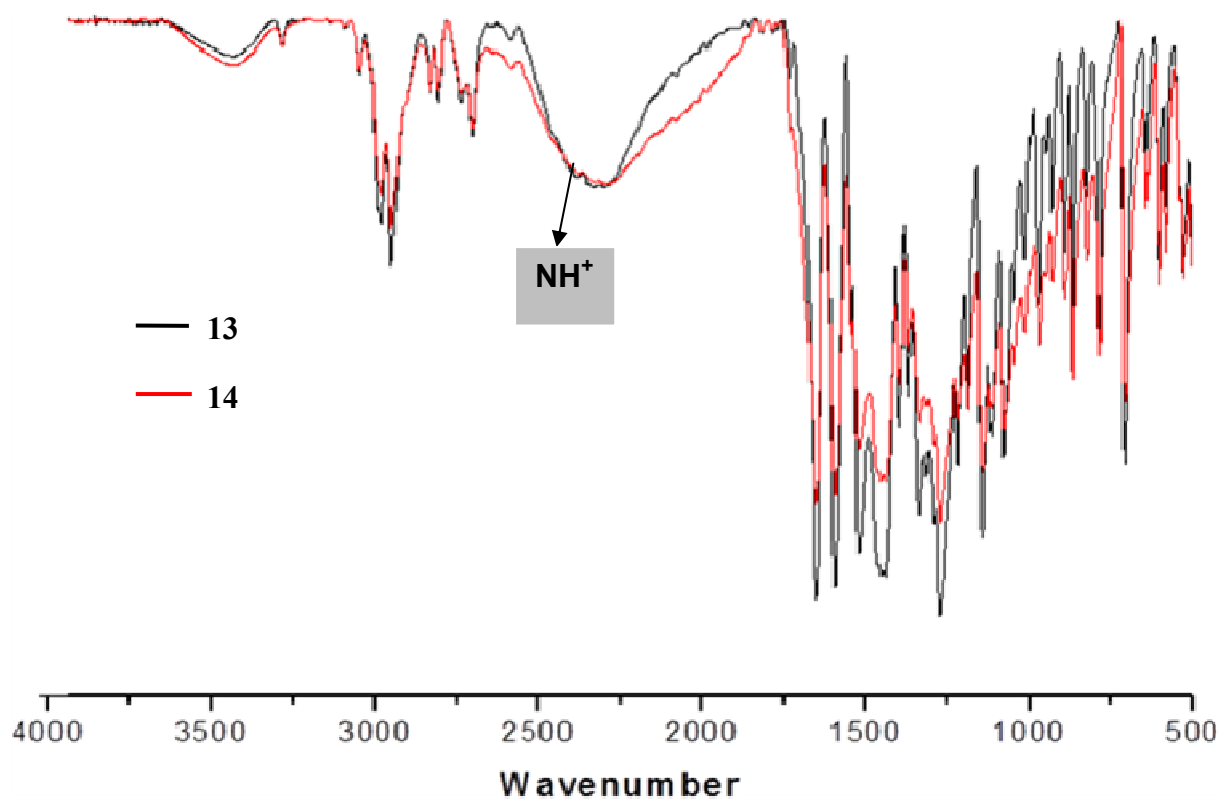


**Figure 38:** IR (KBr) spectra of DEMAVA.

Compound **14** act as pH-responsive monomer in the present study in addition to its hydrophilicity.

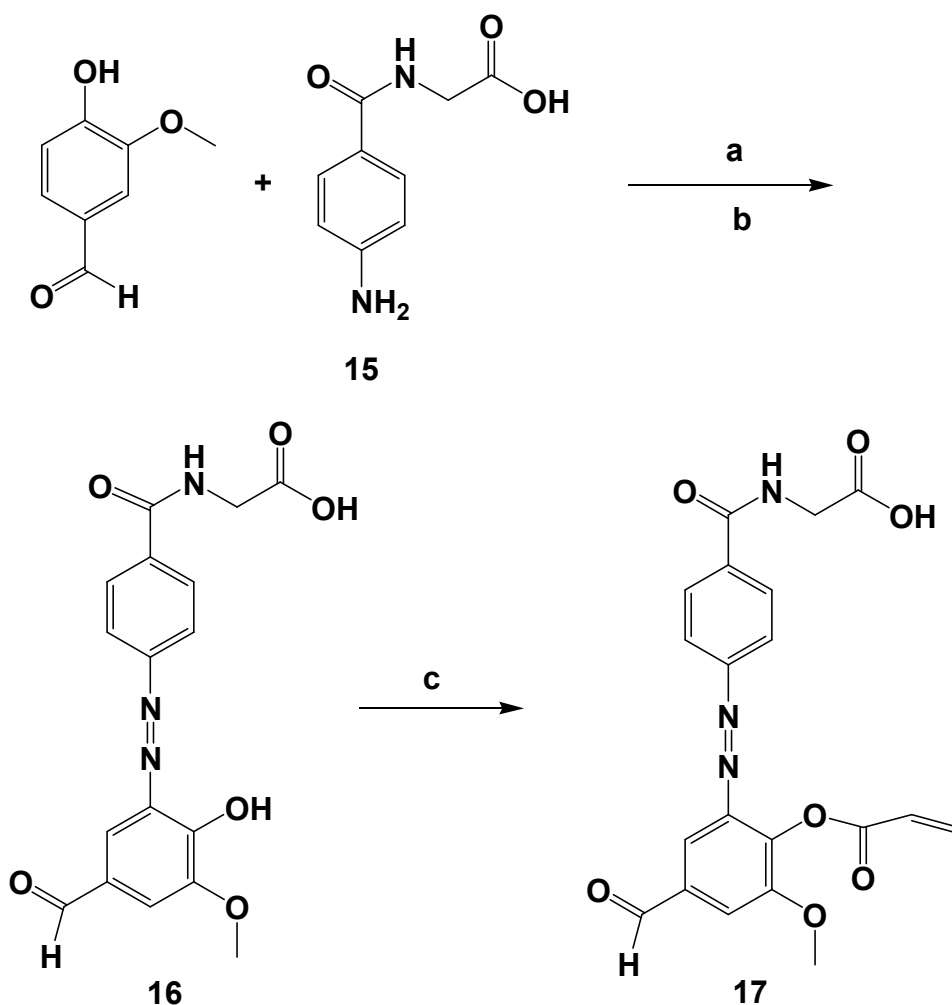
### 3.2.4. [4-[2-(acryloyloxy)-5-formyl-3-methoxyphenyl]diazenyl]benzoyl amino] acetic acid (AHVA).

*Step1: Synthesis of (4-[5-formyl-2-hydroxy-3-methoxyphenyl]diazenyl) benzoyl} amino) acetic acid.*

Synthesis of AHVA was achieved in two steps.

*Step1:* Is the formation of the azo dye. 4-Aminohippuric acid with a free amino group was used in the formation of diazonium salt, which further coupled with vanillin forming compound **16**.

*Step2:* Is the formation of AHVA by reaction with acryloyl chloride in the presence of TEA to give compound **17**.



**Scheme 9:** Synthesis of AVHA.

a. 4-aminohippuric acid / Conc.HCl / NaNO<sub>2</sub>.

b. Vanillin / NaOH

c. CH<sub>2</sub>Cl<sub>2</sub>/Acryloyl chloride/ TEA.

Compounds **16**, and **17** were deduced by <sup>1</sup>H NMR, <sup>13</sup>C NMR, and IR, all data were in a good agreement with the chemical structure. The <sup>1</sup>H NMR and IR spectrums for both **16** and **17** were shown below.

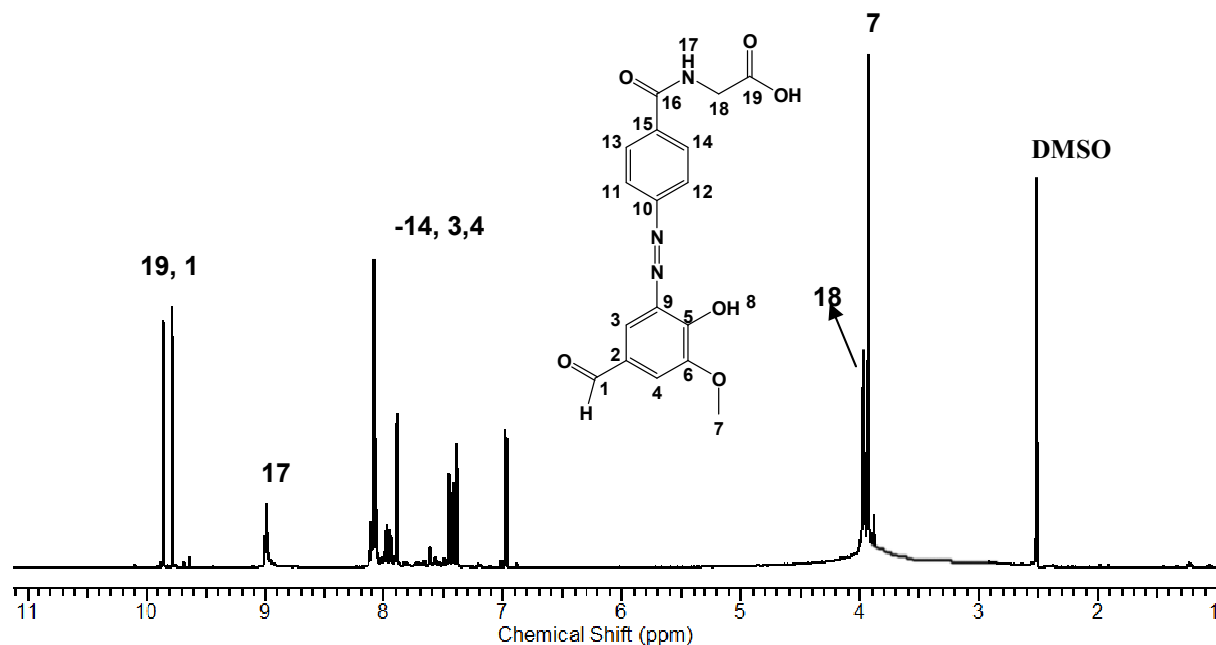


**Figure 39:** <sup>1</sup>H NMR spectra (DMSO) of synthesis of ((4-[5-formyl-2-hydroxy-3-methoxyphenyl]diazanyl) benzoyl) amino) acetic acid.

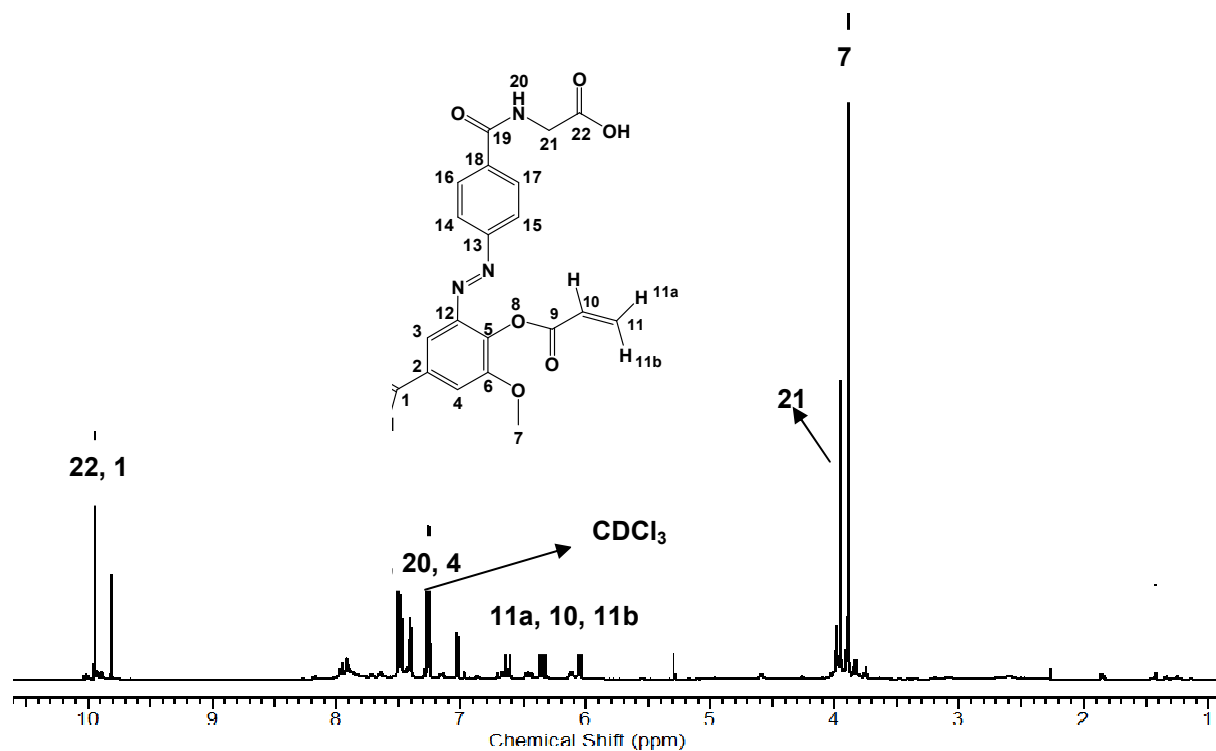


**Figure 40:** <sup>1</sup>H NMR (CDCl<sub>3</sub>) of AVHA.

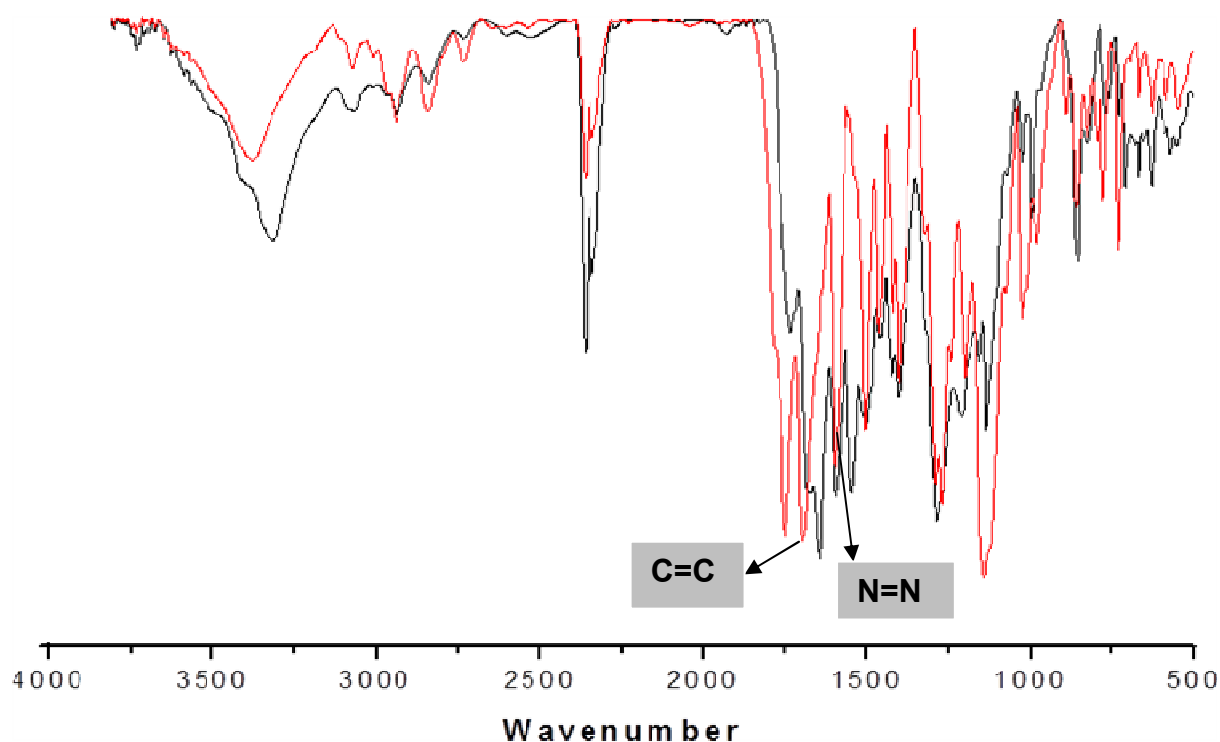
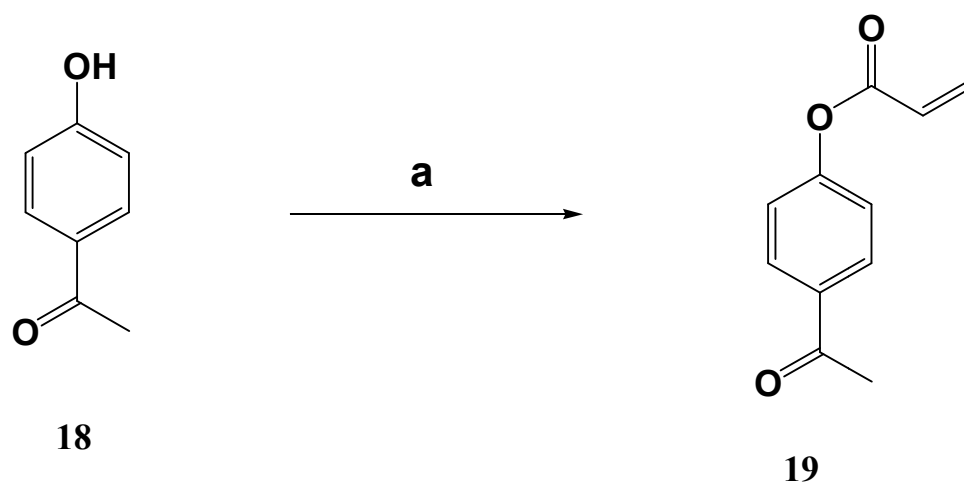


**Figure 41:** FTIR spectra of **16** and **17**.

### 3.2.5. Synthesis of 4-acetylphenyl acrylate.

This monomer was synthesized in one step by reaction of 4-hydroxyacetophenone with acryloyl chloride in presence TEA. This Monomer was used in the synthesis of terpolymer (**45**); and further used in the graft reaction over gold surface.

Monomer (**19**) was investigated by  $^1\text{H}$ NMR,  $^{13}\text{C}$  NMR, IR and elemental analysis. Overall analysis were in a good agreement with the chemical structure **Figure 42**.



**Scheme10:** Synthesis of 4-acetylphenyl acrylate.

a.  $\text{CH}_2\text{Cl}_2$ /Acryloyl chloride/ TEA.

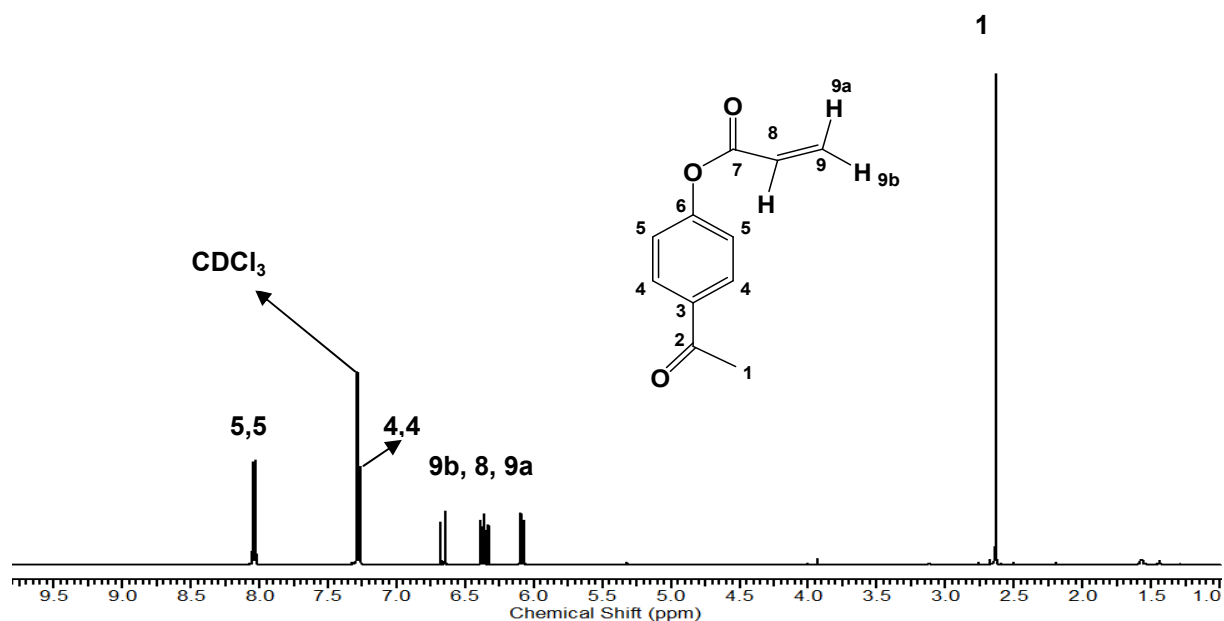
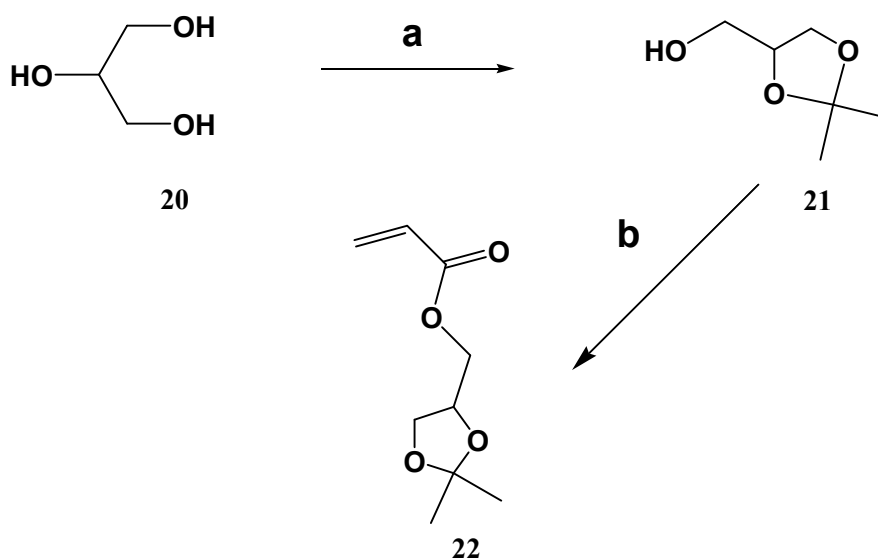


Figure 42:  $^1\text{H}$  NMR ( $\text{CDCl}_3$ ) of APA.

### 3.2.6. Synthesis of 2,2-dimethyl-1,3-dioxolane-4-yl-methylacrylate (Solketalacrylate) (SKA).

SKA is a hydrophobic monomer used in the preparation homo and copolymers. The main object was demonstrated in copolymerization with NIPAAm, to study the change of LCST ( $T_c$ ) in the polymer solution. Furthermore, the swelling of hydrogel thin film, see **section (4.5.5)**. On the other hand, the synthesis of DHPA can be performed which acts as hydrophilic compound. Here we will discuss the synthesis of SKA which has been done in two steps as described in **scheme 11**.

Both compound **21** and **22** were investigated by  $^1\text{H}$ NMR,  $^{13}\text{C}$  NMR and IR. Overall analysis were in a good agreement with the chemical structure (**Figure 43**).



Scheme11: Synthesis of 2,2-dimethyl-1,3-dioxolane-4-yl-methylacrylate

a. Acetone / p-Toluene sulphonic acid.  $\text{CHCl}_3$  /  $80^\circ\text{C}$ . 8h.

b.  $\text{CH}_2\text{Cl}_2$ /Acryloyl chloride/ TEA.

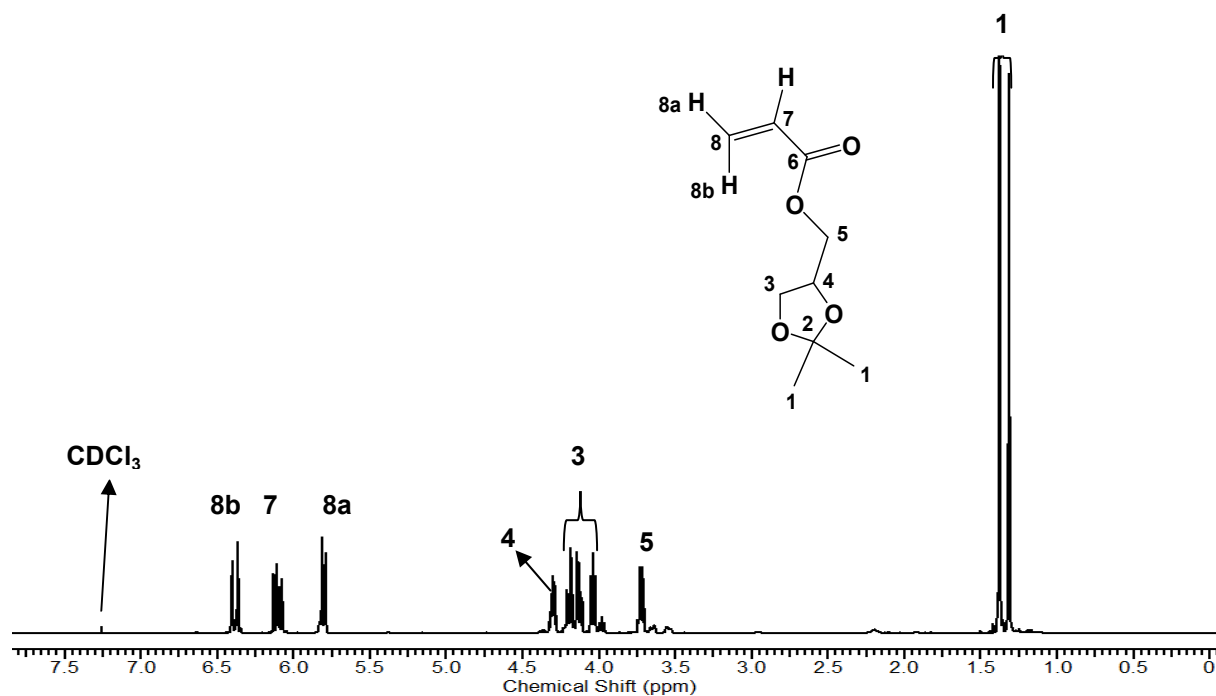
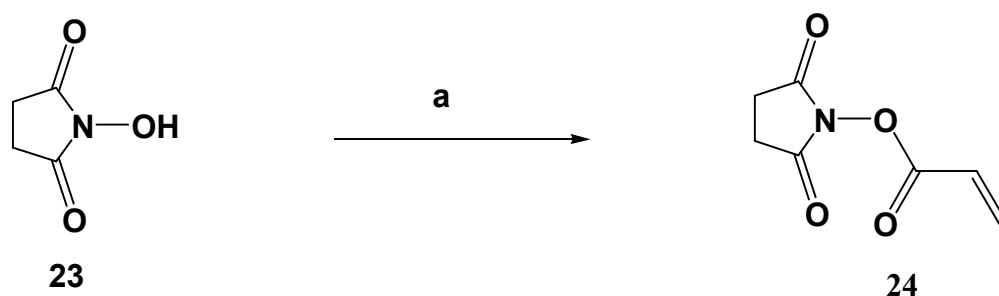


Figure 43:  $^1\text{H}$  NMR ( $\text{CDCl}_3$ ) of SKA.

### 3.2.7. Synthesis of 1-(acryloyloxy)pyrrolidine-2,5-dione ( NASI ).

NASI is a hydrophobic monomer used in the preparation homo and copolymers with NIPAAm. Compound **24** was synthesized in one step as elimination reaction between N-hydroxysuccinimide and acryloyl chloride in base catalysis as illustrated in **scheme12**.

Compound **24** was investigated by  $^1\text{H}$ NMR,  $^{13}\text{C}$  NMR, IR and elemental analysis. Overall analysis was in a good agreement with the chemical structure.



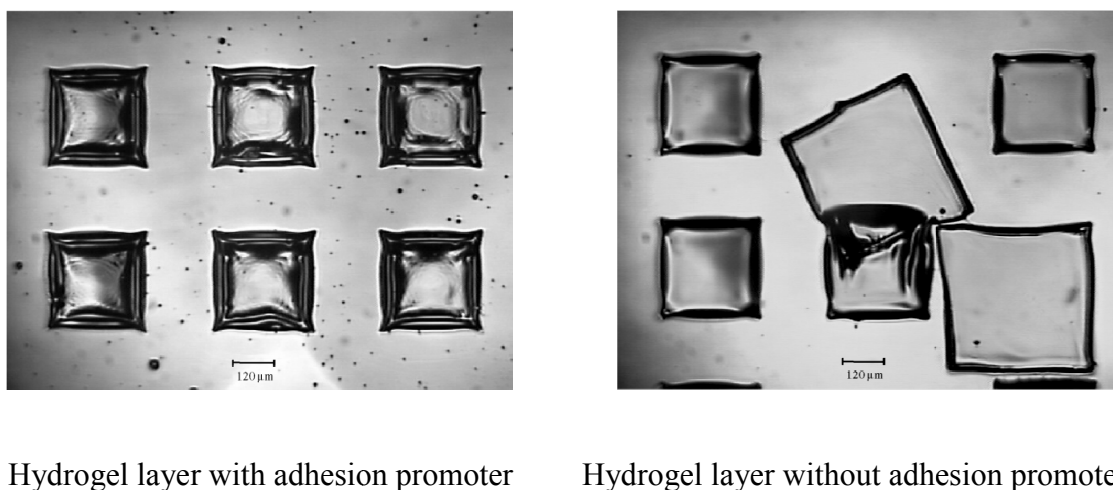
Scheme12: 1-(Acryloyloxy) pyrrolidine-2,5-dione ( NASI )

a.  $\text{CH}_2\text{Cl}_2$ /Acryloyl chloride/ TEA.

### 3.3. Adhesion promoters.

The adhesion promoter for gold was synthesized for the covalent attachment of thin hydrogel layer to these substrates. It has been observed that physisorbed hydrogel layers detach from the surface (**Figure 44**). To avoid such shortcomings, adhesion promoters were synthesized. Synthesized adhesion promoters have a surface-active group ( $-\text{SCOCH}_3$ ) and a terminal group (maleimide) separated by spacer methylene groups <sup>(48)</sup>. The surface-active group is responsible for the chemisorption on the substrate. The molecular surface interactions are covalent Au-S bonds.

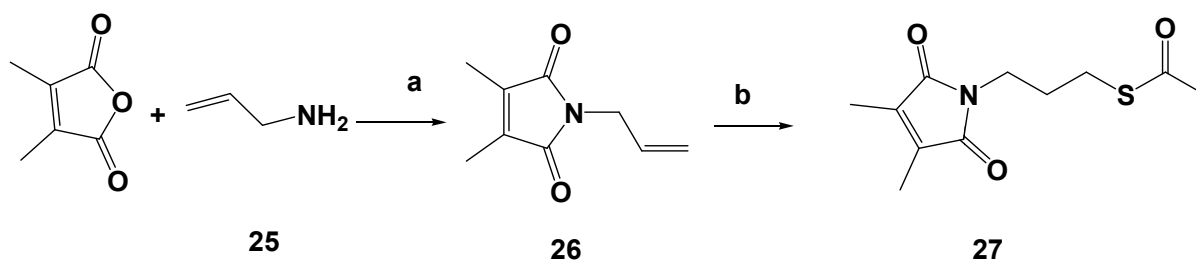
The adhesion promoter for gold (DMITAc) (**27**) was synthesized in a two-step process as shown in **Scheme 13**. First step involved reaction of allyl amine with dimethyl maleic anhydride and removal of water as a byproduct. In the second step, compound (**26**) was reacted with thioacetic acid in presence of AIBN to yield product (**26**). This compound can be used for further modification of the polymers.



Hydrogel layer with adhesion promoter

Hydrogel layer without adhesion promoter

**Figure 44:** Effect of adhesion promoter on swelling of thin hydrogel layers <sup>(48)</sup>.



**Scheme 13:** Synthesis of thioacetic acid 3-(3,4-dimethyl-2,5-dioxo-2,5-dihydro-pyrrol-yl)-propyl ester (DMITAc).

(a) Toluene, 135 °C, 4 h.

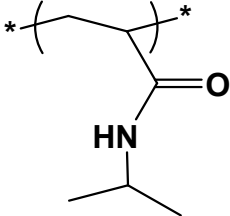
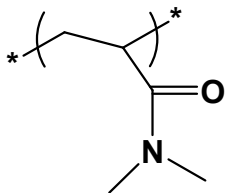
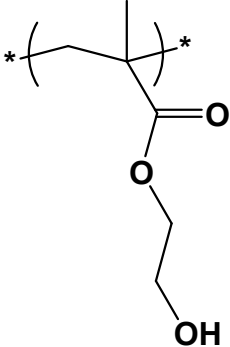
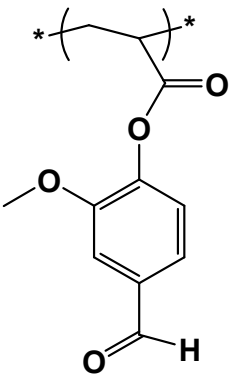
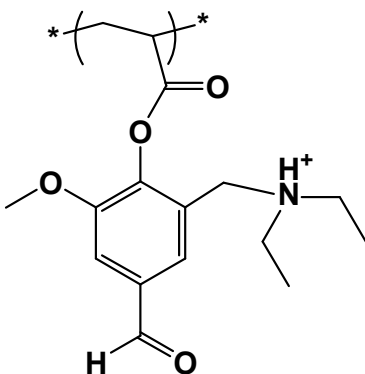
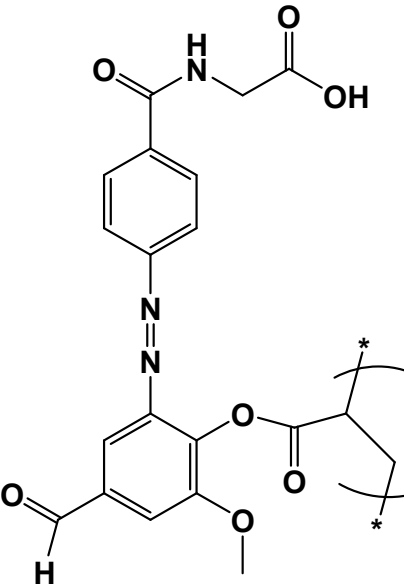
(b) Thioacetic acid, 80 °C, 4.5 h.

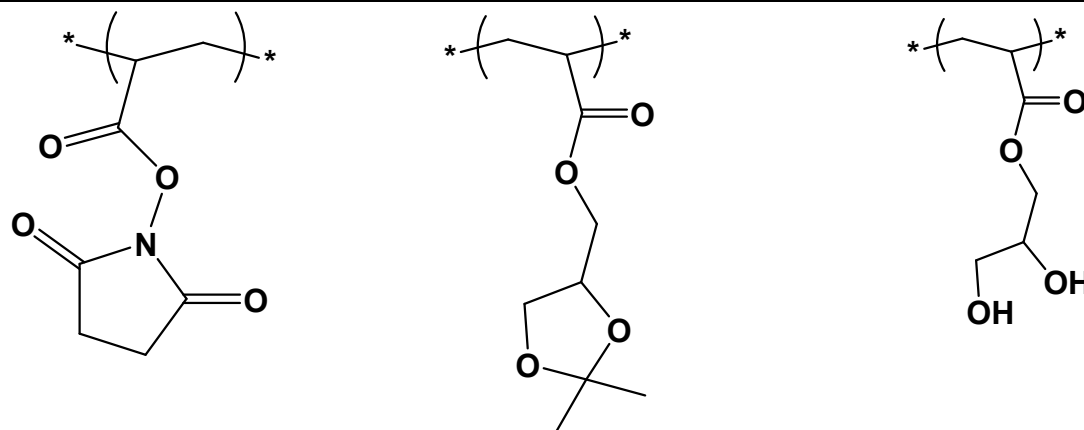
### 3.4. Polymers characterizations.

#### 3.4.1. Homopolymers.

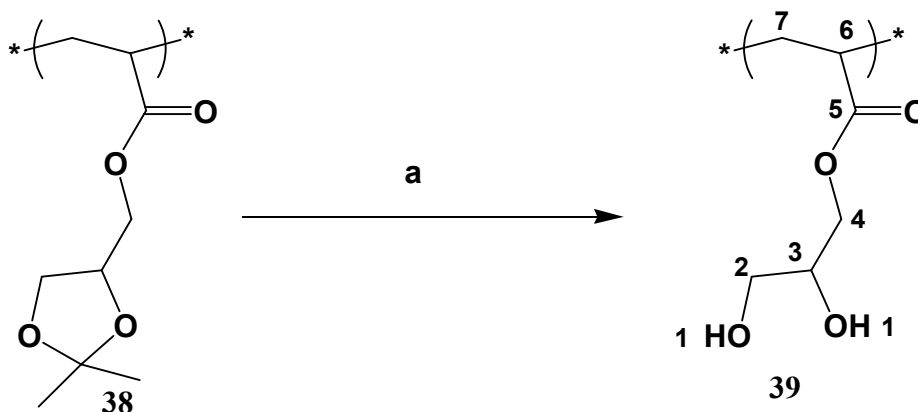
It is necessary before the synthesis of co- and terpolymers to synthesize and characterize the homopolymer of the corresponding monomer and see its characterization. Therefore we will discuss the characterizations of homopolymers used in our study. **Table 48** shows the structures of the most of the homopolymers.

**Table 48:** The structures of homopolymers.

PNIPAAm (29)	PDMAAm (31)	PHEMA (33)
		
PVA (34)	PDEAMVA (35)	PAHVA (36)
		
PNASI (37)	PSKA (38)	PDHPA (39)



Overall homopolymers were synthesized by random free radical polymerization in 1,4-dioxane and AIBN as initiator. Further, polymer **39** was synthesized by the ring opening of polymer (**38**) as illustrated in **scheme14**.



**Scheme14:** Synthesis of Poly (2,3-dihydroxypropyl acrylate) (DHPA).

(a) THF, glacial acetic acid/reflux, 90, 6h

The characterization was summarized in the **Table 49** below. Table cleared yield which calculated as relative yield and both average molecular weight and polydispersity indices as measured by gel permission chromatography (GPC, the polymer solution was 6g/L in DMAc).

The glass transition temperature was measured by DSC as a change in the heat capacity as the polymer goes from glass state to rubber; the transition appeared as a step transition. Polymer **36** shows higher  $T_g$ , due to the chemical structure, and presence of benzene ring, which restrict the free rotation. All polymers showed amorphous state, except polymers **38**, and **39** showed viscous-elastic polymers at room temperature and semi-crystalline state by cooling under  $-20^\circ\text{C}$  and pressure  $10^{-2}$  Pa.

The transition temperature of PNIPAAm is a distinguished character that appeared lower critical solution temperature (LCST) behavior, due to the balance between the hydrophilic CONH group and the hydrophobic dimethyl group, and CH<sub>2</sub> groups in the backbone. Two techniques were used to show this appearance and measure the value of T<sub>c</sub>. The first method was DSC of polymer solutions in deionized water, showing a peak at 33°C. The second technique is the turbidity test using UV-vis.Spectroscopy, as a change in the transmittance with temperature at a constant absorbance (500nm) for 1 wt% of polymer solution in deionized water. The change of transmittance was low till the T<sub>c</sub> point, at which a fast change was occurred. 50% transmittance corresponds to the cloud point of polymer. Above this point the polymer solution was almost completely turbid and no transparency occurred. The same experiment has been done for polymers **37** and **38** in pH11 but, they did not show any change.

**Table 49:** Yield, molecular weight, polydispersity, glass temperature and transition temperature of homopolymers.

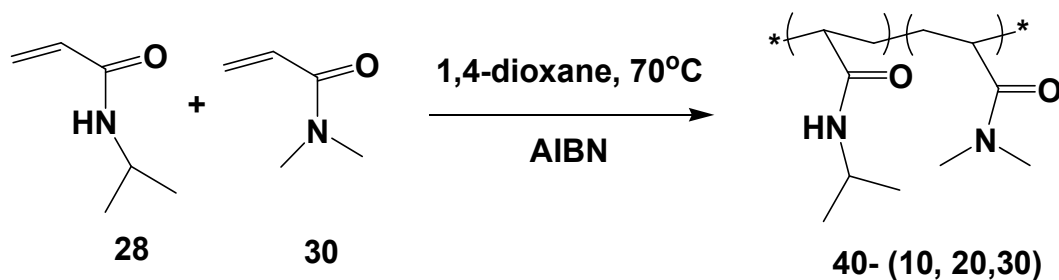
<b>Polymer</b>	<b>Yield (%)</b>	<b>Mw (g/mol) 10<sup>4</sup></b>	<b>PD</b>	<b>T<sub>g</sub> (°C)</b>	<b>T<sub>c</sub> (°C)</b>
<b>29</b>	95	7.17	3.15	140	33
<b>31</b>	93	6.09	1.45	93	-
<b>33</b>	95	3.52	1.93	67	-
<b>34</b>	88	1.53	2.44	187	-
<b>35</b>	20	0.64	1.98	106	-
<b>36</b>	32	0.57	1.69	180	-
<b>37</b>	96	1.64	1.75	135	-
<b>38</b>	57	0.78	2.07	-	-
<b>39</b>	23	0.33	1.30	-	-

### 3.4.2. PNIPAAm copolymers.

The aim of this section is the interpretation of the analysis of copolymers based on PNIPAAm which acts as temperature responsive polymers. The effect of incorporation of hydrophilic or hydrophobic moiety with different mole ratios on the lower critical solution temperature behavior was our interest.

#### 3.4.2.1. Poly(NIPAAm-Co-DMAAm).

The incorporation of DMAAm which act as hydrophilic moiety in PNIPAAm main chain with different mole ratios start from (10 mol% till 30mol%) were done by random free radical polymerization as described in **scheme15**.



**Scheme15:** Synthesis of Poly(NIPAAm-Co-DMAAm).

The  $^1\text{H}$ NMR analysis illustrated the presence of DMAAm in the polymer main chain, was calculated from the integration for (CH) at 3.99-4 ppm of NIPAAm and (2CH<sub>3</sub>) with (CH) backbone at 2.77 - 3.14 ppm of DMAAm, the actual compositions of DMAAm are cleared in **Table 50**.

The  $T_c$  for all copolymers in water solutions were measured by UV-vis.Spectroscopy. Polymer solutions below  $T_c$  were clear and complet transperance related to the hydrogen bonding between the hydrophilic groups in polymers molecules and water molecules resulting in polymer dissolution. After raising the temperature above the  $T_c$  hydrophobic interactions dominates leading to polymer precipitation and lead to phase separation which appears as solution turbidity. **Table 50** clears the increasing of  $T_c$  from polymer **40-10** to **40-30** with 30mol% DMAAm. Moreover, **Figure45** describe the method used for the determination of  $T_c$  and  $C_p$  for polymer aqueous solution, while  $T_c$  was taken as the intersection point between the highest plateau and the straight part as shown in **Figure 45** and  $C_p$  was taken as 50% transmittance at this point the solution look like white cloud or milky solution.

**Table 50:** Yield, composition, molecular weight, polydispersity, glass temperature and transition temperature of poly(NIPAAm-Co-DMAAm).

Polymer	Yield %	Composition		Mw (g/mol) $10^4$	PD	$T_g$ °C	$T_c$ °C
		$^1\text{HNMR}$					
		DMAAm (mol%)					
40-10	90	9.8		2.28	3.15	130.2	36.5
40-20	93	14		3.23	2.34	128.9	42.2
40-30	95	19		4.27	1.89	116.3	43.9

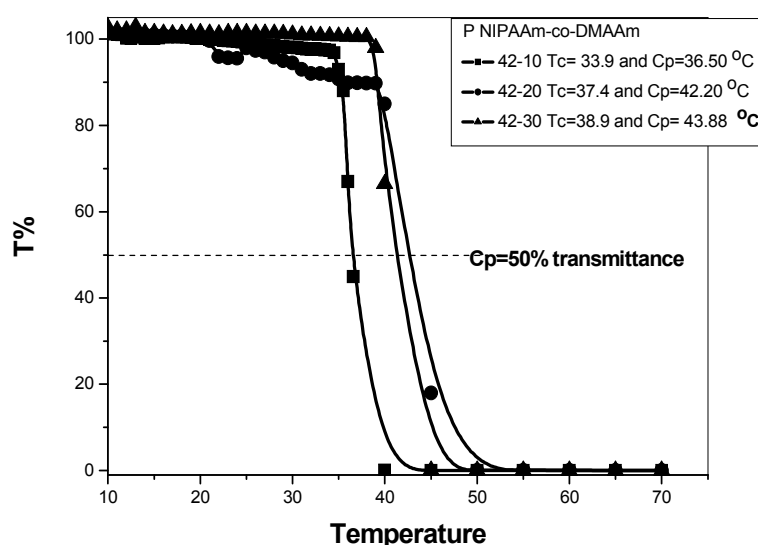
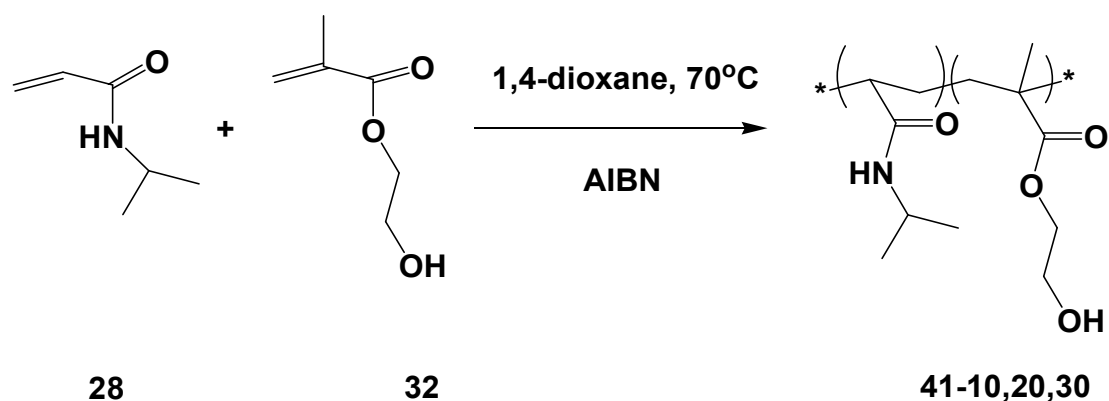


**Figure 45:** Change in turbidity with temperature for determination of  $T_c$  of P(NIPAAm-Co-DMAAm) using UV-vis. Spectroscopy using 1wt% of polymer solution in deionized water.

#### 3.4.2.2. Poly(NIPAAm-Co-HEMA).

The aim of the synthesis of this series of polymers was to get thermoresponsive polymers with high degree of hydrophilicity 2-Hydroxyethyl methacrylate (HEMA) is a hydrophilic monomer. It is water-soluble while, the polymer has a limited solubility.

Polymers were synthesized by free radical polymerization in 1,4-dioxane and AIPN as initiator according to **scheme16**.



**Scheme 16:** Synthesis of Poly(NIPAAm-Co-HEMA)

In this study we will focus on the interpretation of phase transition temperature as the addition of HEMA with different mole ratios of 10, 20, and 30 mol%. These polymers were characterized by  $^1\text{H}$ NMR and IR. The composition of HEMA was determined from the integration using 6H (2CH<sub>3</sub>) of NIPAAm at 0.71-1.16ppm and OH of HEMA at 4.81-5.15ppm. The weight average molecular weight, number average molecular weight and polydispersity were measured by GPC.  $T_g$  decreased with increasing HEMA composition.

The  $T_c$  for all copolymers in aqueous solutions (except polymer **41-30** a mixture of methanol and water 4:1) were measured by UV-vis.Spectroscopy. (**Figure46**). **Table 51** clears the increasing of  $T_c$  from polymer **41-10** to **41-30** with 30mol% HEMA.

**Table 51:** Yield, composition, molecular weight, polydispersity. glass temperature, and transition temperature of poly(NIPAAm-Co-HEMA).

Polymer	Yield %	Composition	Mw	PD	$T_g$ °C	$T_c$ °C
		$^1\text{H}$ NMR	(g/mol)			
		DMAAm (mol%)	$10^4$			
<b>41-10</b>	95	10	5.57	3.37	135.5	34
<b>41-20</b>	95	19.85	5.52	3.47	110.6	37.7
<b>41-30</b>	97	22.20	5.38	3.14	104.6	40

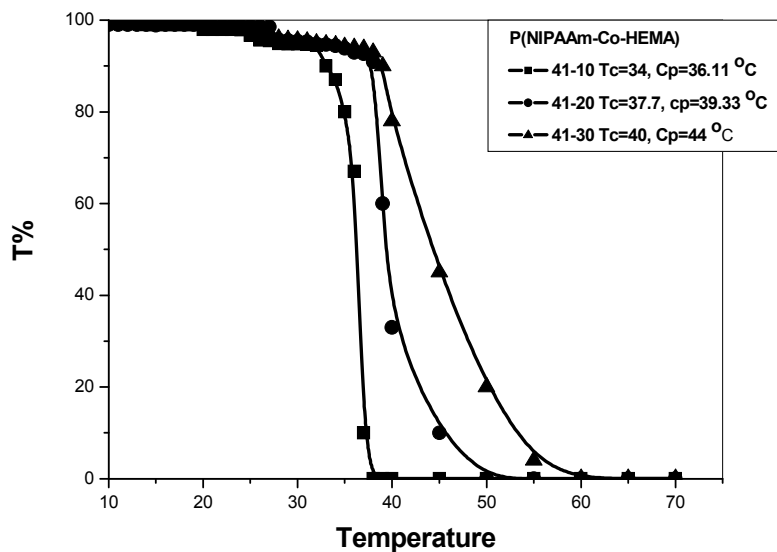
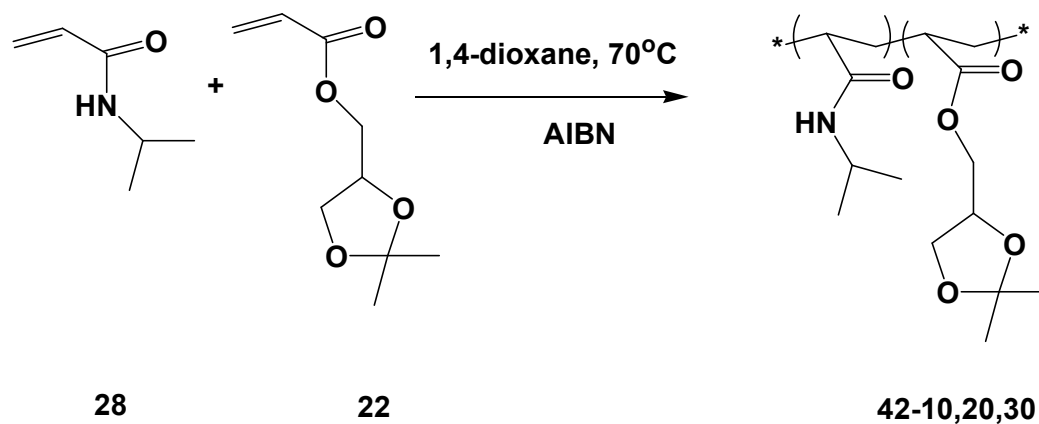


**Figure 46:** Change in turbidity with temperature for determination of  $T_c$  of P(NIPAAm-Co-HEMA) using UV-vis. Spectroscopy using 1wt% of polymer solution in deionized water.

### 3.4.2.3. Poly(NIPAAm-Co-SKA).

In this series of copolymers NIPAAm was synthesized by free radical polymerization in 1,4-dioxane and AIBN as initiator as illustrated in **scheme17**.



**Scheme 17:** Synthesis of Poly(NIPAAm-Co-SKA).

The incorporation of hydrophobic moiety should effect sharply in the phase transition temperature. Therefore, different mole ratios from 10 to 30% of monomer **22** were copolymerized with NIPAAm to see the effect on the molecular weight and glass transtion temperature ( $T_g$ ) and finally most important is the phase transition temperature ( $T_c$ ) (**Table 52**). It was observed that the glass transtion temperature decreased with increasing the hydrophobic moiety in the main chain.

The  $T_c$  of polymers **42-10.20.30** were measured by UV-vis. Spectroscopy as a change in transmittance with temperature. **Figure 47** shows lower  $T_c$  with increasing in the rate of **SKA** composition in the main chain.

**Table 52:** Yield, composition, molecular weight, polydispersity, glass temperature and transition temperature of poly(NIPAAm-*Co*-SKA).

Polymer	Yield %	Composition	Mw (g/mol) $10^4$	PD	$T_g$ °C	$T_c$ °C
		$^1\text{HNMR}$				
		DMAAm (mol%)				
<b>42-10</b>	90	5.88	8.00	2.12	126.4 °C	18.3
<b>42-20</b>	78	15.45	7.57	2.34	123.6 °C	14.4
<b>42-30</b>	60	22.3	3.24	1.80	96.4 °C	10.3

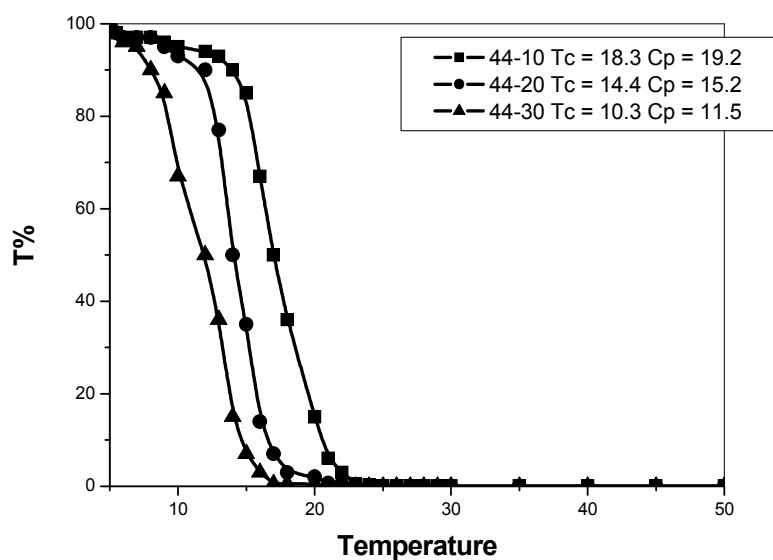
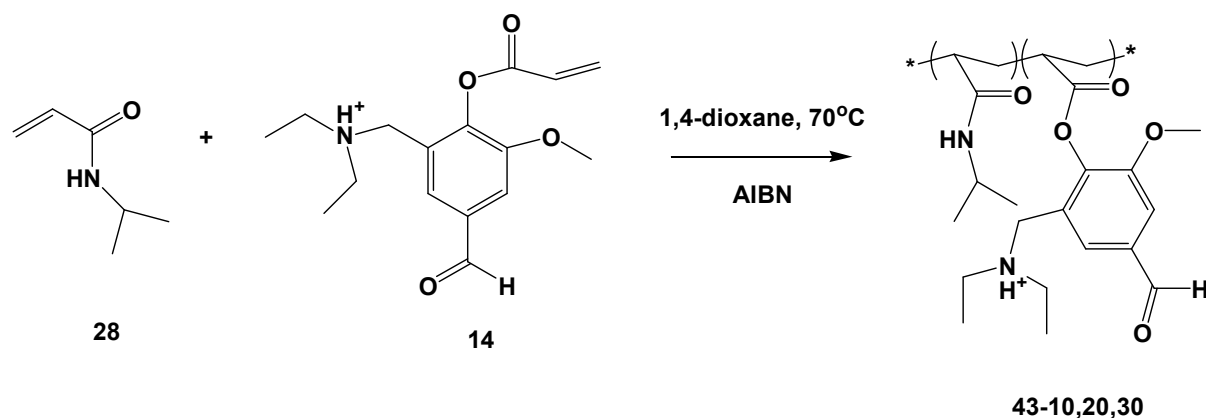


**Figure 47:** Change in turbidity with temperature for determination of LCST of P(NIPAAm-*Co*-SKA) using UV-VIS. spectroscopy using 1Wt% of polymer solution in mixture of deionized water and ethanol.

### 3.4.2.4. Poly(NIPAAm-Co-DEMAVA).

Using the same method Poly(NIPAAm-Co-DEMAVA) was synthesised as illustrated in **scheme18**.



**Scheme 18:** Synthesis of Poly( NIPAAm-Co-DEMAVA).

The aim of the synthesis of this kind of polymer was the formation of polymers with dual responsive in which **NIPAAm** act as temperature responsive as known while, the new monomer **DEMAVA** act as pH-responsive. Three different polymers were synthesized with different mole ratios of **DEMAVA**.

The phase separation for each polymer was studied by UV-vis. Spectroscopy in different pH buffer solutions (pH2, pH7, pH11).

Due to the presence of hydrophilic **DEMAVA** in the polymer chain an increase in the **LCST** with increasing **DEMAVA** content in the polymer chain was observed. The second effect was seen in the pH responsiveness of the polymer solution.

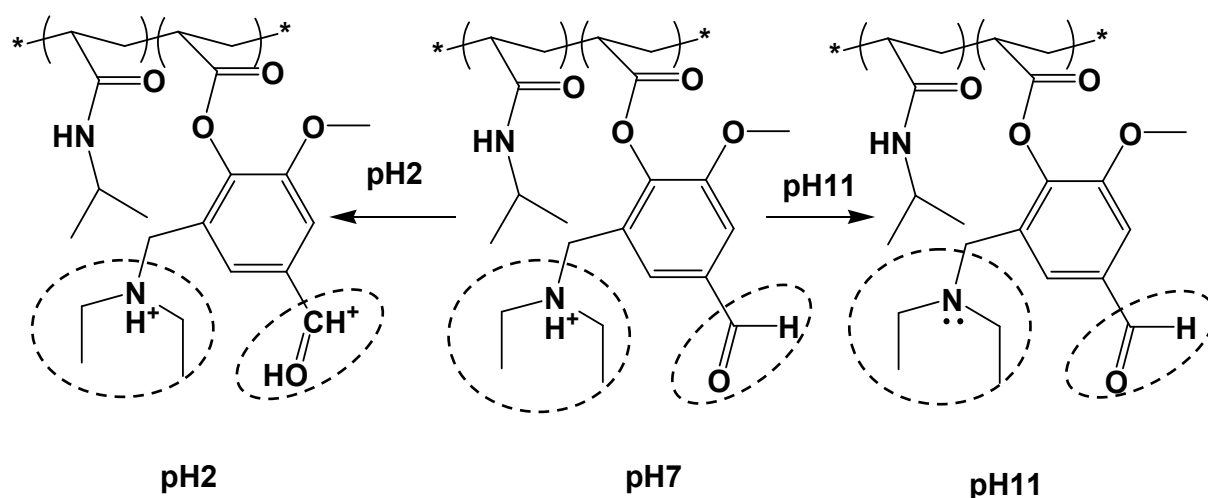
UV-vis Spectroscopy for measuring the absorbance maximum of the polymer solution 1 wt% in pH2, pH7, and pH11 was used. Absorption maxima at pH2  $\lambda_{\max.} = 308$  nm due to the  $n-\pi^*$  transition of C=O aldehyde, 256 nm for  $\pi-\pi^*$  transition of C=C-C=C aromatic conjugated system, and 235 nm for  $n-\pi^*$  transition of C=O amide group. However at pH7 weak absorption at  $\lambda_{\max.} = 345$  nm due to the  $n-\pi^*$  and  $\pi-\pi^*$  transition of C=O ionized carboxylic group 255 nm for  $\pi-\pi^*$  transition of C=C-C=C aromatic conjugation system, and 233nm for  $n-\pi^*$  transition of C=O amide group. At pH11 the spectra showed  $\lambda_{\max.} = 349$  nm due to the  $n-\pi^*$  transition of C=O related to oxidation of aldehyde, 256 nm for  $\pi-\pi^*$  transition of C=C-C=C aromatic conjugated system, and 235nm for  $n-\pi^*$  transition of C=O amide group.

According to these effects the polymer **43** with different mole ratios of DEMAVA demonstrate different  $T_c$  as follows.

- ❖  $T_c$  increases as the DEMAVA increased in the polymer chain as cleared in **Table 53** occurred for polymers in pH2 and pH7. This might be interpreted as the generation of charge along the polymer backbone causing electrostatic repulsion (**Scheme 19**)
- ❖ At **pH2** the polymer has protonated tertiary amine. For this reason the hydrophilic groups is more effective than the hydrophobic groups of DEMAVA. Hence, overall the copolymer illustrated higher hydrophilicity.
- ❖ At **pH7** the polymer solution shows unexpected change. Therefore the polymer solutions illustrated higher  $T_c$  more PNIPAAm (**Figure 52**).
- ❖ The last feature at **pH11** which did not show any change in turbidity starting from 10°C to 80°C. **Figure 49** shows the FTIR spectra at different pH value. This behavior is unclear since the tertiary amino group should be completely deprotonate, and, hence, the lowest  $T_c$  should be observed.

**Table 53** : Yield, composition, molecular weight, polydispersity, glass temperature, and transition temperature of poly(NIPAAm-Co-DEMAVA).

Polymer	Yield %	Composition <sup>1</sup> HNMR DMAAm (mol%)	Mw (g/mol) 10 <sup>4</sup>	PD	T <sub>g</sub> °C	T <sub>c</sub> °C		
						pH2	pH7	pH11
43-10	70	4	1.44	2.20	138.4	34.5	44	-
43-20	65	6.3	1.00	2.43	140.0	37.2	53	-
43-30	65	10.5	1.25	2.27	153.6	44.9	62.3	-



**Scheme 19:** The predicted chemical structures of polymer 43 in different pH solution.

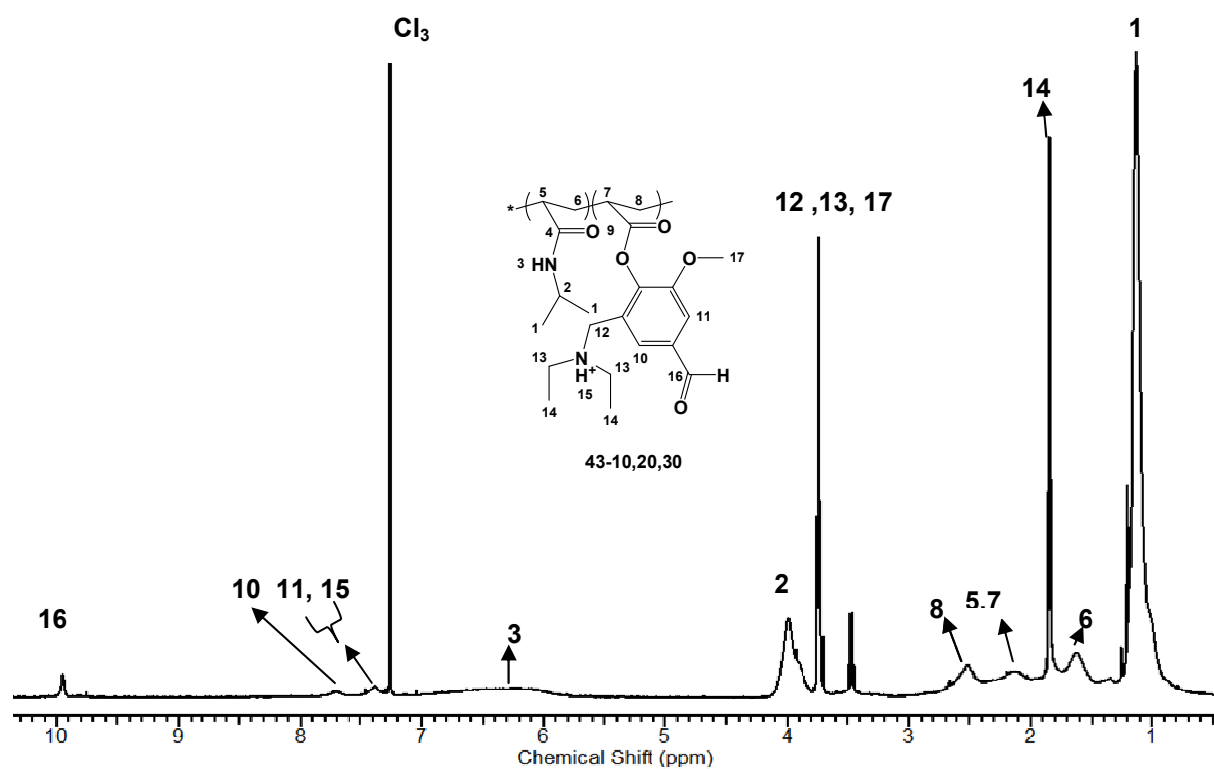


Figure 48:  $^1\text{H}$  NMR spectra ( $\text{CDCl}_3$ ) of polymer 43-20.

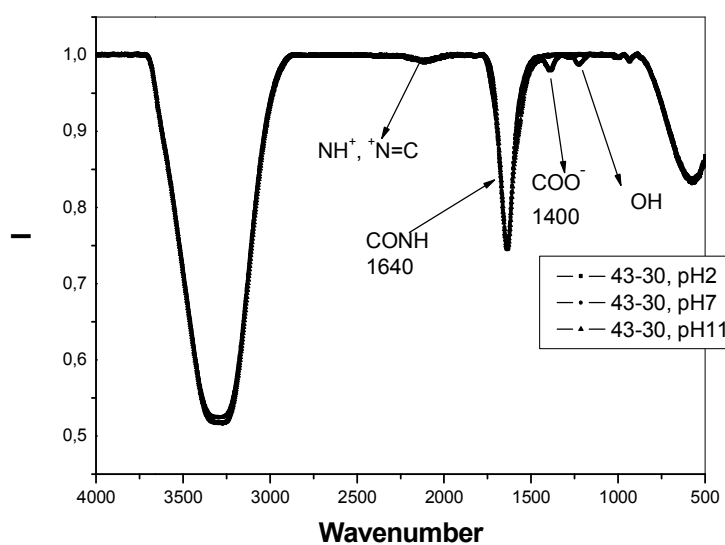
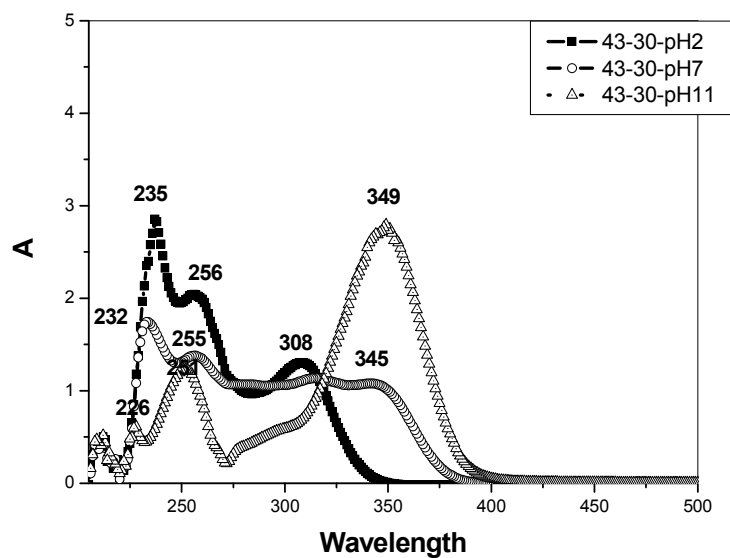
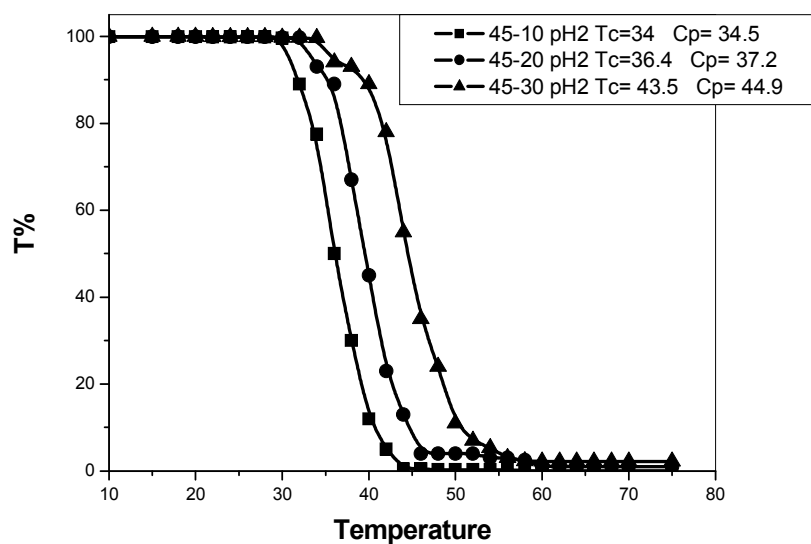


Figure 49: FTIR spectra of polymer 43-30 in different pH-solutions.



**Figure 50:** UV-spectra of polymer 43-30 at pH2, pH7 and pH11.



**Figure 52:** Change in turbidity with temperature for determination of  $T_c$  of P(NIPAAm-Co-DEMAVA) with 10, 20 and 30 mol% of DEMAVA using UV-vis. Spectroscopy using 1Wt% of polymer solution of pH2.

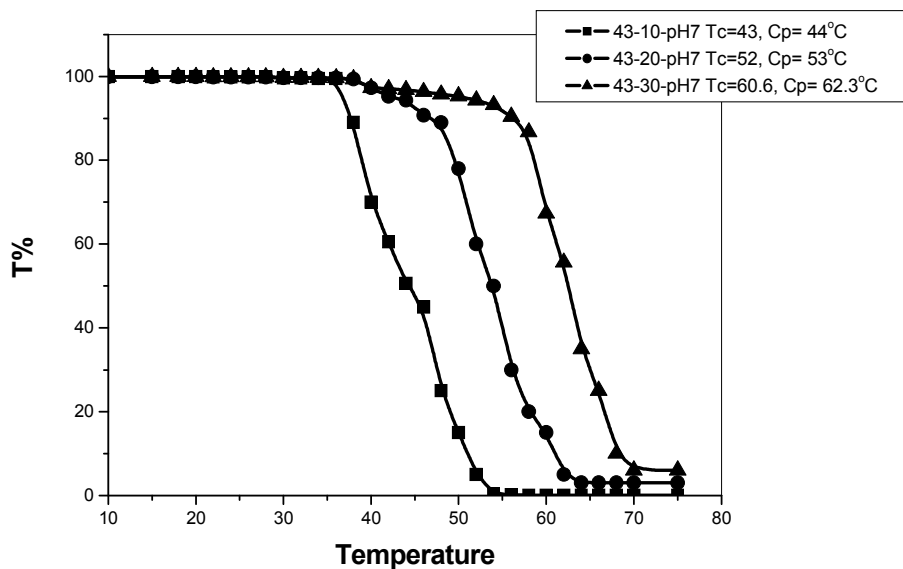
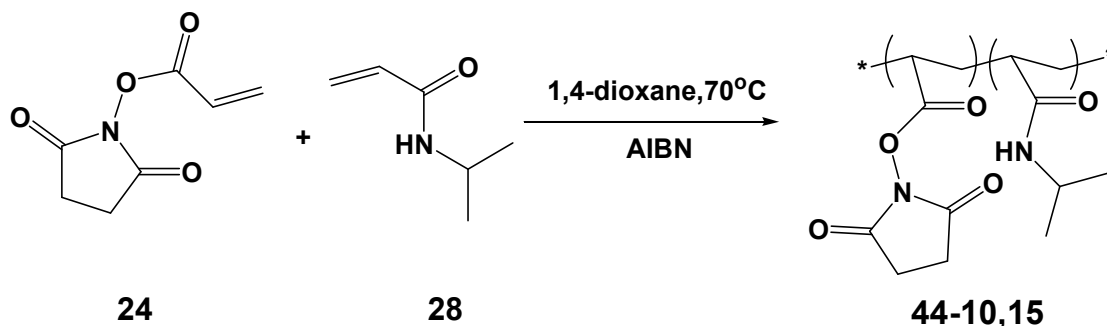


**Figure 51:** Change in turbidity with temperature for determination of  $T_c$  of P (NIPAAm-Co-DEMAVA) with 10, 20 and 30 mol% of DEMAVA using UV-vis. Spectroscopy of 1wt% of polymer solution of pH7.

#### 3.4.2.5. Poly(NIPAAm-Co-NASI).

The synthesis of polymers containing active ester groups has been a recent interest for a variety of applications like drug delivery. The activated ester groups can be substituted by amino group of proteins, amino acids, and other biomolecules.

Here in this section we synthesized this short series of poly(NIPAAm-Co-NASI) 10 and 15 mole % by random free radical polymerization as illustrated in **scheme20**. The polymers were investigated by  $^1\text{H}$ NMR which illustrated the presence of NASI in the polymer main chain with different mole ratio. The composition was calculated from the integration of  $2\text{CH}_2$  of NASI at 2.75-3.01ppm and CH of NIPAAm at 3.87-4.15 ppm (**Table 54**).



**Scheme 20:** Synthesis of poly (NASI-Co-NIPAAm)

The phase transition of polymers solution in deionized water were measured as previously discussed. The  $T_c$  of polymers as illustrated in **Figure 54** demonstrated a reversible relation

between  $T_c$  and the content of NASI in the polymers attributed to the effect of hydrophobic moieties.

**Table 54** : Yield, composition, molecular weight, polydispersity, glass temperature and transition temperature of poly(NIPAAm-*Co*-NASI).

Polymer	Yield %	Composition		Mw (g/mol) $10^4$	PD	$T_g$ °C	$T_c$ °C
		$^1\text{H NMR}$					
		DMAAm (mol %)					
44-10	93	10.0		3.98	2.37	132.6	25.7
44-15	93	12.8		4.31	2.42	129.8	21.8

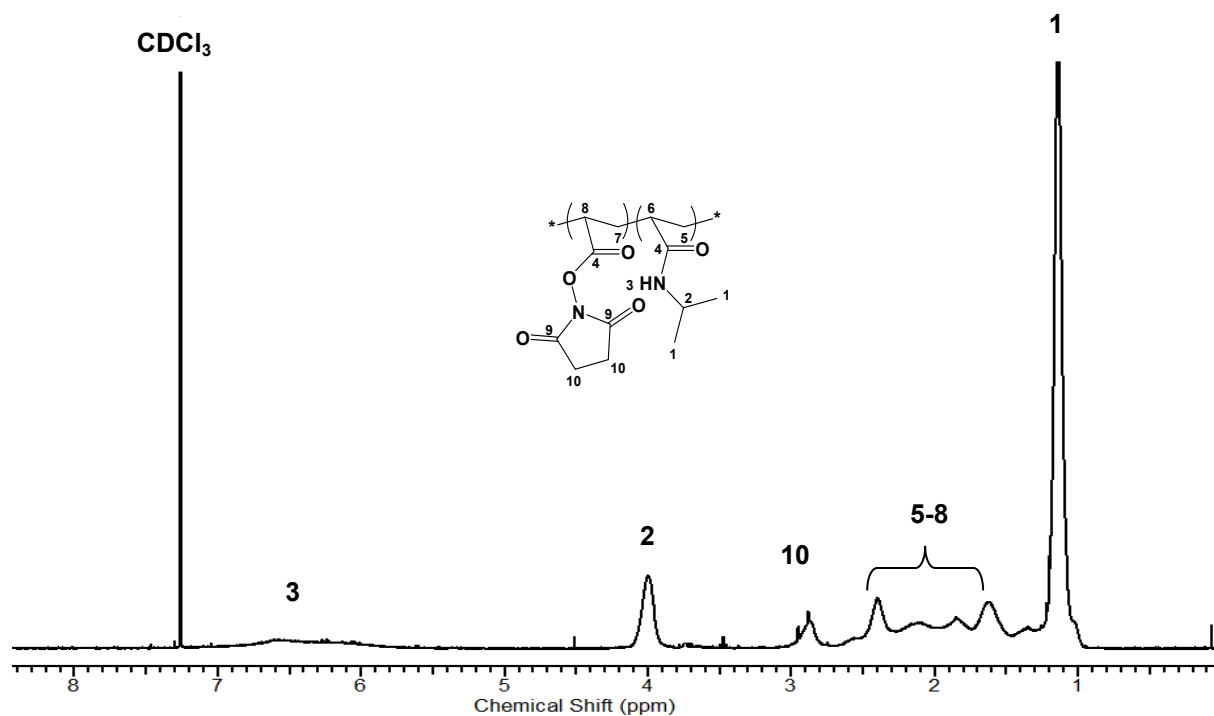


**Figure 53:**  $^1\text{H NMR}$  spectra ( $\text{CDCl}_3$ ) of polymer 44-15.

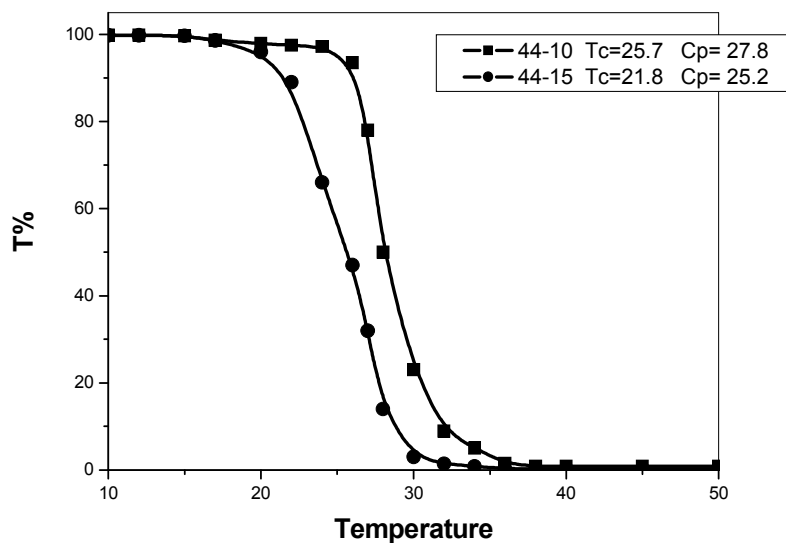
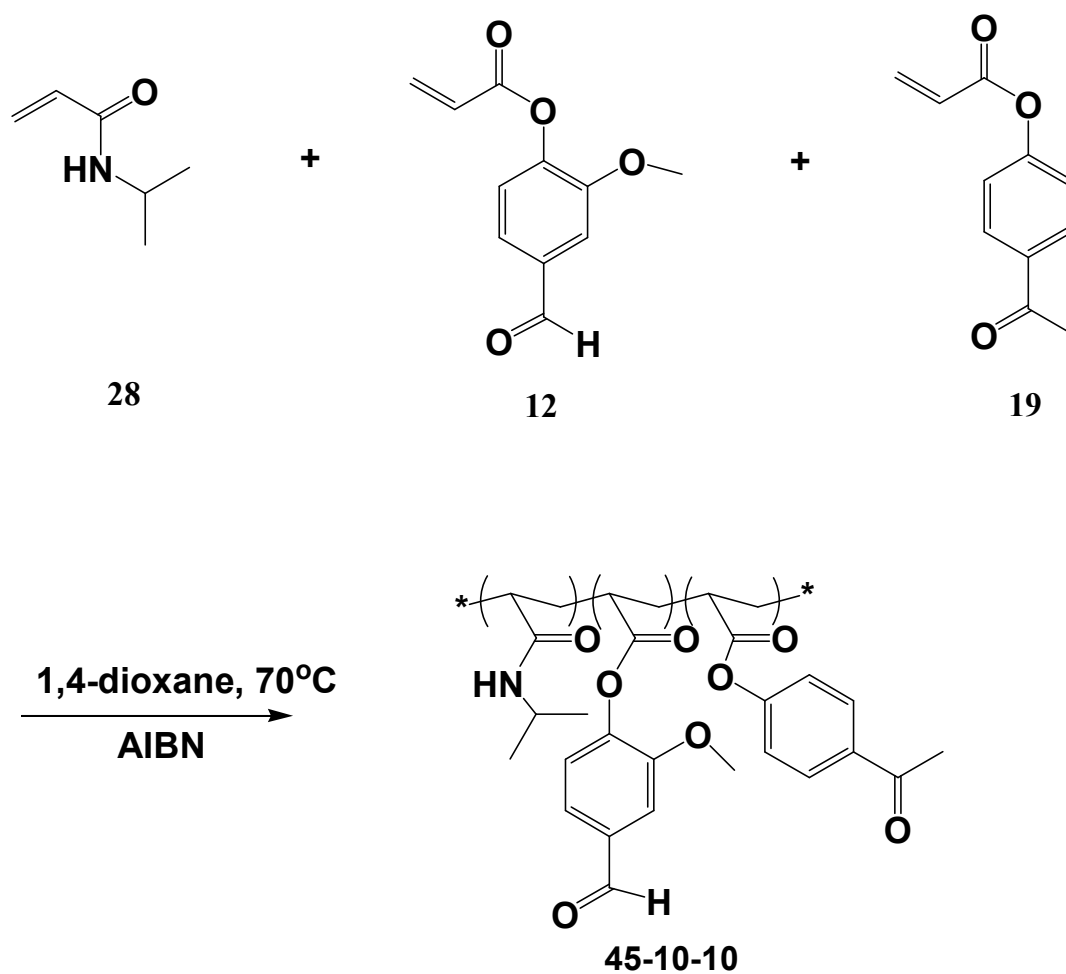


**Figure 54:** Change in turbidity with temperature for determination of  $T_c$  of P(NIPAAm-Co-NASI) with 10 and 15 mol% of NASI using UV-vis. Spectroscopy of 1wt% of polymer solution.

#### 3.4.2.6. Poly (NIPAAm-Co-VA-Co-APA).

The synthesis of polymer (**45**) was aimed to form polymer with bifunctional groups and further increase the hydrophobicity of polymer. The phase separation behavior due to the presence of NIPAAm was also our interest.  $T_c$  was studied by UV-vis. Spectroscopy for the polymer aqueous solution showing 19.7°C. The composition was also determined by integration of the  $^1\text{H}$  NMR spectra; the integration 2.47-2.66 ppm (1 $\text{CH}_3$ ), 3.78-4.19 ppm (17NH), and 9.86-10.04 ppm (13CHO) (**Figure 55**). The polymer was synthesized by free radical polymerization in 1,4-dioxane and AIPN as initiator.



**Scheme 21:** Synthesis of terpolymer of P(NIPAAm-*Co*-VA-*Co*-APA).

**Table 55:** Yield, composition, molecular weight, polydispersity, glass temperature and transition temperature of poly(NIPAAm-*Co*-VA-*Co*-APA).

Polymer	Yield %	Composition		Mw (g/mol) $10^4$	PD	$T_g$ °C	$T_c$ °C
		$^1\text{HNMR}$					
		VA	APA				
45	90	6.5	9.8	4.57	2.50	145.7	15.7

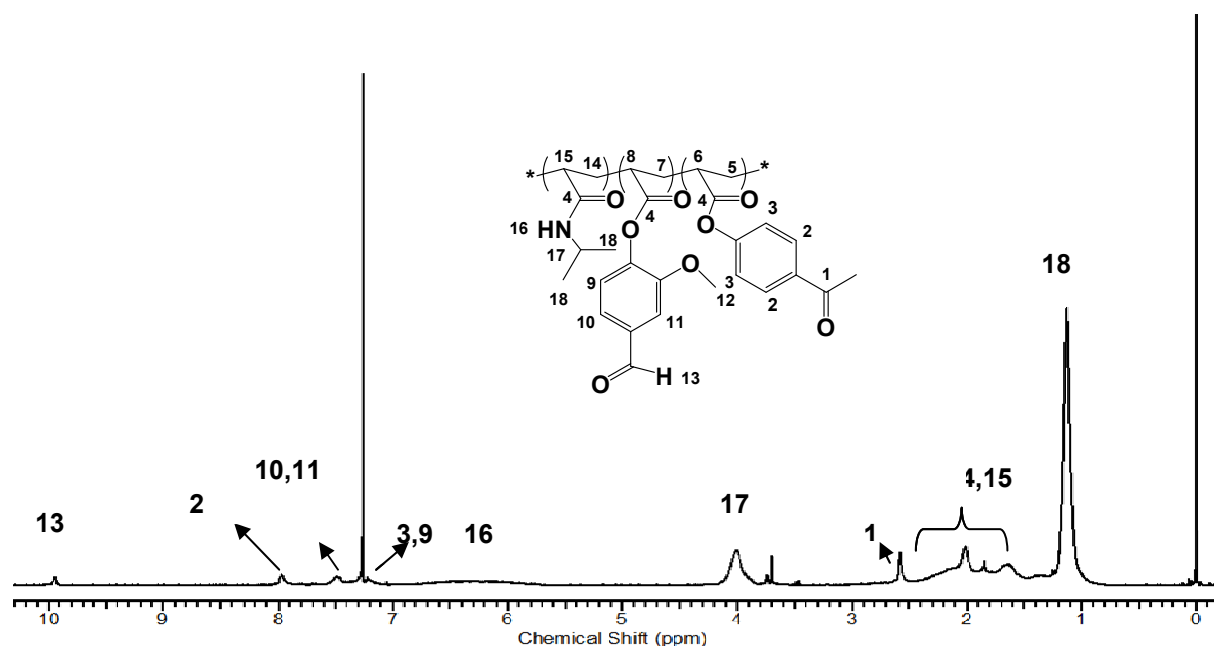


Figure 55:  $^1\text{H}$  NMR spectra ( $\text{CDCl}_3$ ) of polymer 45-10-10.

### 3.5. Photo-crosslinker polymers.

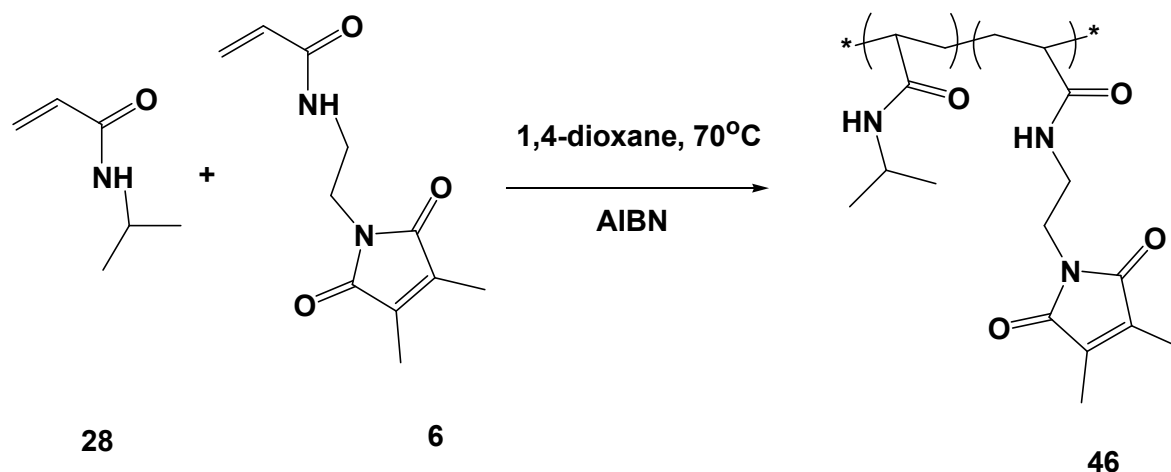
#### 3.5.1. Poly(NIPAAm-*Co*-DMIAAm) with 2, 5 and 10 mol% of maleimido crosslinker.

##### 3.5.1.1. General characterization.

Photo-crosslinkable polymers were synthesized in different composition to obtain temperature sensitive photo-crosslinkable and biocompatible polymers.

The polymers were synthesized by the random free radical polymerization using AIBN as an initiator and 1,4-dioxane as solvent as illustrated in **scheme22**.

2, 5 and 10 mol % of dimethylmalimido acrylamide (DMIAAm) were prepared. Polymers were characterized by  $^1\text{H}$  NMR and UV-vis. Spectroscopy for the determination of DMIAAm composition in the main chain as cleared in (**Table 56**). For  $^1\text{H}$ NMR we used the integration of ( $2\text{CH}_3$ ) at 1.88-1.99 ppm of malimide and ( $\text{CH}$ ) at 3.86-4.12 ppm of NIPAAm. For using UV-vis. Spectroscopy a calibration curve of absorptions of dimethylmalimidoethanol with different concentrations values has been measured. It was noticed that data from UV-spectroscopy were higher than data from  $^1\text{H}$ NMR.



**Scheme 22:** Synthesis of poly(NIPAAm-*Co*-DMIAAm).

The effect of DMIAAm incorporation on the  $T_c$  was measured by two facilities DSC (**Figure 57**) and UV-vis. Spectroscopy or turbidly-metric test (**Figure 56**) and both demonstrated close values of  $T_c$ . It was observed, that an increase in DMIAAc content decreased  $T_c$  values (from 48-02 to 48-10). The small difference between photo-crosslikable PNIAAm and PNIPAAm can be interpreted as increase in the hydrophobic moiety locates in dimethylmaleimide. Further, a decrease of the glass transition temperature and molecular weight of polymers as increasing DMIAAm composition were found, which is in accordance with literature<sup>(24)</sup>.

**Table 56:** Yield, composition, molecular weight, polydispersity, glass temperature and transition temperature of poly(NIPAAm-*Co*-DMIAAm).

Polymer	Yield %	Composition		Mw (g/mol) $10^4$	PD	$T_g$ °C	$T_c$ °C	
		DMIAAm (mol%)					UV	DSC
		$^1\text{HNMR}$	UV					
<b>46-02</b>	93	1.6	1.64	3.94	2.4	132.0	31.0	30.7
<b>46-05</b>	90	4.5	4.95	3.58	2.5	130.2	28.8	28.3
<b>46-10</b>	87	7.3	7.88	2.91	2.5	122.1	27.5	27.6

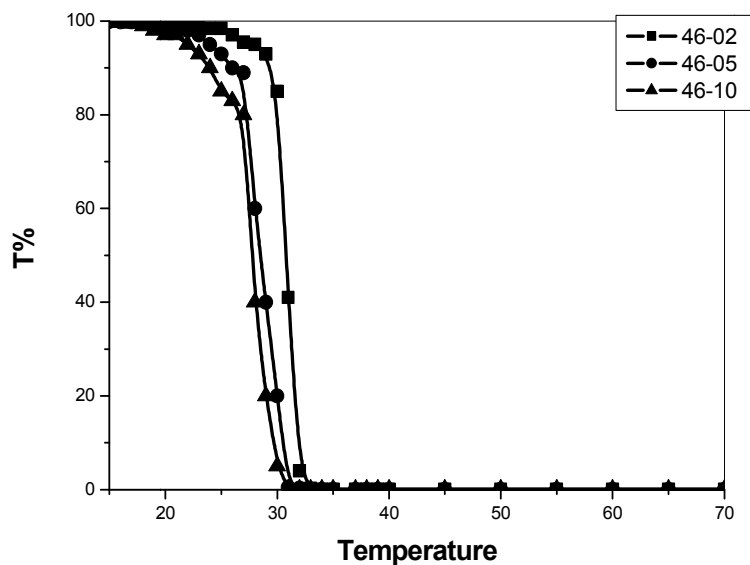


**Figure 56:** Change in turbidity with temperature for determination of  $T_c$  of P(NIPAAm-Co-DMIAAm) with 2, 5 and 10 mol% of DMIAAm using UV-vis. Spectroscopy using 1wt% of polymer solution.

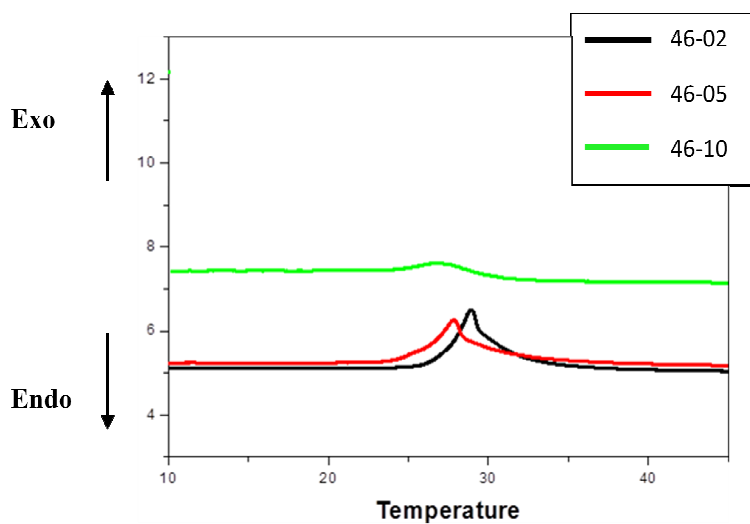
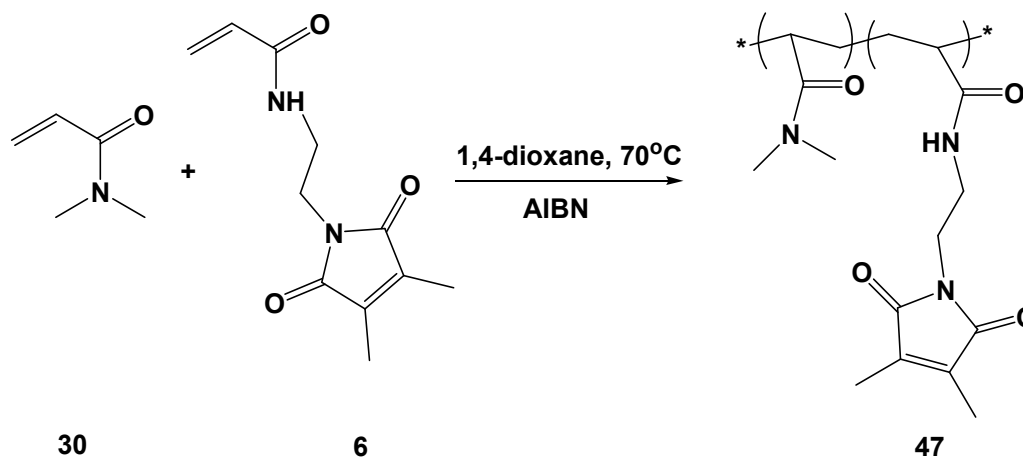


**Figure 57:** DSC of different mol% of P(NIPAAm-Co-DMIAAm) for determination of  $T_c$ .

### 3.5.2. photo-crosslinker poly(DMAAm-*Co*-DMIAAm) with 2, 5 and 10 mol% of maleimido crosslinker.

DMAAm photo-crosslinkable polymers were synthesized by a free radical polymerization of DMAAm with its respective photo-crosslinker as shown in **scheme23**.



**Scheme 23:** Synthesis of photo-crosslinkable poly (DMAAm-*Co*-DMIAAm).

DMAAm is also a hydrophilic monomer like HEMA. The solubility of DMAAm polymers in variety of common solvents makes it more attractive for thin film formation.

The polydispersity indices of DMAAm photo-crosslinkable polymer also decreased with increasing mol-% of DMIAAm. The molecular weights were in the range of  $M_w = 35918$  to 74925. The amount of DMIAAm in DMAAm photo-crosslinkable polymers was estimated by  $^1\text{H}$  NMR and UV-vis. Spectroscopy (**Table 57**).

The comparison between the integration of (2CH<sub>3</sub>) from DMIAAm at 1.88-1.99 ppm and (CH) of DMAAm backbone with (2CH<sub>3</sub>) group in one integration 2.74-3.22 ppm in  $^1\text{H}$  NMR was used in the determination of the actual amount of DMIAAm.

**Table 57:** Yield, composition, molecular weight, polydispersity, and glass temperature of poly(DMAAm-*Co*-DMIAAm).

Polymer	Yield %	Composition		Mw (g/mol) 10 <sup>4</sup>	PD	T <sub>g</sub> °C
		<sup>1</sup> HNMR	UV			
47-02	93	1.87	1.89	7.49	1.59	120.2
47-05	90	3.65	4.21	6.42	1.46	119.7
47-10	87	9.33	9.56	3.59	1.33	116.5

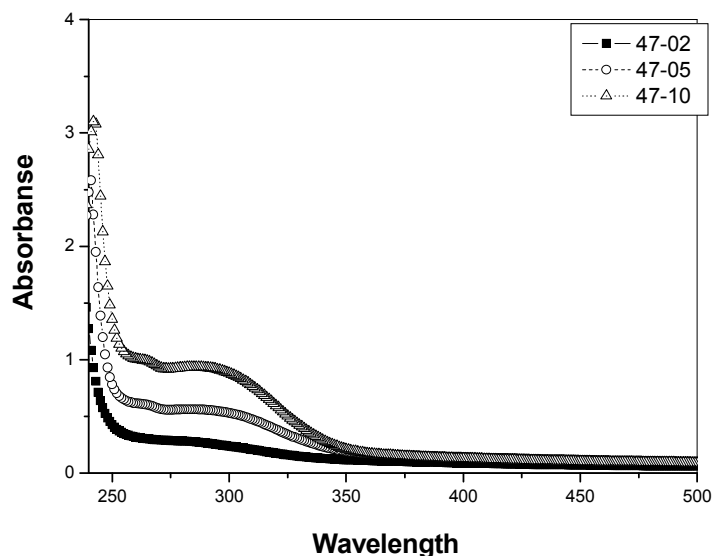
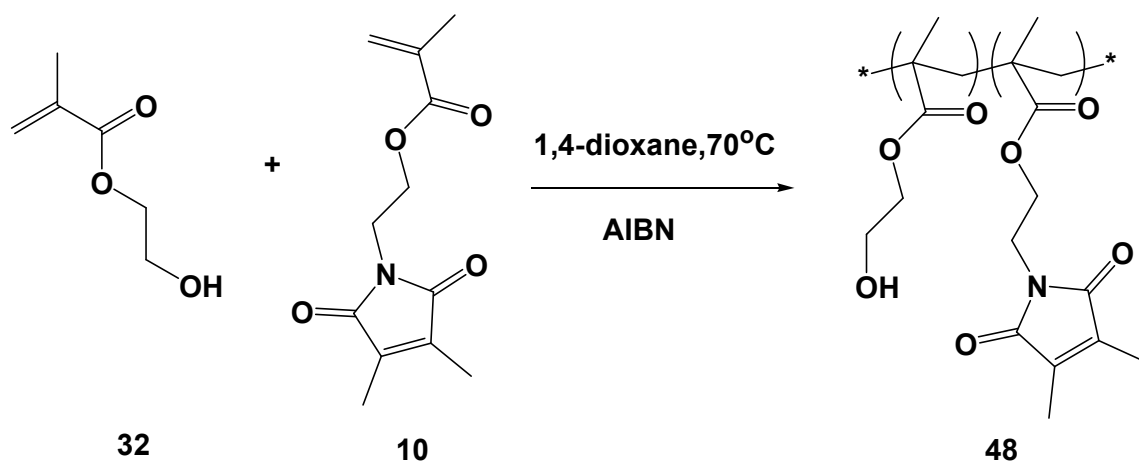


**Figure 58:** UV-vis. Spectroscopy for determination the composition of maleimide crosslinker in polymer 47.

### 3.5.3. Photo-crosslinker poly (HEMA-*Co*-DMIMA) with 2, 5 and 10 mol% of maleimido crosslinker.

Poly(2-hydroxyethyl methacrylate) (PHEMA) has received considerable attention as a biocompatible hydrogel. PHEMA and related copolymers have been used in a multitude of biomaterial applications, including soft contact lenses<sup>(264)</sup>, artificial corneas<sup>(265)</sup>, potential substrates for artificial skin<sup>(266)</sup>, rhinoplasty surgery<sup>(267)</sup> and in drug delivery systems<sup>(268,269)</sup>. The biocompatibility and hydrophilic nature of cross-linked PHEMA hydrogels provide a suitable platform for investigating potential scaffold materials to support tissue growth. Polymeric scaffolds used in tissue engineering applications generally require an open-pore morphology, in which the pores are larger than 10 mm diameter<sup>(270-276)</sup>, interconnected, and uniform throughout the material. This type of pore morphology has been proposed as the optimum to allow for cellular proliferation and tissue development<sup>(277,278)</sup>.

Here in this section we were interested in the synthesis of photo-crosslinkable HEMA polymers. The copolymers of HEMA with DMIMA as a photo-crosslinker were obtained by the free radical polymerization in 1,4-dioxane using AIBN as initiator.



**Scheme 24:** Synthesis of photo-crosslinker poly(HEMA-*Co*-DMIMA).

To study the effect of photo-cross-linker content on the properties of copolymers, different copolymers with 2, 5 and 10 mol-% of DMIMA were synthesized. The properties investigated were molecular weight, copolymer composition, film formation and swelling behavior. Due to the structural similarity of DMIMA with HEMA it is believed that an ideal copolymer is obtained with randomly distributed photo-crosslinker.

The amount of DMIMA in HEMA photo-crosslinkable polymers was estimated by  $^1\text{H}$  NMR and UV-vis.Spectroscopy (**Table58**). The integration of (OH) from HEMA at 4.68-4.98ppm and ( $\text{CH}_2$ ) backbone of DMIMA were used in the determination of the actual amount of DMIMA. The amount of DMIMA in the polymers correlates well with the content in the feed mixture.

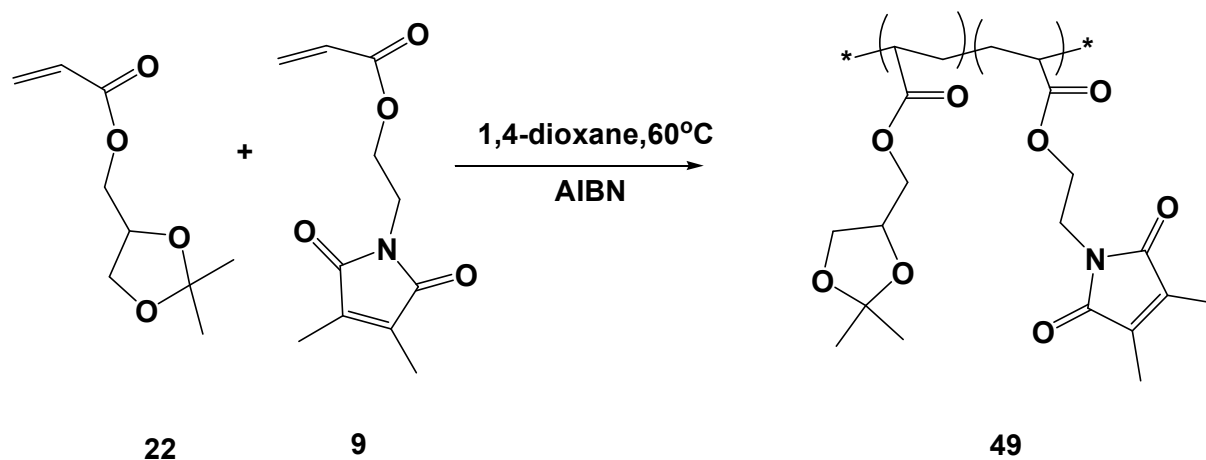
**Table 58:** Yield, composition, molecular weight, polydispersity, and glass temperature of poly(HEMA-*Co*-DMIMA).

Polymer	Yield %	Composition		Mw (g/mol) $10^4$	PD	$T_g$ °C
		DMIAAm (mol%)				
		$^1\text{HNMR}$	UV			
<b>48-02</b>	92	1.89	2.32	12.34	1.72	164.3
<b>48-05</b>	86	4.73	5.75	12.27	2.32	136.6
<b>48-10</b>	82	9.36	9.88	11.81	2.58	115.4

### 3.5.4. Photo-crosslinker poly(SKA-Co-DMIA) with 2, 5 and 10 mol% of maleimido crosslinker.

Solketal-based monomers offer a facile route to obtain hydroxylated polymers. Glycerol monomethacrylate or 2,3-dihydroxypropyl methacrylate obtained from the hydrolysis of solketal methacrylate<sup>(279)</sup> is highly hydrophilic and a constituent of biocompatible networks<sup>(280)</sup>. Moreover, glycerol monomethacrylate finds applications as a replacement for 2-hydroxyethyl methacrylate (HEMA) in contact lenses, photoresists, crosslinkable formulations for paints, and surface modifiers of textile fibers<sup>(281,282)</sup>. Acrylates derived from solketal have been used to synthesize block copolymers as the 2,2-dimethyl-1,3-dioxolane moieties can be converted into hydrophilic glycerol units under mild reaction conditions<sup>(283,284)</sup>. Recently, synthesis of homopolymers and diblock copolymers of solketal acrylate using ATRP (Atom Transfer Radical Polymerization) in cyclohexane has been reported<sup>(285)</sup>. Block copolymers with poly(solketal methacrylate) segments were prepared by Liu et al. using ATRP and anionic polymerization techniques<sup>(286,287)</sup>.

In the present study we focused on the preparation of photo-crosslinkable solketal acrylate by random free radical polymerization as illustrated in **scheme25**.



**Scheme 25:** Synthesis of photo-crosslinker poly (SKA-Co-DMIA).

The change in the molecular weight, polydispersity indices, and glass transition temperature were also determined. Moreover, the polymer was used in the formation of hydrogel thin film through the ring opening of SKA to dihydroxy propylacrylamid which is more hydrophilic as shown in **section 4.5.5**.

The actual compositions of DMIA were determined using UV-vis.Spectroscopy and <sup>1</sup>HNMR. The same method used in the previous polymers used here, the integration of (2CH<sub>3</sub>) in DMIA in a comparison with the integration of (CH<sub>2</sub>) in SKA as shown **Figure59**.

**Table 59:** Yield, composition, molecular weight, polydispersity, and glass temperature of poly(SKA-Co-DMIA).

Polymer	Yield %	Composition DMIAAm (mol%)		Mw (g/mol) $10^4$	PD	T <sub>g</sub> °C
		<sup>1</sup> HNMR	UV			
49-02	45	0.3	0.55	4.76	1.83	97
49-05	50	10.5	11.3	4.63	1.86	119
49-10	47	14.08	16.3	1.00	2.1	128

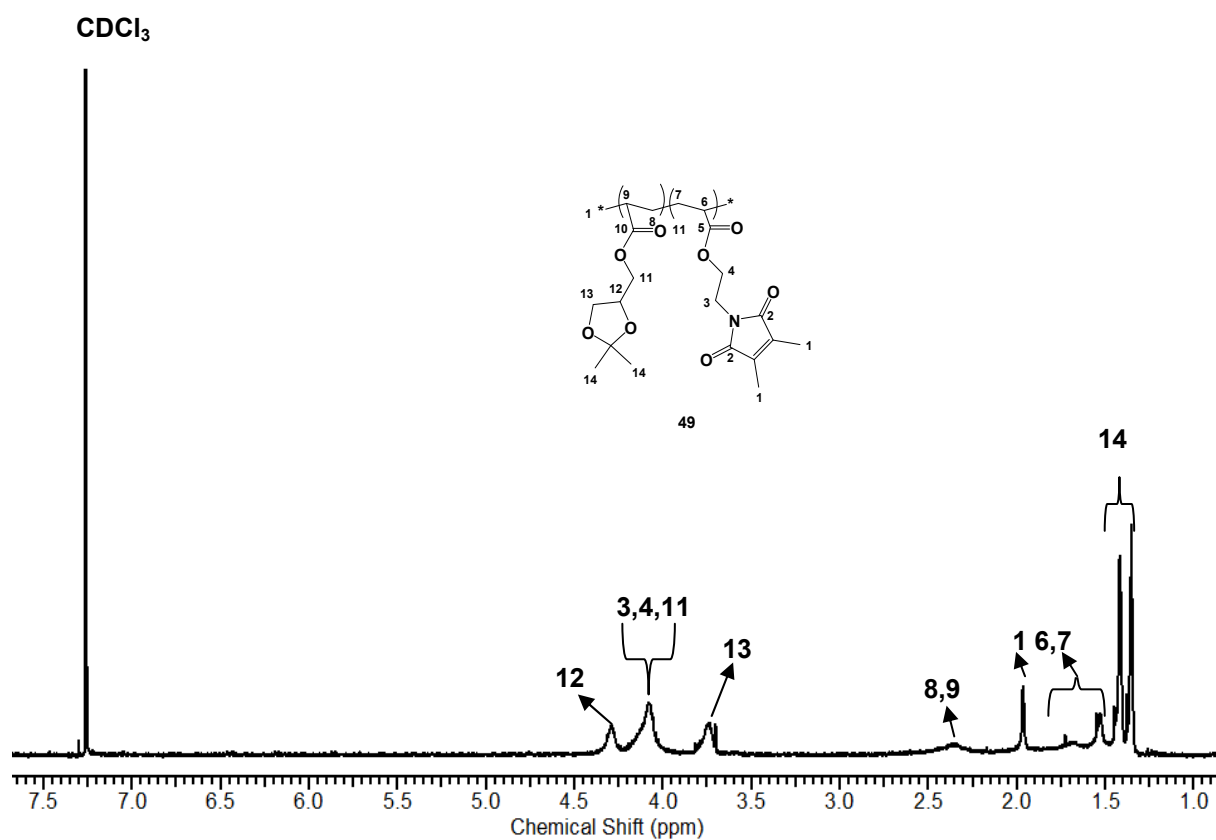


**Figure 59:** <sup>1</sup>H NMR spectra (CDCl<sub>3</sub>) of polymer 49.

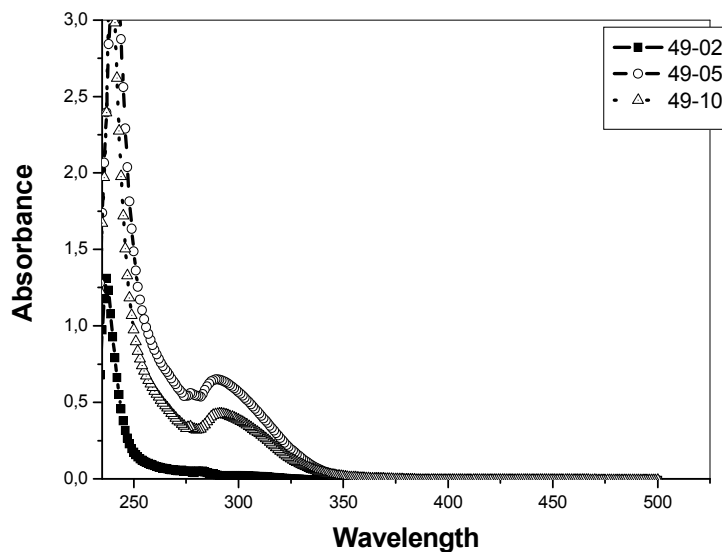
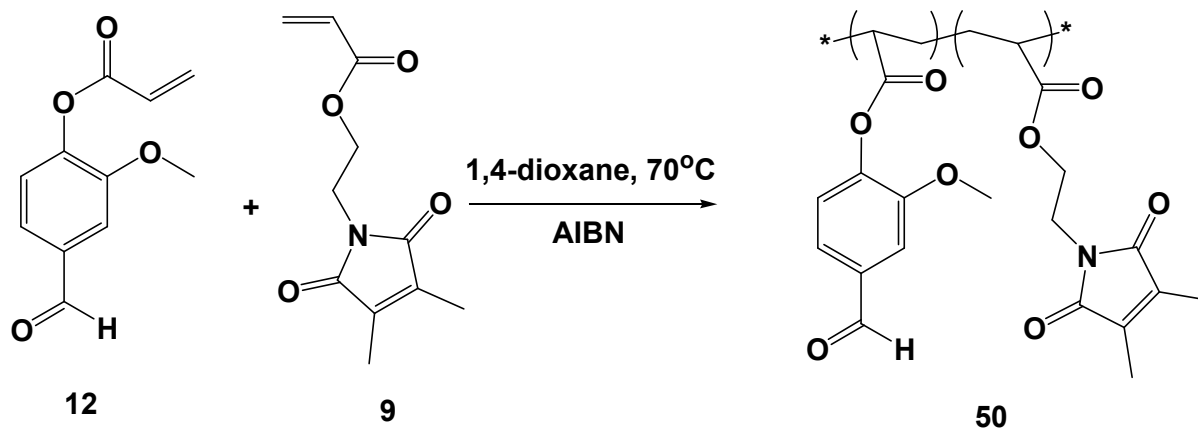


**Figure 60:** UV-vis. Spectroscopy for determination the composition of maleimide crosslinker in polymer (49).

### 3.5.5. Functionalized photo-crosslinker poly(VA-*Co*-DMIA) with 2, 5 and 10 mol% of maleimido crosslinker.

In the recent section we described Vanillin acrylate as homopolymer. In this section our interest was the preparation of new functional photo-crosslinkable polymer by random free radical polymerization as shown in **scheme 26**.



**Scheme 26:** Synthesis of functionalized photo-crosslinker poly(VA-*Co*-DMIA).

The final target was seen in the formation of functional hydrogel thin film. Therefore, the presence of aldehyde groups can play a vital role in the immobilizations of a lot of biomolecular compounds through click reaction between aldehyde and amine group, by the formation of Schiff's base (-CH=N-).

The  $^1\text{H}$ NMR was performed to determine the actual amount of DMIA in the polymer chain. Here, we used the integration (2CH<sub>3</sub>) of DMIA at 1.89-2.21ppm in a comparison with the

integration of (1H) of aldehyde group at 9.86-10.08 ppm. All calculations were in a logic case with the feeding calculation (See Figure 61).

In Figure 62 the absorption band of polymers by UV-vis.Spectroscopy showed two absorption band at 300 for  $\pi$ - $\pi^*$  (C=C) and 250 for  $\pi$ - $\pi^*$  (C=O).

The molecular weight was measured by GPC and demonstrated linear relation with the content of DMIA in the polymer chain. The other observation was remarked in the increase of  $T_g$  linearly with DMIA (Table 62).

**Table 60:** Yield, composition, molecular weight, polydispersity, and glass temperature of poly(VA-Co-DMIA).

Polymer	Yield %	Composition		Mw (g/mol) $10^4$	PD	$T_g$ °C
		DMIAAm (mol%)				
		$^1\text{HNMR}$	UV			
50-02	74	1.83	1.83	0.44	1.22	175.0
50-05	78	5.99	7.11	0.47	1.44	180.0
50-10	73	8.09	9.21	0.51	1.50	184.0

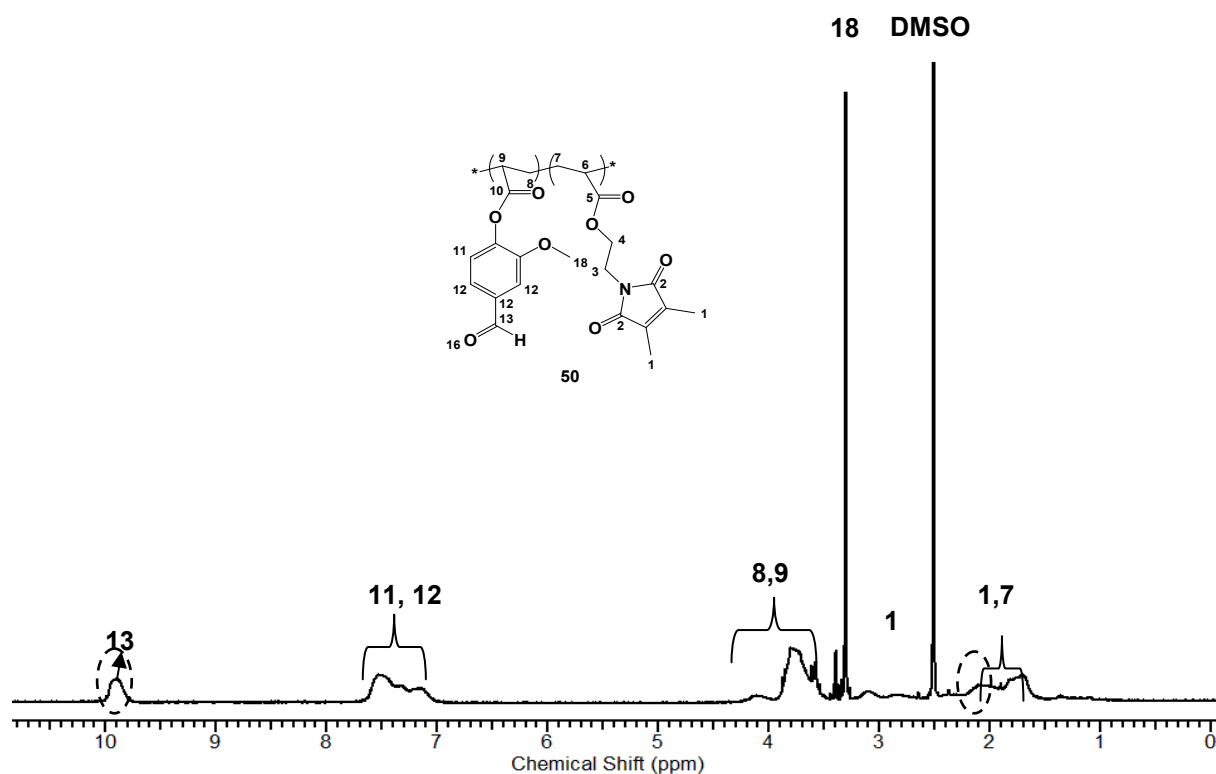


**Figure 61:**  $^1\text{H}$  NMR spectra (DMSO) of polymer 50-10.

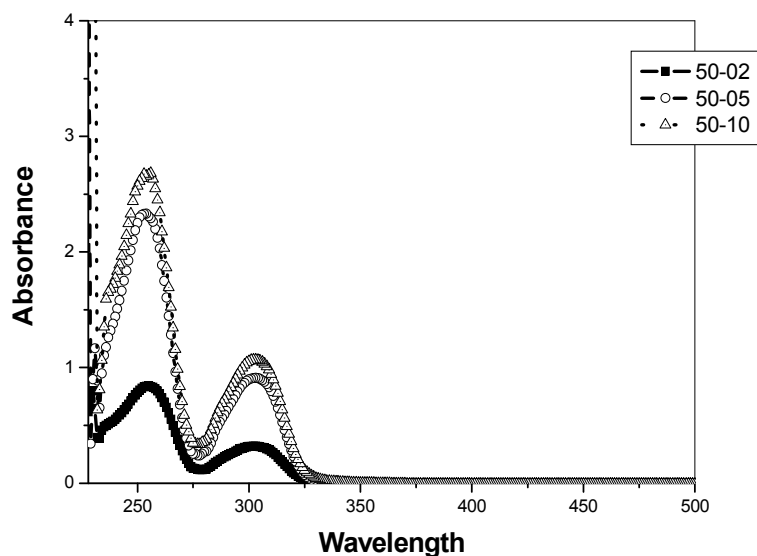
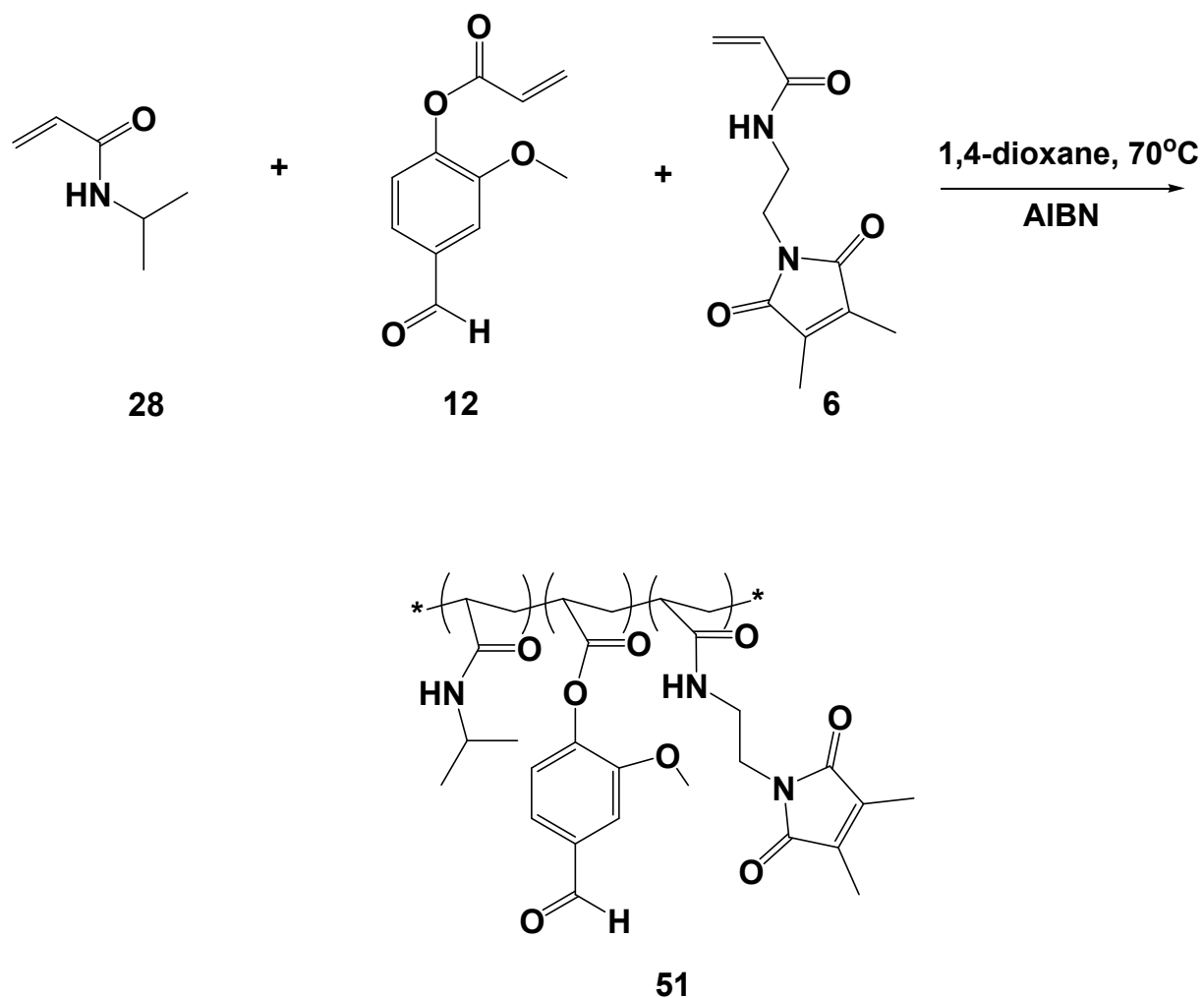


**Figure 62:** UV-vis. Spectroscopy for determination the composition of maleimide crosslinker in polymer 50.

### 3.5.6. Functionalized photo-crosslinker poly(NIPAAm-*Co*-VA-*Co*-DMIAAm) with 2, 5 and 10 mol% of maleimido-crosslinkable and 5, 10 and 15 mol% of VA respectively.

Latterly we synthesized photo-crosslinked VA polymer demonstrating the effect of hydrophobic character in the polymer main chain. Here, we synthesized a series of photo-crosslinked functional polymers in different mole ratios of DMIAAm crosslinker and VA. The effect of VA and DMIAAm on the  $T_c$  of the polymer chain and further the hydrogel will discuss in **section 4.5.7**. For this aim random free radical polymerization was achieved to get polymer 51 (scheme 27).



**Scheme 27:** Synthesis of functionalized photo-crosslinker poly(NIPAAm-Co-VA-Co-DMIAAm).

The  $^1\text{H}$ NMR was performed to estimate the actual amount of DMIAAm and VA in the polymer chain. Here we used three kind of protons integrations the integration ( $2\text{CH}_3$ ) of DMIAAm at 1.89-2.21 ppm, NIPAAm (CH) at 3.87-4.22 ppm in a comparison with the integration of (1H) of aldehyde group at 9.86-10.04 ppm. All calculations were in a logic case with the feeding calculation (See **Figure 63**).

UV.vis. Spectroscopy was used for the determination of absorption band for functional group showed  $\lambda=290\text{nm}$  for  $\pi\text{-}\pi^*$  transition of  $\text{C}=\text{C}$  of DMIAAm, while,  $\lambda_{\text{max.}} = 250\text{ nm}$  for  $\text{n-}\pi^*$  and  $\pi\text{-}\pi^*$  of  $\text{C}=\text{O}$  of aldehydic group in VA as shown in **Figure 64**.

**Table 61:** Yield, composition, molecular weight, polydispersity, glass temperature, and phase transition temperature of poly(NIPAAm-Co-VA-Co-DMIA).

Polymer	Yield %	Composition			Mw (g/mol) $10^4$	PD	T <sub>g</sub> °C	T <sub>c</sub> °C	
		DMIAAm (mol%)		UV				UV	DSC
		<sup>1</sup> HNMR DMIAAm	VA						
51-02-05	85	1.90	4.20	1.96	7.34	3.16	131.3	17.2	-
51-05-10	83	5.88	11.11	5.97	6.45	3.12	133.5	13.8	14.2
51-10-15	75	7.69	14.28	7.85	5.55	2.68	138.0	11.2	-

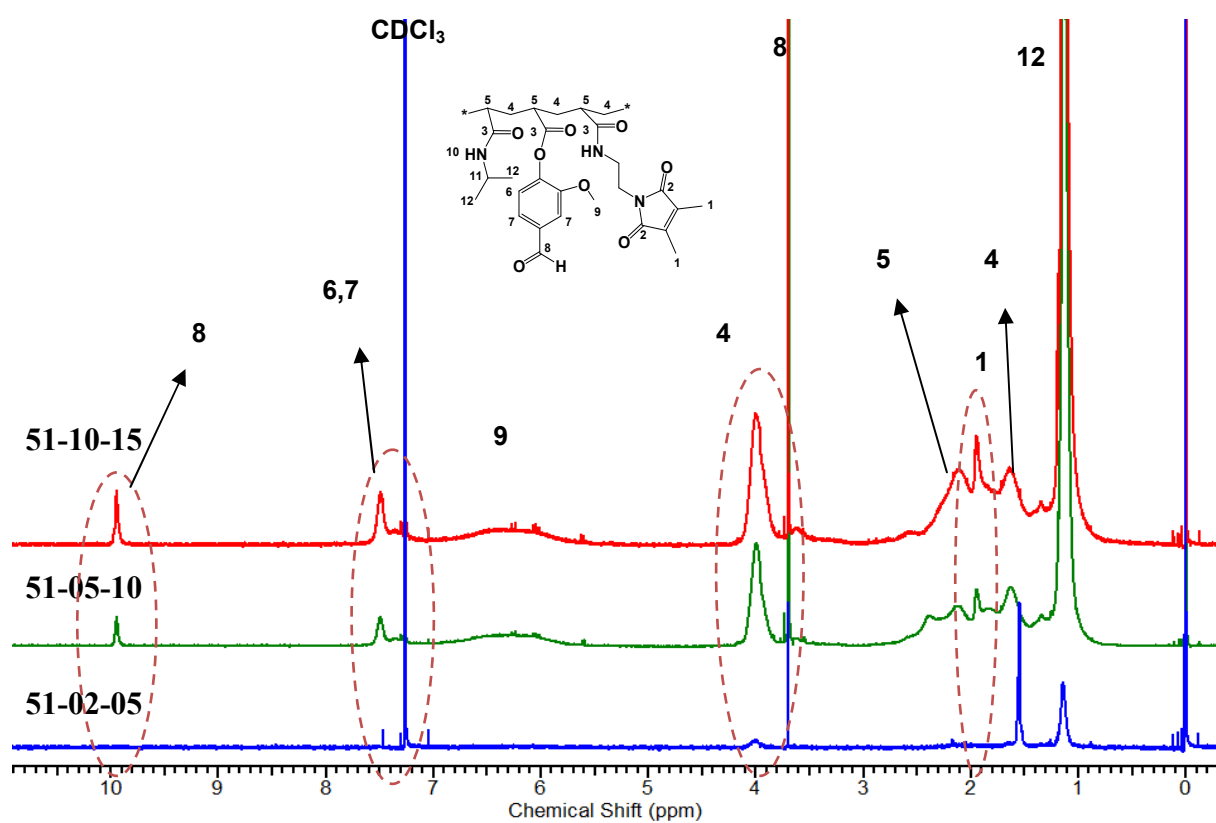
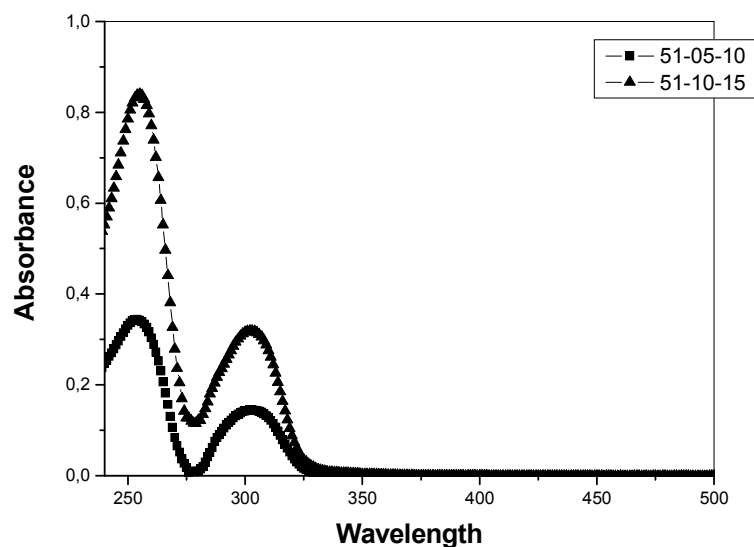
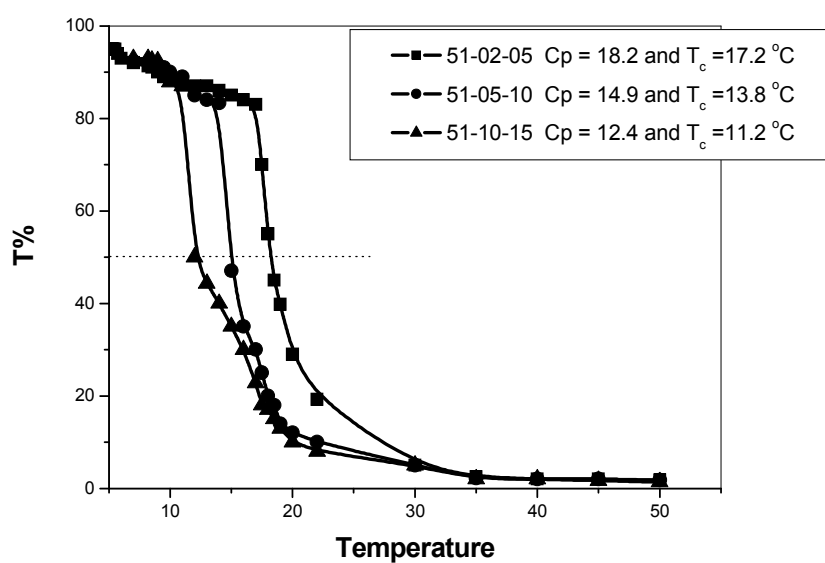


Figure 63: <sup>1</sup>H NMR spectra (CDCl<sub>3</sub>) of polymer 51.



**Figure 64:** UV-vis. Spectroscopy for determination the composition of maleimide cross-linker in polymer 51.



**Figure 65:** The change in turbidity with temperature for determination of  $T_c$  of P(NIPAAm-*Co*-VA-*Co*-DMIAAm) with 2, 5 and 10 mol% of maleimide crosslinker and 5, 10 and 15 mol% of VA respectively using UV-vis. Spectroscopy for 1wt% of polymer solution.

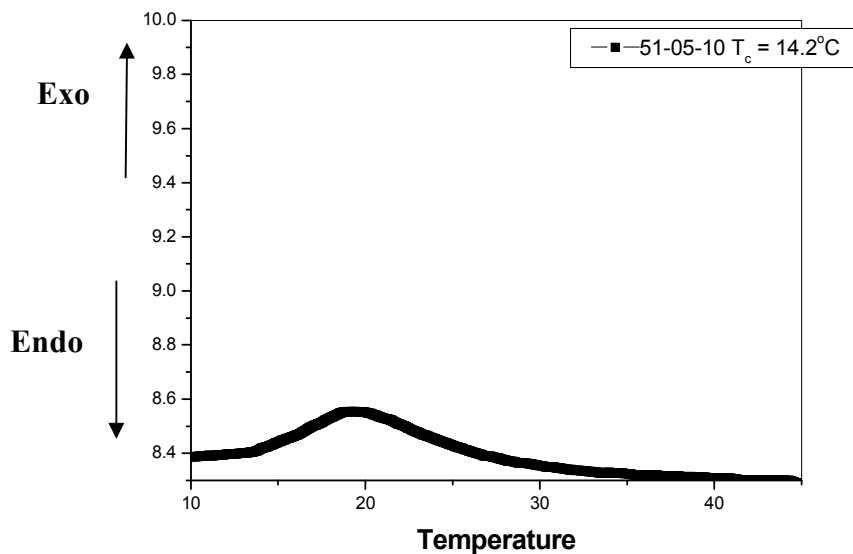
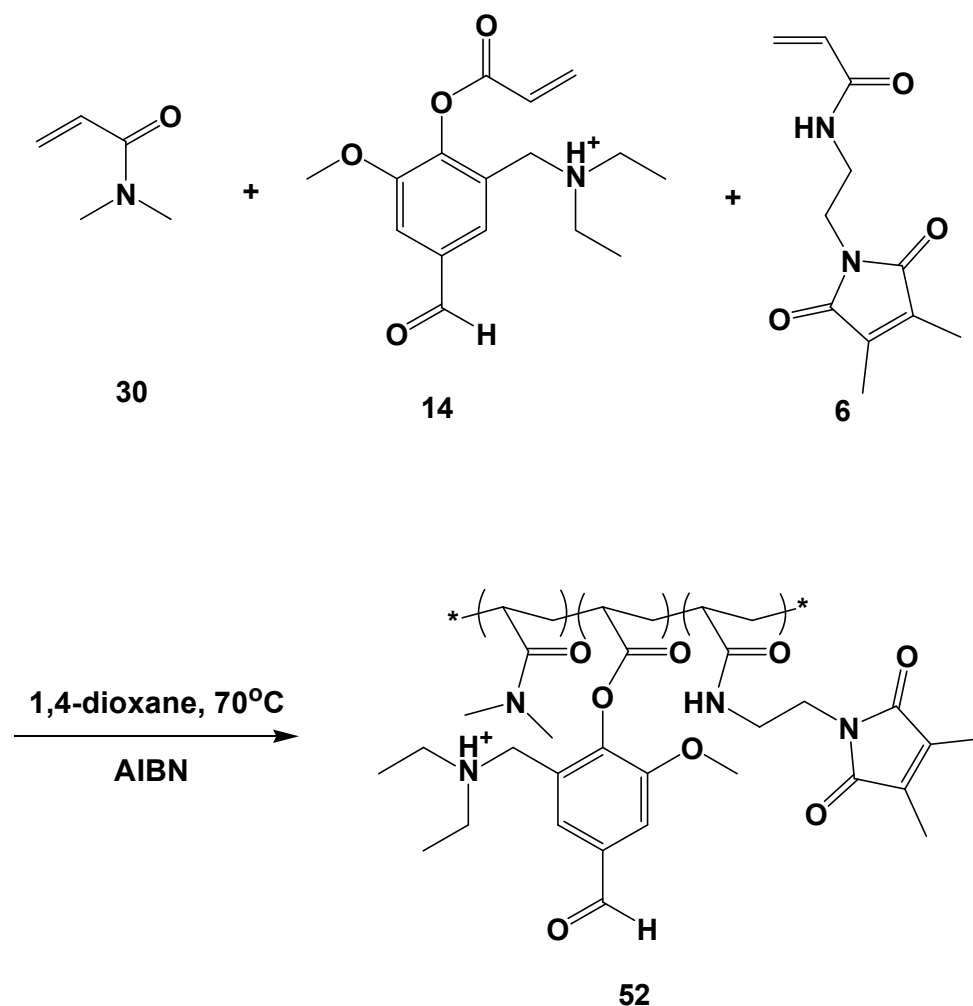


**Figure 66:** DSC of P(NIPAAm-Co-VA-Co-DMIAAm) for determination the  $T_c$ .

**3.5.7. Functionalized photo-crosslinker poly(DMAAm-Co-DEAMVA-Co-DMIAAm) with 2, 5 and 10 mol% of maleimido-crosslinker and 5, 10 and 15 mol% of DEAMVA respectively.**

The free radical polymerization of DMAAm, DEAMVA and DMIAAm were used in the preparation of polymer **52**. The presence of protonated tertiary amine in the polymer chain will achieve pH-responsive polymers, which will be used in the formation of pH-responsive hydrogel layers (see sections 4.5.7).



**Scheme 28:** Synthesis of functionalized photo-crosslinker poly(DMAAm-*Co*-DEAMVA-*Co*-DMIAAm).

$^1\text{H}$ NMR was performed to estimate the actual amount of DMIAAm and VA in the polymer chain. Here, we used three kinds of proton integrations; the integration ( $2\text{CH}_3$ ) of DMIAAm at 1.88-2.04 ppm, DMAAm ( $2\text{CH}_3$ ) at 2.74-3.26 ppm in a comparison with the integration of (1H) of aldehyde group at 9.87-10.01 ppm. All calculations were in a logic case with the feeding calculation, as shown in **Table62** and **Figure67**.

The solubility parameters illustrated the solubility of polymer in water and basic solutions. However, the solubility in acidic solution is dependent on the content of DEAMVA in the polymer chain which might be due to interaction of DEAMVA moieties producing partial soluble polymer (**Table63**).

UV.vis. Spectroscopy was used for the determination of absorption band for functional group showed  $\lambda_{\text{max}} = 300\text{-}280$  nm for  $\pi\text{-}\pi^*$  transition of C=C of DMIAAm, while  $\lambda_{\text{max}} = 250\text{-}220$  nm for  $n\text{-}\pi^*$  and  $\pi\text{-}\pi^*$  of C=O of aldehydic group in VA.

**Table 62:** Yield, composition, molecular weight, polydispersity, and glass temperature of poly(DMAAm-*Co*-DEAMVA-*Co*-DMIAAm).

Polymer	Yield %	Composition			Mw (g/mol) 10 <sup>4</sup>	PD	T <sub>g</sub> °C
		DMIAAm (mol%)					
		<sup>1</sup> HNMR		UV			
DMIAAm	DEAMVA	DMIAAm					
52-02-05	90	4.38	1.46	4.93	2.07	1.91	135.0
52-05-10	65	7.45	4.05	8.54	1.98	2.16	143.0
52-10-15	45	7.75	4.85	8.33	1.41	2.38	140.0

**Table 63:** Solubility parameters of polymer 56 in different pH; (+) completely soluble (±) partially soluble.

pH	pH2	pH5	pH7	pH8	pH11.2
52-02-05	+	+	+	+	+
52-05-10	±	±	+	+	+
52-10-15	±	±	+	+	+

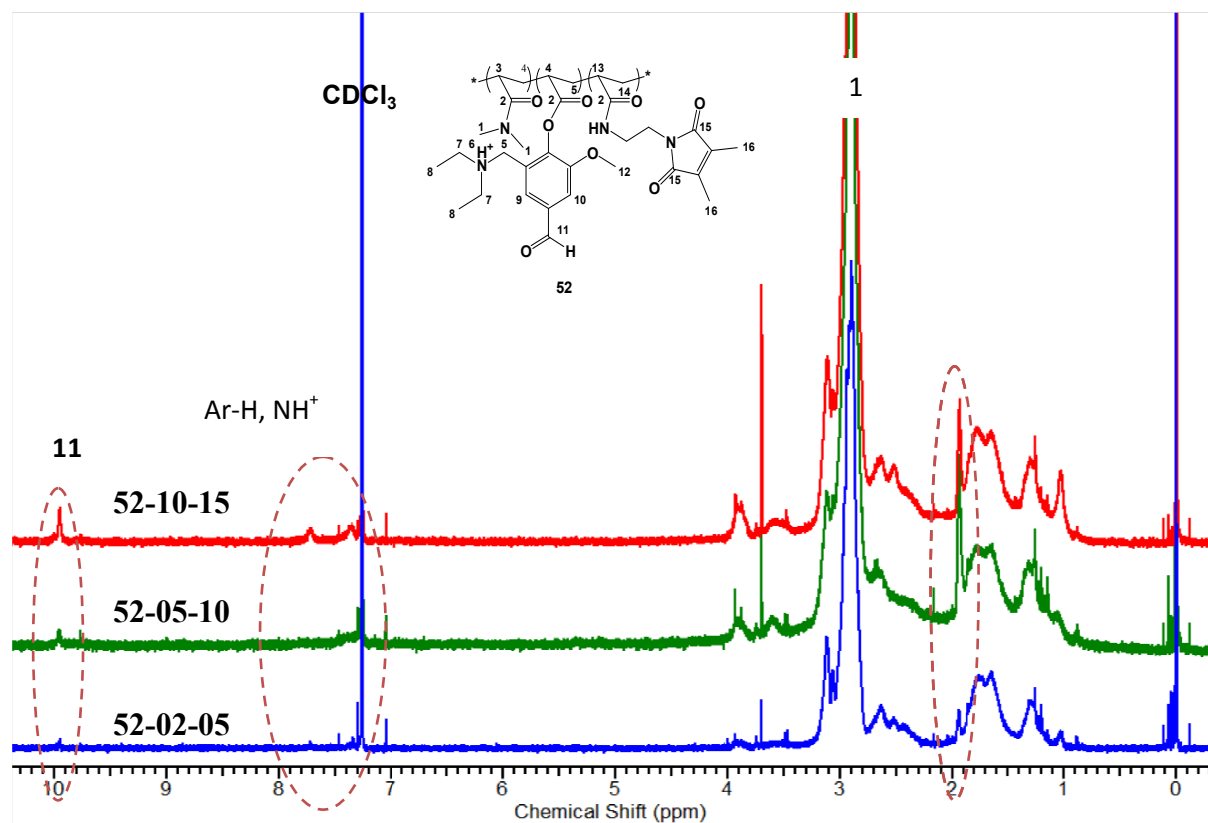
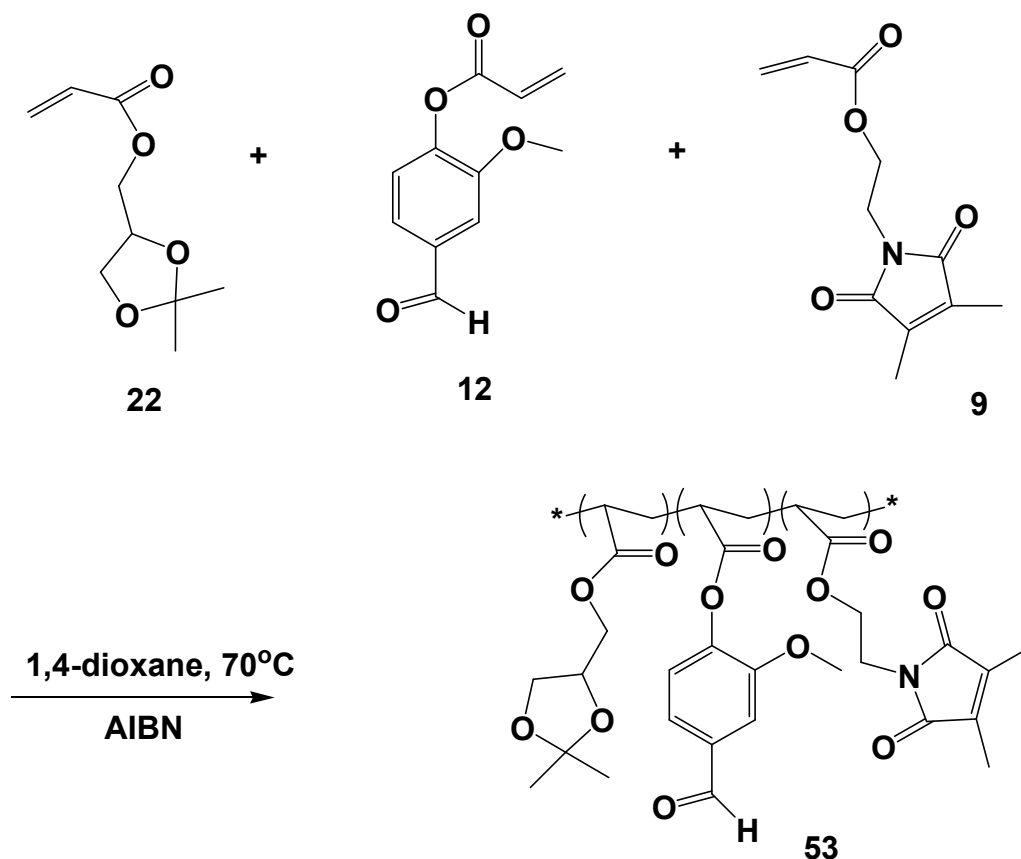


**Figure 67:** <sup>1</sup>H NMR spectra (CDCl<sub>3</sub>) of polymer 52.

**3.5.8. Functionalized photo-crosslinker poly(SKA-Co-VA-Co-DMIA) with 5 and 10 mol% of maleimido crosslinkable, 10 and 15 mol% of VA respectively.**



**Scheme 29:** Synthesis of photo-crosslinker poly(SKA-Co-VA-Co-DMIA).

The polymers were synthesized by random free radical polymerization of SKA, VA and DMIA in different mole ratios of VA and DMIA in the polymer chain. The aim was to introduce further functional groups into PSKA. The swelling properties of such polymers will be discussed in (section 4.5.8).

The  $^1\text{H}$ NMR was performed to estimate the actual amount of DMIA and VA in the polymer chain. Here, we used three kinds of protons integrations; the integration for (2CH<sub>3</sub>) of DMIA at 1.88-2.06 ppm, SKA (2CH<sub>3</sub>) at 1.22-1.47 ppm in a comparison with the integration of (1H) of aldehyde group at 9.85-9.99 ppm. All calculations were in a logic case with the feeding calculation as seen in **Table 64** and **Figure 68**.

The solubility parameters demonstrated formation of partially soluble polymers in basic solutions (**Table 65**).

UV-vis. Spectroscopy was used for the determination of absorption bands for functional group remarked at  $\lambda_{\max} = 300$  nm for  $\pi\text{-}\pi^*$  transition of C=C of DMIAAm, while  $\lambda_{\max} = 250$  nm for  $n\text{-}\pi^*$  and  $\pi\text{-}\pi^*$  of C=O of aldehydic group in VA as shown in **Figure 69**.

**Table 64:** Yield, Composition, molecular weight, polydispersity, and glass temperature of poly(SKA-Co-VA-Co-DMIA).

Polymer	Yield %	Composition			Mw (g/mol) $10^4$	PD	T <sub>g</sub> °C
		DMIAAm (mol%)					
		<sup>1</sup> HNMR		UV			
DMIA	VA	DMIA					
53-05-10	50	4.5	9.0	4.73	1.04	2.3	136.5
53-7.5-15	46	7.3	12.3	8.12	1.13	2.6	138.4

**Table 65:** Solubility parameters of polymer 57 in different pH; (-) insoluble (±) partially soluble.

pH	pH2	pH5	pH7	pH8	pH11.2
53-05-10	–	–	–	–	±
53-7.5-15	–	–	–	–	±

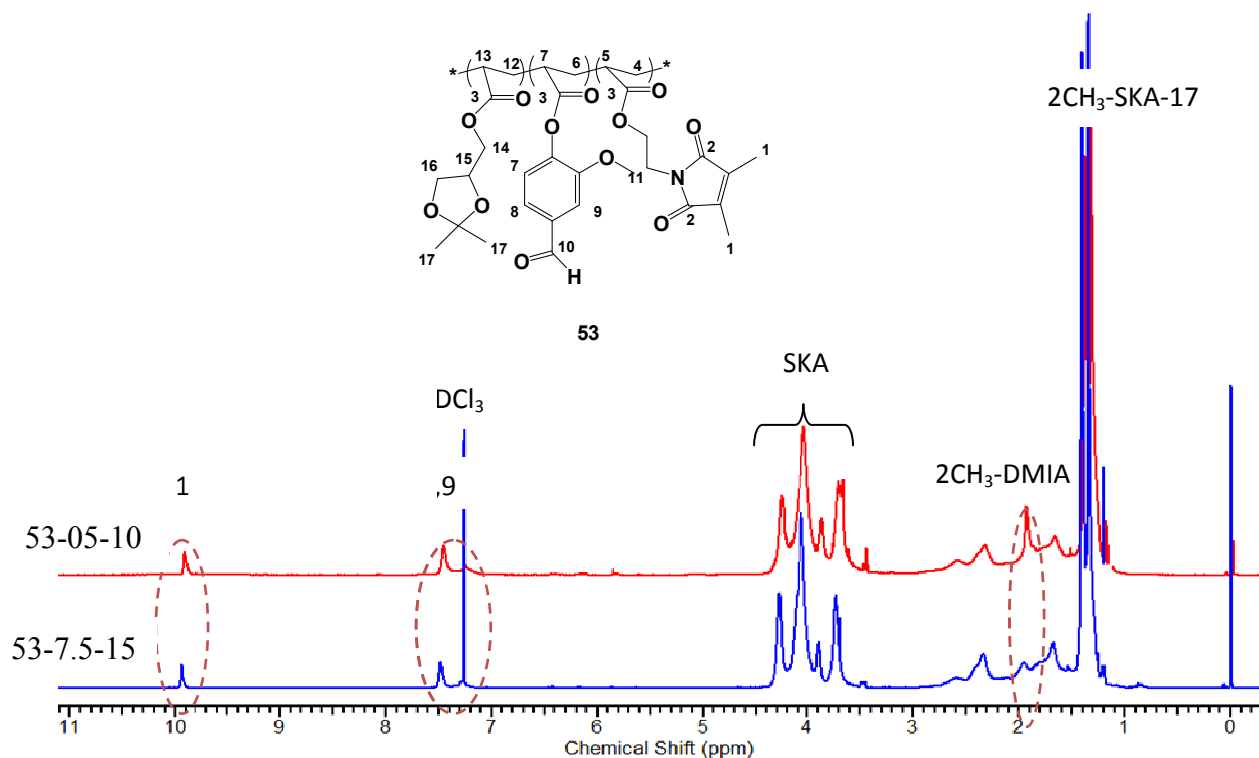


**Figure 68:** <sup>1</sup>H NMR spectra (CDCl<sub>3</sub>) of polymer 53.

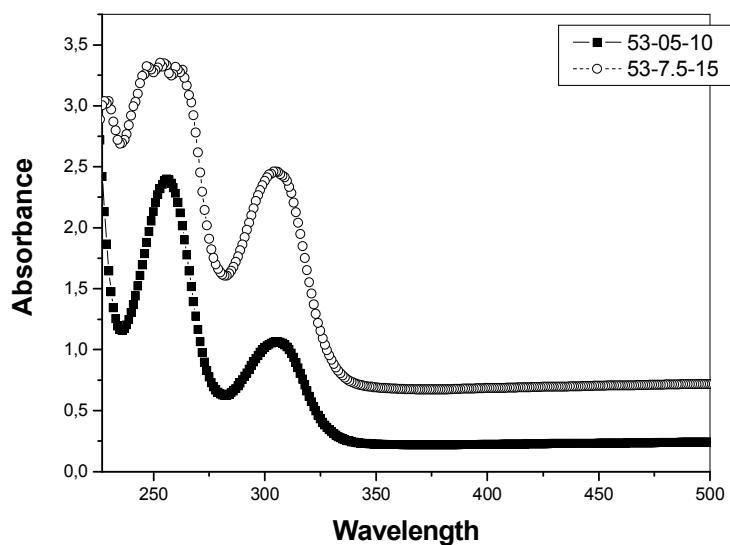
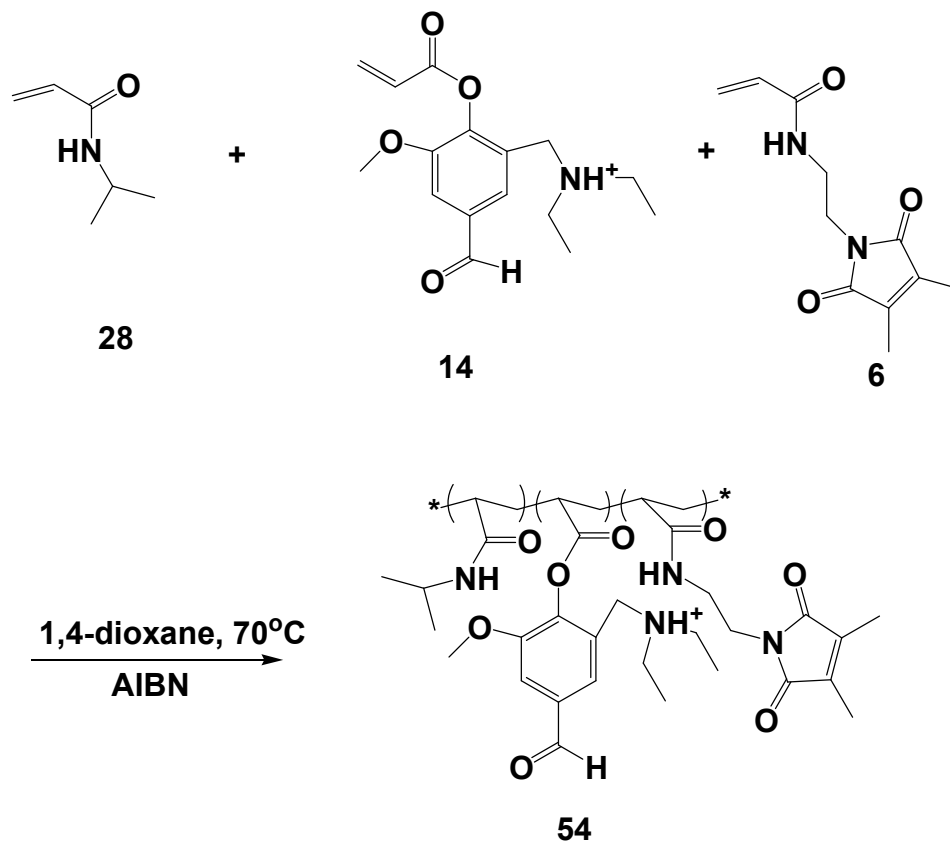


**Figure 69:** UV-Vis. Spectroscopy for determination the composition of maleimide-crosslinker in polymer **53**.

**3.5.9. Functionalized photo-crosslinker Poly(NIPAAm-*Co*-DMEAVA-*Co*-DMIAAm) with 5, 7.5 and 10 mol% of maleimido crosslinkable and 10, 15 and 20 mol% of DEMA VA.**



**Scheme 30:** Synthesis of photo-crosslinker Poly(NIPAAm-*Co*-DMEAVA-*Co*-DMIAAm).

The free radical polymerization of NIPAAm and DEAMVA with DMIAAm was achieved to synthesize dual responsive polymers in temperature and pH. Three different mole ratios of DEAMVA and DMIAAm were used to demonstrate different features. The  $T_c$  was estimated for all polymers in different pH solution.

The  $^1\text{H NMR}$  was performed to estimate the actual amounts of DMIAAm and DEAMVA in the polymer chain. The integration ( $2\text{CH}_3$ ) of NIPAAm at = 0.76-1.30 ppm, DMIAAm ( $2\text{CH}_3$ ) at 1.89-2.02 ppm in a comparison with the integration of (1H) of aldehyde group at 9.79-10.10 ppm. All calculations were in a logic case with the feeding calculation as shown in **Table 66** and **Figure 70**.

The solubility parameters illustrated the solubility of polymers at all pH values at room temperature (**Table 67**). UV-vis. Spectroscopy was used for the determination of absorption band for functional group at  $\lambda_{\text{max}} = 300 \text{ nm}$  for  $\pi\text{-}\pi^*$  transition of  $\text{C}=\text{C}$  of DMIAAm, while  $\lambda_{\text{max}} = 246 \text{ nm}$  for  $n\text{-}\pi^*$  and  $\pi\text{-}\pi^*$  of  $\text{C}=\text{O}$  of aldehydic group in VA.

To demonstrate the effect of DEAMVA content and pH on the  $T_c$ , polymers were prepared in different pH buffer solution as pH2, pH7 and pH11.2. UV-vis. Spectroscopy was used for turbid metric analysis to estimate the  $T_c$  as follow;

- ❖  $T_c$  demonstrated an increase as the DEMAVA increased in the polymer chain (**Table66**). This occurred for polymers in pH2 and pH7. This can be interpreted as increase of the hydrophilicity of the polymers with increasing DEAMVA content (increased amount of charges) (**Table 66** and **Figure 71**).

- ❖ The last feature, at pH11 the polymer solution showed no turbidity from  $10^\circ\text{C}$  to  $80^\circ\text{C}$ .

**Table 66:** Yield, composition, molecular weight, polydispersity, and glass temperature of poly(NIPAAm-*Co*-DEAMVA-*Co*-DMIAAm).

Polymer	Yield %	Composition DMIAAm (mol%)			Mw (g/mol) $10^4$	PD	$T_g$ °C
		$^1\text{H NMR}$		UV			
		DMIAAm	DEAMVA	DMIAAm			
<b>54-05-10</b>	60	4.30	3.00	5.13	2.29	1.66	137.5
<b>54-7.5-15</b>	57	5.50	3.77	5.93	1.92	1.55	145.7
<b>54-10-20</b>	58	7.40	6.54	8.20	1.78	1.45	155.3

**Table Continue 66:** Transition temperature for polymer 56 at pH2 and pH7.

T <sub>c</sub> °C	
pH2	pH7
33.1	36.0
37.7	40.0
43.0	45.0

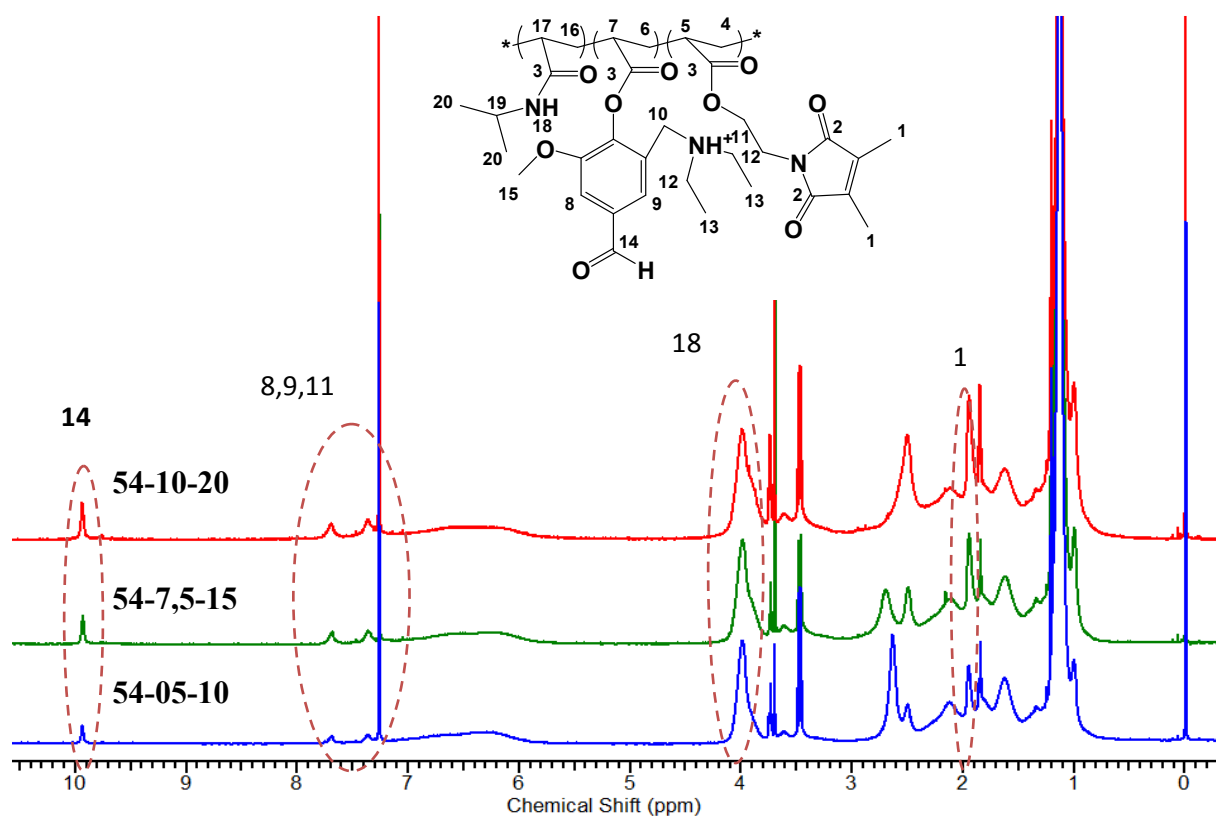
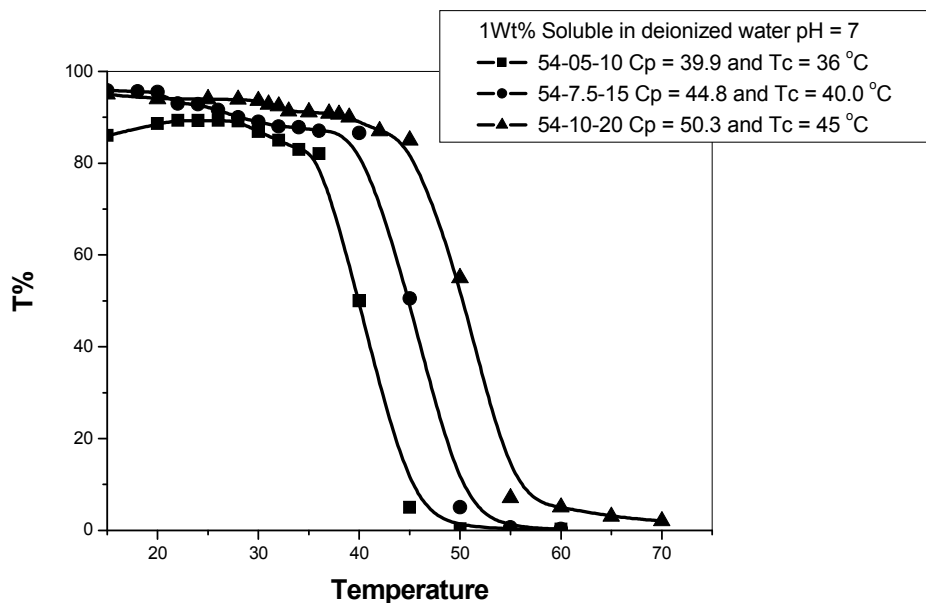


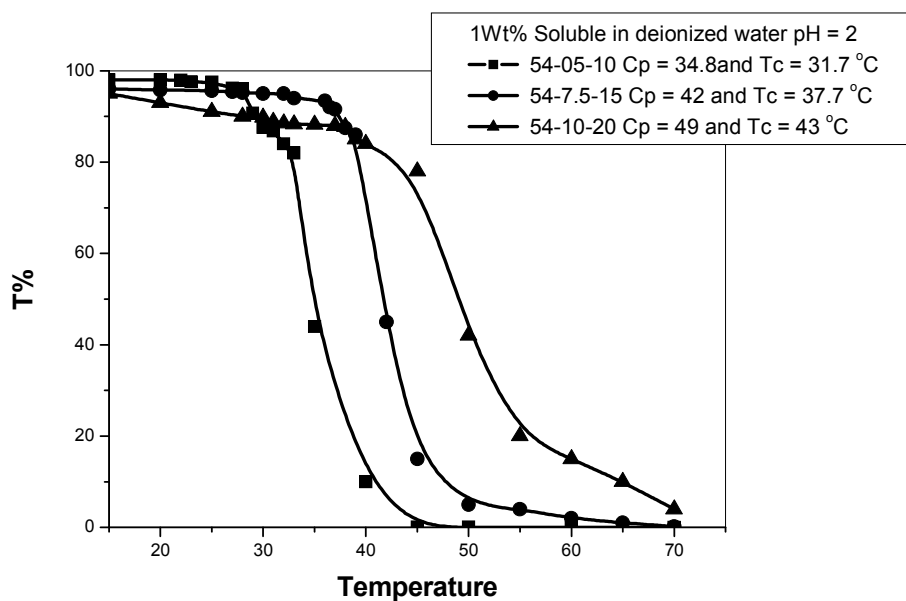
Figure 70: <sup>1</sup>H NMR spectra (CDCl<sub>3</sub>) of polymer 54.

Table 67: Solubility parameters of polymer 54 in different pH; (+) completely soluble.

pH	pH2	pH5	pH7	pH8	pH11.2
54-05-10	+	+	+	+	+
54-7.5-15	+	+	+	+	+
54-10-20	+	+	+	+	+



**Figure 71:** The change in turbidity with temperature for determination the  $T_c$  of P (NIPAAm-*Co*-DEMAVA-*Co*-DMIAAm) with different mol% of DEAMVA and DMIAAm using UV-vis. Spectroscopy for 1wt% of polymer solution in pH7.

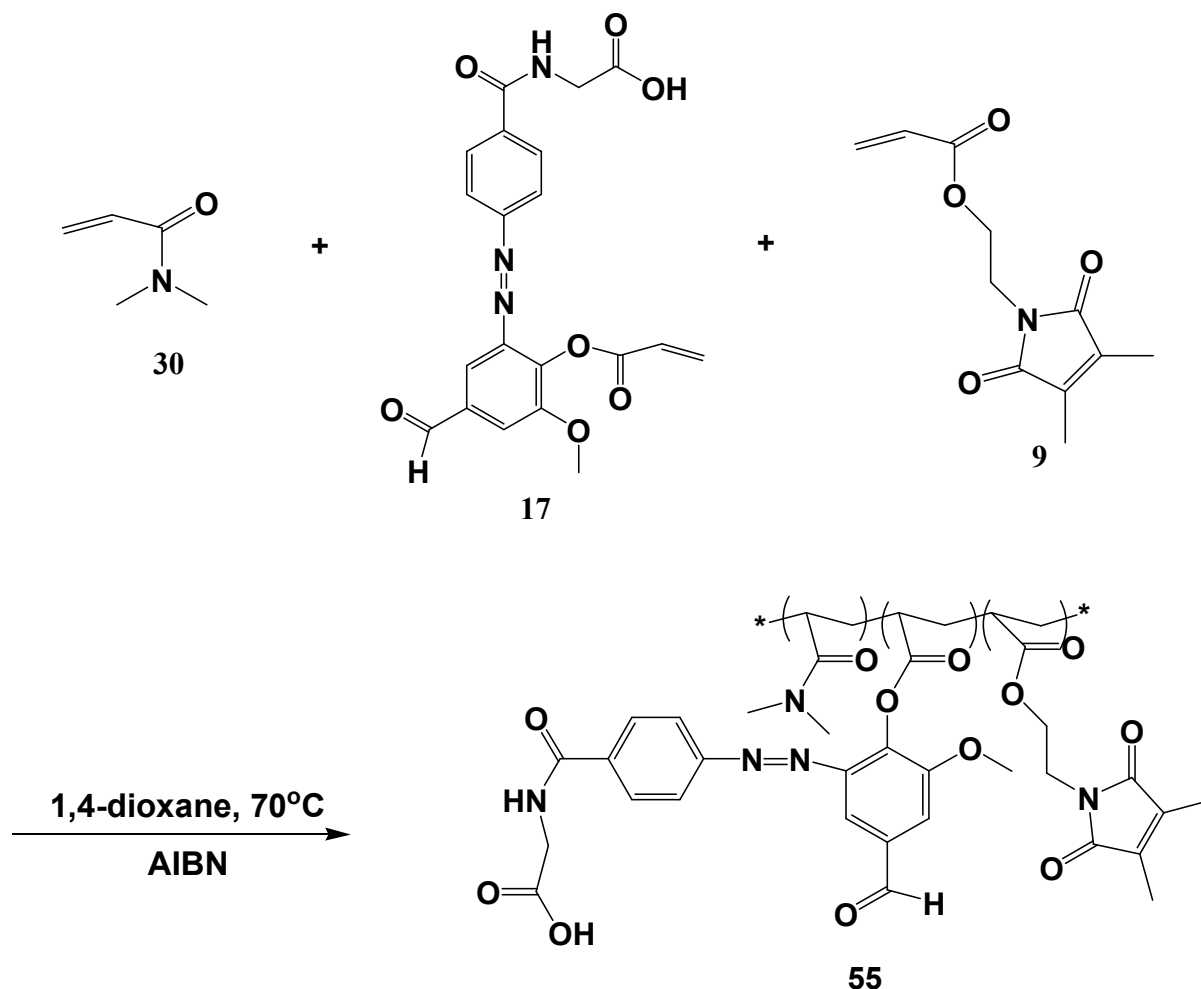


**Figure 72:** The change in turbidity with temperature for determination the  $T_c$  of P (NIPAAm-*Co*-DEMAVA-*Co*-DMIAAm) with different mol% of DEAMVA and DMIAAm, using UV-vis. Spectroscopy for 1wt% of polymer solution in pH2.

### 3.5.10. Azo-dye-functionalized photo-crosslinker polymers.

Azo-dyes were randomly incorporated in the polymer backbone by several working-groups by copolymerization of the dye-functionalized monomer with different monomers<sup>(288)</sup> like NIPAAm,<sup>(289-292,294,296-299)</sup> DMAAm,<sup>(290,293,300)</sup> DMAEMA<sup>(295,301)</sup> and OEGMA.<sup>(290,302,303)</sup> The azobenzene copolymers were studied as light and thermo-sensitive materials. Additionally the effect of the pH value to the LCST<sup>(301)</sup> as well as the complexation of cyclodextrin<sup>(300)</sup> was investigated. Suzuki and Tanaka<sup>(304)</sup> reported about a phase transition of copper chlorophyllin PNIPAAm gels induced by visible light and by temperature, which can be used as switches or as light sensors.

#### 3.5.10.1. Azo-dye-functionalized photo-crosslinker Poly(DMAAm-*Co*-AHVA-*Co*-DMIA) with 5 and 10 mol% of maleimido crosslinker, and 5 and 10 mol% of AHVA.



**Scheme 31:** Synthesis of photo-crosslinker Poly(DMAAm-*Co*-AHVA-*Co*-DMIA).

Two azopolymers were synthesized by free radical polymerization of DMAAm, AHVA and DMIA with different mole ratios of AHVA and DMIA as clear in **Table 68**.

The <sup>1</sup>HNMR showed the actual amounts of DMIA and AHVA in the polymer chain. Also as usual we used the integration comparison for the clearest protons for each monomer. Here we used three kind of integrations; the integration (2CH<sub>3</sub>) of DMAAm at 2.70-3.25 ppm. DMIA, (2CH<sub>2</sub>) at 3.78-4.05 ppm in comparison with the integration of (2H) of aldehyde and carboxyl groups at 9.84-10.09 ppm. All calculations were in a logic case with the feeding calculation, **(Table 68 and Figure 73)**.

The solubility parameters showed the solubility of polymers in basic solutions at room temperature and a partial solubility in water by heating to 70°C.

UV-vis. Spectroscopy was used for the determination of absorption bands for functional groups at pH7 and pH 11.2: At **pH7** the presence of λ=350-300 nm for π-π\* transition of C=C of DMIAAm and azo group -N=N- while, λ = 246 nm for n-π\* and π-π\* of C=O of aldehydic group in AHVA while at pH11.2 an extra absorption band at 500 nm attributed to the conjugation system suggested electrons delocalization for AHVA in basic media as shown in **Figure 74**.

**Table 68:** Yield, composition, molecular weight, Polydispersity, and glass temperature of poly(DMAAm-Co-AHVA-Co-DMIA).

Polymer	Yield %	Composition			Mw (g/mol) 10 <sup>4</sup>	PD	T <sub>g</sub> °C
		DMIAAm (mol%)		UV DMIA			
		<sup>1</sup> HNMR DMIA	AHVA				
<b>55-05-05</b>	65	3.80	3.96	3.96	4.31	2.47	145.0
<b>55-10-10</b>	53	7.64	9.43	7.94	0.51	1.97	154.5

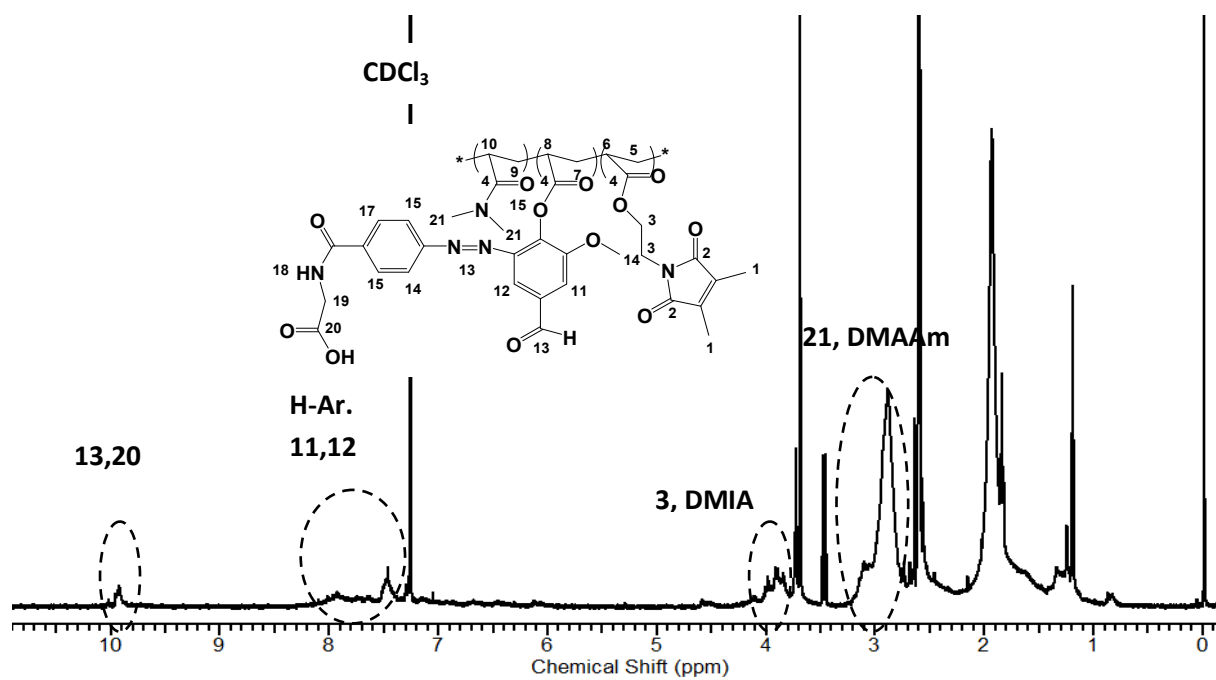


Figure 73:  $^1\text{H}$  NMR spectra ( $\text{CDCl}_3$ ) of polymer **55**.

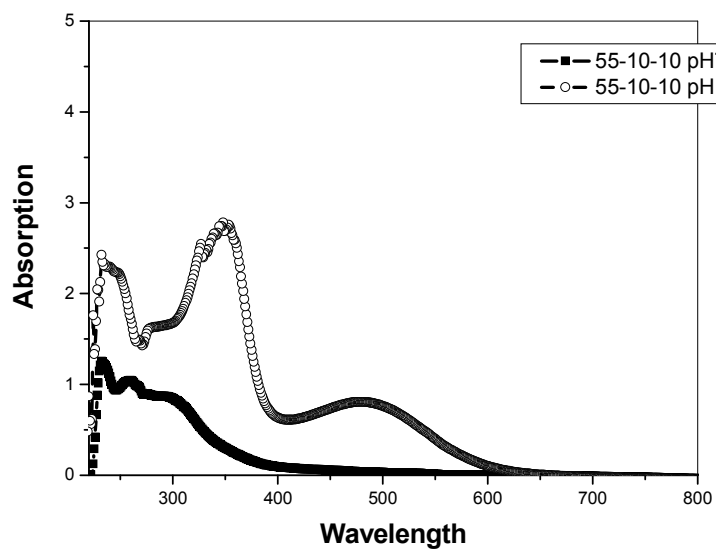
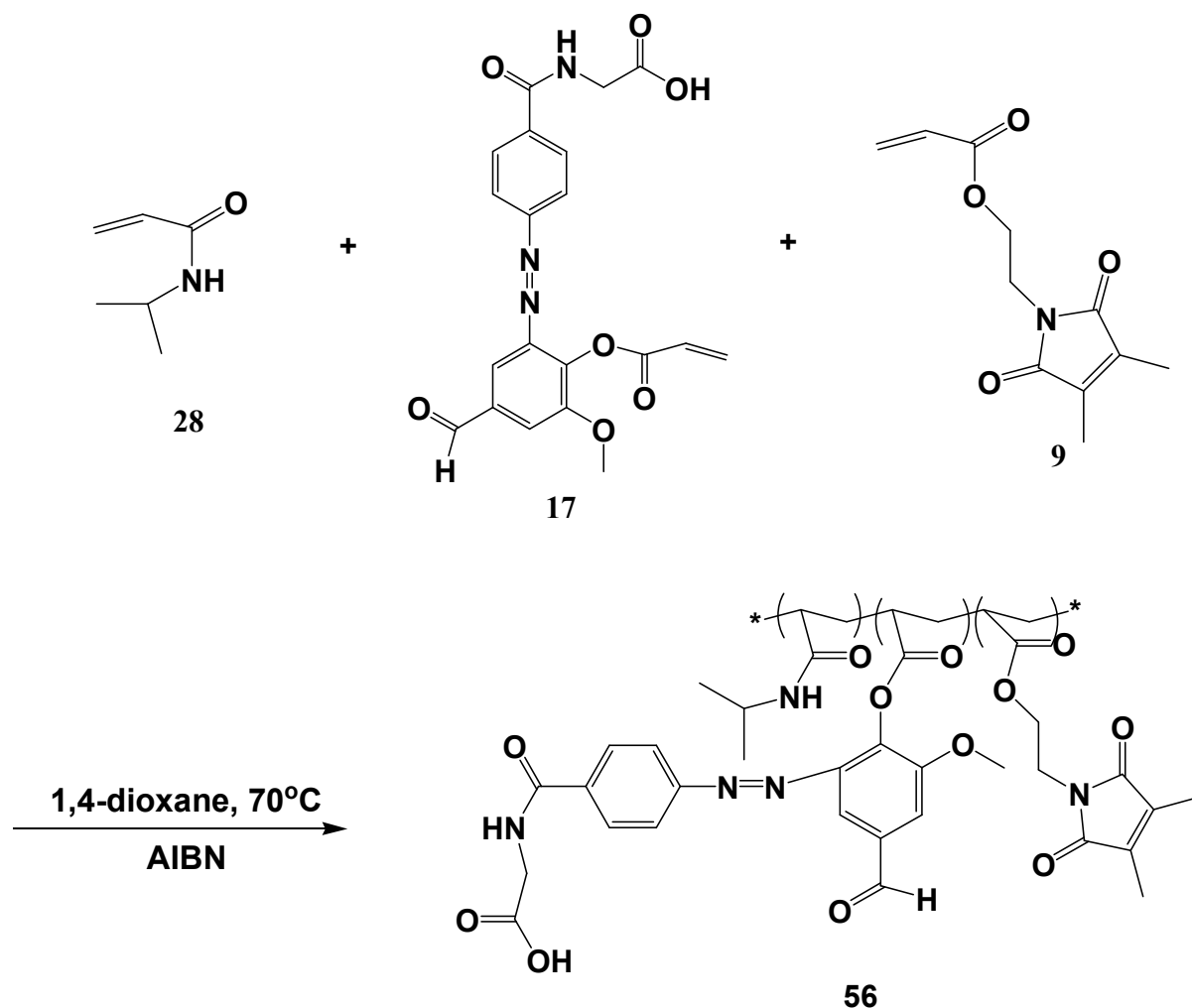


Figure 74: UV-vis. Spectroscopy for polymer **55** in pH7 and pH11.2.

### 3.5.10.2. Azo-dye-functionalized photo-crosslinker Poly(NIPAAm-*Co*-AHVA-*Co*-DMIA) with 10 mol% of maleimido crosslinker and 10 mol% of AHVA.



**Scheme 32:** Synthesis of photo-crosslinker Poly(NIPAAm-*Co*-AHVA-*Co*-DMIA).

In this study free radical polymerization of NIPAAm, AHVA and DMIA were used in the formation of Poly(NIPAAm-*Co*-AHVA-*Co*-DMIA) the aim was to demonstrate the formation of polymers with dual responsive for temperature and pH. The polymer should show LCST behavior, but the presence of AHVA with multi functional groups (azo, carboxyl and also aldehyde) are responsible for the change of this behavior by pH changes. In **section 4.5.9** we will discuss the formation of hydrogel layer and the effect of pH on the transition temperature. The  $^1\text{H NMR}$  was achieved to estimate the actual amounts of DMIA and AHVA in the polymer chain. Here we used three kind of integrations. The integration ( $2\text{CH}_3$ ) of NIPAAm at 0.77-1.13 ppm, DMIA ( $2\text{CH}_3$ ) at 1.78-1.99 ppm in comparison with the integration of ( $2\text{H}$ ) of aldehyde and carboxyl groups at 9.25-10.19 ppm.

The temperature dependent solubility was investigated by UV-vis. Spectroscopy as a function of pH. The investigation has been done at pH2, pH7 and pH11.2.

At pH2 and pH7 no sensitivities were found. However, at pH11.2 an UCST type behavior was found. This might be attributed to the interaction of charged carboxyl groups with the uncharged amide groups. At higher temperatures this interactions were disturbed leading to higher solubility (**Figure 76**).

**Table 69:** Yield, composition, molecular weight, polydispersity, glass temperature and transition temperature of poly(NIPAAm-*Co*-AHVA-*Co*-DMIA).

Polymer	Yield %	Composition			Mw (g/mol) 10 <sup>4</sup>	PD	T <sub>g</sub> °C	T <sub>c</sub> °C
		DMIAAm (mol%)						
		<sup>1</sup> HNMR DMIA	AHVA	UV DMIA				
56-10-20	40	4.1	18.4	4.7	1.12	2.3	162.0	30

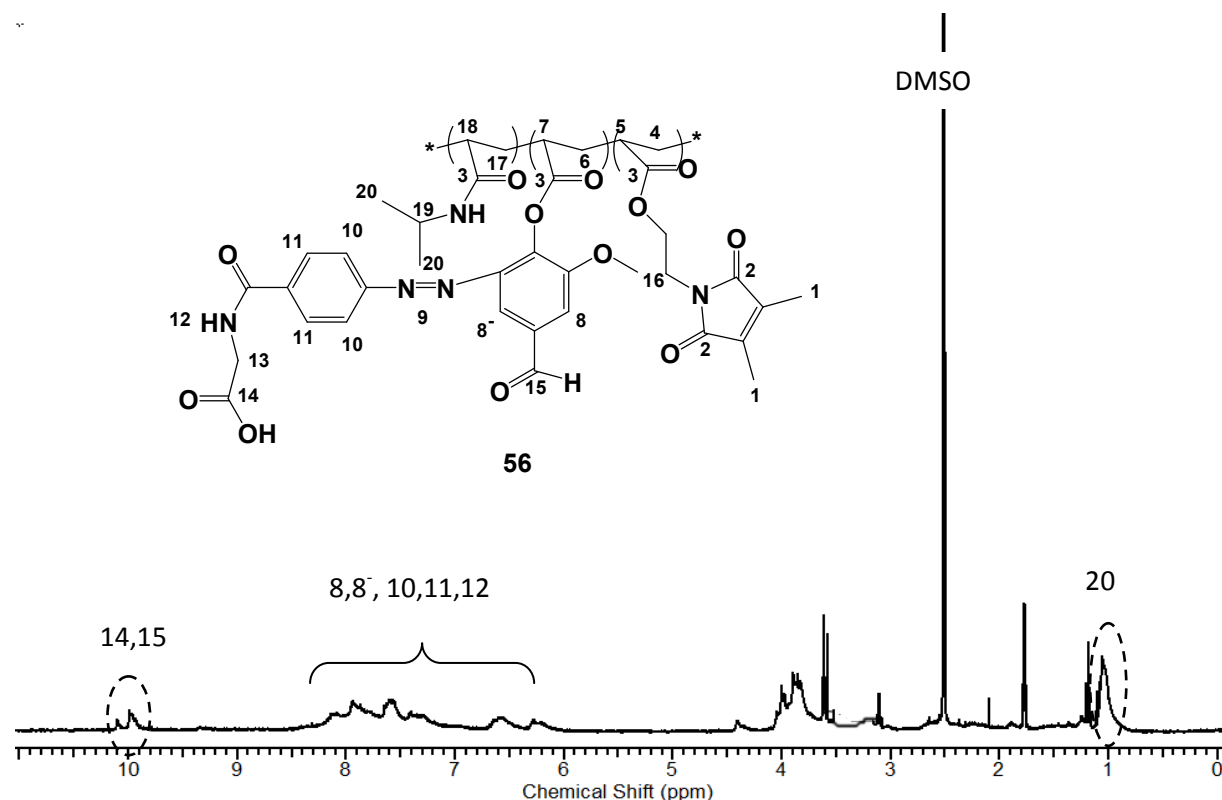


**Figure 75:** <sup>1</sup>H NMR (DMSO) of polymer 56.

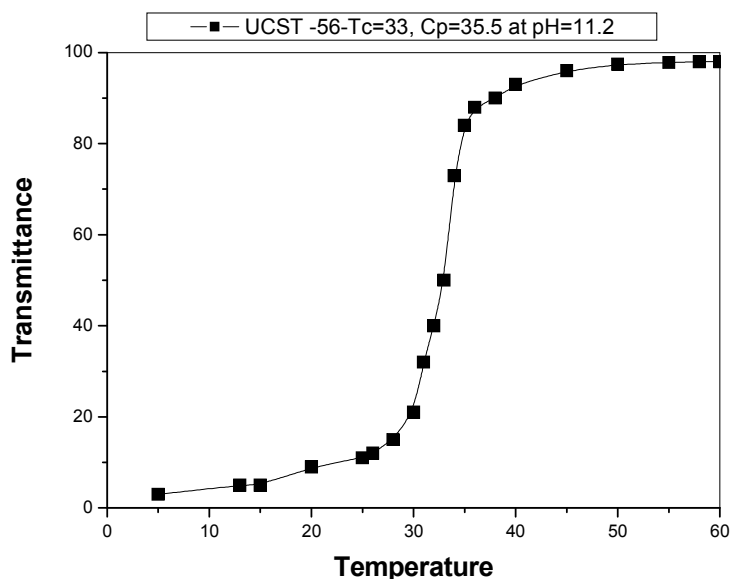
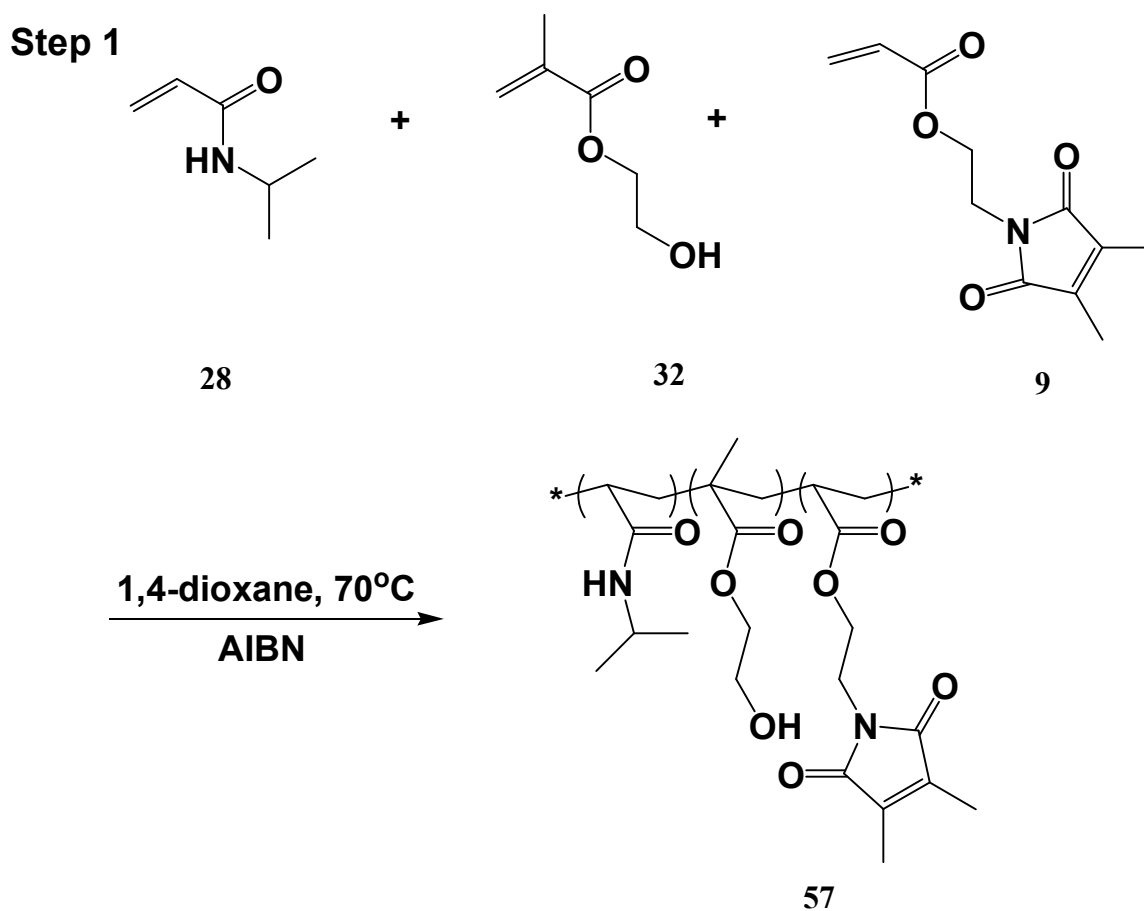


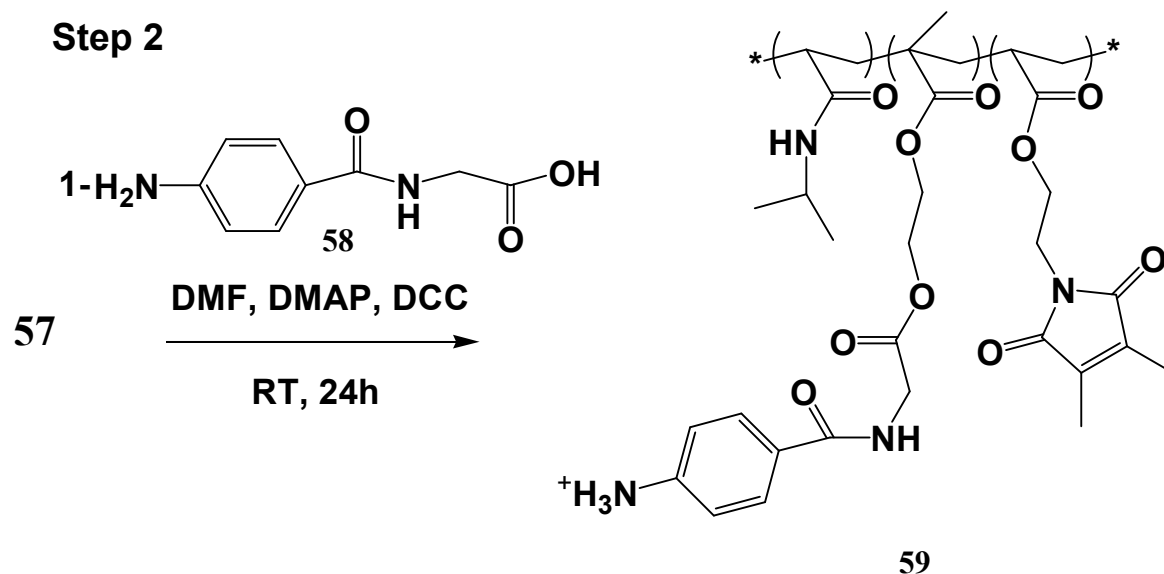
**Figure 76:** The change in turbidity with temperature for determination the  $T_c$  of Poly(NIPAAm-Co-AHVA-Co-DMIA) using UV-vis. Spectroscopy for 1wt% of polymer solution in pH 11.2.

### 3.5.11. Functionalized photo-crosslinker poly(NIPAAm-Co-HEMA-Co-DMIAAm) grafted 4-aminohippuric acid (PAH).

Recently we discussed the effect of HEMA in the copolymerization with NIPAAm demonstrating higher values of  $T_c$  due to the hydrophilic effect (**section 3.4.3.2**). Furthermore, we illustrated the effect of HEMA as photo-crosslinkable polymer in **section 3.5.3**. Here we take the advantages of PHEMA and copolymers in the multitude of biomaterial applications, including contact lenses<sup>(267)</sup>, artificial corneas<sup>(268)</sup>, potential substrate for artificial skin<sup>(269)</sup> and in drug delivery systems<sup>(271,272)</sup> to incorporate it in to NIPAAm and DMIA in order to prepare dual responsive photo-crosslinked polymers. The hydroxyl group of HEMA will be used in the formation of functionalized grafted polymer via esterification. In the recent studies J. Zhang et al. have been synthesized thermo-responsive P(NIPAAm-Co-HEMA)/cellulose hydrogel via “click chemistry”<sup>(305)</sup>. N. Ashok Kumar et al. demonstrated the preparation of nanotubes based on the functionalized PHEMA by chemical grafting HEMA monomer followed by free radical polymerization<sup>(306)</sup>. Young Gwang Ko et al. grafted copolymers of HEMA and NIPAAm, onto tissue culture polystyrene by electron beam irradiation<sup>(307)</sup>. In the present study we prepared poly(NIPAAm-Co-HEMA-Co-DMIAAm) grafted 4-aminohippuric acid in two steps as shown in **scheme 33**. The first step involved the free radical polymerization of NIPAAm, HEMA and DMIA, followed by step 2 including grafting via

esterification of 4-aminohippuric acid. 4-aminohippuric acid or (PAH) was selected due to its biological activity. It is involved in sulfate transport in human neutrophils<sup>(308)</sup>. Its sodium salt is used as a diagnostic aid to measure effective renal<sup>(309)</sup>. Of note, the clearance of PAH is reflective only of RPF to portions of the kidney that deal with urine formation, and thus underestimates actual RPF by about 10 %.)<sup>(310)</sup> Moreover, the preparation of responsive photo-crosslinked polymer for the formation of hydrogel thin film as will be discussed in section 3.6.14.





**Scheme 33:** Synthesis of poly(NIPAAm-*Co*-HEMA-*Co*-DMIAAm)-*g*-4-aminohippuric acid (HA).

**Step 1:** The  $^1\text{H}$ NMR was investigated to determine the actual amounts of DMIA and HEMA in the polymer chain. The integration ( $2\text{CH}_3$ ) of HEMA 4.2-4.30 ppm, DMIA ( $2\text{CH}_3$ ) at 1.92-2.01. As illustrated in **Table 70** and **Figure 77**.

UV-vis. Spectroscopy was used for the determination of absorption band for functional group. The presence of  $\lambda=340\text{-}300$  nm for  $\pi\text{-}\pi^*$  transition of C=C of DMIA was observed.

For the estimation of  $T_c$  of aqueous polymer solution we used both technique DSC and UV-vis. Spectroscopy, giving  $28^\circ\text{C}$  and  $26.5^\circ\text{C}$  respectively (**Figures 78 and 79**).

**Step 2:** The  $^1\text{H}$ NMR spectra was achieved to estimate the actual amounts of NIPAAm, DMIA and HEMA in the polymer chain. The integration ( $2\text{CH}_3$ ) of NIPAAm at 0.79-1.16 ppm, (NH) of HEMA-*g*-PAH 7.88-8.02 ppm, DMIA ( $\text{CH}_2$ ) at 3.56-3.69 ppm. The calculation showed higher value of HEMA-*g*-PHA, which might be attributed to an extra condensation polymerization of HA in the polymer chains (**Table 70 and Figure 77**).

UV-vis. Spectroscopy was used for the determination of absorption band for functional group. The presence of  $\lambda=340\text{-}300$  nm for  $\pi\text{-}\pi^*$  transition of C=C of DMIA was observed.

For the estimation of  $T_c$  of aqueous polymer solution we used UV-vis. Spectroscopy, to achieve turbidimetric as a change in transmittance with temperature. For the dual responsive of polymer we estimated  $T_c$  at different pH.

**Figure 78** illustrates the temperature vs. transmittance of polymer (**57**) and (**59**) at pH2, pH7 and pH11.2.

**Table 70:** Yield, composition, molecular weight, polydispersity, and glass temperature of polymer **57** and **59**.

Polymer	Yield %	Composition DMIAAm (mol%)			Mw (g/mol) $10^4$	PD	$T_g$ °C
		$^1\text{H NMR}$					
		DMIA	HEMA	HEMA-g-HA			
<b>57</b>	90	4.90	7.9	-	5.10	2.56	138.0
<b>59</b>	63	4.76	-	32.5	5.04	1.64	145.0

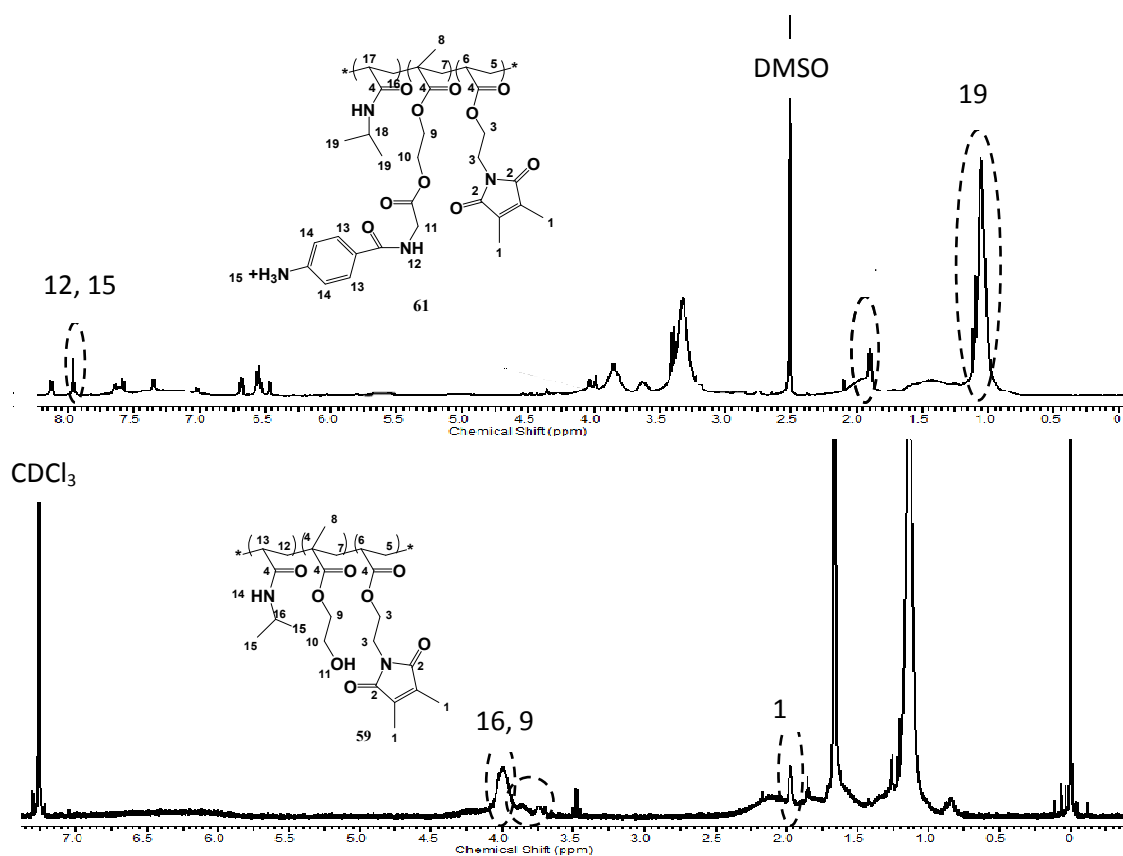


**Figure 77:**  $^1\text{H NMR}$  ( $\text{CDCl}_3$ ) of polymer **57** and **59**.

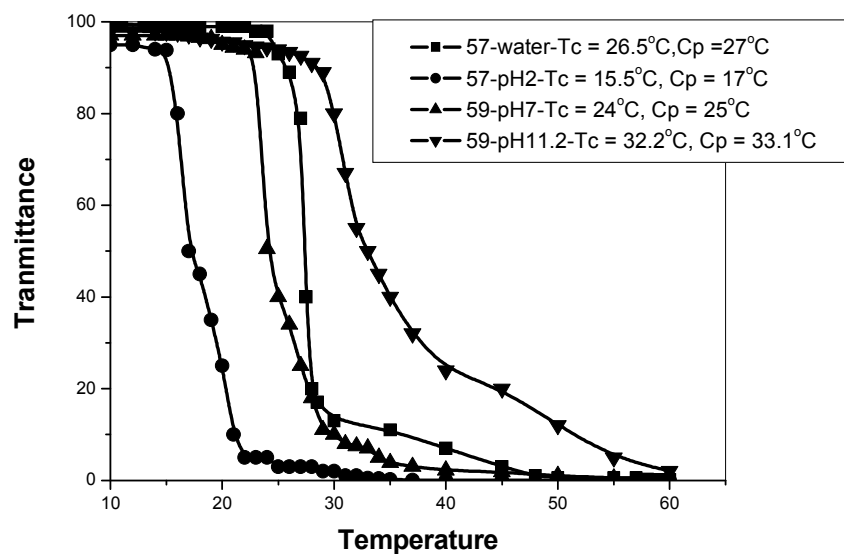


**Figure 78:** The change in turbidity with temperature for determination of  $T_c$  of polymer **57** and polymer **59** (pH2, pH7 and pH 11.2) using UV-vis. Spectroscopy for 1wt% of polymer solution.

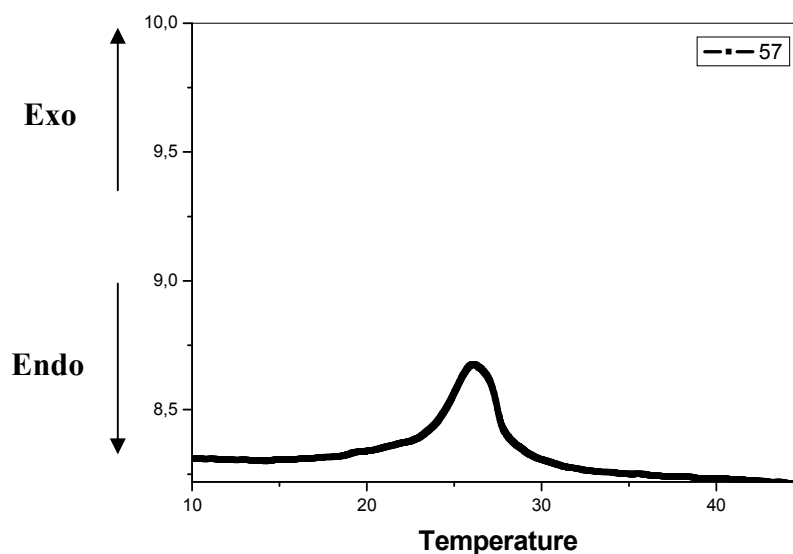


**Figure 79:** DSC of aqueous solution of polymer **57** for determination the LCST.

### **3.6. Formation of photo-crosslinked gel single layer studied by Surface Plasmon resonance and optical waveguide spectroscopy (SPR-OWS).**

#### **3.6.1. Introduction:**

The most important feature in our study is the formation of hydrogel thin film, as mono or bilayers. Therefore, photo-crosslinking has been used to achieve hydrogel formation. Here we used DMIAAm, DMIA and DMIMA as photo-crosslinker for a variety of polymers e.g. NIPAAm, DMAAm....ect. The method for the preparation of gel film is described in **Figure 80**. The method can be described in three stages; the first stage is the evaporation of gold over LaSFN9 glass with 50nm film thickness. After that, the gold slide is immersed in a solution of 5 mM DMITAc adhesion promoter giving 3-5 nm film thickness. The second stage is the spin coating of polymer solution. It was observed that the used solvent affects the homogeneity of the surface. Here we used three kinds of solvents, cyclohexanone, which is best solvent for the formation of homogenous layer, the other is DMSO which acts as bad solvent forming heterogeneous layer; however, is necessary to dissolve polar polymers, and the last one is a mixture of (DMSO + Ethanol) in the ratio of 1:1, which is better than DMSO. The last stage is the UV-irradiation to perform [2+2] cyclodimerization of dimethylmalimide groups. The photo-crossling has been done in the near UV (300- 430 nm). For this reason we always use photosensitizer thioxanthone. It transfers the energy of absorbed light to a polymer's photoreactive moieties causing them to enter the excited state. Factors, which influenced in the photo-crosslinking, are irradiation wavelength and intensity, reaction time, properties and concentration of photo-crosslinker, composition of the photoreactive polymers and presence of photosensitizer. The presence of adhesion promoter resulted in surface attachment of hydrogel to the substrate. The maleimide group in adhesion promoter reacted with a similar group present in the spin coated photo-crosslinkable polymer through above mentioned [2+2] cyclodimerization reaction. Au-S bond on other hand resulted in the co-ordination covalent bond attachment of the hydrogel to the substrate. **Figure 81** shows the formation of mono, and bilayer hydrogel by photocrosslinking using [2+2] cyclodimerization for poly(NIPAAm-Co-DMIAAm).

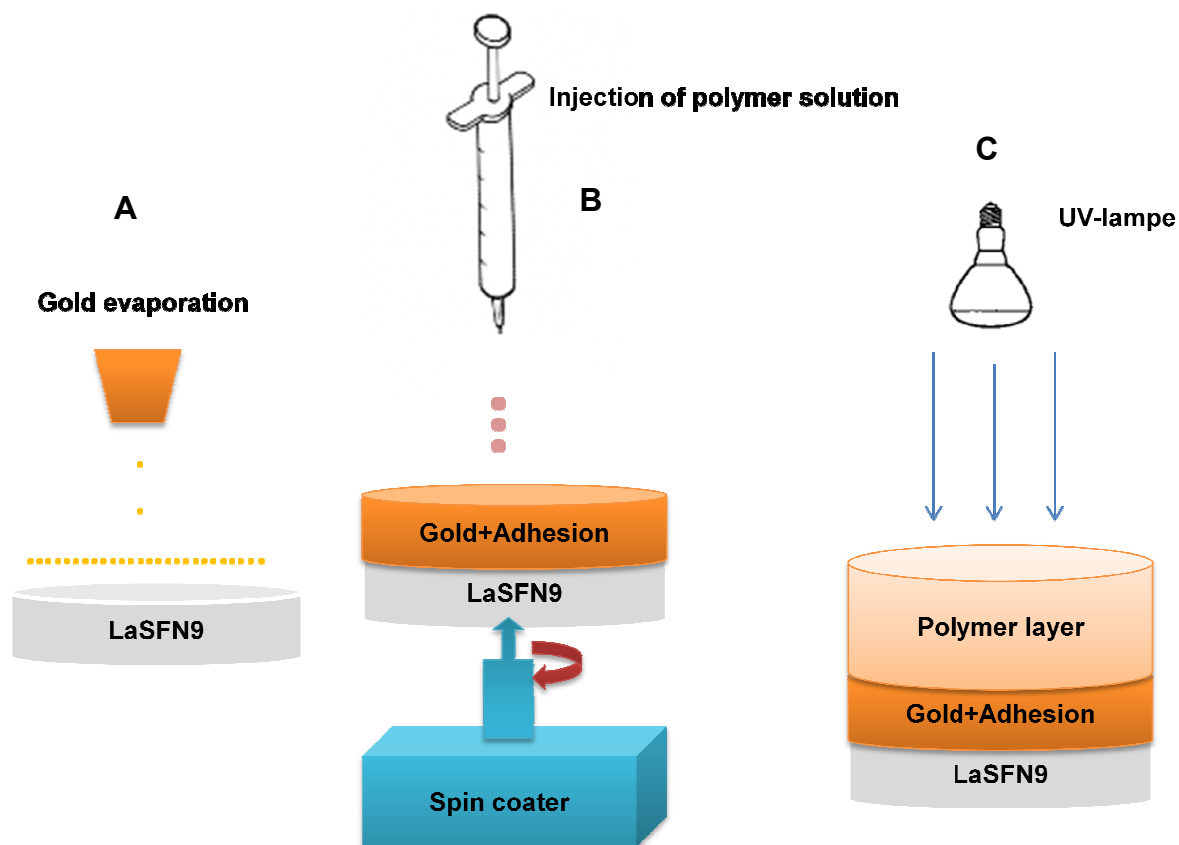


**Figure 80:** Schematic diagram for the formation of gel thin film.

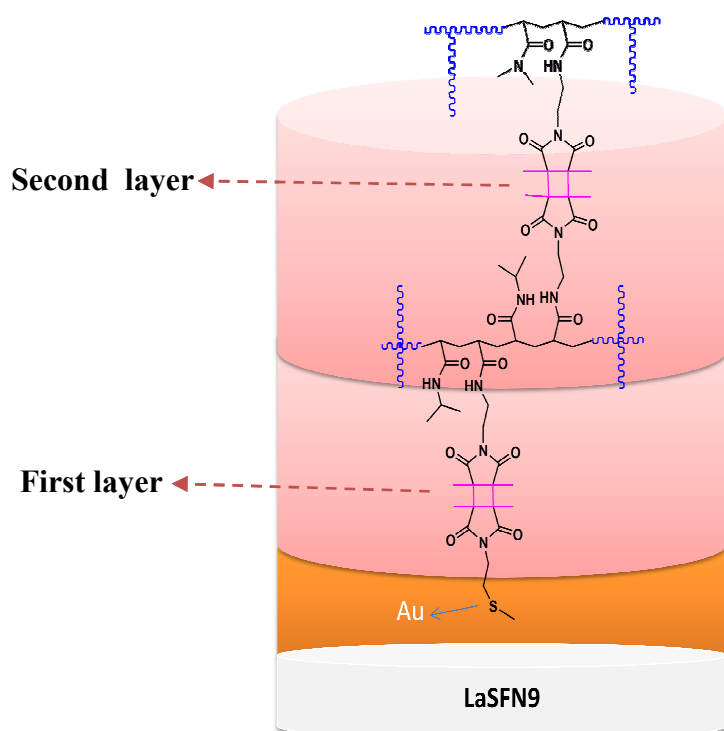


**Figure 81:** Schematic diagram for the formation of single layer of poly(NIPAAm-Co-DMIAAm) and coated by poly(DMAAm-Co-DMIAAm) for the formation of bilayer.

### **3.6.2. Formation of temperature responsive hydrogel thin film based on photo-crosslinked P(NIPAAm-Co-DMIAAm) using SPR/OWS for swelling and thickness measurements.**

In this section we will focus on the formation of hydrogel thin film and interpretation of the swelling properties using SPR-OWS. The different content of the photo-crosslinker effects the formation of hydrogel and further the volume degree of swelling and the refractive index. Therefore, we used three different kinds of polymers 48-(02, 05 and 10) in the formation of hydrogel.

#### **3.6.2.1. General SPR/OWS set up.**

The surface plasmon resonance measurements was carried out according to Kretschmann configuration as described in **chapter 1, section 1.7.2.3**. The LaSFN9 glass (refractive index  $n = 1.8449$ , corresponding to dielectric  $\epsilon = 3.4036$ ,  $n = \sqrt{\epsilon}$ ) was optically matched to the base of the glass prism. Monochromatic light from a He/Ne laser at 633nm was directed through the prism. The external angle of incidence ( $\theta$ ) was varied with a goniometry and then the light was collected with photodiode. The reflection intensity versus angle was recorded. The angle-dependent of the reflectivity was described by solving the Fresnel equation for a multilayer system. The base system for multilayer consisted of LaSFN9 glass, gold ( $d_{Au}$ ,  $\epsilon_{Au}$ ) adhesion promoter (DMITAc) ( $d_{DMITAc}$ ,  $\epsilon_{DMITAc}$ ), and air ( $d_{air}$ ,  $\epsilon_{air}=1$ ), in the case of measurements of bare gold and bare gold + DMITAc. In the case of dry gel case, an additional layer for the gel thin film for determination of  $d_{gel}$  and  $\epsilon_{gel}$ . In the swelling case using deionized water ( $\epsilon = 1.77$ ). The refractive index and thickness of the gel layers change simultaneously during swelling and collapse states. The waveguide modes can be guided within layers thicker than 200 nm in the dry state and 500 nm in the swollen state. For temperature responsive hydrogels temperature control hydrogel was achieved by placing the sample on hot stage, in which the stage was heated resistively and cooled by a cooling mantel surround the stage to adjust the temperature from 15 - 55 °C.

#### **3.6.2.2. SPR-OWS for hydrogel thin film of polymer 46-02.**

In the case of polymer **46-02** with calculated 2 mol% and actually 1.6 mol% of maleimide, solution of 7.5 wt% in cyclohexanone was spin coated on the surface of gold bar with adhesion promoter at 2000 rpm.

**Figure 82** shows the SPR angular scan for gold and (gold + DMITAc), that indicate the thickness of 50 nm. After the self assembling of the adhesion promoter an additional layer was formed giving 55 nm as (50 nm Au + 5 nm AP).

Figure 83 shows a combination for SPR curves for bare gold, bare gold with adhesion promoter and after spin coating and UV crosslinking gel film. In spite of using middle solution concentration (5 wt%) and middle spin coating speed (2000 rpm) it gave a low film thickness (76 nm), due to the lower content of photo-crosslinker in the polymer composition and, hence an increased amount of removable polymers.

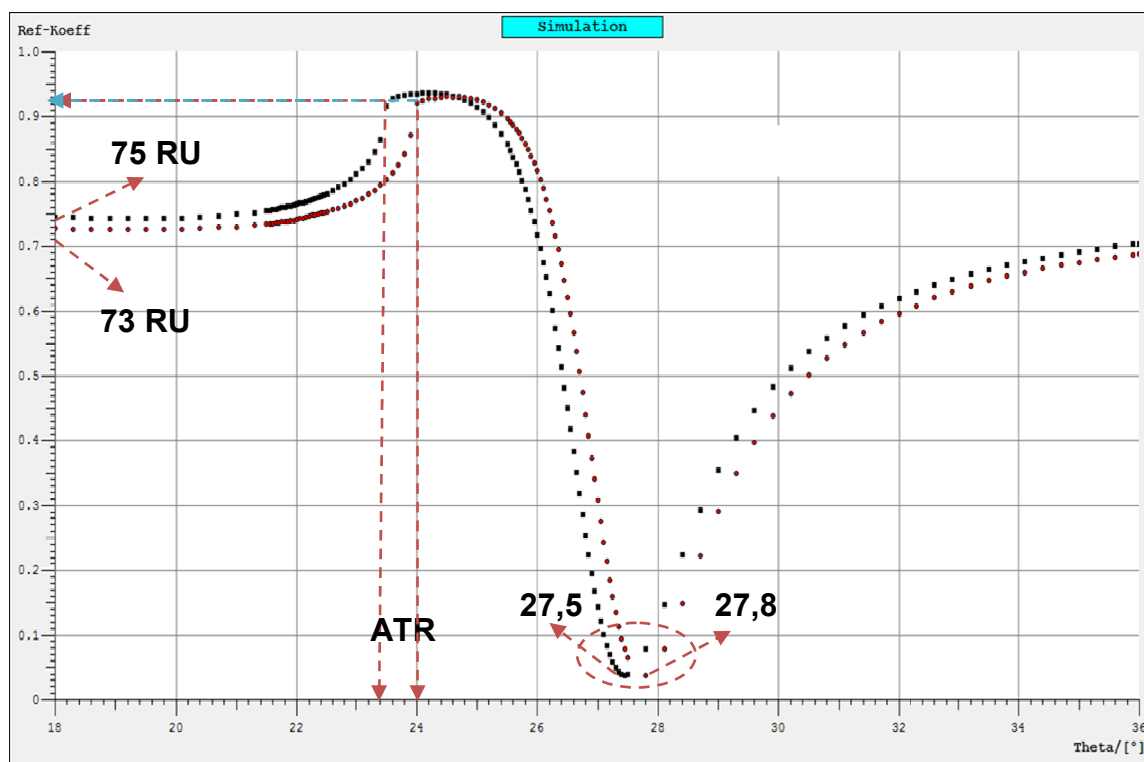


Figure82: SPR angular scan of bar gold ( ... ) and gold with adhesion promoter ( ... ).

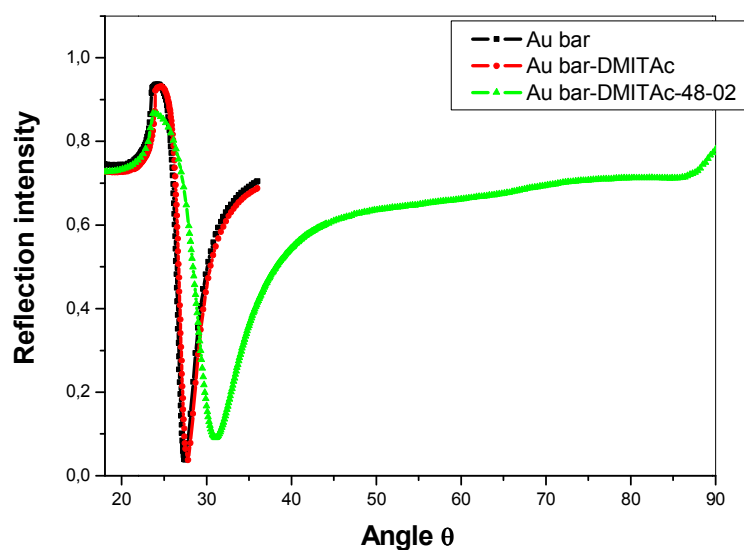


Figure 83: SPR scan of bar Au ( ... ). bar Au + DMITAc ( ... ) and PNIPAAm gel ( ... ).

### ***3.6.2.3. Effect of polymer concentration on the hydrogel formation.***

The same set up as previously described was used for the formation of film thickness from polymer **46-05**. In order to prepare hydrogel thin films 5, 7.5 and 10 wt% of polymer **46-05** in cyclohexanone was spin coated over the surface of (gold+AP), as 40s at 250 rpm and 100s at 2000 rpm, the spin coated slide was removed and dried under vacuum for 20 min., then exposed to UV irradiation for 60 min for the formation of crosslinked hydrogel. The slide with coated hydrogel was washed with deionized water for 5 min to remove the un-crosslinked polymer.

The SPR/OWS measurements were achieved for the dry state at room temperature for three different photo-crosslinker polymer concentrations. The reflection intensity RI versus ( $\theta$ ) angle from 18° to 90° scan was performed. After the measurements of the hydrogel film in the dried state the flow cell was filled by deionised water and the hydrogel was left to swell for about 1 h at 20 °C then an RI versus angle ( $\theta$ ) at constant temperatures was measured. After the completion of the angle scan, the temperature was increased to the second temperature and the hydrogel was left for 15 min to give the thermal equilibrium. Then the angle scan measurement was repeated.

The dry cases for 5, 7.5 and 10 wt% showed a linear increase in the thickness and refractive indices. The scan of the dry cases for 5 wt% showed an attenuated total reflection (ATR) at 22.5°. While 7.5 wt% did not exhibit any ATR but exhibit waveguide mode at 25°. On the other hand 10 wt% exhibited both ATR and waveguide mode at 22.4° and 30° respectively.

The swelling behavior for PNIPAAm hydrogels is temperature dependent. **Figure 86** showed SPR scans for polymer **46-05** at different temperatures. At low temperatures highly swollen case with 830 nm thickness corresponds to 3.608 volume degree of swelling was observed. Furthermore, the scan showed a waveguide mode at 48.5° this waveguide disappeared with increasing temperature till the semi-collapsed state at 50°C, corresponding to highest refractive index at 1.413 RIU and lowest swelling ratio 1.26, which, is close to dry film thickness. Moreover, the Plasmon minima demonstrate change with various temperatures from 64° to 74.2° for 15°C and 50°C respectively.

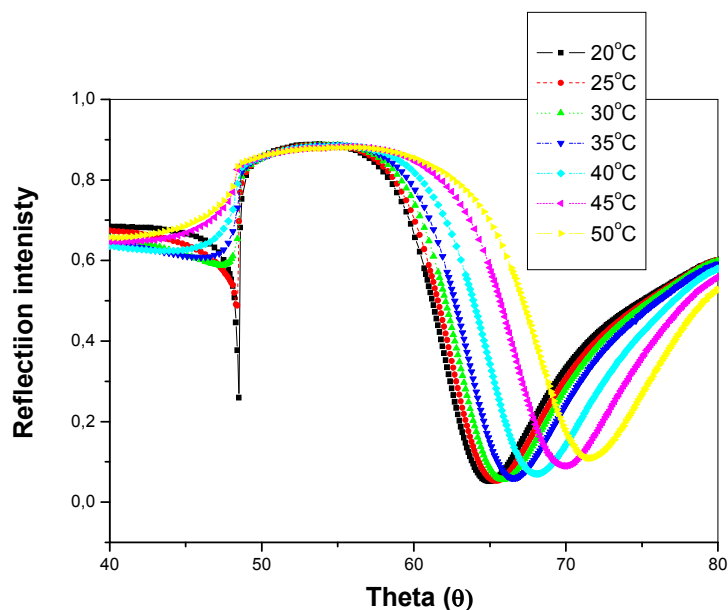


**Figure 84:** SPR scan of photo-crosslinked hydrogel layer 5 mol % DMIAAm and 5 wt% polymer solution swollen in water at different temperature.

The swelling of hydrogel from 7.5 wt% and 10 wt% shown in **Figure 85**, and **Figure 86** respectively. The important values are summarized in **Table 71**

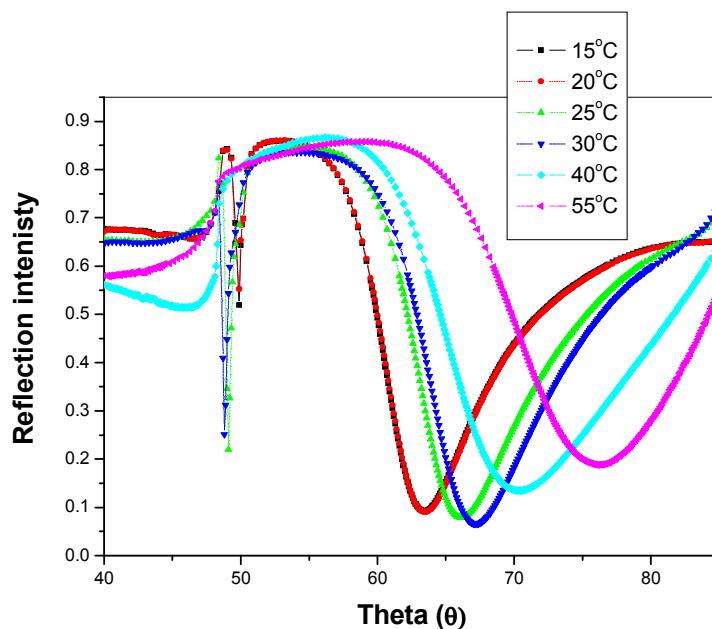


**Figure 85:** SPR scan of photo-crosslinked hydrogel layer 5 mol % DMIAAm and 7.5 wt% polymer solution swollen in water at different temperature.

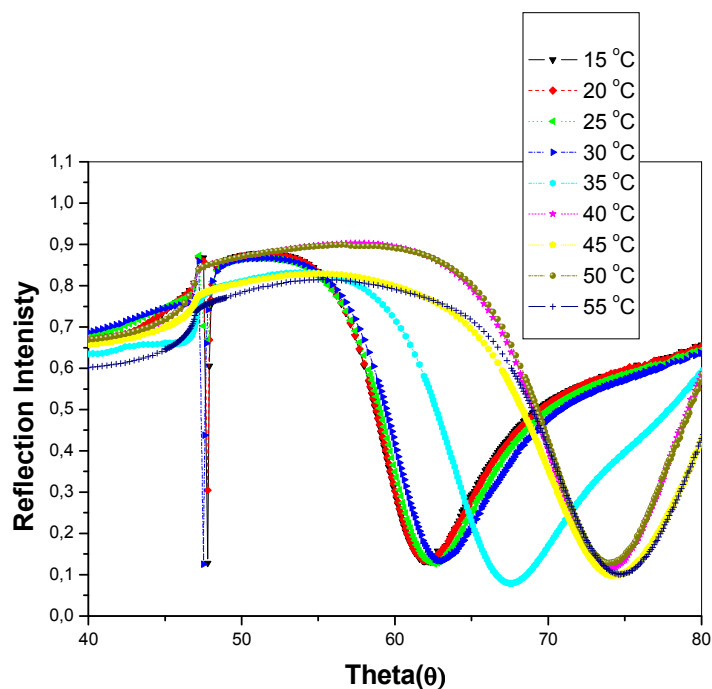


**Figure 86:** SPR scan of photo-crosslinked hydrogel layer 5 mol % DMIAAm and 10 wt% polymer solution swollen in water at different temperature.

**Table 71:** Concentration of polymer, dielectric and refractive indices of polymer 46.

Polymer conc. Wt%	Dry thickness	Dielectric ( $n^2 = \epsilon$ )	n
5	230	2.06	1.435
7.5	275	2.09	1.445
10	389	2.12	1.456

The refractive index extracted from SPR curves was converted to polymer fraction  $\chi_p$  which finally gave volume degree of swelling  $1/\chi_p$  according to the linear equation;<sup>(48)</sup>

$$n = 0.19 \chi_p + 1.33123$$

(n) refers to refractive index, (0.19) calculated constant, and (1.33123) is the refractive index of water corresponding to dielectric  $\epsilon \sim 1.77$ .

The temperature dependent swelling behavior of the three different samples is shown in Figures 87, and 88. The lower critical volume transition temperature was detected as the inflection point in the curve. The  $T_c$  decreased slightly from polymer concentration yielding, 29, 28.5 and 28°C for 5, 7.5, and 10 wt% respectively.

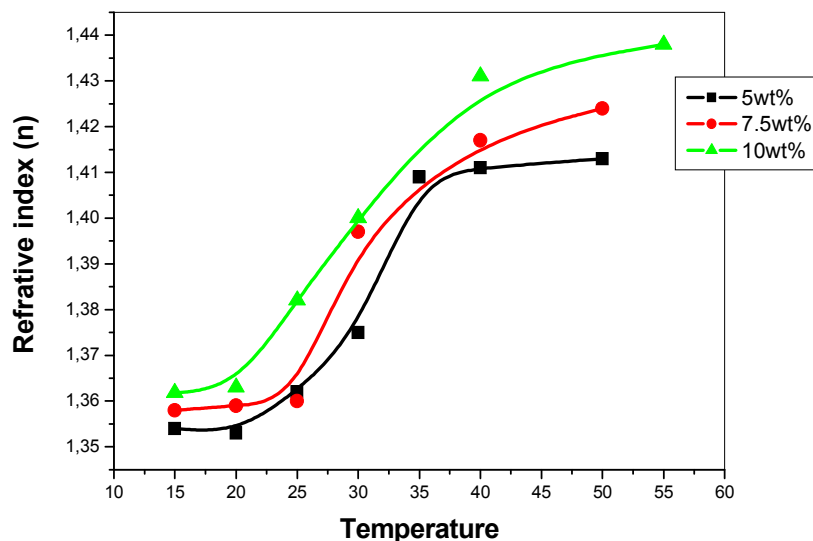


**Figure 87:** Refractive index vs temperature of photo-crosslinked hydrogel layer 5 mol % DMIAAm and 5, 7.5 and 10 wt%.

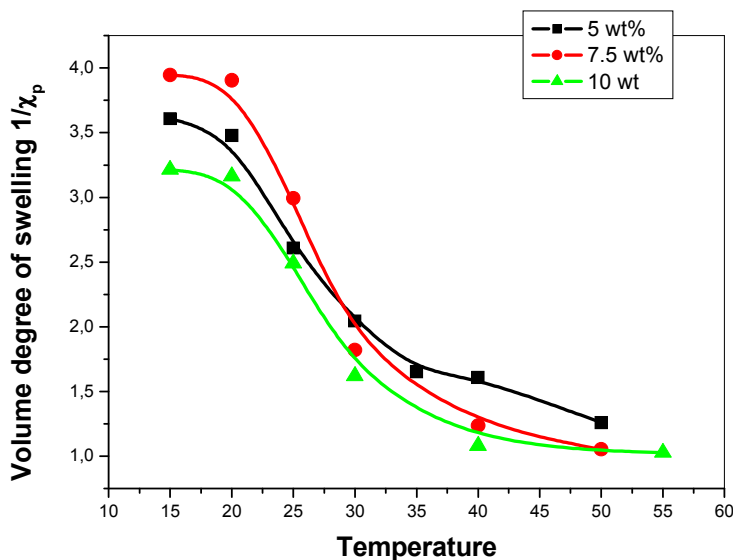


**Figure 88:** Volume degree of swelling vs. temperature of photo-crosslinked hydrogel layer 5 mol % DMIAAm and 5, 7.5 and 10 wt%.

#### 3.6.2.4. SPR/OWS for hydrogel thin film of polymer 46-10 using 7.5 wt%.

In this sub-section we will discuss the swelling behavior of the photo-crosslinked hydrogel based on NIPAAm and 10 wt% DMIAAm.

The temperature dependent swelling behavior for hydrogel was observed in **Figure 89**. At low temperature a swollen film with 1317.5 nm thickness is corresponding to 4.182  $1/\chi_p$ . The collapsed state at 55°C corresponds to highest refractive index at 1.4433 RIU and lowest volume degree of swelling 1.253 and layer thickness of ~400 nm.

The  $T_c$  was determined by the temperature-dependent change in refractive index ( $n$ ) and volume degree of swelling as shown in **Figure 90**. The  $T_c$  decreased with increasing the molar concentration of chromophor in the hydrogel, which is attributed to the hydrophobic effect of chromophor and this is in agreement with DSC and UV-vis. Spectroscopy. However, the  $T_c$  values from SPR measurements are slightly higher. This is most likely due to the difference in how  $T_c$  is defined by the two techniques. The sigmoidal fit defines  $T_c$  as the midpoint or inflection point of the transition, while DSC defines as onset of the transition. Therefore. It was expected that DSC will give slightly lower values<sup>(73)</sup>.

**Table 72:** Concentration of polymer, dielectric and refractive indices for polymer **46-10**.

Polymer conc.	Dry	Dielectric	n
Wt%	Thickness (nm)	( $n^2 = \epsilon$ )	
7.5	315	2.1	1.449

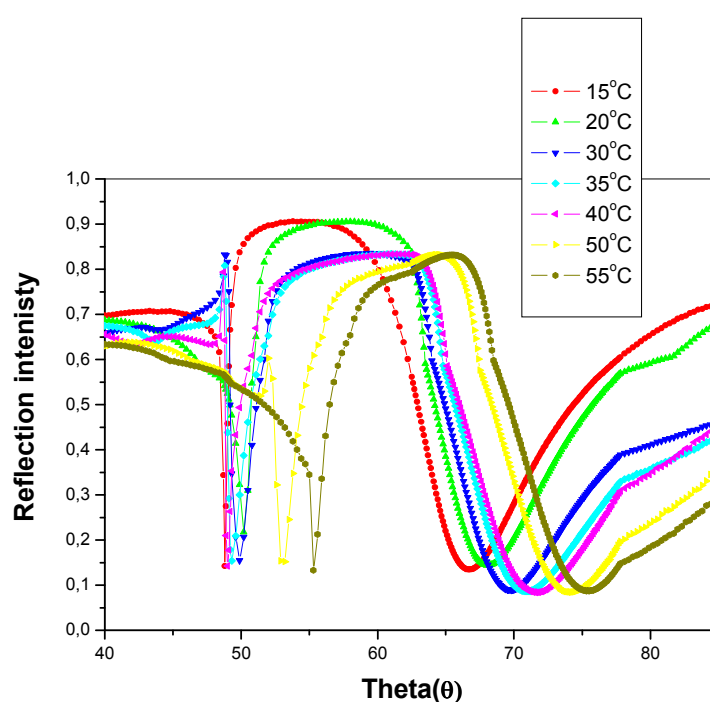


**Figure 89:** SPR scan of photo-crosslinked hydrogel layer 10 mol % DMIAAm and 7.5 wt% polymer solution for both dry case and the swollen case in water at different temperature.

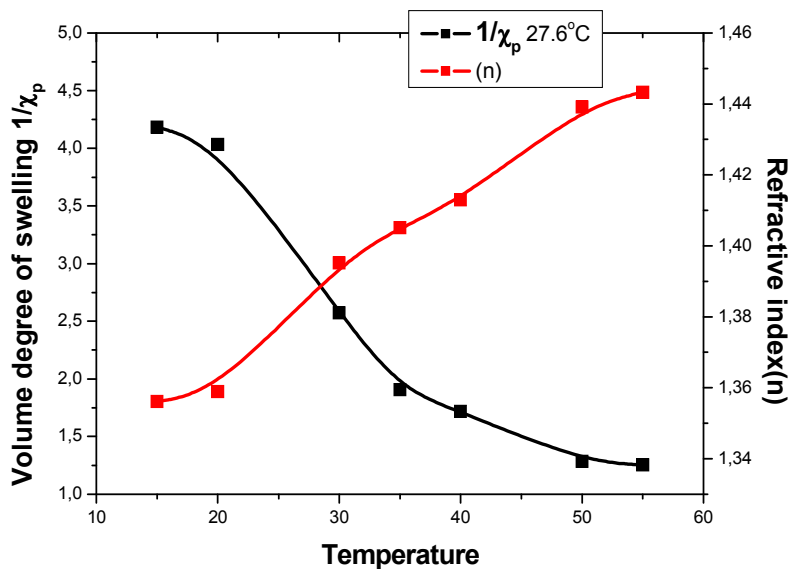


**Figure 90:** Volume degree of swelling and refractive index vs temperature of photo-crosslinked hydrogel layer 10 mol % DMIAAm and 7.5 wt%.

### 3.6.3. Formation of hydrophilic hydrogel thin film based on photo-crosslinked P(HEMA-Co-DMIMA), using SPR/OWS for swelling and thickness measurements.

The swelling behavior of photo-crosslinked HEMA hydrogel layer with 5 mol-% of acrylate photo-crosslinker (DMIMA) was measured in water by SPR. **Figure 91** shows SPR scan RI vs. ( $\theta$ ) for gold+AP (a) and dry hydrogel layer of 10 mol % photo-crosslinker and 5 wt % concentration of the coated photo-crosslinked polymer at 2000 rpm. The SPR/OWS scan showed total reflection at  $23^\circ$  but the ATR is not closed to unity indicating that the homogeneity of the thin film is not good and this is due to the poor solubility of polymer in organic solvent. However, DMSO was used as a suitable solvent, but it is not suitable for the formation of homogenous films.

The swelling for hydrogel is temperature independent and it was performed as shown in **Figure 92**. The film thickness was 450 nm thicknesses corresponding to 2.757 volume degree of swelling and  $\sim 1.4$  RIU. The scan showed ATR at  $48^\circ$  the Plasmon minima at  $70^\circ$  did not change with raising the temperature.

**Table 73:** Concentration of polymer dielectric and refractive indices for polymer 48-05.

Polymer conc. wt%	Dry Thickness (nm)	Dielectric ( $n^2 = \epsilon$ )	n
7.5	189	2.15	1.466

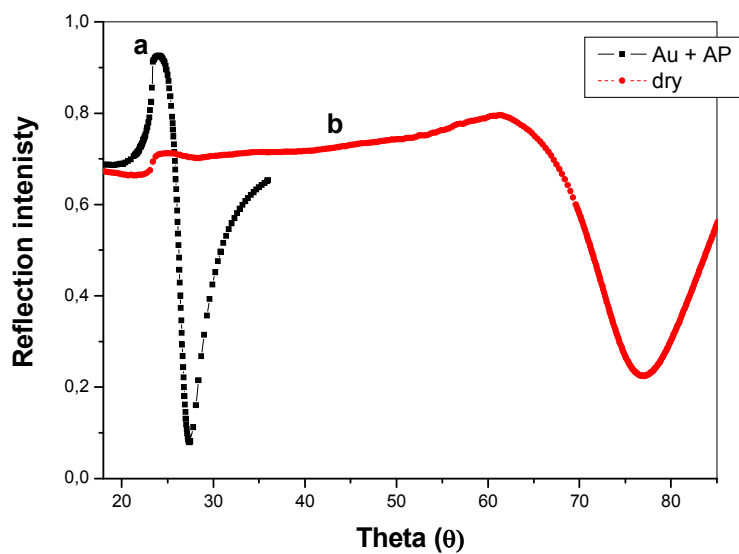


**Figure 91:** SPR scan of Au+AP (a) and dry hydrogel layer (b) of 5 mol % DMIMA and 5 wt% polymer solution.

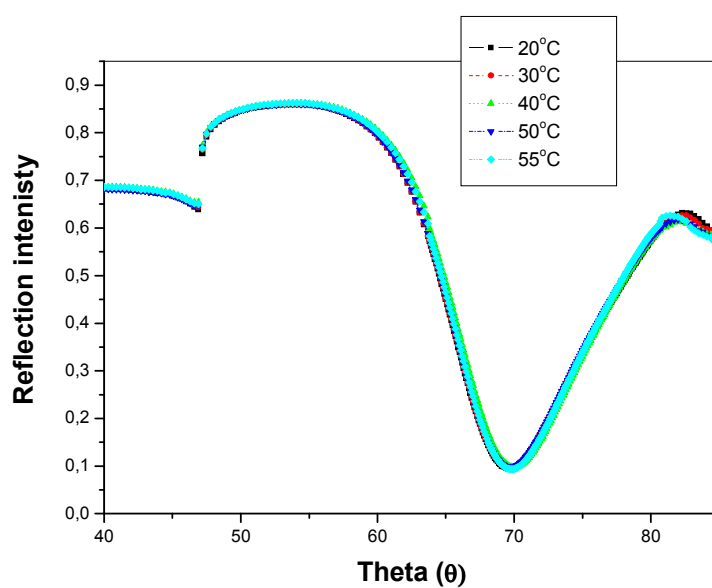


**Figure 92:** SPR scan of photo-crosslinked hydrogel layer 5 mol % DMIMA and 5 wt% polymer solution, swollen in water at different temperature.

### 3.6.4. Formation of hydrophilic hydrogel thin film based on photo-crosslinked P(DMAAm-Co-DMIAAm) using SPR/OWS for swelling and thickness measurements.

The swelling behavior of photo-crosslinked DMAAm hydrogel layer with varying mol-% of acrylamide photo-crosslinker (DMIAAm) was measured in water. It is known that the DMAAm polymers are hydrophilic. Therefore, it is expected that these polymer will exhibit a similar behavior HEMA photo-crosslinkable polymers. Unlike the HEMA based polymers, the DMAAm homo and copolymers are soluble in common organic solvent and hence are more suitable for the thin film formation. Therefore, alternative DMAAm photo-crosslinkable polymers were synthesized.

**Figure 93** shows SPR scan RI vs. ( $\theta$ ) for the bar gold+AP and dry hydrogel layer of 5 mol % photo-crosslinker and 7.5 wt% concentration of the coated photo-crosslinked polymer using 2000rpm. The SPR/OWS scan showed total reflection at 22° and waveguide mode at 24° both indicate the formation of homogenous gel film.

The swelling behavior for this hydrogel is temperature independent as shown in **Figure 94**. The film thickness was 1317.5 nm corresponding to 3.2 volume degrees of swelling and ~1.46 RIU as non sensitive film thickness. The scan showed ATR at 47° and a waveguide mode at 48°. The Plasmon minima at 65° did not change with raising the temperature. **Figure 95** shows a relation between volume degree of swelling and refractive index vs. temperature.

**Table 74:** Concentration of polymer, dielectric and refractive indices.

Polymer conc. wt%	Dry Thickness (nm)	Dielectric ( $n^2 = \epsilon$ )	n
7.5	305	2.12	1.469

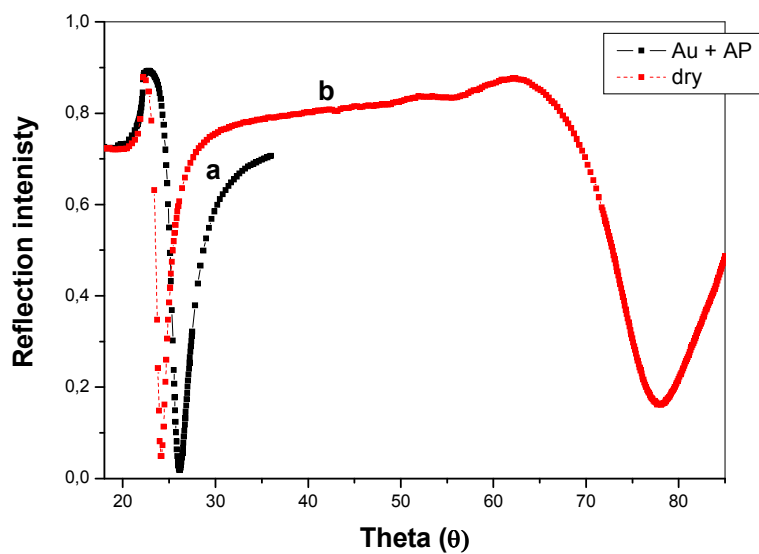


**Figure 93:** SPR scan of Au+AP (a) and dry hydrogel layer (b) of polymer 47-05 with 5 mol % DMIAAm and 7.5 wt% polymer solutions.

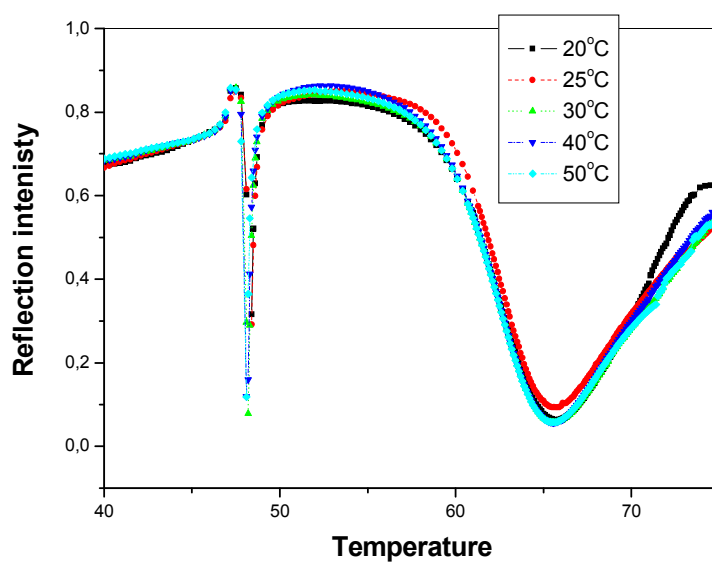


**Figure 94:** SPR scan of photo-crosslinked hydrogel layer of polymer 47-05 with 5 mol % DMIAAm and 7.5 wt% polymer solution, swollen in water at different temperature.

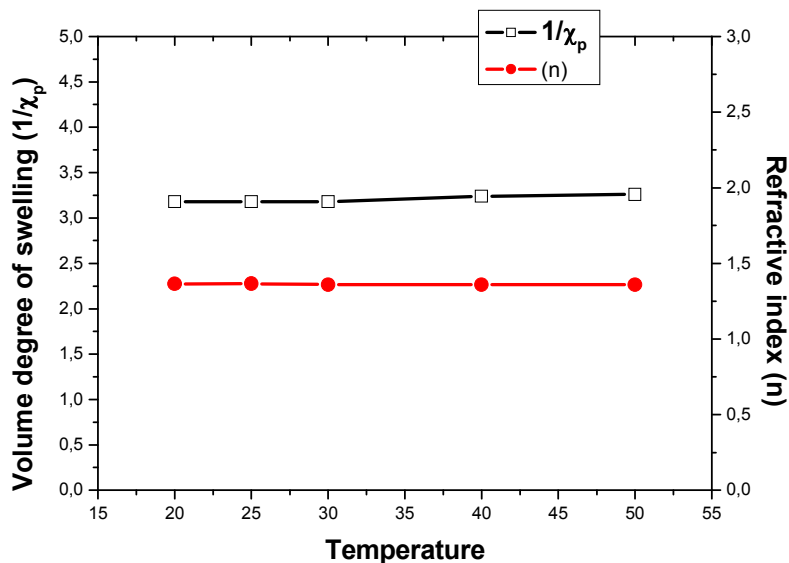


**Figure 95:** Volume degree of swelling and refractive index vs. temperature of photo-crosslinked hydrogel layer 5 mol % DMIAAm and 7.5 wt%.

### 3.6.5. Formation of dual responsive functional hydrogel thin film based on photo-crosslinked P(NIPAAm-*Co*-VA-*Co*-DMIAAm) using SPR/OWS for swelling and thickness measurements.

In section 3.5.6. we discussed the synthesis of functional photo-crosslinked polymers based on NIPAAm, VA and DMIAAm. Different mol ratios of VA and DMIAAm were used. Here we will focus on the formation of hydrogel thin film by photo-crosslinking of polymer **51-05-10** and **51-10-15**, and studying the swelling behavior of the formed hydrogel as temperature dependent and pH-dependent by a combination of SPR/OWS.

#### ❖ *Formation of hydrogel thin film of polymer 51-05-10 and 51-10-15.*

**Dry:** A solution of 10 wt% of photo-crosslinked polymer in cyclohexanone was spin coated on (Au + AP) at 2000 rpm. The scan of RI ( $\theta$ ) showed the presence of ATR at  $\sim 23^\circ$  and waveguide mode at  $\sim 33^\circ$  also plasmon minima at  $\sim 82^\circ$ . All features indicate the formation of homogenous film. The thickness and refractive index were 378.6 nm and 1.468 RIU. The results for **51-05-10** and **51-10-15** are summarized in **Table 75** and **Figure 96**.

**Swelling behavior with variations of temperature:** The swelling was measured by SPR/OWS and using DI water. **Figure 97** and **Figure 98** show the swelling behavior as change in RI ( $\theta$ ). A decrease in the volume degree of swelling and increase the refractive indices with raising temperature occurred and both proved the change of hydrogel state

from the swollen to the collapsed states. Similar behavior was observed for **51-05-10** and **51-10-15** (**Figure 97** and **Figure 99**).

The  $T_c$  was determined by the temperature-dependent change in refractive index ( $n$ ) and volume degree of swelling as shown in **Figure 99**. The transition temperature was detected as the inflection point in the curve. The  $T_c$  showed lower value  $\sim 14.6$  °C than PNIPAAm which is attributed to the hydrophobic effect of (VA). The  $T_c$  for **51-10-15** was  $\sim 12.4$  °C and even lower due to more hydrophobic compounds. (**Figure 101**).

**Swelling behavior with variations of pH values:** The polymers **51-05-10** and **51-10-15** are not supposed to be pH-sensitive. However, for comparison reason the pH dependent swelling was investigated (**Figure 98** and **Figure 102**). The increase of the swelling at higher pH values might be due to a hydrolysis of the maleimide functional group introducing more charges. Hence, best condition for photo-crosslinked film is below pH8.

**Table 75:** Illustrate dielectric and refractive indices of dry states.

Polymer	Dry thickness	Dielectric ( $n^2 = \epsilon$ )	$n = \sqrt{\epsilon}$
<b>51-05-10</b>	378.6	2.1556	1.468
<b>51-10-15</b>	185.61	2.1199	1.455

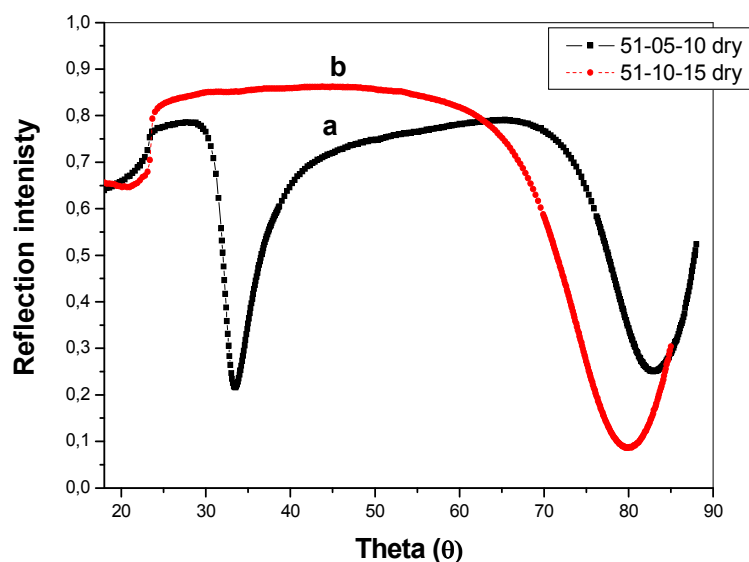


**Figure 96:** SPR/OWS scan of dry hydrogel layers for **51-05-10** and **51-10-15**.

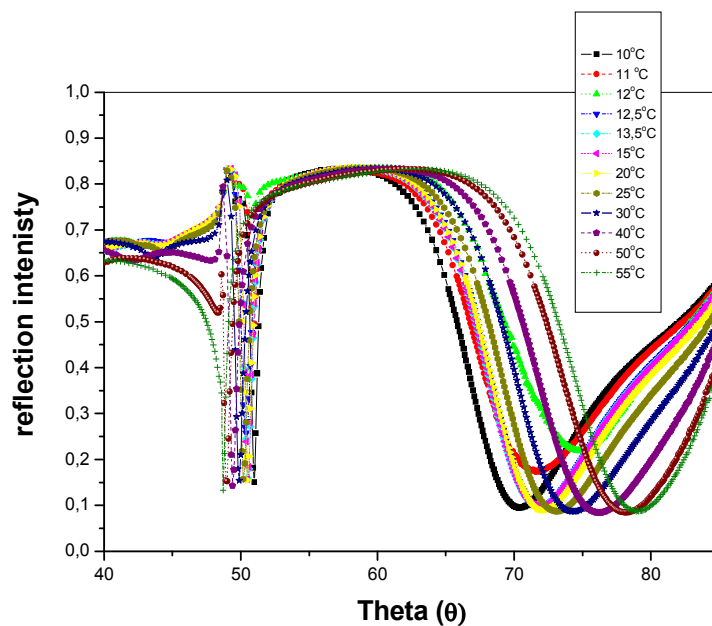


**Figure97:** SPR scan of photo-crosslinked hydrogel layer 10 mol % DMIA and 10wt% polymer solution, swollen in water at different temperature for **51-05-10**

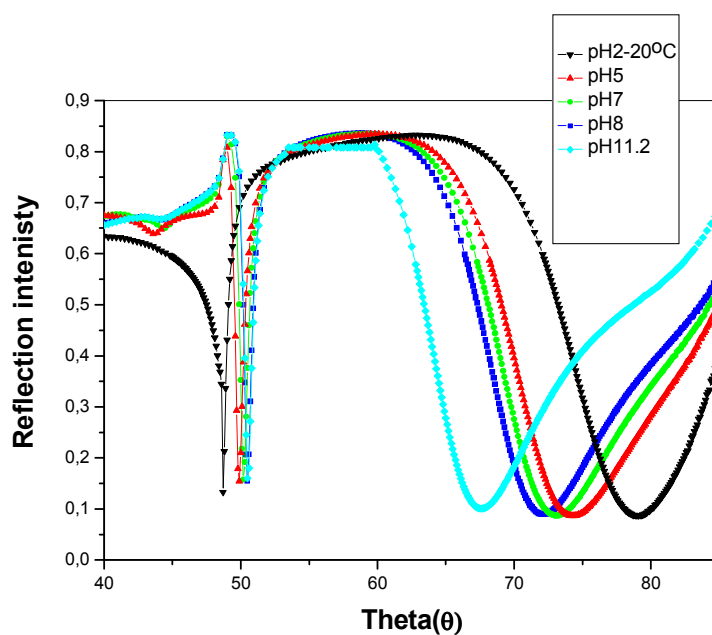


**Figure98:** SPR scan of photo-crosslinked hydrogel layer 10 mol % DMIA and 10wt% polymer solution, swollen in water at pH-values for **51-05-10**

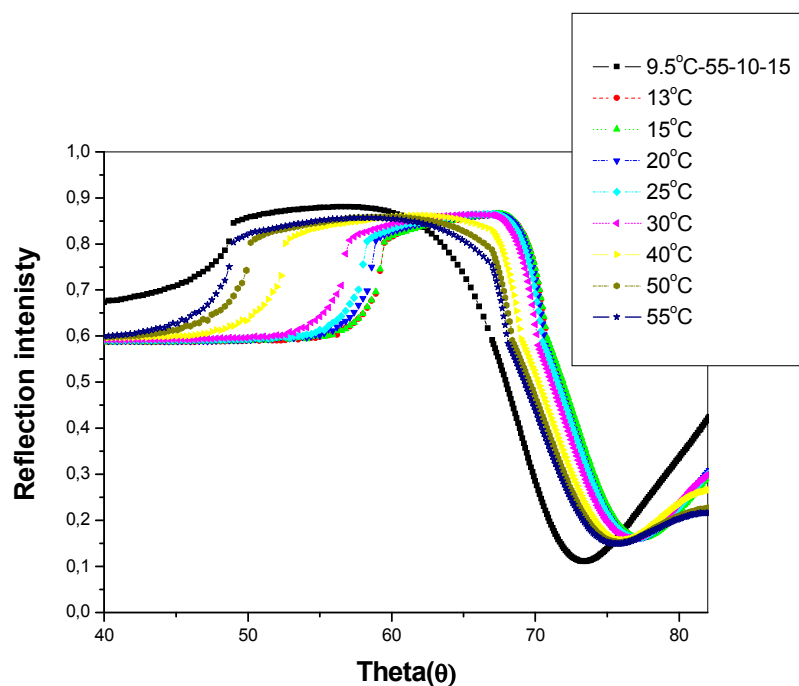


**Figure99:** SPR scan of photo-crosslinked hydrogel layer 10 mol % DMIA and 10wt% polymer solution, swollen in water at different temperatures for **51-10-15**.

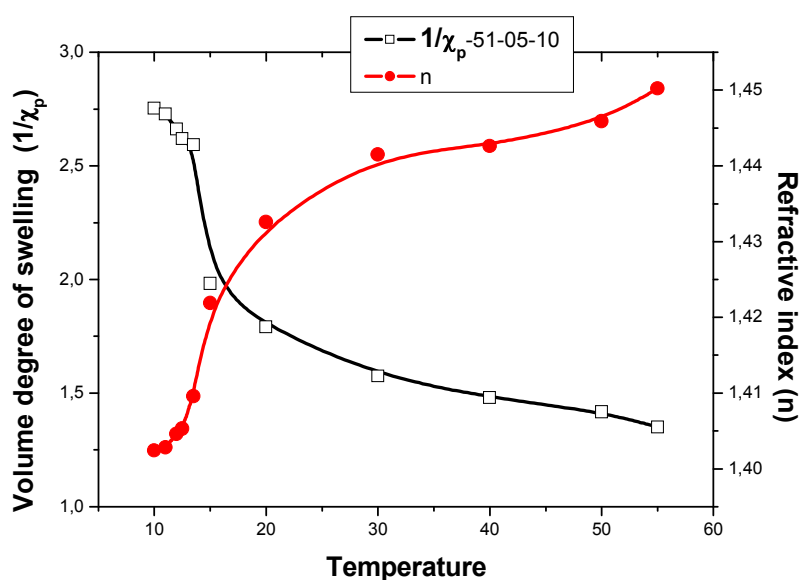


**Figure100:** Volume degree of swelling and refractive index vs. temperature of photo-crosslinked hydrogel layer 5 mol % DMIAAm and 10 wt% for **51-05-10**.

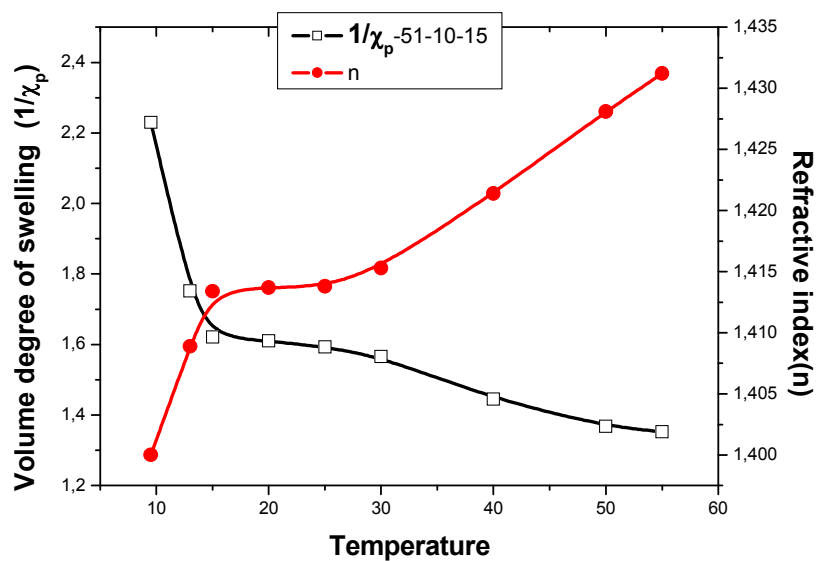


**Figure101:** Volume degree of swelling and refractive index vs. temperature of photo-crosslinked hydrogel layer 10 mol % DMIAAm and 15 wt% for **51-10-15**.

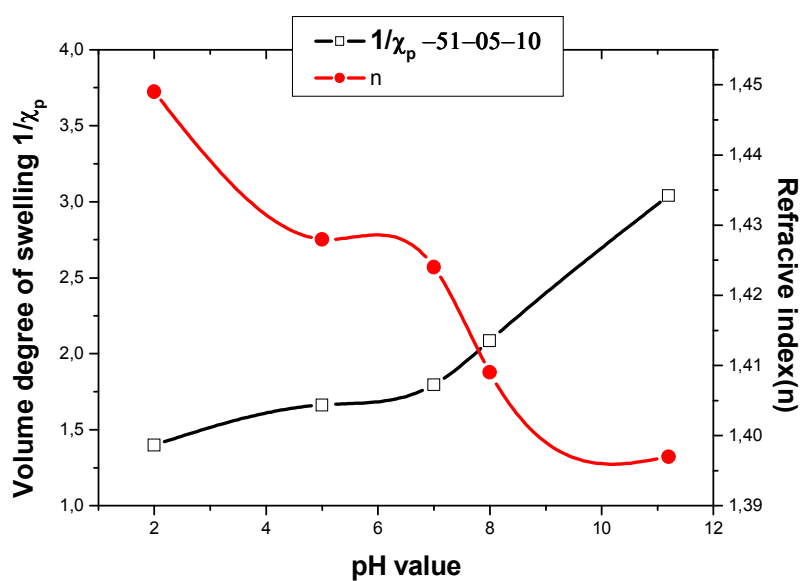


**Figure102:** Volume degree of swelling and refractive index vs pH-values of photo-cross-linked hydrogel layer 10 mol % DMIAAm and 15 wt% for **51-10-15**.

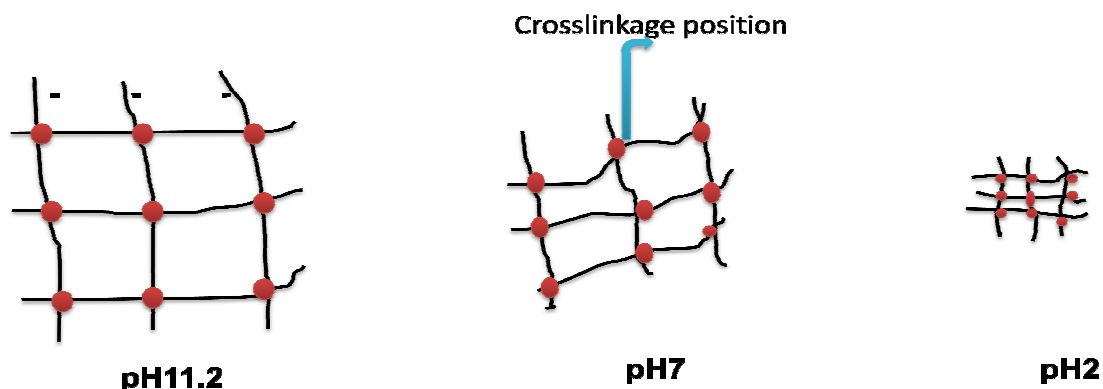


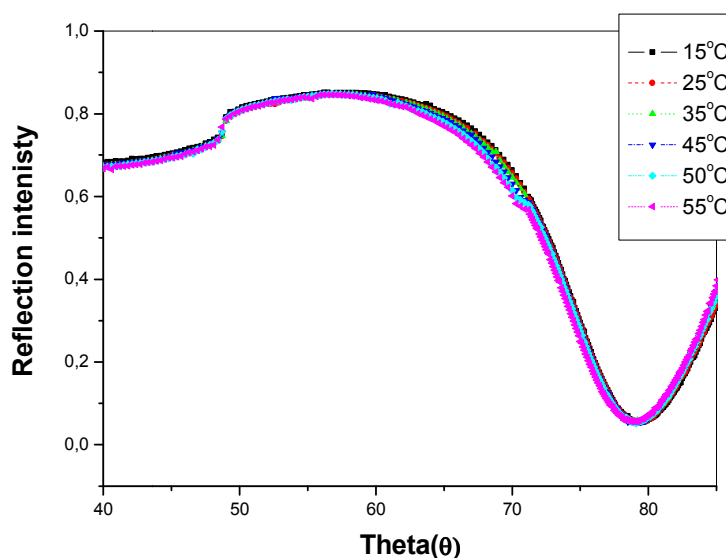
Figure103: Schematic diagram for the effect of pH on the surface of the hydrogel.

**3.6.6. Formation of hydrophobic and functional hydrogel thin film based on photo-crosslinked P(SKA-Co-VA-Co-DMIA) using SPR/OWS for swelling and thickness measurements.**

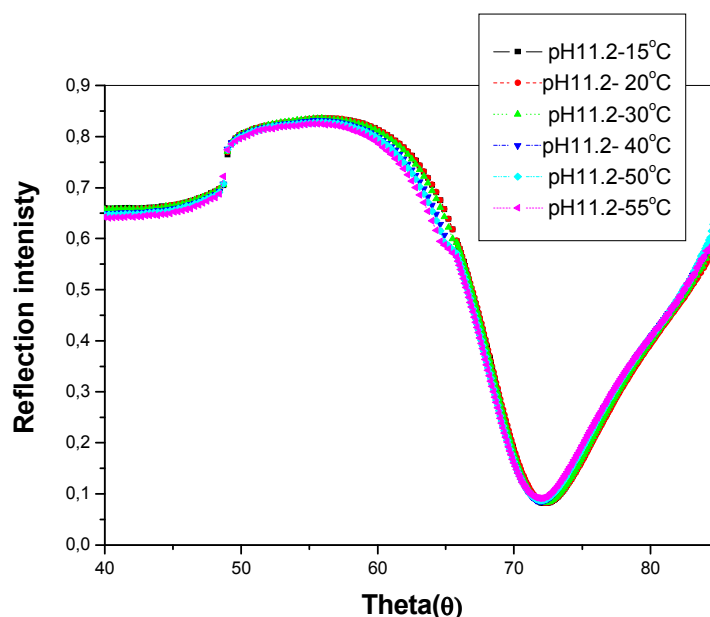
Hydrophobic polymer layers having functional aldehyde groups might be used for the decoration of sensitive hydrogels providing alcohol group. The alcohol groups can be used for further modifications e.g. with proteins. The characteristics of the dry film are summarized in Table 76. The swelling of the layers are temperature independent in water and at pH11.2 (Figure 104 and Figure 105).

Table 76: Illustrate dielectric and refractive indices of dry state.

Polymer	Dry thickness	Dielectric ( $n^2 = \epsilon$ )	$n = \sqrt{\epsilon}$
53-7.5-15	190	2.156	1.4683



**Figure104:** SPR scan of photo-crosslinked hydrogel layer 7.5 mol % DMIA and 5wt% polymer solution swollen in water at different temperatures for 53-7.5-15.



**Figure105:** SPR scan of photo-crosslinked hydrogel layer 7.5 mol % DMIA and 5wt% polymer solution swollen in water at different temperature at pH11.2 for 53-7.5-15.

**3.6.7. Formation of dual responsive functional hydrogel thin film based on photo-crosslinked Poly(NIPAAm-Co-DEAMVA-Co-DMIAAm) using SPR/OWS for swelling and thickness measurements.**

The LCST of photo-crosslinked PNIPAAm is affected by copolymerization with other monomers like (hydrophilic or hydrophobic). Here in this study we will discuss the change in the  $T_c$  of PNIPAAm hydrogel by incorporation of DEAMVA. Overall parameters will be discussed in detail as accomplishment of section3.5.7.

- ❖ **Dry:** Parameters are summarized Table 77.
- ❖ **Swelling behavior with variations of temperature for 54-05-10:** Figure112 and Figure 113 show the swelling behavior as temperature dependent in pure water. The  $T_c$  showed higher value  $\sim 36.7^\circ\text{C}$  than the PNIPAAm hydrogel, due to the higher hydrophilic effect presented in the protonated tertiary amino group of DEMAVA, that play a vital rule in the formation of charged surface. The resulting LCST is in a good agreement with UV-vis. Spectroscopy data.
- ❖ **Swelling behavior with variations of pH values:** The pH-dependence of the polymer or the hydrogel is attributed to the presence of protonated amino groups. Figure109 shows the swelling behavior as change in RI ( $\theta$ ) as pH-dependent. Figures 114, and 115

summarize these observations. However, the observed behavior was unexpected and is still under investigation.

- ❖ **Swelling behavior with variations of temperature for 54-7.5-15:** Similar behavior was found for this polymer (s. **Figure107**). **Figures 112, 113** showed higher  $T_c$  value  $\sim 48.5^\circ\text{C}$  than the previous hydrogel, due to the higher concentration of DEMAVA, which induced the hydrophilicity.
- ❖ **Swelling behavior with variations of pH values:** **Figure 109** shows the swelling behavior as change in RI ( $\theta$ ) as pH-dependent. **Figures 114,115** illustrate the volume degree of swelling and refractive index as pH-dependent and demonstrated the highest ( $1/\chi_p$ ) and lowest ( $n$ ) at pH11.2 as basic dielectric media.
- ❖ **Swelling behavior with variations of temperature for 54-10-20:** The same trends as discussed above can be seen here as well (**Figures 108, 112, 113**).

The  $T_c$  demonstrated highest value  $56.5^\circ\text{C}$ , due to the highest concentration of DEMAVA.

**Swelling behavior with variations of pH values:** **Figure111** shows the swelling behavior as change in RI ( $\theta$ ) as pH-dependent. **Figure114, 115** illustrated the volume degree of swelling and refractive index as pH-dependent and demonstrated the highest ( $1/\chi_p$ ) and lowest ( $n$ ) at pH11.2 as basic dielectric media.

- ❖ **General feature:** The unusual behavior was detected for non-crosslinkable polymers already. There is no reasonable explanation yet.

**Table 77:** Illustrate dielectric and refractive indices of dry state.

Polymer	Dry thickness	Dielectric ( $n^2 = \epsilon$ )	$n = \sqrt{\epsilon}$
<b>54-05-10</b>	161.39	2.0086	1.4442
<b>54-7.5-15</b>	148.78	2.0003	1.4143
<b>54-10-20</b>	165.07	2.0065	1.4165

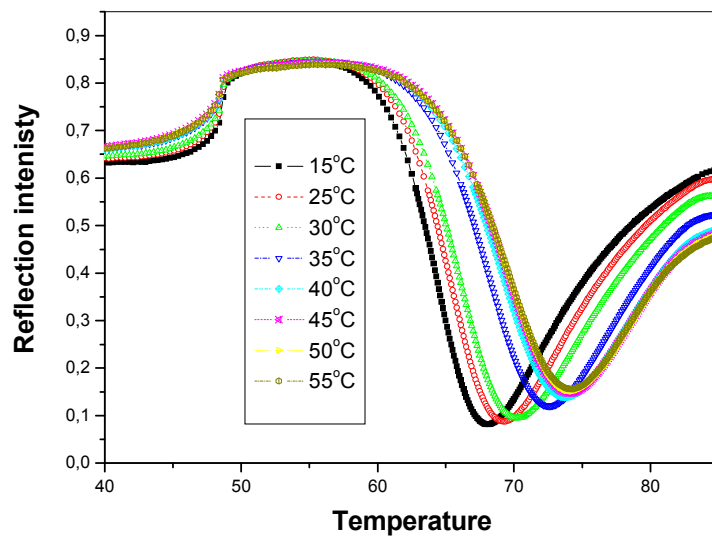


**Figure106:** SPR scan of photo-crosslinked hydrogel layer RI ( $\theta$ ) as temperature dependent for 56-5-10

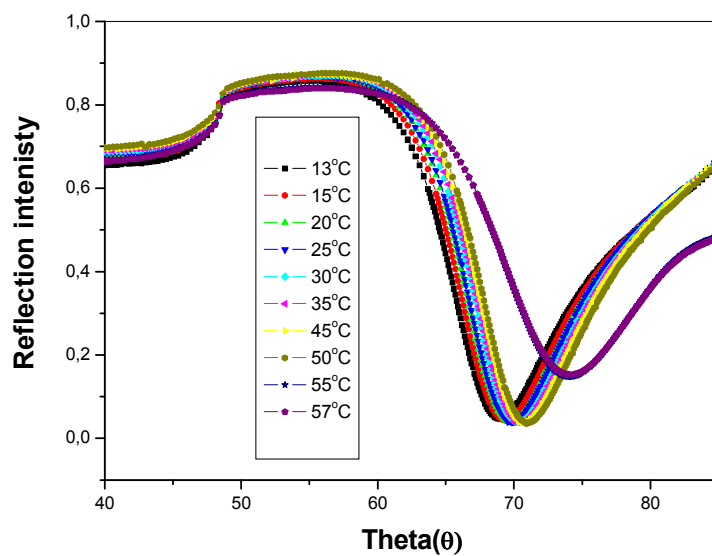


**Figure107:** SPR scan of photo-crosslinked hydrogel layer RI ( $\theta$ ) as temperature dependent for 56-7.5-15

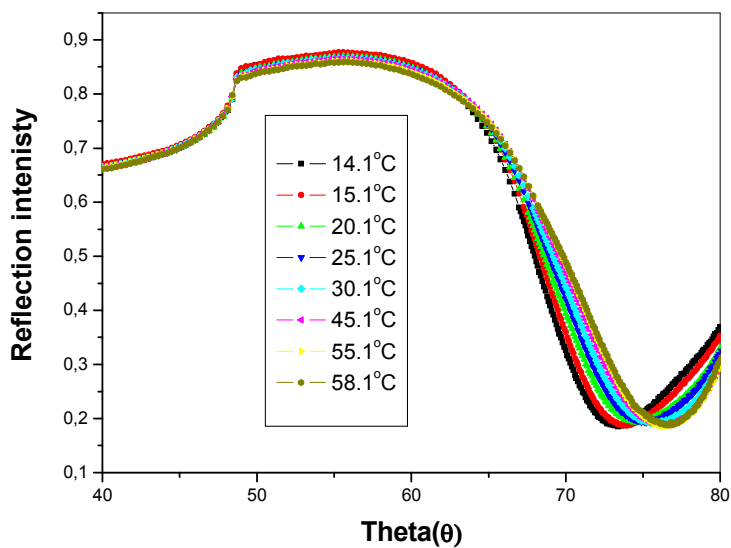


**Figure108:** SPR scan of photo-crosslinked hydrogel layer RI ( $\theta$ ) as temperature dependent for 54-10-20.

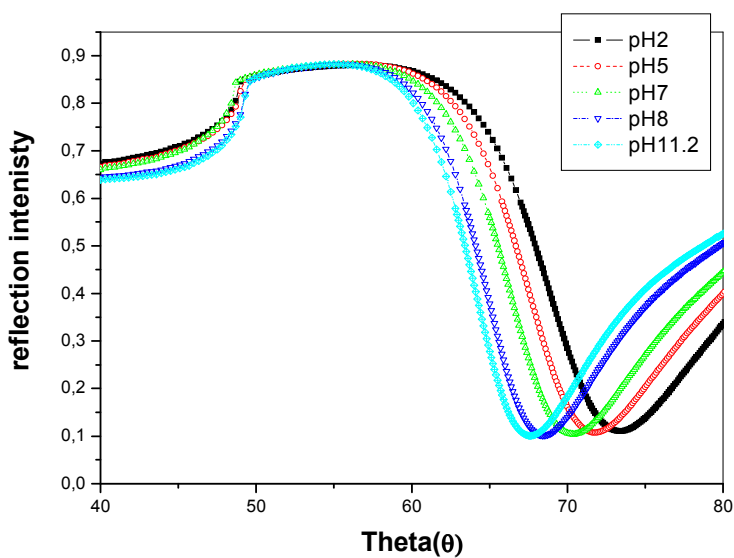


**Figure109:** SPR scan of photo-crosslinked hydrogel layer RI ( $\theta$ ) as pH-dependent for 54-5-10

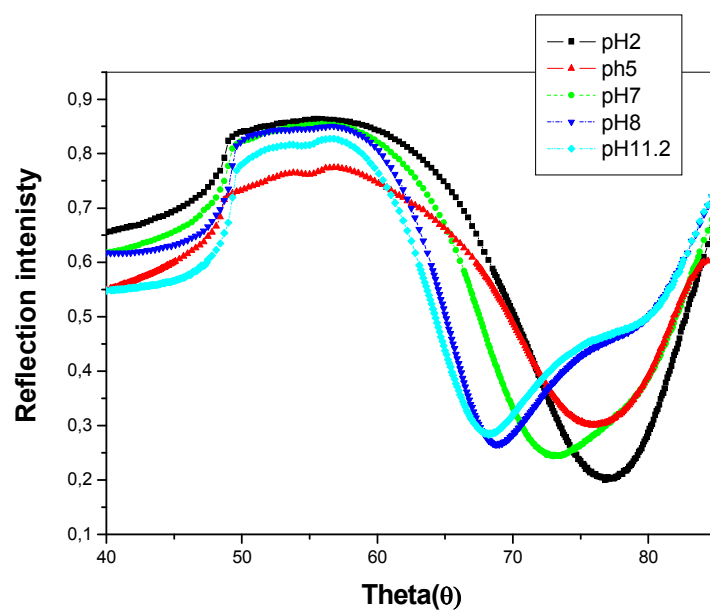


**Figure110:** SPR scan of photo-crosslinked hydrogel layer RI ( $\theta$ ) as pH-dependent for 54-7.5-15.

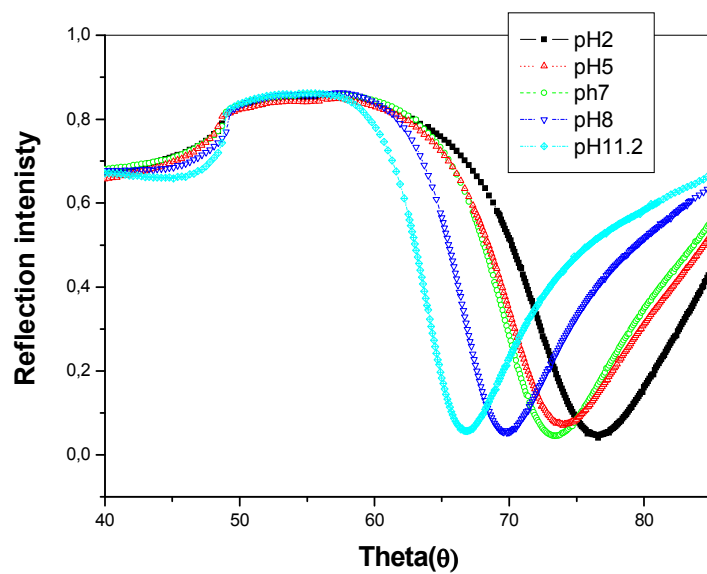


**Figure111:** SPR scan of photo-crosslinked hydrogel layer RI ( $\theta$ ) as pH-dependent for 54-10-20.

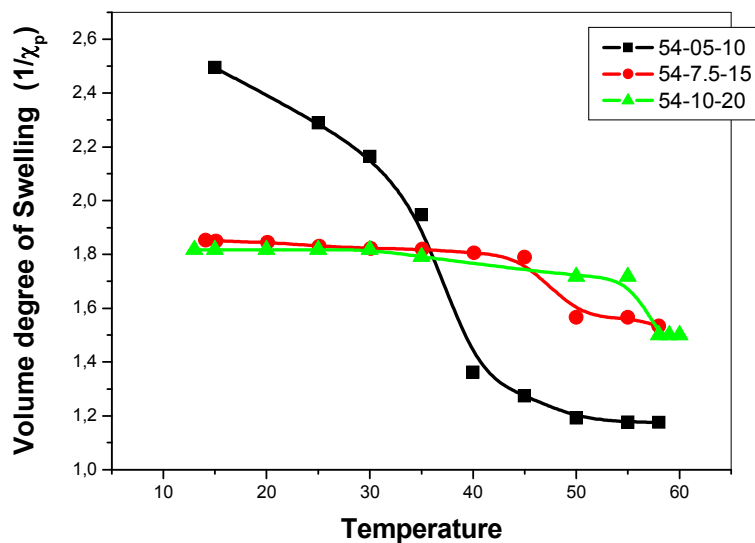


**Figure112:** Volume degree of swelling vs. temperature of photo-crosslinked hydrogel layer for 54.

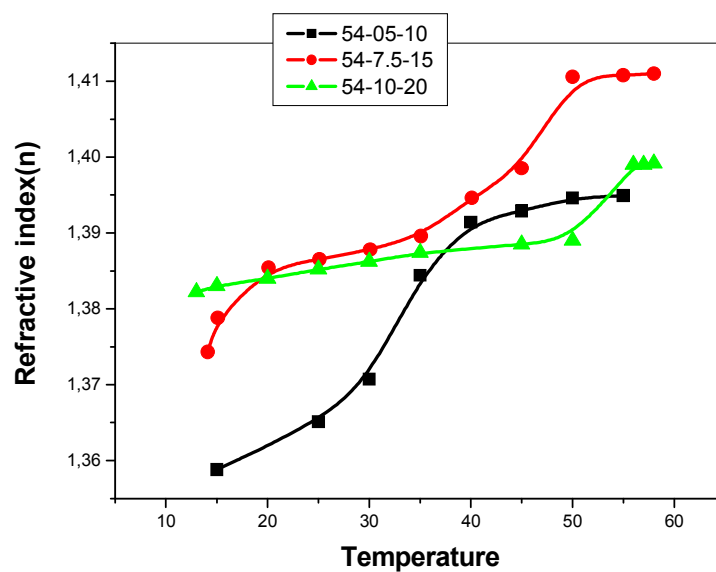


**Figure113:** Refractive index vs. temperature of photo-crosslinked hydrogel layer for 54.

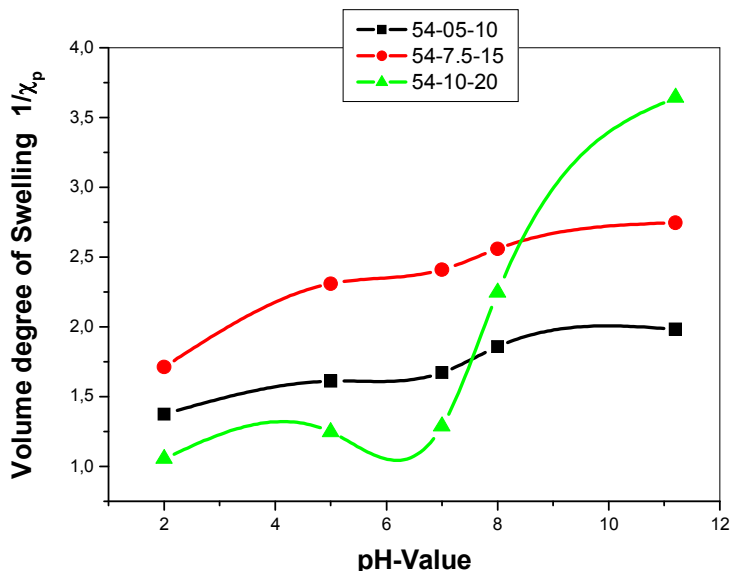


**Figure114:** Volume degree of swelling vs. pH-values of photo-crosslinked hydrogel layer for 54.

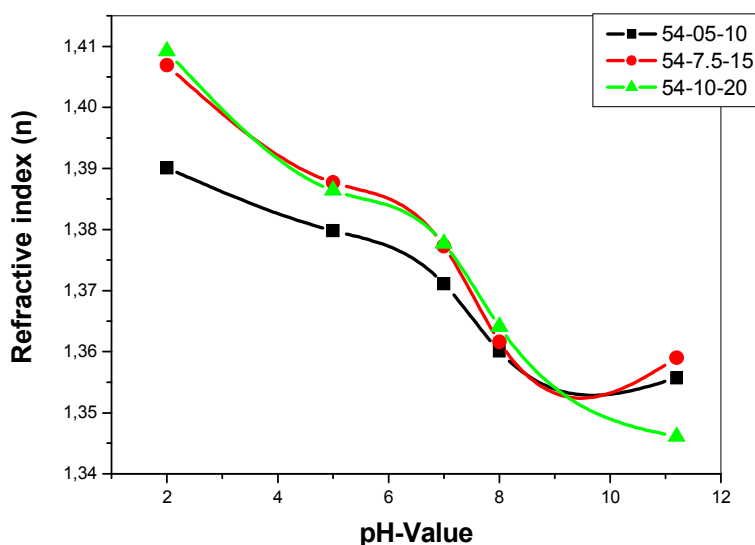


**Figure115:** Refractive index vs. pH-values of photo-cross-liked hydrogel layer for 54.

### 3.6.8. Studying of the conversion of pH-responsive functional hydrogel thin film based on photo-crosslinked P(DMAAm-Co-AHVA-Co-DMIA) to temperature responsive with (UCST).

The first aim of this study was the formation of pH-dependent hydrogels using AHVA with hydrophilic DMAAm. But during our studies we also tried to study the effect of temperature at basic media. We observed that hydrogel showed **upper critical solution temperature (UCST)** behavior, the gel showed highest degree of swelling at the highest temperature and

vice versa for refractive index. In **section 3.5.10.1**, we discussed the turbidity test by UV-vis. Spectroscopy for the polymer solution in acid, neutral and basic media but it did not show any change in the transmittance as temperature changes.

- ❖ **Dry:** The film parameters are summarized in **Table 78**.
- ❖ **Swelling behavior with variations of temperature:** **Figure 116** shows the swelling behavior as a change in RI ( $\theta$ ) as temperature independent in pure water. The volume degree of swelling illustrated nearly no change in volume degree of swelling from  $\sim 1.05$ . Normally the film should swell due to the hydrophilic DMAAm but, the hydrophobic character of the AHVA prevent the film from swelling.
- Swelling behavior with variations of pH values:** The pH-dependent of the hydrogel film is attributed to the presence of functional groups; carboxyl group. **Figure117** shows the swelling behavior as change in RI ( $\theta$ ). **Figure119** shows the volume degree of swelling and refractive index as pH-dependent due to the reversible transition of the carboxylic group from uncharged (pH2) to charged (pH12).
- ❖ **Swelling behavior with variations of temperature at pH 12.5;** the swelling was investigated by SPR and using pH 12.5 buffer solution. **Figure118** shows the swelling behavior of the hydrogel layers.

The UCST was determined from the volume degree of swelling and refractive index at pH 12.5 as shown in **Figure120**  $T_c$  at the midpoint of the straight part of the curve was  $T_c \sim 40^\circ\text{C}$ . The charged carboxylic groups can interact with the polar amide groups leading to small swelling. At elevated temperatures the hydrogen bonding can be overcome resulting in higher swelling ratio.

**Table 78:** Illustrate thickness, dielectric and refractive indices of dry state.

Polymer	Dry Thickness (nm)	Dielectric ( $n^2 = \epsilon$ )	$n = \sqrt{\epsilon}$
55-10-10	196	2.23	1.4933

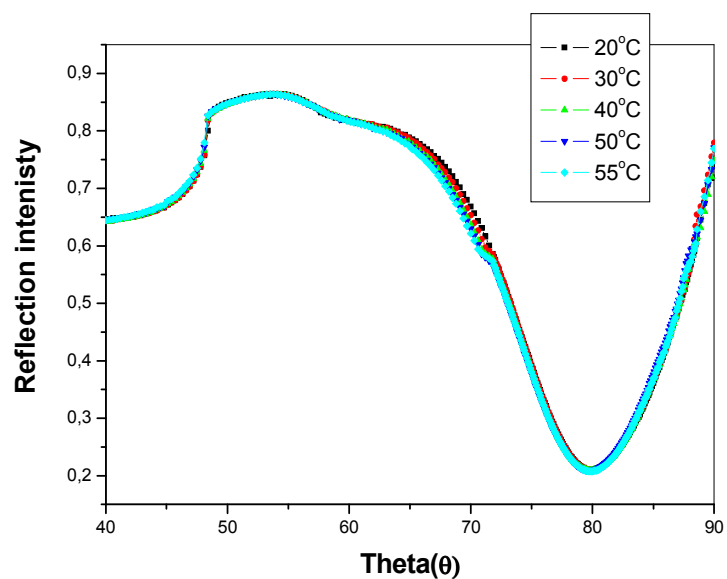


**Figure116:** SPR scan of photo-crosslinked hydrogel layer RI ( $\theta$ ) as temperature dependent for 57-10-20.

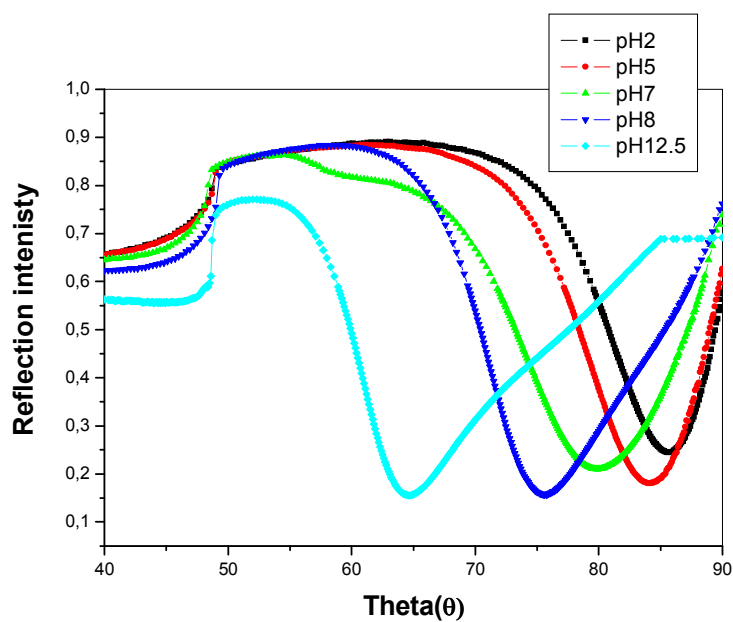


**Figure117:** SPR scan of photo-crosslinked hydrogel layer RI ( $\theta$ ) as pH-dependent for 55-10-10.

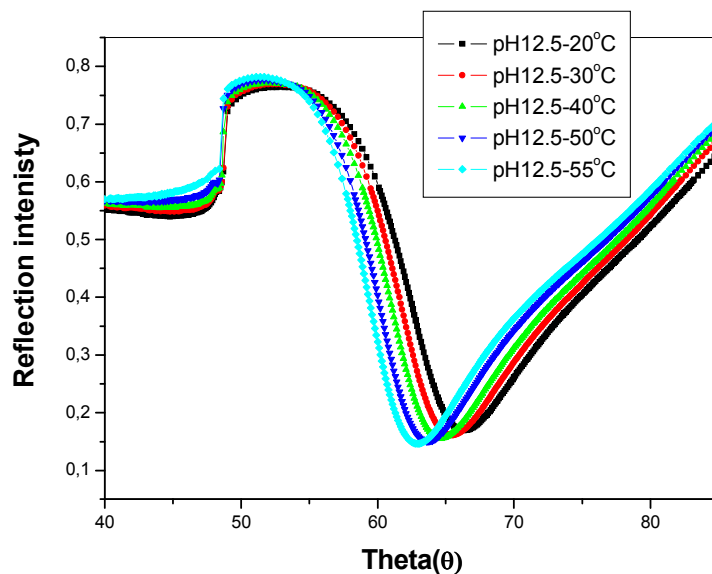


**Figure 118:** SPR scan of photo-crosslinked hydrogel layer RI ( $\theta$ ) as temperature-dependent at pH12.5 for 55-10-10.

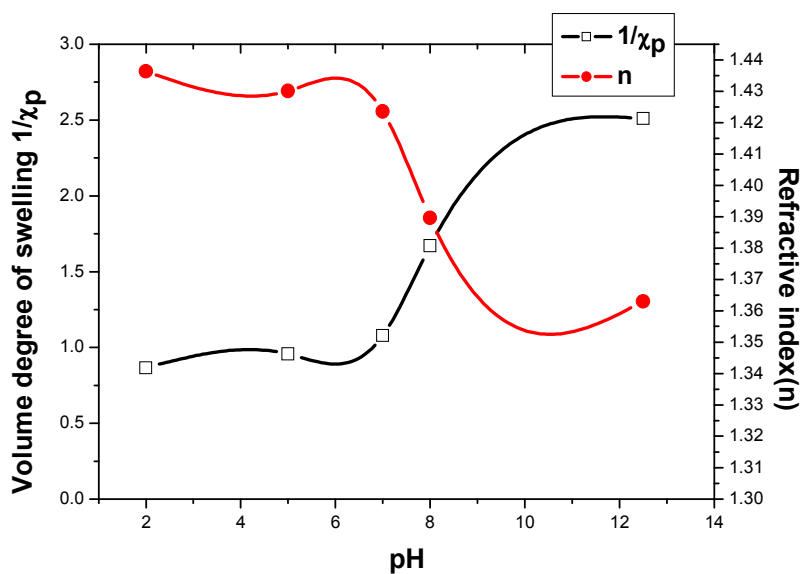


**Figure119:** The volume degree of swelling and refractive index vs. pH-values of photo-crosslinked hydrogel layer for 55-10-10.

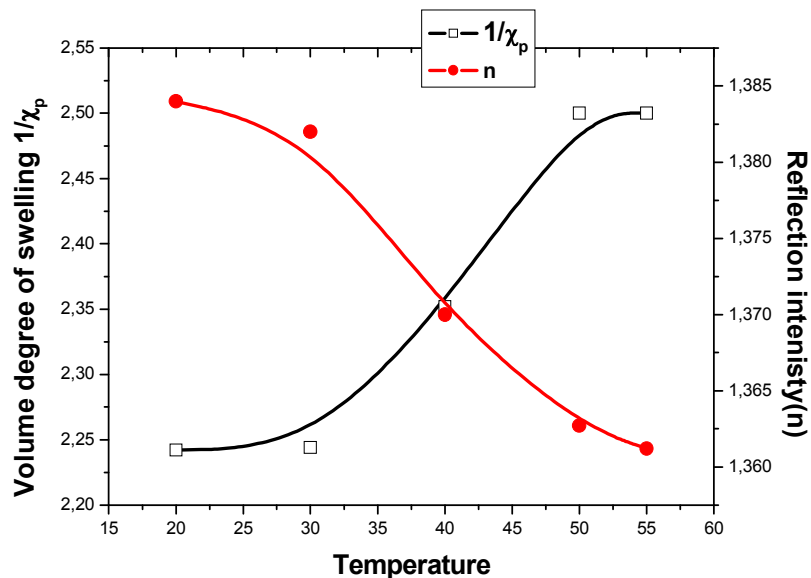


**Figure120:** The volume degree of swelling and refractive index vs. temperature dependent at pH 12.5 of photo-crosslinked hydrogel layer for 55-10-10.

### 3.6.9. Conversion of (T, pH) - dual responsive with LCST to (T, pH)-dual responsive (UCST) functional hydrogel thin film based on photo-crosslinked P(NIPAAm-*Co*-AHVA-*Co*-DMIA), using SPR/OWS for swelling characterization.

As known PNIPAAm and its copolymers in solution have lower critical solution temperature behavior due to the interaction between hydrophobic and hydrophilic moiety in the polymer chains. In this study the incorporation of functional monomer to the photo-crosslinked polymer led to the formation of hydrogels with LCST and UCST behavior depending on pH values.

**Dry:** Parameters are summarized in **Table79**.

❖ **Swelling behavior with variations of temperature:** **Figure121** shows the swelling behavior as temperature independent. The volume degree of swelling and refractive index, showed nearly no change in volume degree of swelling of  $\sim 1.6$  and the refractive indices  $\sim 1.43$  RIU.

**Swelling behavior with variations of pH values:** **Figure122** and **Figure123** show the volume degree of swelling and refractive index as pH-dependent. With increasing the pH the surface became more hydrophilic as changed from an uncharged to charged state.

**Swelling behavior with variations of temperature at pH 11.2;** the swelling was investigated by SPR using pH 11.2 buffer solution. **Figure123** shows temperature dependent.

**The UCST** was determined from the volume degree of swelling and refractive index as temperature dependent at pH 11.2, as shown in **Figure 125**, shows  $T_c \sim 37^\circ\text{C}$  at the midpoint of the straight part of the curve.

**Table 79:** Illustrate thickness, dielectric and refractive indices of dry state.

Polymer	Dry Thickness (nm)	Dielectric ( $n^2 = \epsilon$ )	$n = \sqrt{\epsilon}$
56-10-20	185	2.121	1.4563

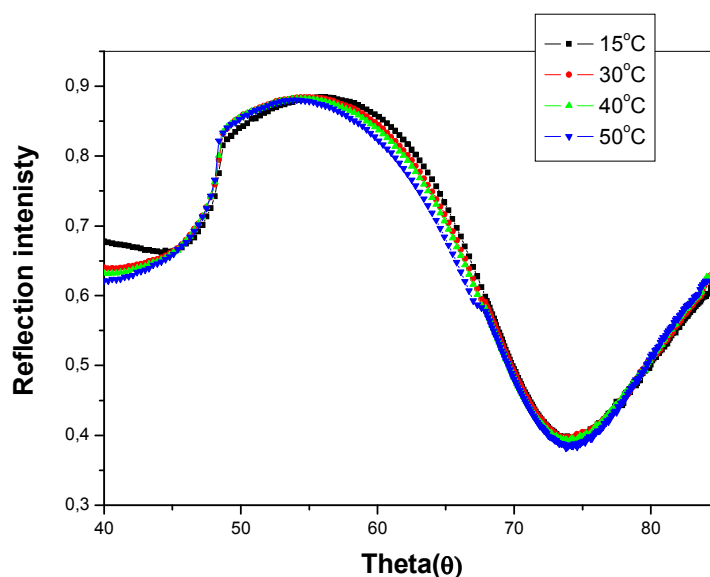


**Figure121:** SPR scan of photo-crosslinked hydrogel layer RI ( $\theta$ ) as temperature-dependent for 58-10-10.

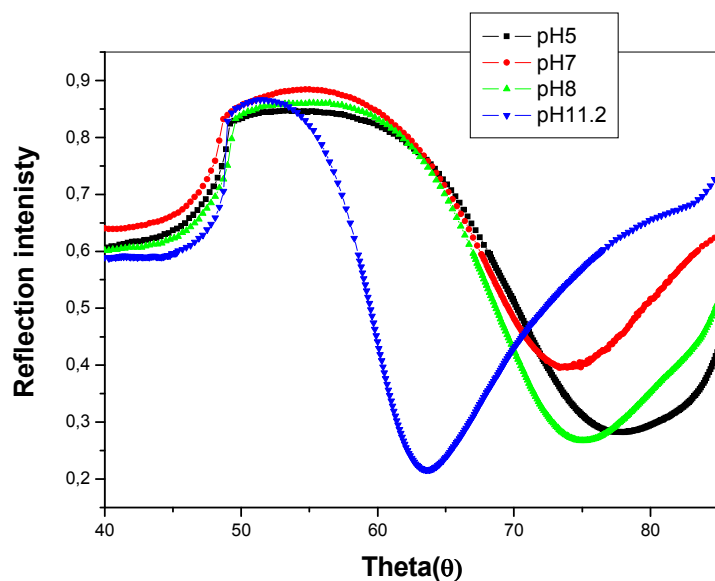


**Figure122:** SPR scan of photo-crosslinked hydrogel layer RI ( $\theta$ ) as pH-dependent for **56-10-10**.

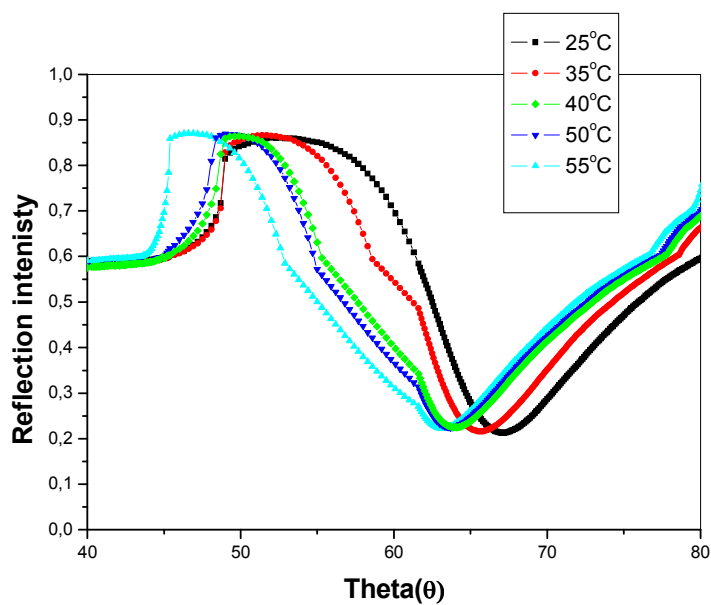


**Figure123:** SPR scan of photo-crosslinked hydrogel layer RI ( $\theta$ ) as temperature-dependent at pH11.2 for **56-10-10**.

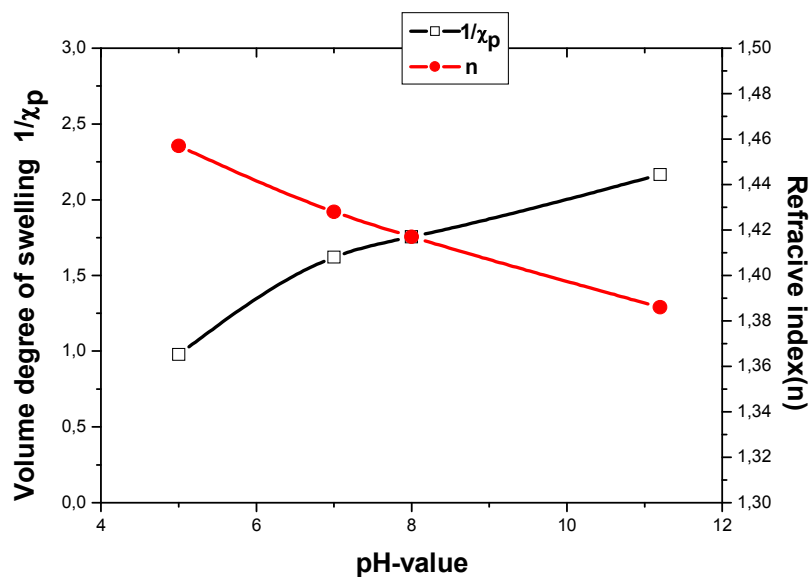


**Figure124:** The volume degree of swelling and refractive index vs. pH of photo-crosslinked hydrogel layer for 56-10-10.

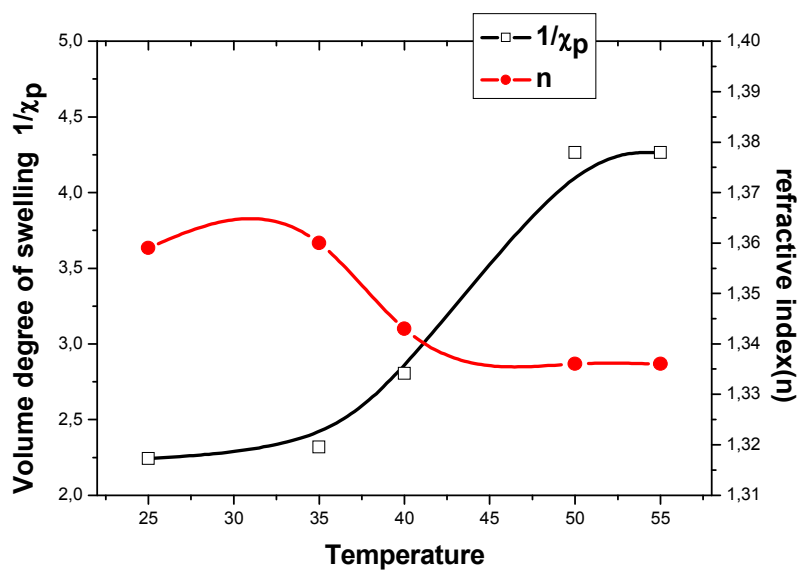


**Figure125:** The volume degree of swelling and refractive index vs. temperature dependent at pH 11.2 of photo-crosslinked hydrogel layer for 56-10-10.

### 3.7. Photo-crosslinked hydrogel bilayer.

*D. Kuckling et al.*<sup>(226)</sup> have been prepared two hydrogel layers based on photo-crosslinkable PDMAAm as base layer and PNIPAAm as top layer forms a bilayer assembly, where the base layer is highly swollen and the top layer shows temperature responsive swelling. Swelling characterization has been done using a combination of surface plasmon resonance spectroscopy and optical waveguide spectroscopy. The PDMAAm and PNIPAAm within the bilayer assembly retain their swelling behavior which they showed as a separate layer.

Hence, after studying the swelling behavior of single layers, we focus on the formation of hydrogel bilayer to describe the combination effect on each layer separately. The main advantage in this case is the interpretation the difference in the swelling behavior as hydrogel single layer and bilayer.

#### 3.7.1. Hydrogel bilayer based on T-responsive as base layer (A) and non-sensitive upper layer (B).

The photo-crosslinked P(NIPAAm-Co-DMIAAm) used as T-responsive base layer and P(DMAAm-Co-DMIAAm) as a non-responsive upper layer as Layer A+B. The first layer was discussed in detail in **section 3.6.2.3**.

The combination of Layer A+ B will be discussed in detail as follow.

- ❖ **Dry:** A solution of 7.5 wt% of photo-crosslinkable 5 mol% P(DMAAm-Co-DMIAAm) in cyclohexanone and were spin coated over **layer A** which consist of [Au + AP + P(NIPAAm-Co-DMIAAm)] at 2000 rpm. SPR/OWS was used for the thickness determination of the dry bilayer set up. **Figure 126** shows the scan of RI ( $\theta$ ) illustrating the presence of ATR at 22° and two waveguide modes at 23° and at 48°, which showed the formation of homogeneous films. The thickness and refractive index was estimated by Fresnel calculation for a model of the dry bilayer film yielding a thickness of 292.3 nm, and ~1.47 RIU (see **Table85** and **Figure 127,128**).
- ❖ **Swelling behavior with variations of temperature for layer A+B:** The swelling was investigated by SPR/OWS, using DI water. **Figure 128** shows the swelling behavior as a change in RI ( $\theta$ ). The change of waveguide modes was discussed by Knoll *et al.* demonstrating that the higher order waveguide modes being found at lower incident angles are more sensitive to thickness changes while the lower order waveguide modes located at higher incident angles are sensitive to refractive index change<sup>(75)</sup>. Moreover the displacement of the plasmon minimum from ~ 65.5° to ~ 68° as changed from swollen to

collapsed states respectively. The Fresnel calculations used for the estimation of the volume degree of swelling and refractive index for each layer gave the following results;

- ❖ **Layer A:** The change in the volume degree of swelling and the refractive indices are temperature responsive performed  $1/\chi_p \sim 3.8$ , 1.386 RIU and  $\sim 2.7$ ,  $\sim 1.41$  RIU for 15°C and 55°C respectively as shown in **Figure 129**.
- ❖ **Layer B:** The volume degree of swelling and the refractive indices are temperature independent  $1/\chi_p \sim 1.8$ , 1.386 RIU as shown in **Figure 130**.

**General features:** It was observed from the information of the double layer provided each layer separately in a comparison with single layer that the volume degree of swelling  $1/\chi_p$  of single layer to layer A at lower temperature 15°C shows 3.9 and 3.8 for single and double layer respectively and vice versa at 55°C performed 1.05 and 2.8 for single and layer A respectively. The slight difference at low temperature was affected on the second layer which rather effect in the physisorbed of the first layer. On the other hand the big difference at higher temperature, performed collapsed state, might be attributed to the formation of double layer lead to increase in the film thickness, and the presence of temperature independent layer is responsible in the formation of wetting in the upper surface which prevents the formation of full collapsed state <sup>(312,313)</sup>. The smaller displacement of Plasmon minima of layer A in DL system than single layer system due to the same reason. Finally, these were proved by the higher value of  $T_c$  in the double layer system than single one which showed 34°C and 29°C for double and single layer respectively.

**Table 80:** The Fresnel calculations of double layers system illustrate thickness, dielectric and refractive index.

<b>Polymer</b>	<b>Dry Thickness (nm)</b>	<b>Dielectric (<math>n^2 = \epsilon</math>)</b>	<b><math>n = \sqrt{\epsilon}</math></b>
<b>Single layer</b>	275.0	2.0900	1.4450
<b>Layer A</b>	275.0	2.1453	1.4628
<b>Layer B</b>	282.3	2.1622	1.4700

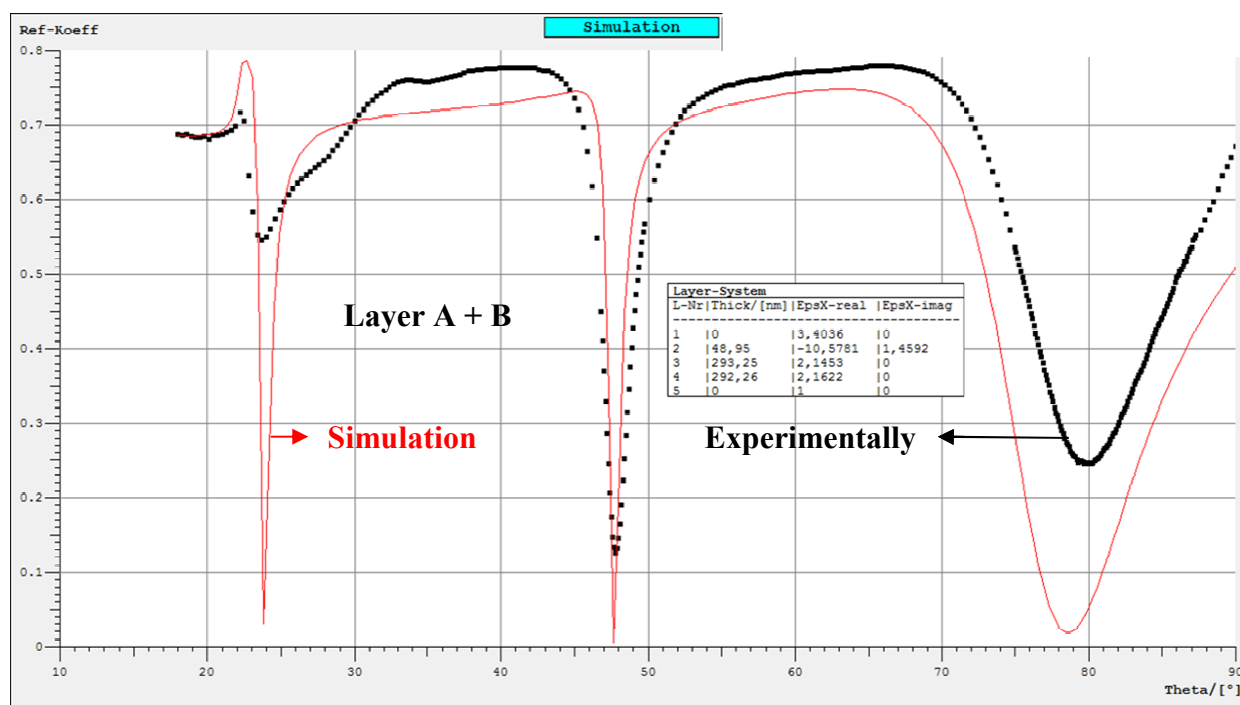


**Figure126:** SPR scan of photo-crosslinked hydrogel layer RI ( $\theta$ ) experimental (■) and simulation (—) and Fresnel calculation in the model box for the dry film thickness of Layer A+B.

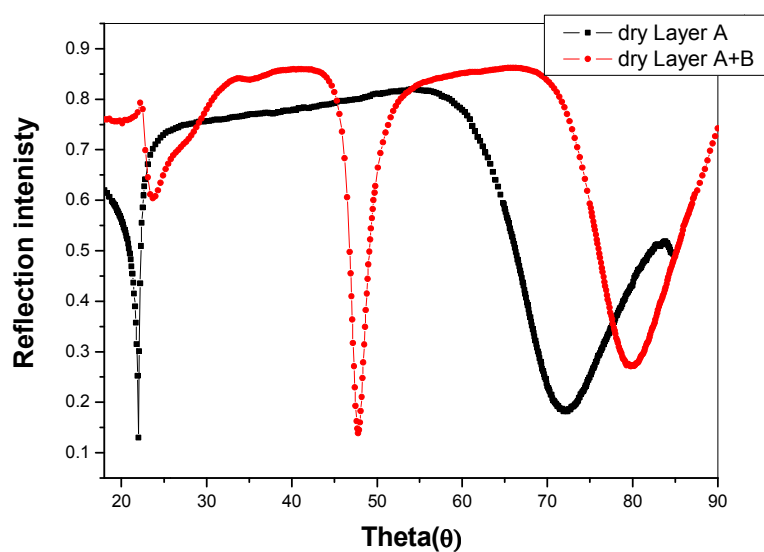


**Figure 127:** SPR scan of photo-crosslinked hydrogel single 46-05 (■) and bilayer (●) RI ( $\theta$ ) for dry cases.

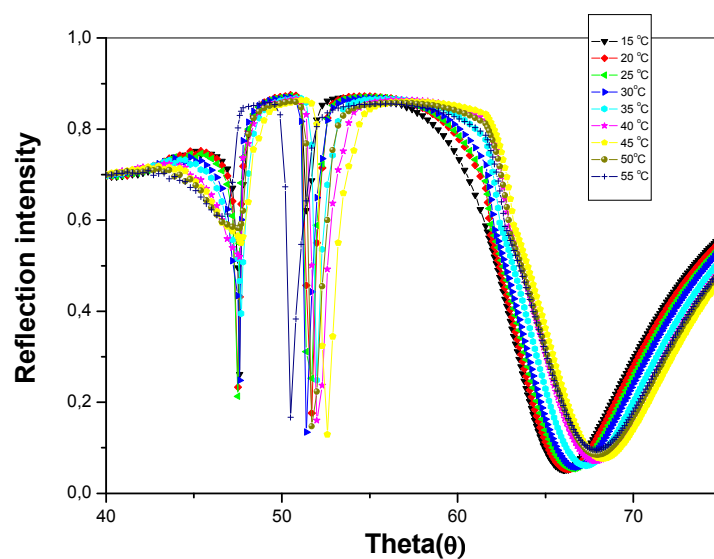


**Figure128:** SPR scan of photo-crosslinked hydrogel bilayer RI ( $\theta$ ) in dependence of temperature.

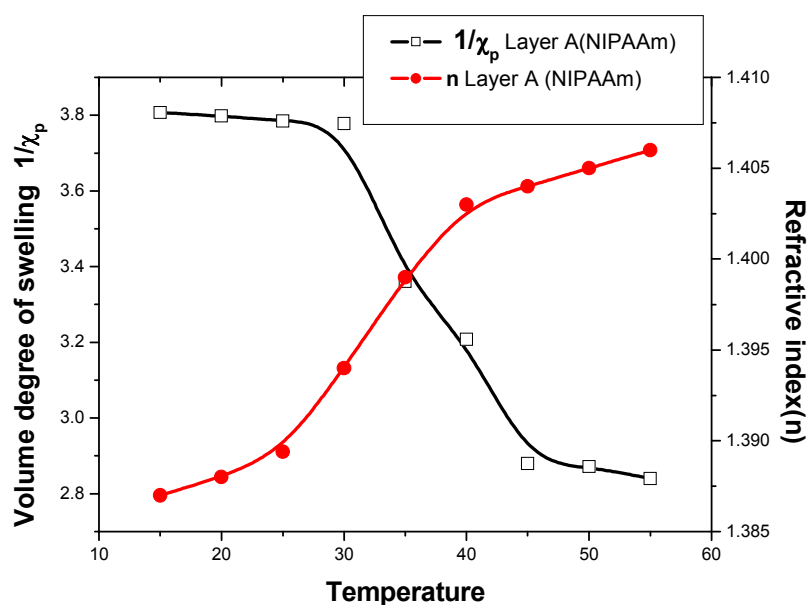


**Figure 129:** The volume degree of swelling and refractive index vs. temperature of photo-crosslinked hydrogel bilayer for layer A.

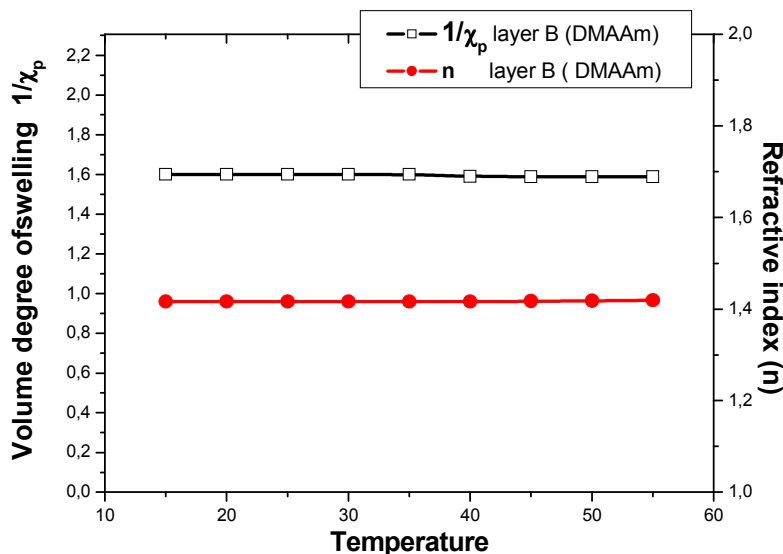


**Figure 130:** The volume degree of swelling and refractive index vs. temperature of photo-crosslinked hydrogel bilayer for layer B

### 3.7.2. Hydrogel bilayer based on non responsive as base layer (A) and T-responsive in the upper layer (B).

To further study the effects on responsive/non-responsive bilayer systems, we reversed the process of bilayer formation consisting of photo-crosslinked P(DMAAm-Co-DMIAAm) as non-responsive base layer and P(NIPAAm-Co-DMIAAm) as T-responsive upper layer as Layer A+B. The first layer was discussed in detail in **section 3.6.4**.

The combination of Layer A+ B will be discussed in detail as follow;

- ❖ **Dry:** A solution of 7.5 wt% of photo-crosslinked 5 mol% P(NIPAAm-Co-DMIAAm) in cyclohexanone and were spin coated over **layer A** which consist of (Au + AP + P(DMAAm-Co-DMIAAm) at 2000 rpm. **Figure 131** shows the scan of RI ( $\theta$ ) illustrating the presence of ATR at  $22^\circ$  and two waveguide modes at  $27^\circ$  and at  $51.5^\circ$  which is attributed to the formation of homogeneous film thickness. Additional waveguide mode at higher scan angle indicated the increase in the film thickness. The Plasmon minima was at  $\sim 82.5^\circ$ . The thickness and refractive index was estimated by Fresnel calculation for a model of the dry bilayer film giving 299 nm, and  $\sim 1.47$  RIU for layer A and 311nm corresponding to 1.51RIU. The total layer thickness should be the sum of Layers A+B producing 610 nm. (See **Table 81** and **Figure 131**).
- ❖ **Swelling behavior with variations of temperature for layer A+B:** **Figure 132** shows the swelling behavior as a change in RI ( $\theta$ ).

- ❖ **Layer A:** The volume degree of swelling and the refractive indices are temperature independent performed  $1/\chi_p \sim 3.7$ , 1.39 RIU as shown in **Figure 133**.
- ❖ **Layer B:** The volume degree of swelling and the refractive indices are temperature responsive:  $1/\chi_p \sim 3.4$ , 1.37 RIU and  $\sim 1.2$ ,  $\sim 1.48$  RIU for 15°C and 55°C respectively as shown in **Figure 134**.
- ❖ **General features:** The volume degree of swelling  $1/\chi_p$  of single layer to layer A of double layer system shows 3.72 and 3.7 for single and double layer respectively. The slight difference can be neglected. Finally,  $T_c$  in the double layer system was higher than single one which showing 35°C for layer B.
- ❖ **From 3.7.1 and 3.7.2:** It is important to discuss the difference of the formation of bilayer hydrogel based on sensitive/non-sensitive or non-sensitive/sensitive order. It was observed that  $T_c$  is higher for the bilayer system than  $T_c$  for single layer due to the affection of the second layer. The great advantage was achieved in the case of sensitive/non-sensitive the sensitive layer was attached directly to the substrate. It illustrated a change in the volume degree of swelling attributed to the sensitivity of the first layer to temperature with respect to non sensation of the second layer; therefore the upper surface was kept wetted. This also affected directly in the formation of completely collapsed state <sup>(312,313)</sup>.

**Table 81:** The Fresnel calculations of double layers system illustrate thickness, dielectric and refractive index.

Polymer	Dry Thickness (nm)	Dielectric ( $n^2 = \epsilon$ )	$n = \sqrt{\epsilon}$
Layer A	299	2.184	1.477
Layer B	311	2.280	1.509

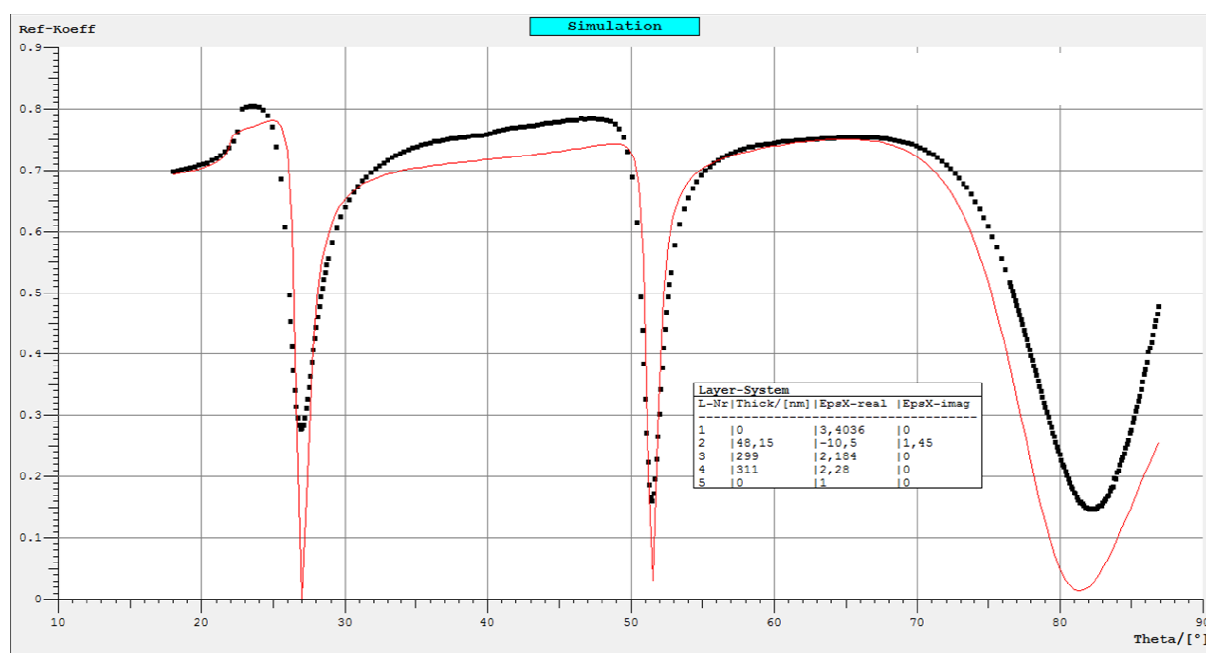


**Figure 131:** SPR scan of photo-crosslinked hydrogel layer RI ( $\theta$ ) as experimentally ( $\blacksquare$ ) and simulation ( $\text{—}$ ) and Fresnel calculations in the model box for the dry film thickness of Layer A+B (47-05 and 46-05).

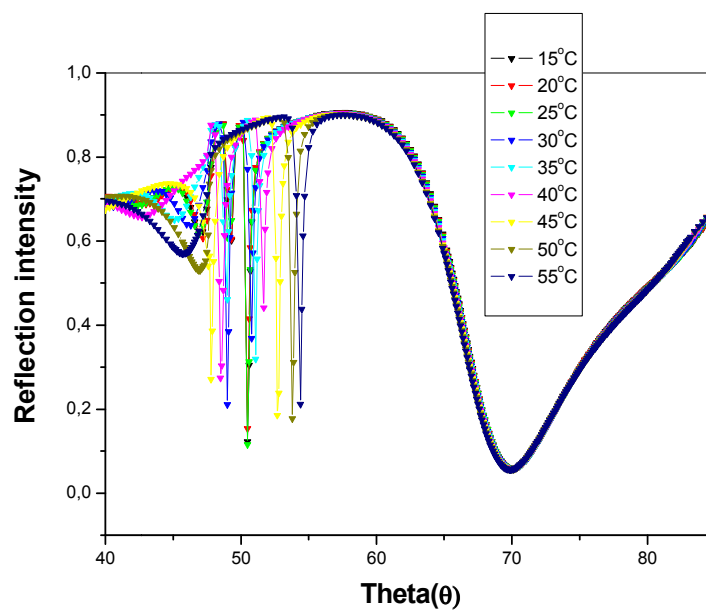


**Figure 132:** SPR scan of photo-crosslinked hydrogel bilayer RI ( $\theta$ ) with temperature variations.

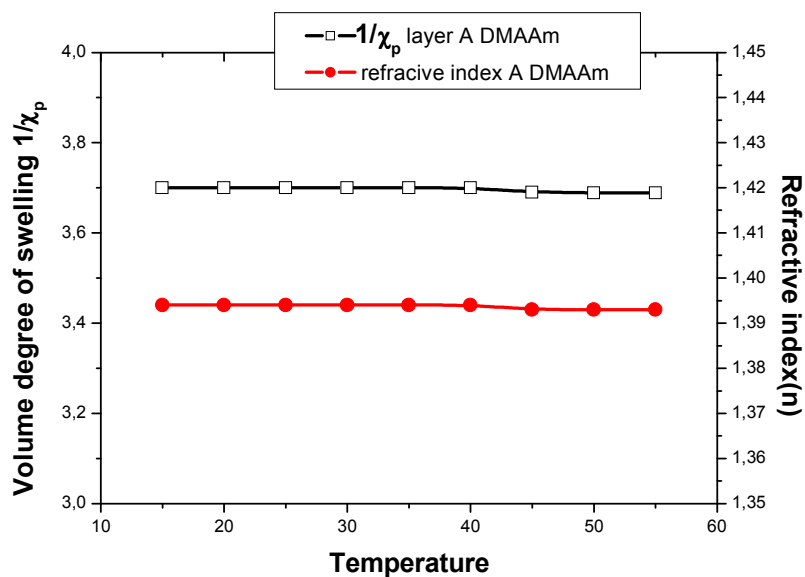


**Figure 133:** The volume degree of swelling and refractive index vs. temperature of photo-crosslinked hydrogel bilayer for layer A.

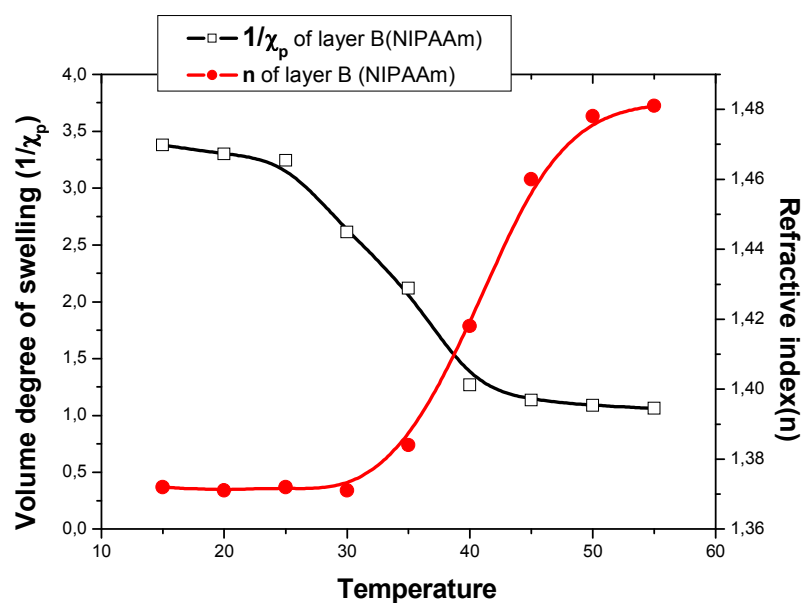


**Figure 134:** The volume degree of swelling and refractive index vs. temperature of photo-crosslinked hydrogel bilayer for layer B.

### 3.7.3. Formation of hydrogel bilayer based on non-sensitive P(DMAAm-Co-DMIAAm) as base layer (A) and pH-responsive (P(DMAAm-Co-DEAMVA-DMIAAm) as upper layer (B).

Bilayer hydrogel thin film was achieved by combining nonresponsive lower layer and pH-responsive top layer of P(DMAAm-Co-DEAMAm-DMIAAm). SPR/OWS were used in the swelling characterization of the crosslinked hydrogel.

**Dry:** A solution of 5 wt% of 5 mol% P(DMAAm-Co-DEAMVA-DMIAAm) in cyclohexanone and was spin coated over **layer A** which consist of (Au + AP + P(DMAAm-Co-DMIAAm) at 3000 rpm. The dry bilayer film was 154 nm and ~1.43 RIU for layer A and 140 nm corresponding to 1.45RIU (**Table 82**).

❖ **Swelling behavior as pH-dependent for Layer A:** The swelling characterizations demonstrated a non responsive behavior. The swelling was ~3 and refractive index 1.38 RIU.

❖ **Swelling behavior as pH-dependent for DL A+B:** The pH-dependence of the hydrogel bilayer system is attributed to the presence of protonated amino group of DEMAVA in Layer B. **Figure 135** shows the swelling behavior as pH-dependent. The unexpected increase of the degree of swelling has been discussed in **section 3.6.7**. (**Figure 137**).

❖ **Layer A:** No change in the volume degree of swelling and the refractive indices were pH independent was observed:  $1/\chi_p \sim 3.12$ , 1.4 RIU (**Figure 136**).

**Layer B:** The volume degree of swelling and the refractive indices were pH dependent (**Figure 137**).

**Table 82:** The Fresnel calculations of double layers system illustrate thickness, dielectric and refractive index.

Polymer	Dry Thickness (nm)	Dielectric ( $n^2 = \epsilon$ )	$n = \sqrt{\epsilon}$
Layer A	154	2.057	1.434
Layer B	140	2.110	1.452

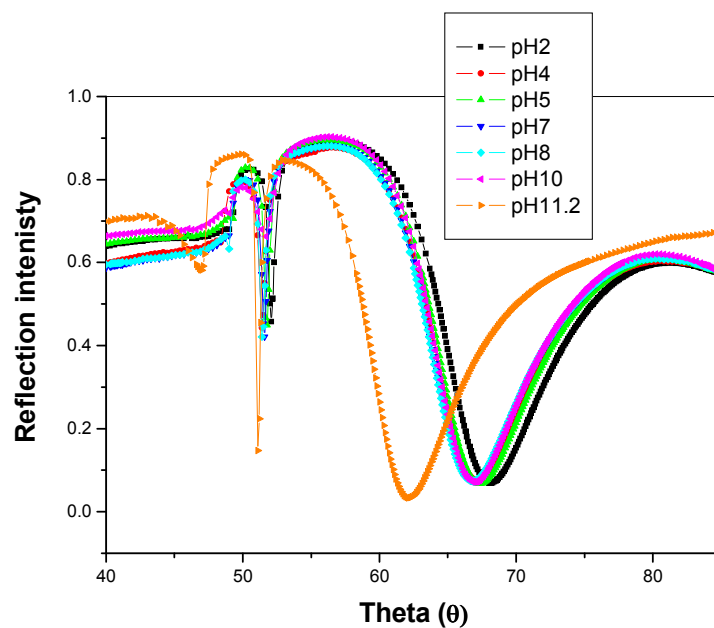


**Figure 135:** SPR scan of photo-crosslinked hydrogel bilayer RI ( $\theta$ ) with pH variations (47-05 and 52-05-10).

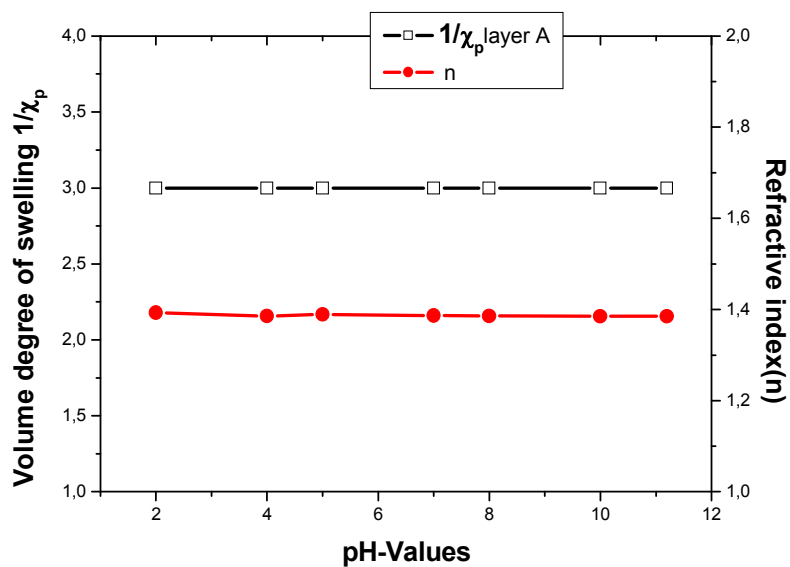


**Figure 136:** The volume degree of swelling and refractive index vs. pH of photo-crosslinked hydrogel bilayer for layer A (47-05).

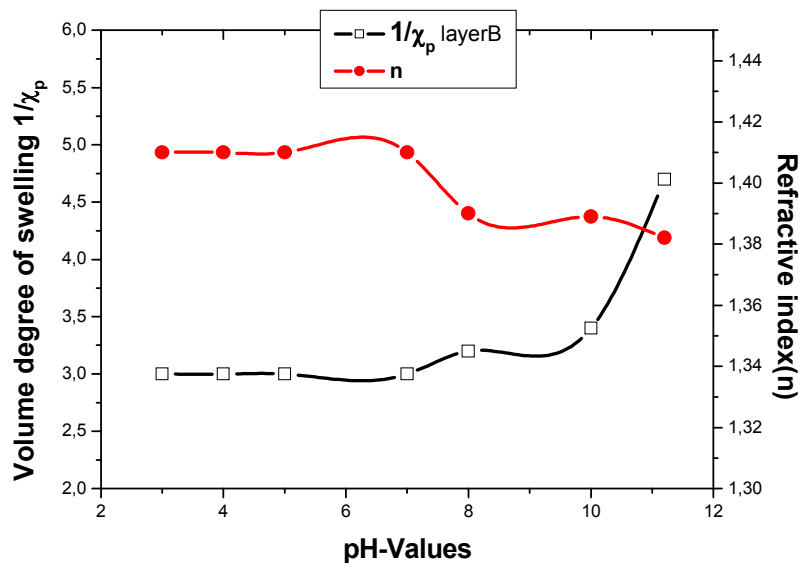


**Figure 137:** The volume degree of swelling and refractive index vs. pH of photo-crosslinked hydrogel bilayer for layer B (52-05-10).

### 3.7.4. Hydrogel bilayer based on dual (T, pH)-responsive P(NIPAAm-Co-DEAMVA-Co-DMIAAm) as base layer (A) and non-responsive P(DMAAm-Co-DMIAAm) as upper layer (B).

The formation of bilayer hydrogel based on dual response in temperature and pH was used as base layer and also DMAAm polymer was used in the formation of the non sensitive layer. The first layer was discussed in **section 3.5.8**. The effect of pH on  $T_c$  and swelling was pH-dependent, and also T-dependent.

- ❖ **Dry :** A solution of 7.5 wt% of 5 mol% P(DMAAm-Co-DMIAAm) in cyclohexanone were spin coated over **layer A** which consist of (Au + AP + P(NIPAAm-Co-DEAMVA-Co-DMIAAm)) at 2000 rpm. **Figure 138** shows the scan of RI ( $\theta$ ). The thickness and refractive index were performed 170 nm and ~1.48 RIU for layer A and 380 nm corresponding to 1.53RIU. The total thickness should be the sum of Layers A+B and was 550 nm (**Table 83 and Figure138**).
- ❖ **Swelling behavior with variations of temperature for DLA+B in DI:** **Figure147** shows the swelling behavior as a change in RI ( $\theta$ ) was a temperature dependent.
- ❖ **Layer A:** The volume degree of swelling and the refractive indices were temperature dependent showing at 15°C as highly swollen state  $1/\chi_p \sim 2.6$ , 1.4 RIU, while at 58°C higher temperature  $1/\chi_p \sim 1.6$ , 1.44 RIU (**Figure 142**).
- Layer B:** The volume degree of swelling and the refractive indices were temperature independent performed nearly for all  $1/\chi_p \sim 1.85$ , 1.45 RIU as shown in **Figure 142**.

**Figure 150** shows the volume degree of swelling and refractive index vs. temperature for each layer separately, illustrating the non sensitivity of layer B and the sensation of layer A with temperature. The  $T_c$  demonstrated higher value of  $\sim 44.3^\circ\text{C}$  than the single layer that demonstrated  $\sim 36.7^\circ\text{C}$ . Moreover, the presence of non responsive layer as a second layer affected directly on the formation of incompletely collapsed state.

- ❖ **Swelling behavior as pH-dependent for DLA+B:** **Figure 140** shows the swelling behavior as pH-dependent. **Figure 151** illustrated the volume degree of swelling and refractive index as pH-dependent and demonstrated the highest ( $1/\chi_p$ ) and lowest ( $n$ ) at pH11.2 as basic dielectric media.

**Layer A:** The volume degree of swelling and the refractive indices were pH dependent. At pH11.2 as highly swollen state with  $1/\chi_p \sim 3.12$ , and 1.39 RIU while at  $58^\circ\text{C}$  the swelling decreased to  $1/\chi_p \sim 1.7$ . 1.43 RIU as shown in **Figure 143**.

**Layer B:** The volume degree of swelling and the refractive indices as temperature independent were nearly for all  $1/\chi_p \sim 2.1$ . 1.45 RIU as shown in **Figure 143**.

- ❖ **Swelling behavior with variations of temperature for DLA+B in pH2:** **Figure 141** shows the swelling behavior a temperature dependent.

**Layer A:** The volume degree of swelling and the refractive indices were temperature dependent showing at  $20^\circ\text{C}$  as highly swollen state  $1/\chi_p \sim 1.7$ , 1.43 RIU as while at  $58^\circ\text{C}$   $1/\chi_p \sim 1.04$ , and 1.45 RIU as shown in **Figure 144**. The  $T_c$  was observed at  $\sim 41^\circ\text{C}$  lower than the previous case attributed to the hydrogel behavior of pH2.

**Layer B:** The volume degree of swelling and the refractive indices were temperature independent performed nearly for all  $1/\chi_p \sim 2.1$ , and 1.45 RIU.

- ❖ **Swelling behavior with variations of temperature for DLA+B of pH11.2:**

- ❖ **Layer A:** Almost no observed change in the volume degree of swelling and the refractive indices as temperature increased from  $20^\circ\text{C}$  to  $55^\circ\text{C}$  ( $1/\chi_p \sim 3.12$ . 1.39 RIU). The reason of this is the behavior of hydrogel in the dielectric as; at pH11.2 the dielectric has negatively and facilitate in the migration of the proton of the tertiary amine to the surface performing highly charged surface, further producing highly swollen state for that reason the expected LCST should be higher than the temperature region allowed to use in SPR technique (**Figure 143**).

**Layer B:** The volume degree of swelling and the refractive indices were temperature independent performed nearly for all  $1/\chi_p \sim 2.1$ . 1.45 RIU (**Figure 142**).

**Table 83:** The Fresnel calculations of double layers system illustrate thickness, dielectric and refractive index.

Polymer	Dry Thickness (nm)	Dielectric ( $n^2 = \epsilon$ )	$n = \sqrt{\epsilon}$
Layer A	170	2.2	1.483
Layer B	380	2.35	1.532

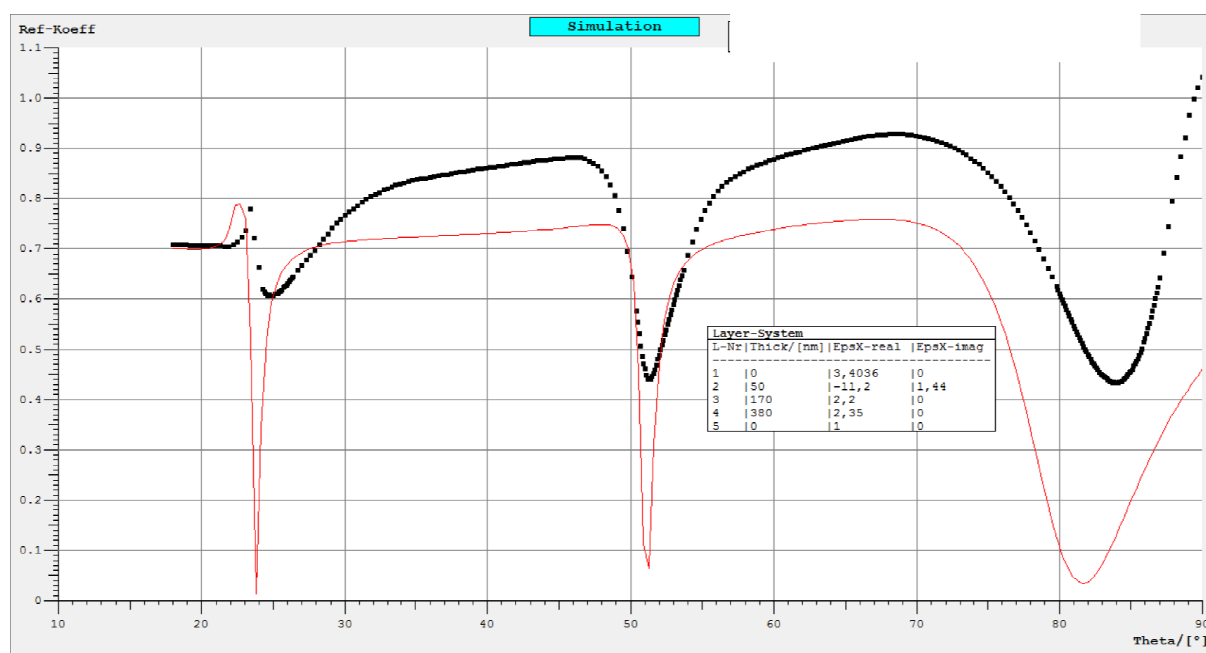


**Figure 138:** SPR scan of photo-cross-liked hydrogel layer RI ( $\theta$ ) as experimentally (■) and simulation (—) and Fresnel calculations in the model box for the dry film thickness of Layer A+B (54-05-10 and 47-05).

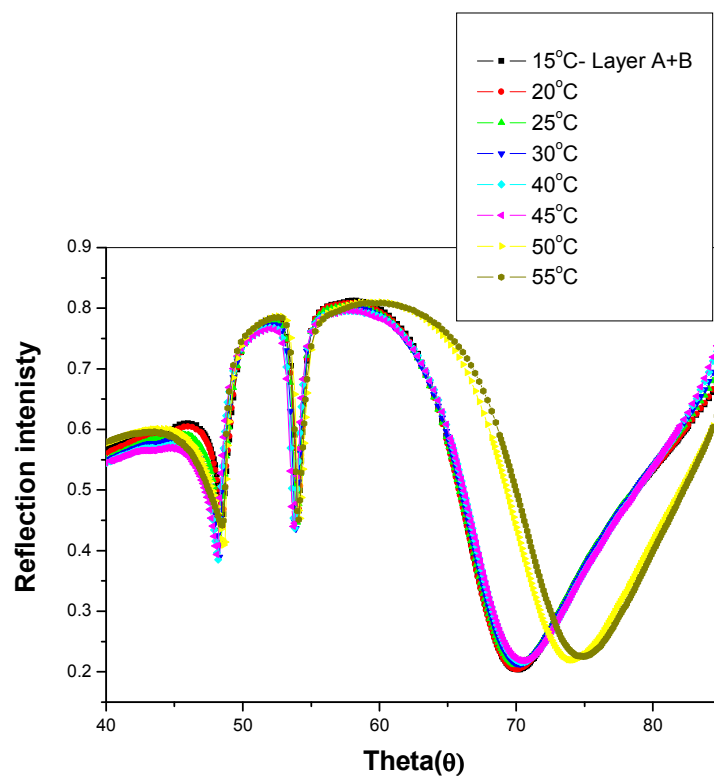


**Figure 139:** SPR scan of photo-crosslinked hydrogel bilayer RI ( $\theta$ ) with temperature variations of bilayer (54-05-10 and 47-05).

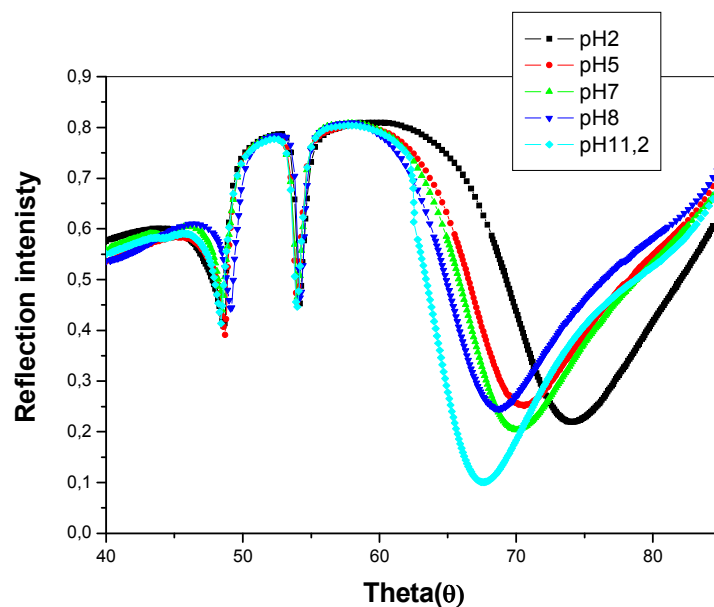


**Figure 140:** SPR scan of photo-crosslinked hydrogel bilayer RI ( $\theta$ ) with pH variations of bilayer (54-05-10 and 47-05).

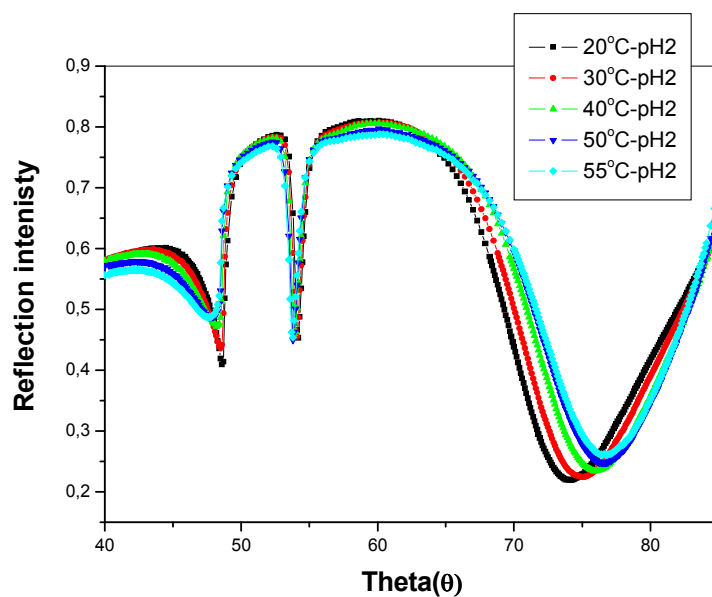


**Figure 141:** SPR scan of photo-crosslinked hydrogel bilayer RI ( $\theta$ ) with temperature variations of bilayer in pH2 (54-05-10 and 47-05).

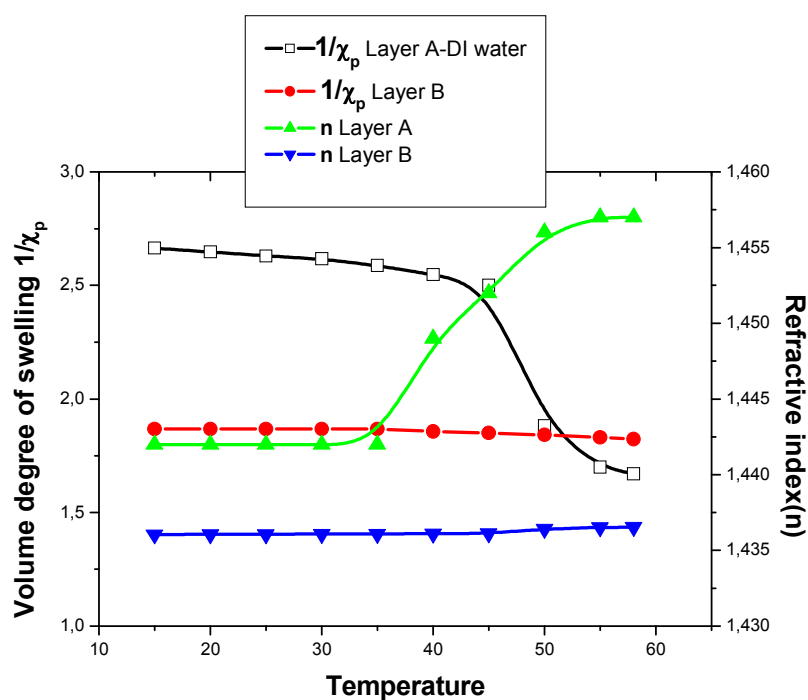


**Figure 142:** The volume degree of swelling and refractive index vs. temperature of photo-crosslinked hydrogel bilayer for layer A and B (54-05-10 and 47-05).

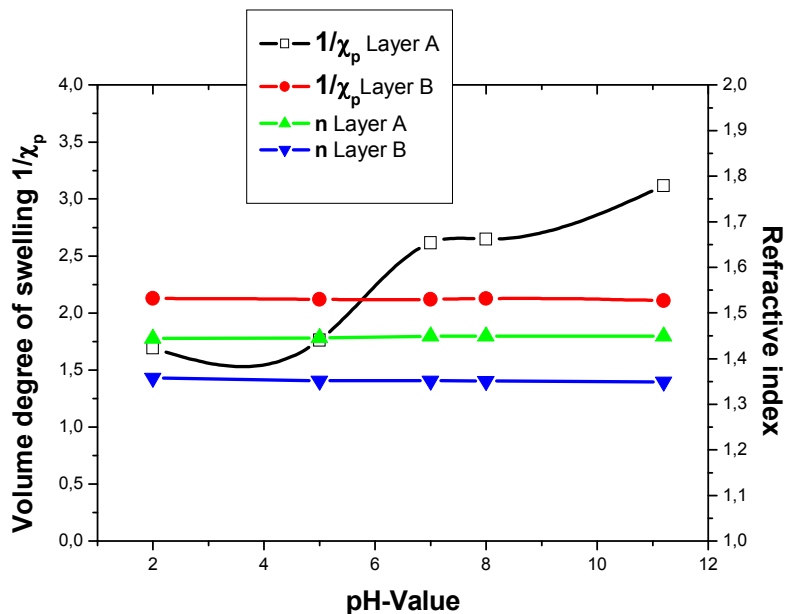


**Figure 143:** The volume degree of swelling and refractive index vs. pH of photo-crosslinked hydrogel bilayer for layer A and B (54-05-10 and 47-05).

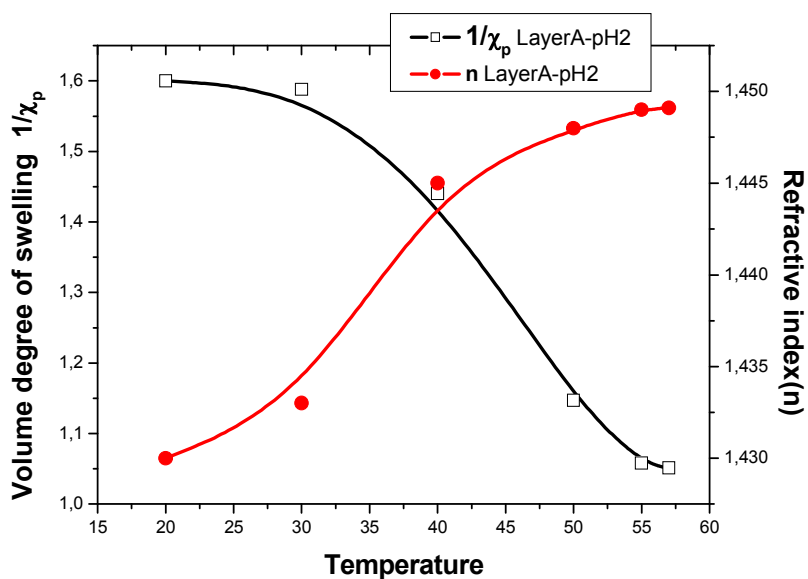


**Figure 144:** The volume degree of swelling and refractive index vs. temperature in pH2 of photo-crosslinked hydrogel bilayer for layer A (54-05-10).

### 3.8. Effect of film thickness on the behavior of hydrogel bilayer.

For this study two kinds of bilayers system were prepared. The first bilayer was built as temperature responsive as base layer and nonresponsive as upper layer. The second was built vice versa. We studied the swelling properties using SPR/OWS for four different bilayers thickness as, 1:1 of responsive: non responsive, and vice versa, also 1:4 of non responsive: responsive, the last case provided 4:1 of responsive: non responsive.

The first two cases were discussed in sections 3.7.1., 3.7.2. Therefore here we focused to interpret the last two cases in detail.

❖ **The third Case: 1 layer A (DMAAm): 4 layer B (NIPAAm).**

❖ **Dry:** A solution of 5 wt% of 5 mol% P(DMAAm-*Co*-DMIAAm) in cyclohexanone was spin coated to achieve **layerA** which photo-crosslinked. This followed by spin coating of a solution of 15 wt% of 5 mol% P(NIPAAm-*Co*-DMIAAm) in cyclohexanone at 2000 rpm to achieve double layer. **Figure 145** shows the scans of RI ( $\theta$ ) for the bilayer the formation of homogeneous film thickness, additional waveguide mode at higher scan angle indicated the increasing in the film thickness. The thickness and refractive index were 200 nm and  $\sim 1.45$  RIU for layer A also 820nm corresponding to  $\sim 1.51$ RIU for layer B. The total thickness should be the sum of Layers A+B and was 1120 nm (**see Table 84 and Figure145**).

❖ **Swelling behavior with variations of temperature for layer A:** **Figure 146** shows the swelling as temperature independent. The volume degree of swelling and refractive index were  $1/\chi_p \sim 3.7$ , and 1.38 RIU respectively.

❖ **Swelling behavior with variations of temperature for layer A+B:** **Figure 147** shows the swelling as a temperature dependent.

❖ **Layer A:** The volume degree of swelling and the refractive indices were temperature independent performed  $1/\chi_p \sim 2.1$ . 1.39 RIU.

❖ **Layer B:** The volume degree of swelling and the refractive indices were temperature responsive showing  $1/\chi_p \sim 2.46$ , 1.38 RIU and  $\sim 1.05$ ,  $\sim 1.48$  RIU for 20°C and 55 °C respectively as shown in **Figure 148**.

❖ **The last Case: 4 layer A (NIPAAm):1 layer B (DMAAm).**

❖ **Dry:** A solution of 7.5 wt% of photo-crosslinked 5 mol% P(NIPAAm-*Co*-DMIAAm) in cyclohexanone was spin coated at 2000 rpm to achieve **layerA** and further photo-crosslinked. This followed by spin coating of a solution of 5 wt% of photo-crosslinked 5 mol% P(DMAAm-*Co*-DMIAAm) in cyclohexanone at 5000 rpm to achieve double layer. **Figure 149** shows the scan of RI ( $\theta$ ) for both single and bi-layer films. The scan of single

layer film gave 300 nm and ~1.452 RIU for single layer, while the bilayer demonstrated layer A 300 nm corresponding to ~1.456 RIU and for layer B 120 nm corresponding to ~1.483RIU. The total thickness should be the sum of Layers A+B and was 420 nm see (Table 84 and Figure 149).

- ❖ **Swelling behavior with variations of temperature for layer A:** The swelling was investigated by SPR/OWS and using DI water as dielectric media. The scan of theta ( $\theta$ ) vs. RI for variations of temperature has been performed. **Figure 150** shows the swelling behavior as a change in RI ( $\theta$ ) as a temperature dependent. The Fresnel calculations used for the estimation the volume degree of swelling and refractive index demonstrated  $1/\chi_p$  ~4.18, 1.36 RIU and ~1.15, ~1.45 RIU for 15°C and 55 °C respectively as shown in **Figure 151**.
- ❖ **Swelling behavior with variations of temperature for layer A+B:** **Figure152** shows the swelling behavior as temperature dependent.
- ❖ **Layer A:** The volume degree of swelling and the refractive indices were temperature responsive  $1/\chi_p$  ~2.7, 1.38 RIU and ~1.58, corresponding to ~1.41 RIU for 1<sup>5</sup>°C and 5<sup>5</sup>°C respectively as shown in **Figures 153,154**.
- ❖ **Layer B:** The volume degree of swelling and the refractive indices were temperature independent  $1/\chi_p$  ~2.3, 1.39 RIU as shown in **Figures 153,154**.
- ❖ **General features:** We observed that  $T_c$  is dependent on the thickness of bilyayer hydrogel and the order of the T-responsive layer to the substrate. Therefore, the  $T_c$  demonstrates the highest values in the case of 1:1 (NIPAAm layer B) and 1:4, but lowest values for 1:1(NIPAAm layerA) and 4:1. The reason might be attributed to the effect of wettability of the non-responsive layer.

**Table 84:** The Fresnel calculations of double layers system illustrating thickness, dielectric and refractive index and transition temperature.

Polymer	Dry Thickness (nm)	Dielectric ( $n^2 = \epsilon$ )	$n = \sqrt{\epsilon}$	$T_c$ °C
<b>1: layer A (NIPAAm):1 layer B (DMAAm). App.</b>				
Single layer	275.00	2.090	1.445	29
Layer A	275.00	2.145	1.463	34
Layer B	282.26	2.162	1.470	No
<b>1: layer A (DMAAm):1 layer B (NIPAAm). App.</b>				
Single layer	305.00	2.120	1.469	No

<b>Layer A</b>	299.00	2.184	1.476	No
<b>Layer B</b>	311.00	2.280	1.509	35
<b>1 layer A (DMAAm): 4 layer B (NIPAAm). App.</b>				
<b>Single layer</b>	200.00	2.070	1.438	No
<b>Layer A</b>	200.00	2.110	1.452	No
<b>Layer B</b>	820.00	2.290	1.513	35
<b>1: layer A (NIPAAm):0.3 layer B (DMAAm). App.</b>				
<b>Single layer</b>	300.00	2.110	1.452	29
<b>Layer A</b>	300.00	2.120	1.456	32
<b>Layer B</b>	120.00	2.200	1.483	No

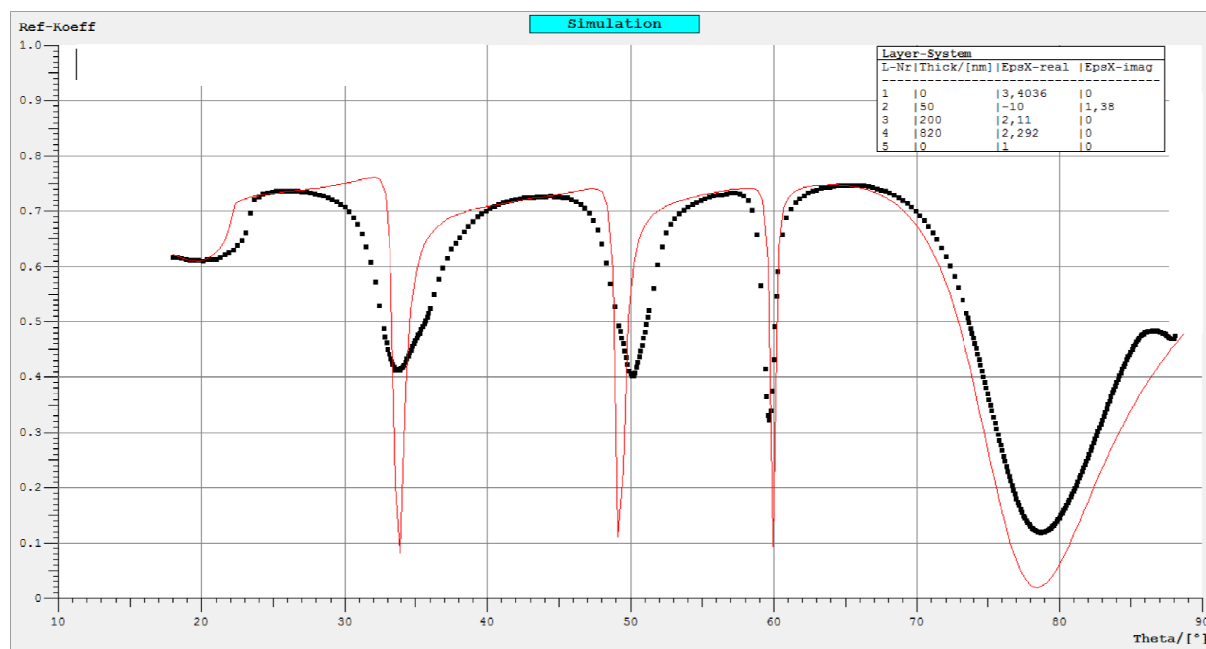


**Figure145:** SPR scan of photo-crosslinked hydrogel bilayer RI ( $\theta$ ) with temperature variations of bilayer 1:4 ratios.

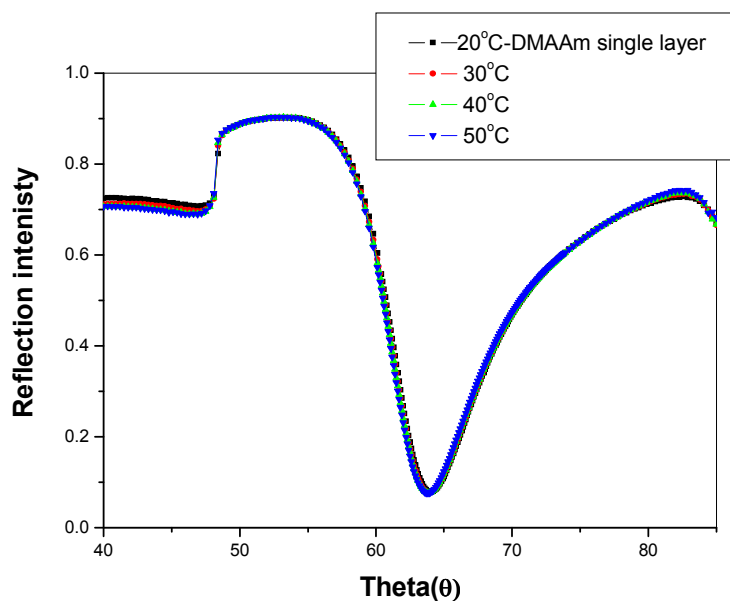


**Figure146:** SPR scans of photo-crosslinked hydrogel single layer RI ( $\theta$ ) as temperature dependent for single layer of 1:4 ratios.

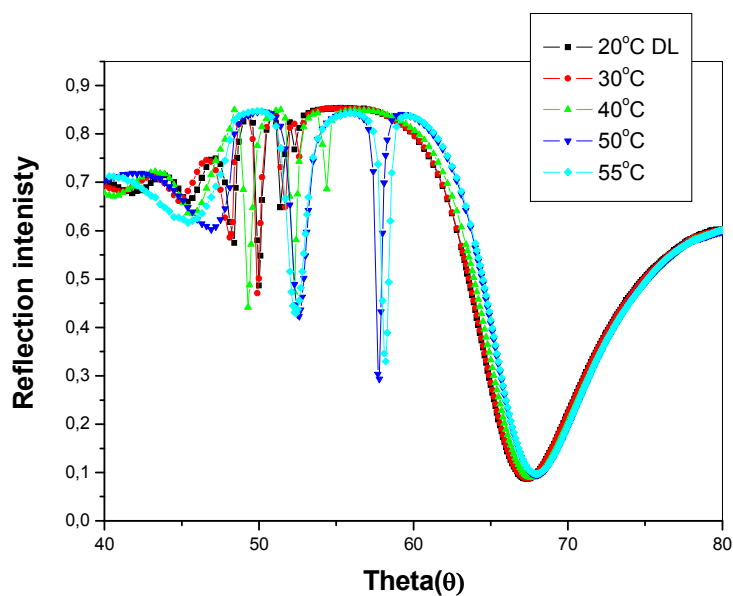


**Figure147:** SPR scan of photo-crosslinked hydrogel layer RI ( $\theta$ ) as temperature dependent for bilayer of 1:4 ratios (46-05, and 47-05).

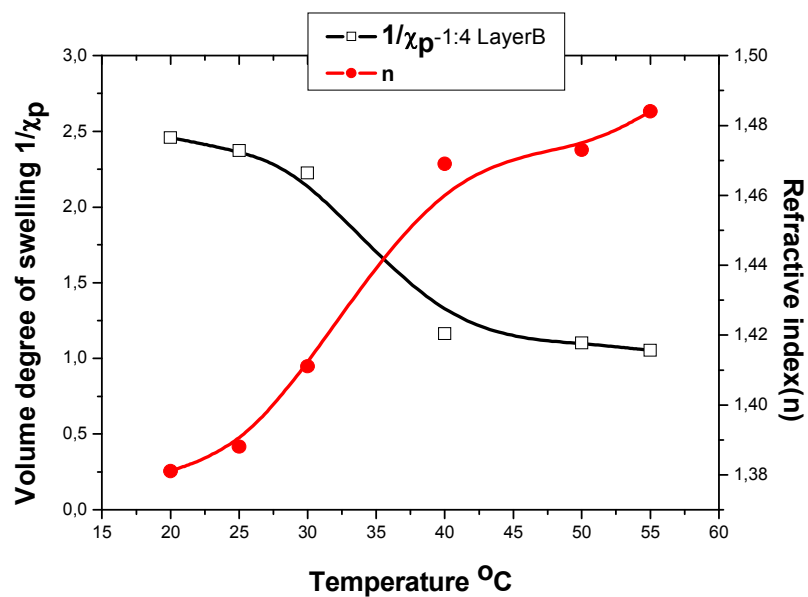


**Figure148:** Volume degree of swelling and refractive index vs. temperature of photo-crosslinked hydrogel bilayer 1:4 ratios of layer B (46-05, and 47-05).

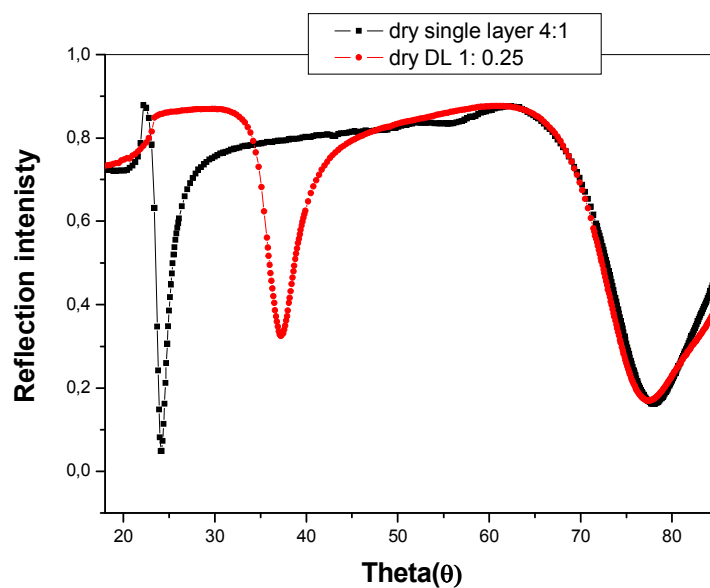


**Figure 149:** SPR/OWS scan of dry hydrogel single and bilayers for 4:1ratios (46-05, and 47-05).

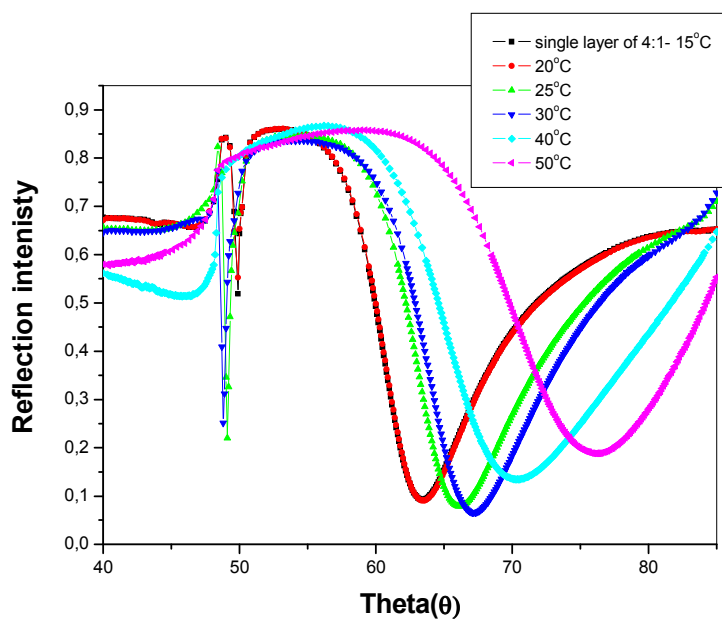


**Figure150:** SPR scan of photo-crosslinked hydrogel layer RI ( $\theta$ ) as temperature dependent for single layer of 4:1 ratios.

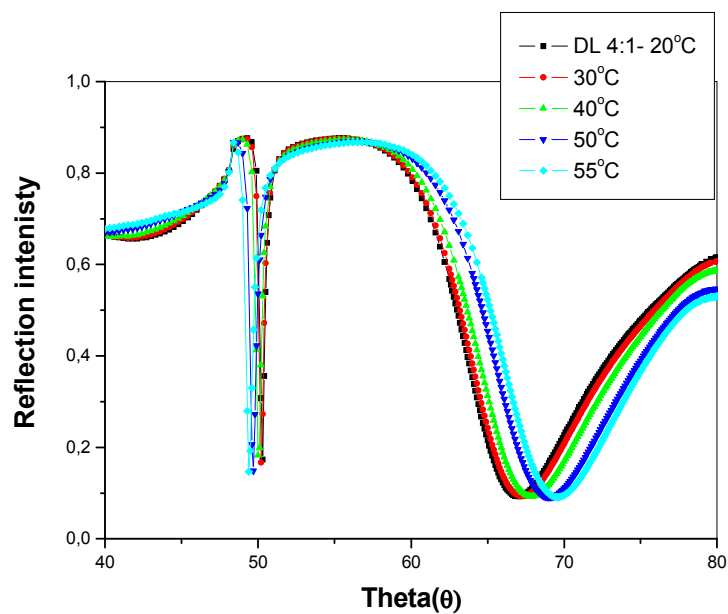


**Figure151:** SPR scan of photo-crosslinked hydrogel layer RI ( $\theta$ ) as temperature dependent for bilayer of 4:1 ratios.

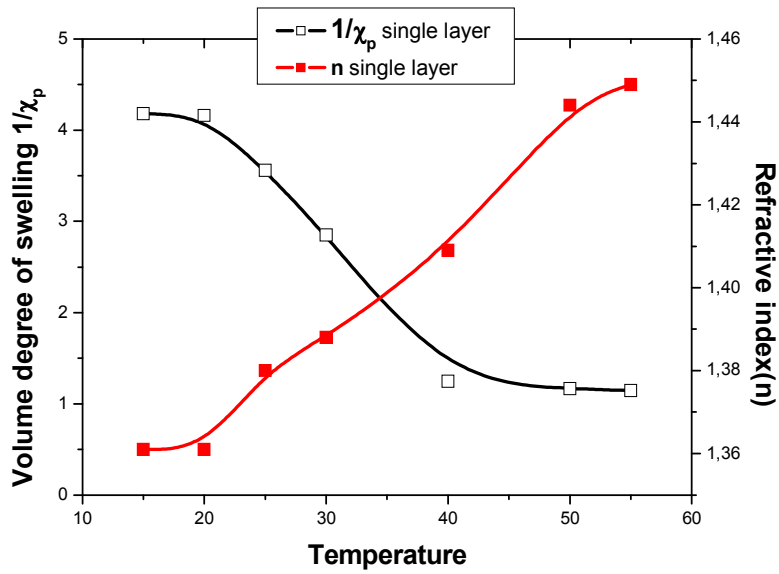


**Figure152:** Volume degree of swelling vs. temperature of photo-crosslinked hydrogel single layer 4:1 ratios of layer B.

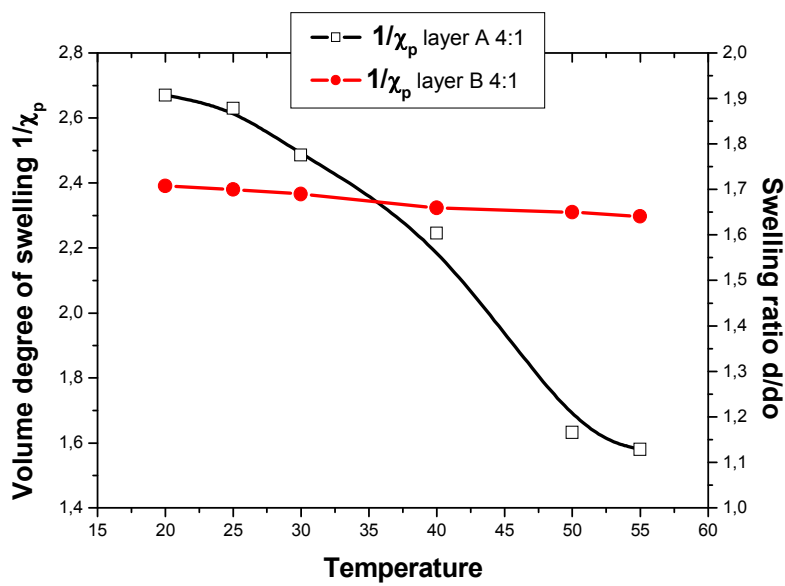


**Figure153:** Volume degree of swelling vs. temperature of photo-crosslinked hydrogel bilayer 4:1 ratios of layer B.

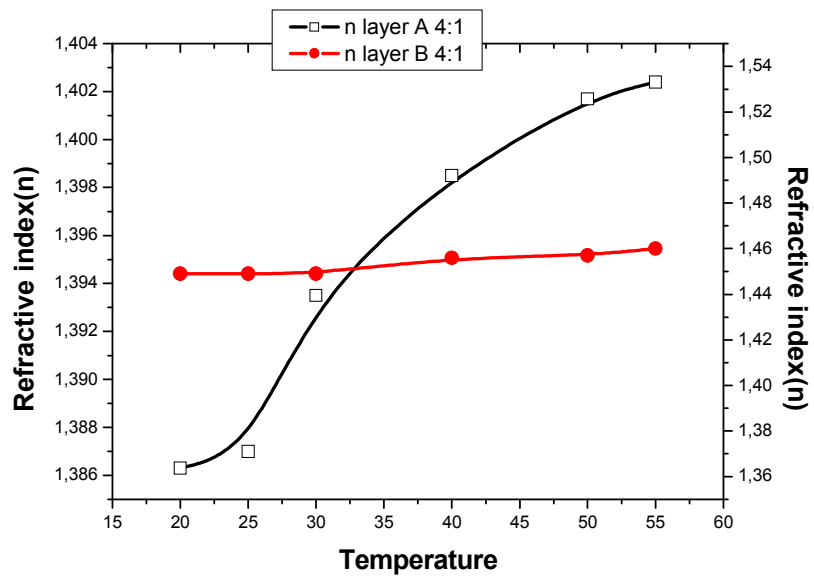


**Figure154:** Refractive index vs. temperature of photo-crosslinked hydrogel bilayer 4:1 ratios of layer B.

## 4- Summary.

In this thesis, surface attached photo-crosslinked thermo-responsive, pH, dual-responsive, hydrophilic and hydrophobic thin gel layers were synthesized and their transition temperature  $T_c$ , pH or combined T-pH effect were investigated for both soluble polymers and crosslinked gel.

Our study can be summarized as followed;

- ❖ First of all we focused on the synthesis of new functional monomers; therefore, we used vanillin as start compound in the synthesis of three monomers (VA, DEAMVA and AHVA). All of these monomers have additional functional groups and they were used in the copolymerization with DMAAm and NIPAAm.

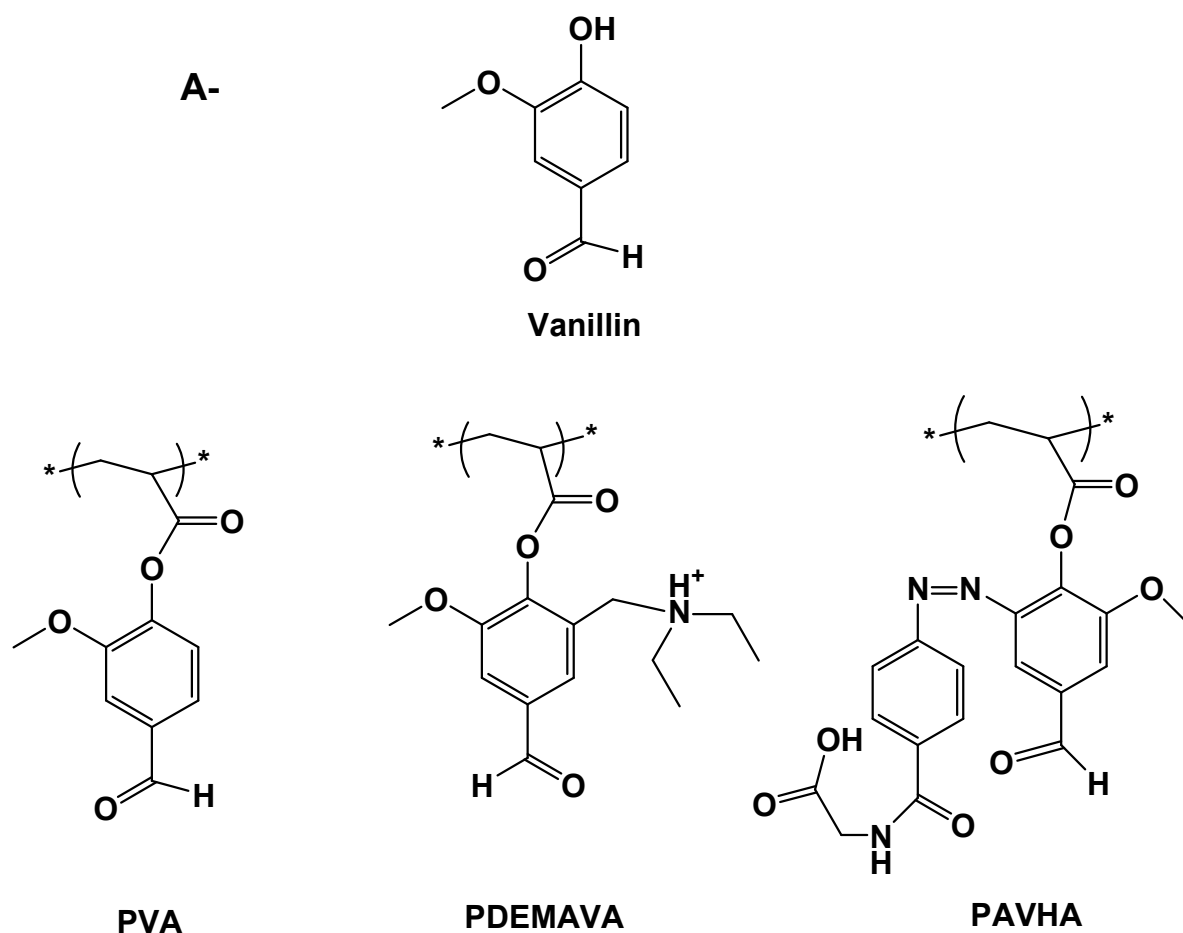


**Figure 4.1:** New polymers based on vanillin.

- ❖ Homopolymers were synthesized by random free radical polymerization of the specific monomers. These were investigated by  $^1\text{H}$ NMR, FTIR, GPC and DSC. After

that it was important to synthesize copolymers based on NIPAAm and study the effect of the incorporated monomers which are hydrophilic (DMAAm, and DEAMVA) or hydrophobic (SKA and NASI) on the lower critical solution temperature ( $T_c$ ). We observed an increase in ( $T_c$ ) with increased hydrophilic monomer content and vice versa for hydrophobic monomers.

- ❖ Dimethylmaleimide (DMI) moieties were incorporated in the polymers chains to introduce photo-crosslinking by [2+2] cyclodimerization reaction in the presence of UV irradiation. The photo-crosslinkers based on DMI group were DMIAAm, DMIA, and DMIMA as shown in **Figure 4.2**. Random free radical polymerization of a photo-crosslinker with its respective monomer resulted in formation of photo-crosslinkable polymers of (a) NIPAAm, (b) DMAAm, (c) HEMA, (d) VA, (e) SKA, (f) NIPAAm/VA, (g) DMAAm/DEAMVA, (h) SKA/VA, (i) NIPAAm/DEAMVA, (j) DMAAm/AHVA and (k) NIPAAm/AHVA. The properties of these polymers were investigated by  $^1\text{HNMR}$ , UV-vis. Spectroscopy, GPC and SPR. Thin hydrogel layers were prepared by spin coating on gold-coated LaSFN9 glass. The covalent attachment to the surface was achieved through an adhesion promoter.

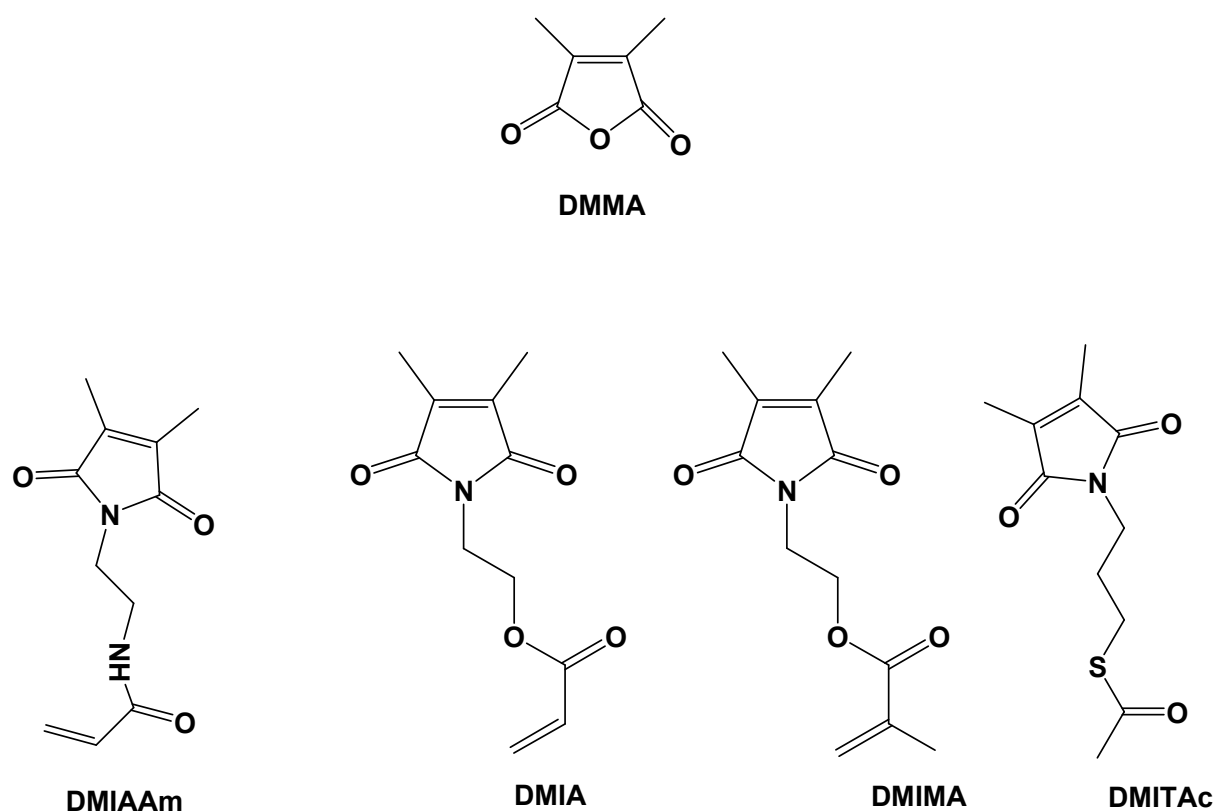


**Figure4.2:** Dimethylmaleic anhydride and the related photo-crosslinkers and also adhesion promoter.

- ❖ Swelling behavior of the thin polymer gel layers was investigated by Surface Plasmon Resonance (SPR) and Optical Waveguide Spectroscopy (OWS). SPR and OWS gave a wide range of information regarding the film thickness ( $d$ ), swelling ratio ( $d/d_0$ ) and refractive index ( $n$ ) and volume degree of swelling ( $1/\chi_p$ ) of the thin hydrogel layer.
- ❖ For T-responsive polymer hydrogel, RI versus angle ( $\theta$ ) at constant temperatures was measured. After the completion of the angle scan, the temperature was increased to the second temperature and the hydrogel was left for 15 min to give the thermal equilibrium, then the angle scan measurement was repeated. Fresnel calculations were used for the determination of film thickness and dielectric which further converted to volume degree of swelling and refractive index. The volume degree of swelling or refractive index vs. temperature was used in the determination of  $T_c$ .
- ❖ For pH-responsive polymer gel, RI versus angle ( $\theta$ ) at different pH-values start from pH 2.2 till pH 11.2 was measured; the hydrogel was left for 25 min to give the pH-equilibrium. Fresnel calculations were used for the determination of film thickness and dielectric which further converted to volume degree of swelling and refractive index. The volume degree of swelling or refractive index vs. pH-values was plotted.
- ❖ For dual-responsive polymer hydrogels with temperature and pH, both of the previously methods were used in the determination of  $T_c$ . This means that the swelling was done as temperature change at different pH buffer solutions.
- ❖ Hydrogel layers were investigated for all kinds of polymers to illustrate different responsive films as temperature responsive (NIPAAm) or pH-responsive (DEAMVA). Furthermore, hydrophilic photo-crosslinked polymer gels based on DMAAm and HEMA or hydrophobic photo-crosslinked polymer gels based on SKA and VA were prepared.
- ❖ Formation of dual-responsive polymers and hydrogels were taken in our study as the incorporation of temperature responsive moieties(NIPAAm) with pH-responsive (DEAMVA) and studying the change in  $T_c$  as a change in pH solution. We observed the increasing of  $T_c$  as change from acidic to neutral to basic buffer solution demonstrating higher  $T_c$  in basic solutions.
- ❖ We observed that all  $T_c$  values calculated by SPR were in agreement with UV.vis.Spectroscopy and DSC with respect of little change related to the different definitions for each technique.
- ❖ One interesting observation in our study is seen in azo polymer hydrogel as AVHA is incorporated into DMAAm or NIPAAm polymers showing pH-response and dual-

response respectively. We observed the formation of upper critical solution temperature (UCST) or change of phase separation from LCST to UCST during swelling at pH 11.2.

- ❖ After the formation of single layer it was of interest to build bilayer hydrogels. Therefore, we built bilayer hydrogels as temperature responsive (NIPAAm) as base layer and non-responsive (DMAAm) as top layer and vice versa. The swelling behavior was calculated by adding a new layer to the Fresnel calculations. The lower critical solution temperature was determined as function of  $1/\chi_p$  or refractive index for each layer.
- ❖ The formation of bilayers based on dual-responsive polymers in the base layer and non-responsive in the upper layer or vice versa was done. The swelling was done as a function of both temperature and pH.

**Table 4.1:** The hydrogel film used in our study as single or bilayer.

<b>Photo-crosslinked polymer</b>	<b>Solvent</b>	<b>No. of polymer layer</b>	<b>Surface responsive to or not.</b>
P(NIPAAm- <i>Co</i> -DMIAAm)	Cyclohexanone	Single	T-responsive
P(DMAAm- <i>Co</i> -DMIAAm)	Cyclohexanone	Single	Non, hydrophilic
P(HEMA- <i>Co</i> -DMIMA)	DMSO	Single	Non, hydrophilic
P(SKA- <i>Co</i> -DMIA)	Cyclohexanone	Single	Non, hydrophobic
Poly ( VA- <i>Co</i> -DMIA)	Cyclohexanone	Single	Non, hydrophobic
Poly ( VA- <i>Co</i> -DMIA)-g-(AA)	Cyclohexanone	Single	Non, hydrophobic
Poly( VA- <i>Co</i> -DMIA)-g-(AA)-g-(NIPAAm)	Cyclohexanone	Single	Non, hydrophobic/hydrophilic
P(NIPAAm- <i>Co</i> -VA- <i>Co</i> -DMIAAm)	Cyclohexanone	Single	T-responsive
P(DMAAm- <i>Co</i> -DEAMVA- <i>Co</i> -DMIAAm)	Cyclohexanone	Single	pH-responsive
P(SKA- <i>Co</i> -VA- <i>Co</i> -DMIA)	Cyclohexanone	Single	hydrophobic

## Summary

Poly (NIPAAm- <i>Co</i> -DEAMVA- <i>Co</i> -DMIAAm)	Cyclohexanone	Single	Dual-responsive
P(DMAAm- <i>Co</i> -AHVA- <i>Co</i> -DMIA)	Cyclohexanone	Single	Hydrophobic in pH7/pH-responsive/T-responsive UCST pH11.2
P(NIPAAm- <i>Co</i> -AHVA- <i>Co</i> -DMIA)	Cyclohexanone	Single	Hydrophobic in pH7/pH-responsive/T-responsive UCST pH11.2
P(NIPAAm- <i>Co</i> -HEMA- <i>Co</i> -DMIA)	Cyclohexanone	Single	T-responsive
Poly (NIPAAm- <i>Co</i> -HEMA- <i>Co</i> -DMIAAm)-g-HA	Cyclohexanone	Single	Dual-responsive
P(NIPAAm- <i>Co</i> -DMIAAm) + P(DMAAm- <i>Co</i> -DMIAAm)	Cyclohexanone	Bilayer	T-responsive + Hydrophilic
P(DMAAm- <i>Co</i> -DMIAAm) + P(NIPAAm- <i>Co</i> -DMIAAm)	Cyclohexanone	Bilayer	Hydrophilic + T-responsive
P(DMAAm- <i>Co</i> -DMIAAm) + P(DMAAm- <i>Co</i> -DEAMVA-DMIAAm)	Cyclohexanone	Bilayer	Hydrophilic + pH-responsive
P(NIPAAm- <i>Co</i> -DEAMVA- <i>Co</i> -DMIAAm) + P(DMAAm- <i>Co</i> -DMIAAm)	Cyclohexanone	Bilayer	Dual-responsive + Hydrophilic
P(NIPAAm- <i>Co</i> -DMIAAm) + P(NIPAAm- <i>Co</i> -VA- <i>Co</i> -DMIAAm)	Cyclohexanone	Bilayer	T-responsive + T-responsive

P(DMAAm-Co-AHVA-Co-DMIAAm) + P(NIPAAm-Co-DMIAAm)	Cyclohexanone	Bilayer	Hydrophobic in pH7/pH-responsive/T- responsive UCST pH11.2 + T-responsive
--	---------------	---------	--

- ❖ The last point was the study of bilayer hydrogel assemblies with different relative film thickness. For this purpose we used four kinds of bilayer thickness as temperature responsive and non-responsive. It was shown that the layer thickness of the non-responsive film as well as the order of assembly has an influence on  $T_c$ .

## References

1. Holm, C.; Kremer, K. T.; and Vilgis, A.; *Physikalische Blätter*.; Polyelektrolyte.; **1998**, *54*, 1013-1016.
2. Machacek, O.; *US-Patent 3985593*, Water gel explosives, **1976**.
3. Wichterle, O.; *US-Patent 3408429*, Method for centrifugal casting a contact lens.; **1968**.
4. Buchholz, F. L.; *Chemtech*.; Keeping Dry with Superabsorbent Polymers. **1994**, *24*, 38-43.
5. Rawlings, A. V. and Watkinson, A.; *US-Patent 5554366*; Skin care method and composition; **1996**.
6. Barry, E. F. and Grob, R. L.; *Modern practice of gas chromatography*; Wiley-Interscience **2004**, Part I, 163.
7. Hennink, W.E.; Nostrum, van C.F. *Adv. Drug Deliv. Rev.* **2002**, *54*, 13-36.
8. Baldwin, S.P.; W.M. Saltzman, W.M. *Adv. Drug Deliv. Rev.* **1998**, *33*, 71-86.
9. Park, K.; Shalaby, W.S.W.; Park, H. (Eds.), Technomic, Basle, **1993**.
10. Hoffman, R.; Wells, P.; Morrison, H. *J. Org. chem.* **1971**; *1*:102-108.
11. Cohen M.D.; Schmidt, J.M.G. *J. Chem. Soc.; Topochemistry. A, survey*; **1964**, 1996-2000.
12. Rennert, J.; Ruggiero, E.M. *Rapp, J. Photochem. Photobiol.* **1967**, *6*, 29-34.
13. Oikawa, S.; Tsuda, M.; Ueno, N.; Sugita, K. *Chem Phys Lett.* **1980**, *74*, 379-383.
14. Tsuda, M. *J. Polym. Sci A.* **1964**, *2*, 2907-2916.
15. Egerton, P.L.; Pitts, E.; Reiser, A. *Macromolecules.* **1981**, *14*, 95-100.
16. Nakayama, Y.; Matsuda, T. *J. Polym. Sci A.* **1992**, *30*, 2451-2457.
17. Minsk LM, Smith IG, Wright JF. *J. Appl. Polym. Sci.* **1959**, *2*, 302-307.
18. Robertson, E.M.; Van Deusen, W.P.; Minsk, LM. *J. Appl. Polym. Sci.* **1959**; *2*:308-311.
19. Coqueret, X. *Macromol. Chem. Phys.* **1999**, *200*, 1567-1579.
20. Williams, J.L.R.; Farid, S.Y.; Doty, J.C.; Daly, R.C.; Specht, D.P.; Searle, R.; Borden, D. G.; Chang, H.; and Martic, P. A. *Pure Appl. Chem.* **1977**, *49*, 523-538.
21. Ngai, T.; Wu, C. *Macromolecules.* **2003**, *36*, 848-854.
22. De Schryver, F.C.; Feast, W.J.; Smets, G. *J. Polym. Sci. A.* **1970**, *8*, 1939-1948.
23. De Schryver, F.C.; Boens, N.; Smets, G. *J. Polym. Sci. A.* **1972**; *10*:1687-1699.
24. Kuckling, D.; Adler, H.J.P.; Ling, L.; Habicher, W.D.; Arndt, K.F. *Polym. Bull.* **2000**, *44*, 268-276

25. Duan Vo, C.; Kuckling, D.; Adler, HJP.; Schönhoff, M. *Colloid Polym Sci.* **2002**, 280, 400-409.
26. Kuckling, D.; Duan Vo, C.; Wohlrab S.E. *Langmuir.* **2002**, 18, 4263-4269.
27. Kuckling, D.; Duan Vo, C.; Adler, H.J.P.; Völkel, A.; Cölfen, H. *Macromolecules.* **2006**, 39, 1585-1591.
28. Seiffert, S., Oppermann, W.; Saalwächter, K. *Polymer*, **2007**, 48, 5599-5611.
29. Cockburn, E.S.; Davidson, R.S.; Pratt, J.E. *J. Photochem. Photobiol.* **1996**, 94, 83-88.
30. Schinner, R.; Wolff, T.; Kuckling, D. *Ber Bunsen-Ges Phys Chem.* **1998**, 102, 1710-1714.
31. Hammond, G.S.; Turro, N.J.; Leermakers, P.A. *J. Phys. Chem.* **1962**, 66, 1144-1147.
32. Schenck GO, Steinmetz R. *Bull. Soc. Chim. Belg.* **1962**, 71, 78.
33. Kaur, G.; Chang, S.L.Y.; Bell, T.D.M.; Hearn, M.T.W.; Saito, K. *J. Polym Sci A.* **2011**, 19, 4121-4128.
34. Zhang, L.; Wang, H. *Polymer*, **2011**, 52, 3146-3154.
35. Eagland, D.; Crowther, N.J.; Butler, C.J. *Eur. Polym. J.* 1994, 30, 767-773.
36. Bell, C.L.; Peppas, N.A. *J. Controlled Release* **1996**, 39, 201-207
37. Mathur, A.M., Hammonds, K.F.; Klier, J. A.B. Scanton. *J. Controlled Release* **1998**, 54, 177-184.
38. Haglund, B.O.; Joshi, R.; Himmelstein, K.J. *J. Controlled Release* **1996**, 41, 229-235.
39. Arndt, K.F.; Schmidt, T.; Richter, A.; Kuckling, D. *Macromol. Symp.* **2004**, 207, 257-268.
40. Tanaka, T. *Phys. Rev. Lett.* **1978**, 40 (12), 820-823.
41. Richter, A.; Paschew, G.; Klatt, S.; Lienig, J.; Arndt, K.F.; and Adler, H. *J. P. Sensors Rev.* **2008**, 8, 561-581.
42. Flory, P.J.; Rehner, J. *J. Chem. Phys.* **1943**, 11, 512-520.
43. Flory P.J.; Rehner, J., *J. Chem. Phys.* **1943**, 11, 521-526.
44. Huggins, M.L. *J. Chem. Phys.* **1941**, 9, 440.
45. Harmon, M. E.; Kuckling, D.; Pareek, P.; Frank, C. W. *Langmuir* **2003**, 19, 10947-10956.
46. Gao, J.; Frisken, B. J. *Langmuir* **2003**, 19, 5217-5222.
47. Takeoka, Y.; Watanabe, M.; *Langmuir* **2003**, 19, 9104-9106.
48. Pradeep Pareek. PhD, thesis, Faculty of Mathematics and Natural Sciences Technical University Dresden. **2006**, 9.

## References

---

49. Siegel, R.A.; Firestone, B.A. *Macromolecules* **1988**, 21, 3254-3259.
50. Ding, Z.; Chen, G.; Hoffman, AS. *J Biomed Mater Res* **1998**, 39, 498-505.
51. Stayton, PS.; Shimoboji, T.; Long, C. *Nature* **1995**, 378, 472-474.
52. Packhaeuser, CB.; Schnieders, J; Oster, CG; Kissel, T. *Eur. J. Pharm. Biopharm.* **2004**, 58, 445-455.
53. Jeong, B.; Gutowska, B. *Trends Biotechnol.* **2002**, 20, 305-311.
54. Gil, ES.; Hudson, SM. *Prog. Polym. Sci.* **2004**, 29, 1173-1222.
55. Fujishige, S.; Ando, KKI. *J. Phys. Chem. A.* **1989**, 93, 3311-3313.
56. Zhang, X.; Zhuo, R.; Yang, Y. *Biomaterials.* **2002**, 26, 1313-1318.
57. Brown, W.; Schillen, K.; Hvidt, S. *J. Phys. Chem.* **1992**, 96, 6038-6044.
58. Kazakov, S.V., Revokatov, O.P., and Chernova, N.I. *Doklady Physics*, **1998**, 43, 137-140,
59. Saeki, S.; Kuwahara, N.; Nakata, M.; Kaneko, M. *Polymer*, **1976**, 17, 685-689.
60. Bae, Y. C.; Lambert, S. M.; Soane, D. S.; Prausnitz, J. M. *Macromolecules*, **1991**, 24, 4403-4407.
61. Iwao Teraoka. *Polymer Solutions: An Introduction to Physical Properties.*, Copyright © **2002**, John Wiley & Sons, Inc. 99-100.
62. Kazakov, S.V. and Chernova, N.I. *Russ. J. Phys. Chem.* 2002, 76, 1236-1241.
63. Galaev, I.Y. and Mattiasson, B., Eds., *Smart Polymers for Bioseparation and Bioprocessing*, Taylor & Francis, London and New York, **2002**.
64. Taylor, L.D.; Cerankowski, L.D.J. *J. Polym. Sci. A.* **1975**, 13, 2551-2570.
65. Fujishige, S.; Kubota, K.; and Ando, I. *J. Phys. Chem.* 1989, 93, 3311-3313.
66. Overstreet, D.J.; Dhruv, H.D.; Vernon, B.L. *Biomacromolecules.* **2010**, 11, 1154-1159.
67. Rathfon, J.M.; Tew, G.N. *Polymer.* **2008**, 49, 1761-1769.
68. Kotsuchibashi, Y.; Kuboshima, Y.; Yamamoto, K.; Aoyagi, T. *J. Polym. Sci. A.* **2008**, 46, 6142-6150.
69. Kuckling, D.; Pareek, P. *J. Polym. Sci. A.* **2003**, 41, 1594-1602.
70. Grinberg, N. V.; Dubovik, A. S.; Grinberg, V. Y.; Kuznetsov, D. V.; Makhaeva, E. E.; Grosberg, A. Y.; Tanaka, T. *Macromolecules.* **1999**, 32, 1471-1475.
71. Kuckling, D.; Adler, H-J. P.; Arndt, K-F.; Ling, L.; Habicher, W. D. *Macromol. Chem. Phys.* **2000**, 201, 273-280.
72. Barker, I.C.; Cowie, J. M. G.; Huckerby, T. N.; Shaw, D. A.; Soutar, I.; Swanson, L. *Macromolecules.* **2003**, 36, 7765-7770.

## References

---

73. Kuckling, D.; Harmon, M. E.; Frank, C. W. *Macromolecules*. **2002**, *35*, 6377-6383.
74. Harmon, M. E.; Kuckling, D.; Frank, C. W. *Macromolecules* **2003**, *36*, 162-172.
75. Nan Zhang, N.; Knoll, W. *Anal. Chem.* **2009**, *81*, 2611-2617.
76. Anac, I.; Aulasevich, A.; Junk, M.J.N.; Jakubowicz, P.; Roskamp, R.F.; Menges, B.; Jonas, U.; Knoll, W. *Macromol.Chem. phys.* **2010**, *211*, 1018-1025.
77. Hoffman, A.S.; Stayton, P.S.; Bulmus, V. *J. Biomed. Mater. Res.* **2000**, *52*, 577-586
78. Schild, H.G. *Progr. Polym. Sci.*, **1992**, *17*, 163-249.
79. NetopiliP, M.; Bohdanecký, M.; Chytrý, V.; Ulbrich, K. *Macromoleculesl. Rapid. Commun.* **1997**, *18*, 107-111.
80. Platè,N.A.; Lebedeva, T.L.; Valuev,L. *Polym. J.* **1999**, *31*, 21-27.
81. Idziak, I.; Avoce, D.; Lessard, D.; Gravel, D.; Zhu, X.X. *Macromolecules*. **1999**, *32*, 1260-1263.
82. Cho, S.H.; Jhon, M.S.; Yuk, S.H. *Europ. Poly. J.* **1999**, *35*, 1841-1845.
83. Akaash, M.; Nakano, S.; Kishida, A. *J. Polym. Sci. A.* **1996**, *34*, 301-303.
84. Ichijo, H.; Hirasa, I.; Kishi, R.; Oowada, M.; Sahara, K.; Kokufut, E.; Kohno, S. *Radiat. Phys. Chem.* **1995**, *46*, 185-190.
85. Ataman, M. *Colloid Polym. Sci.* **1987**, *265*, 19-25.
86. Chen,F.P.; Ames, A.E.; Taylor,L.D. *Macromolecules*. **1990**, *23*, 4688-4695.
87. Winnik, F.M. *Macromoleculesl.*, **1987**, *20*, 2745-2750.
88. Dinarvand, R.D.; Emanuele, A. *J. Controlled Release.* 1995,*36*,221-227.
89. Chun, S.W.; Kim, J.D. *J. Controlled Release.* **1996**, *38*, 39-47.
90. Ichikawa, H.; Fukumori, Y. *J. Controlled Release.* **2000**, *63*, 107-119.
91. Yoshida, T. *J. Polym. Sci. A.* **2003**, *41*, 779-787.
92. Kumashiro, Y.; Lee, W.K.; Ooya, T.; Yui, N. *Macromol. Rapid Comm.* **2002**, *23*, 407-410
93. Vernon, B.; Kim, S.W.; Bae, Y.H. *J. Biomed. Mater. Res.* **2000**, *51*, 69-79.
94. Spohr, R.; Spohr, R.; Reber, N. J. *Controlled Release* **1998**, *50*, 1-11.
95. Li, S.K.; D'Emanuele, A. *J. Controlled Release.* **2001**, *75*, 55-67.
96. Nath, N.; Chilkoti, A. *Adv. Mater.* **2002**,*14*,1243-1247.
97. Kim, Y.S.; Lim, J.Y.; Donahue, H.J.; Lowe, T.L. *Tissue Eng.* **2005**, *11*, 30-40.
98. Webb, D.; An, Y.H.; Gutowska, A.; Mironov, V.A.; Friedman, R.J. *MUSC. Orthop. J.* **2000**, *3*, 18-21.
99. Aguilar, M.R.; Elvira, C.; Gallardo, A.; Vázquez, B.; Román, J.S. *Topics in Tissue Engineering*, **2007**, *3*.

## References

---

100. Qiu, Y.; Park, K. *Adv. Drug Deliver. Rev.* **2001**, 53, 321-339.
101. Park, S.Y.; Bae, Y.H. *Macromol. Rapid Comm.* **1999**, 20,269-273.
102. Jeong B, Bae YH, Kim SW. *J. Biomed. Mater. Res.* **2000**, 50, 171-177.
103. Jin Woo Lee, Doo Sung Lee, Sung Wan Kim. *Macromol.Res.* 2003, 11, 3,189- 193.
104. Lou, L.; Kato, M.; Tsuruta, T.; Kataoka, K.; Nagasaki, Y. *Macromolecules.* **2000**, 33, 4992-4994.
105. Nagasaki, Y.; Luo, L.; Tsuruta, T.; Kataoka, K. *Macromol. Rapid Comm.* **2001**, 22, 1124-1127.
106. Davaran, S.; Hanaee, J.; Khosravi, A. *J. Controlled Release.* **1999**, 58, 279-287
107. Gallardo, A.; Rodriguez, G.; Aguilar, M.R.; Fernández, M.M.; Román, S. J. *Macromolecules.* **2003**, 36, 8876-8880.
108. Sauer, M.; Streich, D.; Meier, W. *Adv. Mater.* **2001**, 13, 1649-1651.
109. Jones R. *Nat. Mater.* **2004**, 3, 209-210.
110. Liu, Y.Y.; Fan, X.D.; Kang, T.; Sun, L. *Macromol. Rapid Comm.* **2004**, 25, 1912-1916
111. Godbey, W.T.; Mikos, A.G. *J. Controlied Release.* **2001**, 72, 115-125.
112. Borchard, G. *Adv. Drug Deliv. Rev.* **2001**, 52, 145-150.
113. Corsi, K.; Chellat, F.; Yahia, L.; Fernandes, J.C. *Biomaterials.* **2003**, 24, 1255-1264.
114. Erbacher, P.; Zou, S.; Bettinger, T.; Steffan A.M.; Remy, J.S. *Pharm. Res.* 1998, 15, 1332-1339.
115. Ishii, T.; Okahata, Y.; Sato, T. *Biochim. Biophys. Acta.* **2001**, 1514, 51-64.
116. Leong, K.W.; Mao, H.Q.; Truong, L.; Roy, K.; Walsh, S.M.; August, J.T. *J Controlled Release.* **1998**, 53, 183-193.
117. Lim, Y.B.; Han, S-A.; Kong, H-U.; Park, J-S.; Jeong, B.; Kim, S.W. *Pharm. Res.* **2000**,17, 811-816.
118. Kataoka, K. 4-5. **2004.** *Ref Type: Conference Proceeding*
119. Stayton, P.S.; Hoffman, A.S. Murthy, N. *J. Controlled Release.* **2000**, 65, 203-220.
120. Stayton, P.S.; El Sayed, M.E.; Murthy, N. *Orthodontics & craniofacial research.* 2005, 8, 219-225.
121. Stayton, P.S.; El Sayed, M.E.H.; Hoffman, A.S. *Expert. Opin. Biol. Th.* 2005, 5, 23-32.
122. El Sayed, M.E.H.; Hoffman, A.S.; Stayton, P.S. *J. Controlled Release.* 2005, 101, 47-58
123. Podual, K.; Doyle, III.; Peppas, N.A. *Polymer.* **2000**, 41, 3975-3983.

124. Guenther, M.; Kuckling, D.; Corten, C.; Gerlach, G.; Sorber, J.; Suchaneck, G.; Arndt, K.F. *Sens. Actuators, B*. **2007**, 126, 97–106.
125. Matsukuma, D.; Yamamoto, K.; Aoyagi, T. *Langmuir*, **2006**, 22, 5911–5915.
126. Chen, Y.; Pang, X.-H.; Dong, C.-M. *Adv. Funct. Mater.* **2010**, 20, 579–586.
127. Bulmus, V.; Ding, Z.; Long, C.J.; Stayton, P.S.; Hoffman, A.S. *Bioconjug. Chem.* **2000**, 11, 78-83.
128. Brazel, C.S.; Peppas, N.A. *Macromolecules*. **1995**, 28, 8016-8020.
129. Zareie, H.M.; Volga Bulmus, E.; Piskin, E.; Gunning, A.P.; Morris, V.J.; Hoffman, A.S. *Polymer*. **2000**, 41, 6723-6727.
130. Leung, M.F.; Zhu, J.; Li, P.; Harris, F.W. *Macromol. Symp.* **2005**, 226, 177-185.
131. Rodríguez-Cabello, J.C.; Reguera, J.; Girotti, A.; Alonso, M.; Testera, A.M. *Prog Polym Sci* **2005**, 30, 1119-1145.
132. Alonso, M.; Rebotto, V.; Guiscardo, L.; Martin, A.S.; Rodríguez-Cabello, J.C. *Macromolecules*. **2000**, 33, 9480-9482.
133. Kurata, K.; Dobashi, A. *J. Macromol. Sci.* 2004, 41, 143-164.
134. Ramkissoon-Ganorkar, C.; Baudys, M.; Wan Kim, S. *J. Biomat. Sci. Polym. Ed.* **2000**, 11, 45-54.
135. Ju, H.K.; Kim, S.Y.; Kim, S.J.; Lee, Y.M. *J. Appl. Polym. Sci.* **2002**, 83, 1128-1139
136. Benrebouh, A.; Avoce, D.; Zhu, X.X. *Polymer*. **2001**, 42, 4031-4038.
137. Ning, L.; Min, Y.; Maolin, Z.; Jiuqiang, L.; Hongfei, H. *Radiat Phys Chem* **2001**, 61, 69-73.
138. Mallapragada SK, Anderson BC. Ref Type: Conference Proceeding 2002, 1, 486-487.
139. Gan, L.H.; Gan, Y.Y.; Roshan Deen, G. *Macromolecules*, **2000**, 33, 7893-7897
140. Mitchellb, R.-R.; Vasilea, C. *Polym Int.* **2011**, 60, 222–233.
141. Chen, D.; Liu, H.; Kobayashib, T.; Yu, H. *J. Mater. Chem.* **2010**, 20, 3610–3614
142. George Pasparakisa and Maria Vamvakaki. *Polym. Chem.* **2011**, 2, 1234
143. Beck, J. B.; Rowan, S. J. *J. Am. Chem. Soc.* **2003**, 125, 13922–13923.
144. Xia, F.; Ge, H.; Hou, Y.; Sun, T.; Chen, L.; Zhang, G.; Jiang, L. *Adv. Mater.* **2007**, 19, 2520–2524.
145. Bousquet, A.; Ibarboure, E.; Papon, E.; Labrugère, C.; J. Rodríguez-Hernández, J. *Polym. Sci. A*. **2010**, 48, 1952–1961
146. Gauthier, M. A.; Gibson, M. I.; Klok, H. A. *Angewandte Chemie International Edition* **2009**, 48, 48–58,

147. Fuchs, A. D.; Tiller, J. C. *Angewandte Chemie-International Edition*. **2006**, 45, 6759–6762.
148. Zolotukhin, M. G.; Colquhoun, H. M.; Sestiaa, L. G.; Rueda, D. R.; Flot, D. *Macromolecule*, **2003**, 36, 4766–4771.
149. Schneider, B. H.; Dickinson, E. L.; Vach, M. D.; Hoijer, J. V.; Howard, L. V.; *Biosensors & Bioelectronics* **2000**, 15, 13–22.
150. Vaisocherova, H.; Yang, W.; Zhang, Z.; Cao, Z. Q.; Cheng, G.; Piliarik, M.; Homola, J.; Jiang, S. Y. *Analytical Chemistry*, **2008**, 80, 7894–7901.
151. Wark, A. W.; Lee, H. J.; Corn, R. M.; *Analytical Chemistry*, **2005**, 77, 3904–3907
152. Lakhari, H.; Okano, T.; Nurdin, N.; Luthi, C.; Descouts, P.; Muller, D.; Jozefonvicz, J. *Biochimica Et Biophysica Acta-General Subjects*, **1998**, 1379, 303–313.
153. Kanazawa, H.; Yamamoto, K.; Matsushima, Y.; Takai, N.; Kikuchi, A.; Sakurai, Y.; Okano, T.; *Analytical Chemistry*, **1996**, 68, 100–105.
154. Bhattacharya, S.; Eckert, F.; Boyko, V.; and Pich, A. *Small*, **2007**, 3(4), 650–657.
155. Xulu, P. M., Filipcsei, G., and Zrinyi, M., *Macromolecules*, **2000**, 33(5), 1716–1719.
156. Robert Fokko Roskamp. *Ph.D thesis, Max Plank institute for polymer*, **2009**, 7.
157. Brooks, Y.- E.; Kizhakkedathu, J.N. *Macromolecules*, **2008**, 41, 5393-5405.
158. Tokarev, I.; Minko, S. *Soft Matter*, **2009**, 5, 511–524.
159. Harmon, M. E.; Jakob, T. A. M.; Knoll, W.; Frank, C. W. *Macromolecules*, **2002**, 35, 5999-6004.
160. Bhatta, D.; Christie, G.; Madrigal-Gonzalez, B.; Blyth, J.; Lowe, C. R. *Biosens. Bioelectron.* **2007**, 23, 520-527.
161. Bashir, R.; Hilt, J. Z.; Elibol, O.; Gupta, A.; Peppas, N. A. *Appl. Phys. Lett.* **2002**, 81, 3091-3093.
162. Liang, L.; Feng, X. D.; Peurrung, L.; Viswanathan, V. J. *Membr. Sci.* **1999**, 162, 235-246.
163. Reuber, J.; Reinhardt, H.; Johannsmann, D. *Langmuir*, **2006**, 22, 3362.
164. Gabai, R.; Sallacan, N.; Chegel, V.; Bourenko, T.; Katz, E.; Willner, I. *J. Phys. Chem. B.* **2001**, 105, 8196-8202.
165. Wang, X. J.; Bohn, P. W. *J. Am. Chem. Soc.* **2004**, 126, 6825-6832.
166. Pan, Y. V.; Wesley, R. A.; Luginbuhl, R.; Denton, D. D.; Ratner, B. D. *Biomacromolecules*, **2001**, 2, 32-36.
167. Tamirisa, A.; Hess, D. W. *Macromolecules*, **2006**, 39, 7092-7097.

## References

---

168. Bullett, N. A.; Talib, R. A.; Short, R. D.; McArthur, S. L.; Shard, A. G. *Surf. Interface Anal.* **2006**, 38, 1109-1116.
169. Forch, R.; Chifen, A. N.; Bousquet, A.; Khor, H. L.; Jungblut, M.; Chu, L. Q.; Zhang, Z.; Osey-Mensah, I.; Sinner, E. K.; Knoll, W. *Chem. Vapor Depos.* **2007**, 13, 280-294.
170. K. Chan, K.; Gleason, K. K. *Langmuir*, **2005**, 21, 8930-8939.
171. Gupta, S.; Kuckling, D.; Kretschmer, D.; Choudhary, V.; Adler, H. J. J. *Polym. Sci. A.* **2007**, 45, 669-679.
172. Recum, von H.A.; Kim, S. W.; Kikuchi, A.; Okuhara, M.; Y. Sakurai, Y.; Okano, T, *J. Biomed. Mater. Res.* **1998**, 40, 631-639.
173. Matsukuma, D.; Yamamoto, K.; Aoyagi, T. *Langmuir*, **2006**, 22, 5911-5915.
174. Heijl, J. M. D.; Du Prez, F. E. *Polymer*. **2004**, 45, 6771-6778.
175. Hoffmann, J.; Plotner, M.; Kuckling, D.; Fischer, W. J. *Sens. Actuators, A.* **1999**, 77, 139-144.
176. Liu, H. C.; Ito, Y. *J. Biomed. Mater. Res. A.* **2003**, 67A, 1424-1429.
177. Aussenegg, F. R.; Brunner, H.; Leitner, A.; Lobmaier, C.; Schalkhammer, T.; Pittner, F. *Sens. Actuators B.* **1995**, 29, 204-209.
178. Schmaljohann, D.; Beyerlein, D.; Nitschke, M.; Werner, C. *Langmuir*, **2004**, 20, 10107-10114.
179. Nitschke, M.; Zschoche, S.; Baier, A.; Simon, F.; Werner, C. *Surf. Coat. Tech.*, **2004**, 185, 120-125.
180. Sukhishvili, S. A. *Curr. Opin. Colloid Interface Sci.* **2005**, 10, 37-44.
181. D. Lee, D.; Nolte, A. J.; Kunz, A. L.; Rubner, M. F.; Cohen, R. E. *J. Am. Chem. Soc.*, **2006**, 128, 8521-8529.
182. Dai, J. H.; Jensen, A. W.; Mohanty, D. K.; Erndt, J.; Bruening, M. L. *Langmuir*, **2001**, 17, 931-937.
183. Quinn, J. F.; Johnston, A. P. R.; Such, G. K.; Zelikin, A. N.; Caruso, F. *Chem. Soc. Rev.*, **2007**, 36, 707-718.
184. Quinn, J. F.; Caruso, F. *Langmuir*. **2004**, 20, 20-22.
185. Kharlampieva, E.; Kozlovskaya, V.; Tyutina, J.; Sukhishvili, S.A. *Macromolecule*, **2005**, 38, 1052310531.
186. Mendelsohn, J.D.; Barrett, C.J.; Chan, V.V.; Pal, A.J.; Mayes, A.M.; Rubner, M.F. *Langmuir*, **2000**, 16, 5017-5023.
187. Fery, A.; Scholer, B.; Cassagneau, T.; Caruso, F. *Langmuir*, **2001**, 17, 3779-3783.

## References

---

188. Dubas, S.T.; Schlenoff, J.B. *Macromolecules*, **2001**, 34, 3736-3740.
189. Sukhishvili, S.A.; Granick, S. *J. Am. Chem. Soc.* **2000**, 122, 9550-9551.
190. M. K. Park, M.K.; S. X. Deng, S.X.; Advincula, R.C. *J. Am. Chem. Soc.* **2004**, 126, 13723-13731.
191. Kang, E.H.; Liu, X.K.; Sun, J.Q.; Shen, J.C. *Langmuir*, **2006**, 22, 7894-7901
192. Serizawa, T.; Matsukuma, D.; Nanameki, K.; Uemura, M.; Kurusu, F.; Akashi, M. *Macromolecules*, **2004**, 37, 6531-6536.
193. Such, G.K.; Quinn, J.F.; Quinn, A.; Tjipto, E.; Caruso, F. *J. Am. Chem. Soc.* **2006**, 128, 9318-9319.
194. Such, G.K.; Tjipto, E.; Postma, A.; Johnston, A.P.R.; Caruso, F. *Nano Lett.* **2007**, 7, 1706-1710.
195. Connal, L.A.; Kinnane, C.R.; Zelikin, A.N.; Caruso, F. *Chem. Mater.* **2009**, 21, 576-578.
196. Tong, W.; Gao, C.; H. Meohwald, H. *Macromol. Rapid Commun.* **2006**, 27, 2078-2083.
197. Johnston A. P. R.; Caruso, F. *Small*, **2008**, 4, 612-618.
198. Johnston, P. R.; Mitomo, H.; Read, E. S.; Caruso, F. *Langmuir*, **2006**, 22, 3251-3258.
199. Jaber, J. A.; Schlenoff, J. B. *Macromolecules*, **2005**, 38, 1300-1306.
200. Fulghum, T. M.; Estillore, N. C.; Vo, C. D.; Armes, S. P.; Advincula, R. C. *Macromolecules*, **2008**, 41, 429.
201. Chu, L. Y.; Li, Y.; Zhu, J. H.; Chen, W. M. *Angew. Chem. Int. Edit.*, **2005**, 44, 2124-2127.
202. Tokarev, I.; Orlov, M.; Minko, S. *Adv. Mater.* **2006**, 18, 2458-2460.
203. Richter, A.; Bund, M. K.; Arndt, K. F. *Sens. Actuators B.* **2004**, 99, 579-585.
204. Harnish, B.; Robinson, J. T.; Pei, Z. C.; Ramstrom, O.; Yan, M. D. *Chem. Mater.*, **2005**, 17, 4092-4096.
205. Kanekiyo, Y.; Ono, Y.; Inoue, K.; Sano, M.; Shinkai, S. *J. Chem. Soc. Perk. T. 2*, **1999**, 557-562.
206. Hilt, J. Z.; Gupta, A. K.; Bashir, R.; Peppas, N. A. *Biomed. Microdevices*, **2003**, 5, 177-184.
207. Yamada, N.; Okano, T.; Sakai, H.; Karikusa, F.; Sawasaki, Y.; Sakurai, Y. *Macromol. Rapid Commun.* **1990**, 11, 571.
208. Da Silva, R. M. P.; Mano, J. F.; Reis, R. L. *Trends Biotechnol.*, **2007**, 25, 577-583.

## References

---

209. Yang, J.; Yamato, M.; Nishida, k.; Ohki, T.; Kanzaki, M.; Sekine, H.; Shimizu, T.; Okano, T. *J. Control. Release*, **2006**, 116, 193-203.
210. Tsuda, Y.; Shimizu, T.; Yarnato, M.; Kikuchi, A.; Sasagawa, T.; Sekiya, S.; Kobayashi, J.; Chen, G.; Okano, T. *Biomaterials*, **2007**, 28, 4939-4946.
211. Tsuda, Y.; Kikuchi, A.; Yamato, M.; Chen, G. P.; Okano, T.; *Biochem. Biophys. Res. Commun.* **2006**, 348, 937-944.
212. Ronald Lee Earp Jr. Ph.D. thesis, *Department of Chemistry Virginia Polytechnic Institute and State Univeristy*, **1997**, Chapter 2,8.
213. Maier, S. A. *Plasmonics: Fundamentals and Applications*; Springer: New York, 2007.
214. Drude, P. *Ann. Phys.* **1900**, 1, 566-613.
215. Drude, P. *Theory of Optics*; Longmans, Green, New York, 1922; Dover, New York, **1968**.
216. Wood, R. W. *Phil. Magm.* **1902**, 4, 396-402.
217. Maxwell, J. C. *A Treatise on Electricity & Magnetism*; Dover Publications: New York, **1873**.
218. Zenneck, J. *Ann. Phys.* **1907**, 23, 846-866.
219. Otto, A. *Z. Phys.* **1968**, 216, 398-410.
220. Kretschmann, E.; Raether, H. *Z. Naturforsch.* **1968**, 23a, 2135-2136.
221. Samantha S. Bokatzian-Johnson. Literature, Department of Chemistry, University of Alabama, **2008**.
222. Haes, A. J.; Zou, S.; Schatz, G. C.; Van Duyne, R. P. *J. Phys. Chem. B.* **2004**, 108, 109-116.
223. Green, R. J.; Frazier, R. A.; Shakesheff, K. M.; Davies, M. C.; Roberts, C. J.; Tendler, S. J. B. *Biomaterials.* **2000**, 21, 1823-1835.
224. Homola, J.; Yee, S. S.; Gauglitz, G. *Sens. Actuators, B.* **1999**, 54, 3-15.
225. Odom, T. W.; Nehl, C. L. *ACS Nano.* **2008**, 2, 612-616.
226. Kuckling, D.; Pareek.; P. *Polymer*, **2008**, 49, 1435-1439
227. Lofas, S.; Johnsson, B.; Edstrom, A.; Hansson, A.; Lindquist, G.; Hillgren, R. M. M.; Stigh, L. *Biosens. Bioelectron.* **1995**, 10, 813-822.
228. Yang, N.; Su, X. D.; Tjong, V.; Knoll, W. *Biosens. Bioelectron.* **2007**, 22, 2700.
229. Fong, C. C.; Wong, M. S.; Fong, W. F.; Yang, M. S. *Anal. Chim. Acta.* **2002**, 456, 201-208.

## References

---

230. Mack, N. H.; Wackerly, J. W.; Malyarchuk, V.; Rogers, J. A.; Moore, J. S. R. Nuzzo, G. *Nano Lett.* **2007**, *7*, 733-737.
231. Hutter, E.; Fendler, J. H. *Adv. Mater.* **2004**, *16*, 1685.
232. Ghosh, S. K.; Pal, T. *Chem. Rev.* **2007**, *107*, 4797-4862.
233. Lee, S.; Perez-Luna, V. H. *Langmuir*, **2007**, *23*, 5097-5099.
234. Marshall, J.; Blyth, J.; Davidson, C. A. B.; Lowe, C. R. *Anal. Chem.* **2003**, *75*, 4423-4431.
235. Marshall, J.; Young, D. S.; Kabilan, S.; Hussain, A.; Blyth, J.; Lowe, C. R. *Anal. Chim. Acta.* **2004**, *527*, 13-20.
236. Mayes, G.; Blyth, J.; Kyrolainen-Reay, ; Millington, R. B.; Lowe, C. R. *Anal. Chem.* **1999**, *71*, 3390-3396.
237. Mayes, A. G.; Blyth, J.; Millington, R. B.; Lowe, C. R. *Anal. Chem.* **2002**, *74*, 3649-3657.
238. Gonzalez, B. M.; Christie, G.; Davidson, C. A. B.; Blyth, J.; Lowe, C. R. *Anal. Chim. Acta.* **2005**, *528*, 219-228.
239. Marshall, J.; Young, D. S.; Blyth, J.; Kabilan, S.; Lowe, C. R. *Anal. Chem.* **2004**, *76*, 1518-1523.
240. Kabilan, S.; Marshall, A. J.; Sartain, F. K.; Lee, M. C.; Hussain, A.; Yang, X. P.; Blyth, J.; Karangu, N.; James, K.; Zeng, J.; Smith, D.; Domschke, D.; Lowe, C. R. *Bioelectron.* **2005**, *20*, 1602-1610.
241. Dubendorfer, J.; Kunz, R. E.; Jobst, G.; Moser, I.; Urban, G. *Sens. Actuators, B.* **1998**, *50*, 210-219.
242. Clark, L. C.; Wolf, R.; Granger, D.; Taylor, Z. *J. Appl. Physiology.* **1953**, *6*, 189-193.
243. Liedberg, B.; Nylander, C.; Lunstrom, I. *Sens. Actuators.* **1983**, *4*, 299-304.
244. Jennifer, S. S.-P.; Campbell, C. T. *Analytical Chemistry*, **2004**, *76*, 4, 907-917.
245. Linda S. J.; Campbell, C.T.; Chinowsky, T. M.; Mar, M. N.; Sinclair S. Y. *Langmuir*, **1998**, *14*, 5636-5648.
246. Stenberg, S.; Persson, B.; Roos, H.; Urbaniczky, C. *Journal of Colloid and Interface Science*, **1991**, *143*, 513-526.
247. arima, Y.; Toda, M.; Iwata, H. *Adv. drug deliv. rev.* **2011**, *63*, 988-999
248. Badia, A. *Litrature, Faculty of science, Chemistry department, McGill University.* **2007**.
249. Schuck, P. *Annu. Rev. Biophys. Struct.* **1997**, *26*, 541-566.

250. Schasfoort, R.B.M.; Tudos, A. J. *Handbook of Surface Plasmon Resonance, The Royal Society of Chemistry*, **2008**,6,181.
251. Myszka, D.G. *J. Mol. Recognit.* **1999**, 12, 279-284.
252. Nagata, K. *Significance of the real-time analysis of biological interactions, in Real-Time Analysis of Biomolecular Interactions, K. Nagata, H. Handa, (Eds.), Springer.* **2000**, 3–9.
253. Wild, D. (Ed.) *the Immunoassay Book, Stockton Press, New York.* **1994**.
254. Murai, M.; Yoshida, M. *Molecular Chaperones in Part 4 Chapter 1, in Real-Time Analysis of Biomolecular Interactions, K. Nagata, H. Handa.*
255. Nelson, B.P.; Frutos, A.G.; Brockman, J.M.; Corn, R.M. *Anal. Chem.* **1999**, 71, 3928-3934.
256. de Mol, N.J.; Plomp, E.; Fischer, M.J.; Ruijtenbeek, R. *Anal. Biochem.* **2000**, 279, 61-70.
257. Kipping, M.; PhD Thesis. Faculty of mathematics and science *Technical univeristy Dressden* **2008**.
258. Berger RG, KU. *Appl Microbiol Biotechnol.* **1998**, 49: 1
259. Hocking MB. *J Chem Ed.* **1997**, 74: 1055
260. Gumí, T; Gascón, S.; Torras, C.; Garcia-Valls, R. *Desalination*, **2009**, 246 396–402
261. Zou, Y.; Brooks, DE.; Kizhakkedathu, J.N. *Macromolecules*, **2008**, 41, 5393-5405.
262. Heredia, K.L.; Maynard, H.D. *Org. Biomol.Chem.* **2007**, 5, 45-53.
263. Han, S.; Hagiwara, M.; Ishazone, T. *Macromolecules*, **2003**, 36, 8312-8319.
264. Wichterle O.; Lim, D. *Nature* **1960**,185:117–8.
265. Peppas, NA.; Mikos, AG. Preparation methods and structure of hydrogels. In: Peppas NA. *Hydrogels in medicine and pharmacy*, vol. 1. Boca Raton, Florida: CRC Press, Inc; **2000**, p. 1–25.
266. Lee, KY.; Mooney, DJ. *Chem Rev* **2001**, 101, 1869–79.
267. Lai, YC.; Wilson, AC.; Zantos, SZ. Contact lenses. In: Howe-Grant M, editor. Kirk-Othmer. *Encyclopedia of Chemical Technology*, vol. 7. New York, NY: John Wiley and Sons, Inc.; **1993**, p. 192–218.
268. Chirila, TV. *Biomaterials.* **2001**, 22, 11–7.
269. Young, C-D.; Wu, J-R.; Tsou, T-L. *Biomaterials.* **1998**, 19, 1745–1752.
270. Voldrich, Z.; Tomanek, Z.; Vacík, J.; Kopecek J. *J Biomed Mater Res.* **1975**, 9, 675–685
271. Lou, X.; Munro, S.; Wang, S. *Biomaterials.* **2004**, 25:5071–80.

## References

---

272. Dziubla, TD.; Torjman, MC.; Joseph, JI.; Murphy-Tatum, M.; Lowman, AM. *Biomaterials*. **2001**, 22, 2893–2899.
273. Sharkawy, AA.; Klitzman, B.; Truskey, GA.; Reichert, WM. *J Biomed Mater Res* **1998**, 40, 598–605.
274. Sharkawy, AA.; Klitzman, B.; Truskey, GA.; Reichert, WM. *J Biomed Mater Res*. **1998**, 40, 586–97.
275. Sharkawy, AA.; Klitzman, B.; Truskey, GA.; Reichert, WM. *J Biomed Mater Res*. **1997**, 37, 401–12.
276. Chirila, TV.; Constable, JI.; Crawford, GJ.; Vijayasekaran, S.; Thompson, DE.; Chen, Y-C. *Biomaterials* **1993**, 14, 26–38.
277. Vacanti, JP.; Morse, MA.; Saltzman, WM.; Domb, AJ.; Perez-Atayde, A.; Langer, R. *J. Pediatr Surg*. **1988**, 23, 3–9.
278. Cima, LG.; Vacanti, JP.; Vacanti, C.; Ingbar, D.; Mooney, D.; Langer, R. *J Biomech Eng -T ASME*. **1991**, 113, 143–51.
279. Save, M.; Weaver, J. V. M.; Armes, S. P. *Macromolecules*, **2002**, 35, 1152-1159.
280. Haigh, R.; Rimmer, S.; Fullwood, N. J. *Biomaterials*, **2000**, 21, 735-739.
281. Lewis, A. L.; Cumming, Z. L.; Stratford, P. W.; *Biomaterials*, **2001**, 22, 99-111.
282. Weiss, K. D. *Prog. Polym. Sci.* **1997**, 22, 203-245.
283. Feng, X. S.; Pan, C. Y.; Wang, J. *Macromol. Chem. Phys.* **2001**, 202, 2986-2991.
284. Pan, C. Y.; Tao, L.; Wu, D. C. *J. Polym. Sci. Polym. Chem.* **2001**, 39, 3062-3072.
285. Zhen, Y.; Wan, S.; Liu, Y.; Yan, H.; Shi, R.; Wang, C. *Macromol. Chem. Phys.* **2005**, 206, 607-612.
286. Zhang, Z. R.; Liu, G. J.; Bell, S. *Macromolecules*, **2000**, 33, 7877-7883.
287. Li, Z.; Liu, G. J. *Langmuir*, **2003**, 19, 10480-10486.
288. Pietsch, C.; Schubert, U.; Hoogenboom, R. *Chem. Commun.*, **2011**, 47, 8750–8765
289. Kungwachakun, D.; Irie, M. *Makromol. Chem. Rapid Commun.* **1988**, 9, 243–246.
290. Zhao, Y.; Tremblay, L.; Zhao, Y. *J. Polym. Sci., Part A: Polym. Chem.* **2010**, 48, 4055–4066.
291. Irie, M.; Kungwachakun, D. *Proc. Jpn. Acad., Ser. B, Phys. Biol. Sci.* **1992**, 68, 127–132.
292. Akiyama, H.; Tamaoki, N. *J. Polym. Sci., Part A: Polym. Chem.* **2004**, 42, 5200–5214.
293. Yuan, W.; Jiang, G.; Wang, J.; Wang, G.; Song, Y.; Jiang, L. *Macromolecules*, **2006**, 39, 1300–1303.
294. Desponds, A.; Freitag, R. *Langmuir*, **2003**, 19, 6261–6270.

## References

---

295. Ravi, P.; Sin, S. L.; Gan, L. H.; Gan, Y. Y.; Tam, K. C.; Xia, X. L.; Hu, X. *Polymer*, **2005**, 46, 137–146.
296. Akiyama, H.; Tamaoki, N. *Macromolecules*, **2007**, 40, 5129–5132.
297. Jochum, F. D.; Theato, P. *Polymer*, **2009**, 50, 3079–3085.
298. Jochum, F. D.; Forst, F. R.; Theato, P. *Macromol. Rapid Commun.* **2010**, 31, 1456–1461.
299. Jochum, F. D.; Theato, P. *Chem. Commun.* **2010**, 46, 6717–6719.
300. Luo, C.; Zuo, F.; Ding, X.; Zheng, Z.; Cheng, X.; Peng, Y. *J. Appl. Polym. Sci.* **2008**, 107, 2118–2125.
301. Tang, X.; Liang, X.; Gao, L.; Fan, X.; Zhou, Q. *J. Polym. Sci., Part A: Polym. Chem.* **2010**, 48, 2564–2570.
302. Jochum, F. D. Borg, L zur.; Roth, P. J.; Theato, P. *Macromolecules*, **2009**, 42, 7854–7862.
303. Xiang, X.; Xue, X.; Zhu, J.; Zhang, Z.; Zhang, W.; Zhou, N.; Zhu, X. *Polym. Chem.* **2010**, 1, 1453–1458.
304. Suzuki, A.; Tanaka, T. *Nature*, **1990**, 346, 345–347
305. Zhang, J.; Xu, X-D.; Wu, D-Q.; Zheng, X.; Zhuo, R-X. *Carbohydrate polymers*, **2009**, 77, 583-589.
306. Kumar, NS.; Ganapathy, HS.; Kim, JS.; Jeong, YS.; Jeong, YT. *European Polymer Journal*, **2008**, 44, 579–586.
307. Kim, YH.; Cho, C-S.; Kang, I-K.; Kim, SY.; Kwon, OH. *Key Engineering Materials*. **2007**, 342-343, 245-238.
308. Simchowit, A.O. *Davis, J. Gen. Physiol.* **1989**, 94, 95-124.
309. Phillips, R. A.; P. B. Hamilton. *Am J Physiol February 29*, **1948** 152, (3) 523- 530.
310. Costanzo, L. *Physiology*, 4th Edition. Philadelphia: Lippincott Williams and Wilkins, **2007**, 156-160.
311. Sanong Ekgasit, S.; Chuchaat Thammacharoen, C.; Wolfgang Knoll, W. *Analytical chemistry*, **2004**, 76, 561-568
312. Yang. X. M.; Peters. R. D.; Nealey. P. F.; Solak. H. H.; Cerrina. F. *Macromolecules*, **2000**, 33, 9575-9582.
313. Fondecave. R.; Wyart. F. B. *Macromolecules*, **1998**, 31, 9305-9315.

## *Acknowledgements*

*I am equally grateful thanks to my Professor, Prof. Dr. Dirk Kuckling. He gave me moral support and guided me in different matters regarding the topic. He had been very kind and patient while suggesting me the outlines of this project and correcting my doubts. I thank him for his overall supports.*

*I am very thankful for my lovely wife. She supported me, for i have completed my project effectively and moreover on time.*

*I would like to thank my parents who helped me a lot in my life.*

*Special thanks to my dear Dr. Antje Britze , She helped me a lot in gathering different information, collecting data and guiding me from time to time in making this project.*

*Also I thank my Dear collage Nebia Greving for her kindly helping.*

*My grateful thanks for my collages Dr. Wolfgange Birnbaum and Dr. Artjom Döring for their helping along my work.*

*I also wish to express my deep sense of gratitude to my collages Agnes Wycisk and Simon Schmücker.*

*I also wish to convey my sincere thanks to Angelika Kröber , Annette Lefarth and Mariola Zukowski .*

*I gratefully acknowledge the assistance of the following people: Ralf Hamann, Andrea Harbarth and Susanne Keuker-Baumann for their invaluable help in the characterization of various compounds.*

*Momen Ali*